

An Investigation into a Lower Temperature and Low Cost Direct Reduction Process for Iron-Making

A dissertation submitted in the
School of Chemical Engineering

by

Reubendran Chellan
[B.Sc. (Eng.)]
University of Natal, Durban

In fulfillment of the requirements for the degree of
Master of Science in Engineering (Chemical)

July 2003

UNIVERSITY OF NATAL
SCHOOL OF CHEMICAL ENGINEERING



**An investigation into a lower temperature and low cost
Direct Reduction process for iron-making**

By: Reubendran Chellan

Supervisor: Dr J. Pocock

Co-supervisor: Prof D. Arnold

Abstract

The blast furnace process for the reduction of iron ore to pig iron faces problems such as emission of air pollutants, high investment cost and the current major problem of decreasing supplies of coke. Coke is used in large quantities to promote a combination of direct and indirect reduction within the furnace. Due to the lack of good coking coal within South Africa, and dwindling supplies worldwide, new iron-making processes, are being developed using coal and/or natural gas to replace coke as the reductant.

The new processes allow efficient use of carbon, fed in the form of coal pellets (coal-based processes) or natural gas (gas-based processes), as the reducing agent. Presently, most coal-based processes use an excess of coal, up to 500% stoichiometric addition, and are run at temperatures up to $\pm 1200^{\circ}\text{C}$, although reduction tends to proceed at $\pm 850^{\circ}\text{C}$.

This project developed a low temperature process using mixed pellets of fine waste iron oxide and fine domestic coal with a natural carbonaceous binder (a by-product from local pulping industry).

Reduction tests performed on composite pellets in a tube furnace and thermobalance indicated, upon analysis by X-Ray Diffraction and Scanning Electron Microscope, that reduction occurred gradually at 900°C . Implementing induction heating of bulk pellets reduced heating times substantially. Induction heating also resulted in direct reduced iron [DRI] containing 75 – 80% metallic iron. Energy consumption based on coal usage amounted to 23.71 GJ/ton DRI, which compares with the calorific consumption of most coal-based processes, i.e. coal consumption range between 15 and 25 GJ/ton DRI. Energy consumed during induction heating amounted to 9.94 GJ/ton DRI, as electricity. This energy consumption value does not take into account the efficiency of the primary energy required to generate electricity.

Preface

The work presented in this thesis was performed at the University of Natal, Durban from April 2001 to April 2003. The work was supervised by Dr J. Pocock and Prof. D. Arnold.

This thesis is presented as the full requirement for the degree of M.Sc. in Chemical Engineering. All the work presented in this thesis is original unless otherwise stated and has not, in whole or part, been submitted previously to any tertiary institute as part of a degree.

R. Chellan

Date

Supervisor

Date

Co - Supervisor

Date

Acknowledgements

I would like to acknowledge the following people for their respective contributions to this work:

- My supervisor, Dr J. Pocock, for his guidance, motivation and creative thinking that always complemented my work. I will cherish the experience gained while working with him.
- My co-supervisor, Prof. D. Arnold, for always showing a keen interest and contributing with his wealth of experience towards my work.
- Lignotech South Africa for sponsorship during my degree.
- Roy and Pat, from the Geology Department of Natal University, and Prof. J. Dunlevey, from the Geology Department of University of Durban Westville for respective X-Ray Diffraction analysis which was always efficiently performed in the minimum period.
- Fiona Graham, from the SEM Unit of Natal University, for always being available to perform analysis (with a smile).
- My colleagues (a special mention of Dr. Jalari Rajasekhar), for their positive criticism and more importantly their friendship.
- On a more personal note, my family, namely, David, Kantha and Niven Chellan, Maliga Moodley, and both my grandmothers, for always believing in my capabilities.
- My dear Tash, for being the pillar of strength I can and always will count on.

And finally, I wish to thank our beloved Almighty, as belief in him gives us the strength and fortitude to reach our goals, in the most demanding yet most enjoyable way possible.

TABLE OF CONTENTS

	<i>Pg</i>
<i>Abstract</i>	<i>i</i>
<i>Preface</i>	<i>ii</i>
<i>Acknowledgements</i>	<i>iii</i>
<i>List of Tables</i>	<i>viii</i>
<i>List of Figures</i>	<i>ix</i>
<i>List of Graphs</i>	<i>x</i>
<i>Nomenclature</i>	<i>xii</i>
<i>Chapter 1</i>	
1. Introduction	1
<i>Chapter 2 – Literature Survey</i>	
2.1 Direct Reduction of Pellets	
2.1.1 Mechanism of Direct Reduction of Pellets	6
2.1.1.1 Direct and Indirect Reduction	6
2.1.1.2 Reaction Pathways in Pellet	7
2.1.1.3 Effect of Temperature on Iron Oxide Phases	11
2.1.2 Kinetic Rate Equations	14
2.1.2.1 Kinetics of Ore/Coal Systems	14
2.1.2.2 Kinetics of Fluidised Beds	19
2.1.2.3 Thermogravimetric Methods	21
2.1.3 Conclusion	24
2.2 Iron-making Processes	
2.2.1 The Blast Furnace Operation	26

2.2.1.1	The Blast Furnace Set-up	26
2.2.1.2	Role of Coke in the Blast Furnace	30
2.2.1.3	Other Raw Materials and Products	32
2.2.2	Commercial Direct Reduction Processes	36
2.2.2.1	Midrex Direct Reduction Process	37
2.2.2.2	Danarex Process	39
2.2.2.3	SL/RN Process	41
2.2.2.4	Fastmet Process	42
2.2.2.5	Corex Process	44
2.2.2.6	The HIs melt Process	46
2.2.2.7	New Technologies	48
2.2.2.8	Overview of Iron-Making Processes	52
2.2.3	Conclusion	55

Chapter 3 – Pelletization

3.1	Pelletization Theory	57
3.2	Pellet Manufacture	
3.2.1	Properties of fines	60
3.2.2	Pelletization Experimental Set-up	65
3.3	Evaluation of Pellets	
3.3.1	Ball Size	68
3.3.2	Compression Strength	68
3.3.3	Drop Strength	71
3.3.4	Resistance to Abrasion	71
3.3.5	Moisture Content	72
3.3.6	Tests with Bentonite	72
3.4	Conclusion	73

Chapter 4 – Reduction in Tube Furnace

4.1	Experimental Set-up	74
4.2	Results of Tube Furnace Tests	75
4.3	Discussion of Tube Furnace Tests	81
4.4	Conclusion	82

Chapter 5 – Reduction in Thermobalance

5.1	Experimental Set-up	83
5.2	Results of Thermobalance Tests	85
5.3	Discussion of Thermobalance Tests	91
5.4	Conclusion	92

Chapter 6 – Reduction in Induction Furnace

6.1	Theory of Induction Heating	93
6.2	Advantages of Induction Heating	94
6.3	Induction Furnace Set-up	96
6.4	Results and Discussion of Induction Furnace Testing	98
6.4.1	Reduction of Pellets containing coal < 100 μ m	98
6.4.2	Effect of Varying Magnetite/Coal Ratios	100
6.4.3	Effect of Varying Coal Particle Size	102
6.4.4	Effect of Using Air Atmosphere	103
6.5	Optimising Reduction in Induction Furnace	105
6.5.1	Parameters for Optimised Run	105
6.5.2	Results and Discussion of Optimised Run	106
6.5.3	Slag Formation	108

6.5.4	Energy Consumption of Induction Furnace	108
6.5.5	Advantages of the DRI Process	109
6.5.6	Uses of the DRI Process	110
6.6	Conclusion	111

Chapter 7 – Conclusion and Recommendations

7.1	Conclusion	112
7.2	Recommendations	114

<i>References</i>	115
-------------------	-----

Appendices

Appendix A:	Kinetic Analysis of Reduction	121
Appendix B:	X-Ray Diffraction	123
Appendix C:	Kinetic Evaluation using Thermobalance Data	128
Appendix D1:	Detail of Mapham Induction Heater	137
Appendix D2:	Induction Heating Experimental Procedure	139
Appendix D3:	Calculation of Percent Metallic Iron Produced	140
Appendix D4:	Calculation of Energy Consumption of Process	142
Appendix E:	Equipment Pictures	143
Appendix F:	Calibration curves	145
Appendix G:	SEM Images	149
Appendix H:	XRD Analytical Data	151

LIST OF TABLES

	<i>Pg</i>
2.1 Typical Analysis of Coke	30
2.2 Typical Analysis of Pig Iron	33
2.3 Typical Analysis of Blast Furnace Slag	33
2.4 Typical Analysis of Product Gas	34
2.5 Raw Materials and Products for Production of 1 ton Pig Iron	35
2.6 Process Parameters	54
3.1 Elemental Analysis of Feed Material	60
3.2 Surface Areas and Size of Feed Material	62
3.3 Elemental Analysis of Lignobond	64
3.4 Abrasion Index of Mixed Magnetite/Coal Pellets	72
5.1 Mass Percent of Elements in Pellet Reduced in Thermobalance	90
6.1 SEM Elemental analyses of reduced pellets containing coal < 100 μm	99
6.2 SEM Elemental analyses of reduced pellets, magnetite/coal = 2:1	101
6.3 SEM Elemental analyses of reduced pellets containing coal < 20 μm	102
6.4 SEM Elemental analyses of pellets reduced in air atmosphere	104
6.5 SEM Elemental analyses of pellets for Optimised Run	106
B1 D-Spacing of Respective Compounds	127
D3.1 Atomic Masses of Elements	140
D3.2 Mass Percent of Elements in pre-reduced pellet	140

LIST OF FIGURES

	<i>Pg</i>
2.1 Schematic diagram of the mode of gaseous reduction of a spherical sample of ferric oxide	8
2.2 Section of the Blast Furnace	27
2.3 Simulated gas temperature map for typical Blast Furnace	29
2.4 Shaft Furnace detail	38
2.5 Chemical Reactions in the Danarex reactor	40
2.6 The SL/RN process flow-sheet	41
2.7 Flowsheet of Fastmet Process	43
2.8 Flowsheet of Corex Process	45
2.9 The HISmelt Reduction Vessel (SRV)	47
2.10 Flow sheet of the Comet Process	48
2.11 Apparatus for Direct Reduction of Metal Agglomerates	51
3.1 Mechanism of ball formation	57
3.2 Motion of Material in a disc pelletizer revolving at various speeds	65
3.3 Typical arrangements of feeding and spraying in a disc pelletizer	66
3.4 Strength Tester	69
4.1 Experimental Set-up of Tube Furnace Testing	74
5.1 Thermobalance Experimental Set-up	83
6.1 Principle of Induction Heating	93
6.2 Induction furnace Experimental Set-up	96
B1 Reflection of X-Rays from two planes of atoms in a solid	123
B2 X-Ray Powder Diffractometer	124
D1 Detail of Mapham Induction Heater	137

LIST OF GRAPHS

	<i>Pg</i>
2.1 Plot of $p_{CO}/(p_{CO} + p_{CO_2})$ versus temperature for pressure of 1 atm, showing areas of stability of ferrite, austenite, wustite, magnetite and graphite	13
2.2 Conversion of Magnetite to iron using Reddy et al (1991) kinetics	18
3.1 Malvern Size Analysis of Magnetite	61
3.2 Malvern Size Analysis of Coarser Coal	63
3.3 Malvern Size Analysis of Finer Coal	63
3.4 Strength of Magnetite/Coal Pellets	70
4.1 XRD Analysis of feed Pellets	76
4.2 – 4.5 XRD Analysis of Pellets reduced in Tube Furnace	76 – 80
5.1 Temperature profiles for 3 Thermobalance Runs	85
5.2 – 5.4 Ginstling – Brounshtein Model for Thermobalance Runs	86 – 87
5.5 Arrhenius Plot	88
5.6 – 5.9 XRD Analysis of Pellets reduced in Thermobalance Furnace	89
6.1 – 6.3 XRD Analysis of reduced pellets containing coal < 100 μm	98 - 99
6.4 – 6.5 XRD Analysis of reduced pellets containing different ratios of magnetite/coal	100
6.6 – 6.7 XRD Analysis of reduced pellets containing coal < 20 μm	102
6.8 XRD Analysis of pellets reduced in air atmosphere	103
6.9 XRD Analysis of reduced pellets for optimised run	106
C1.1 Temperature Profile Thermobalance Run 1	128
C1.2 Mass of Pellet during Run 1	129
C1.3 Fraction of Reaction During Run 1	129
C1.4 Ginstling – Brounshtein Model for Run 1	130
C1.5 Jander Model for Run 1	131
C1.6 Spherical Symmetrical Model for Run 1	131

C2.1	Temperature Profile Thermobalance Run 2	132
C2.2	Mass of Pellet during Run 2	133
C2.3	Fraction of Reaction During Run 2	133
C2.4	Ginstling – Brounshtein Model for Run 2	134
C3.1	Temperature Profile Thermobalance Run 3	134
C3.2	Mass of Pellet during Run 3	135
C3.3	Fraction of Reaction During Run 3	135
C3.4	Ginstling – Brounshtein Model for Run 3	136
F1.1	Strength Tester Calibration Curve	145
F1.2	Calibration Curve for N ₂ Rotameter	145
F1.3	Calibration Curve for Water Rotameter	146
F2.1 – F2.3	Induction Heater Calibration Curves at different Power settings, without susceptor	147
F2.4 – F2.6	Induction Heater Calibration Curves at different Power settings, with susceptor	148

NOMENCLATURE

A	Pre – exponential factor,	min^{-1}
C^*	Equilibrium concentration of CO at the given temperature,	mol / g
C^*	Concentration of CO at the reaction interface,	mol / g
C_A	Concentration of A,	mol / g
C_{A0}	Initial concentration of A,	mol / g
D	Diameter,	m
d	Space between crystalline layers,	nm
DR/dt	Rate of Reduction,	l / min
E	Activation Energy	kJ / mol
f	Fraction of Reaction	
$G(x)$	Ginstling – Brounshtein Model	
I/I_1	Relative Intensity	
$J(x)$	Jander Model	
k	Kinetic Rate Constant,	min^{-1}
K	Ratio of weight of iron to that of oxygen in the ore	
L	Length,	m
M	Ratio of initial concentrations of reactants	
n_{crit}	Critical number of revolutions per minute,	min^{-1}
n_{opt}	Optimum number of revolutions per minute,	min^{-1}
O	Number of Oxygen atoms,	mol
P_{CO}	Partial Pressure of Carbon Monoxide,	kPa
P_{CO_2}	Partial Pressure of Carbon Dioxide,	kPa
R	Gas constant,	$(8.314) \text{ kJ / kmol.K}$
$-r_A$	Rate of Reduction of A,	mol / g.s
$S(x)$	Spherical Symmetrical Model	
T	Temperature,	K
X_A	Fractional conversion of A	
ΔG^o	Gibbs Free Energy,	kJ / mol
Θ	Angle	
α	Degree of Reduction	
ρ	Density,	kg / m^3

Chapter 1: Introduction

The production of pig iron in the blast furnace ranks foremost amongst all the iron-making processes. In 2001 the blast furnace production of pig iron amounted to approximately 580 million tons, which constituted 59% of the world iron production (Moore, 2001). The iron blast furnace is a tall, vertical shaft, which employs carbon, mainly in the form of coke to reduce iron oxides to metallic iron. Coke is used in large quantities in iron blast furnaces to promote a combination of direct and indirect reduction within the furnace. Direct reduction involves the carbon reacting directly with the iron oxide to form iron; while indirect reduction involves the carbon monoxide, which is a product of direct reduction, becoming the reducing agent to form metallic iron. The product is a liquid 'pig iron', containing up to 5% carbon and 1% silicon (Percy and Davenport, 1979). The extensive use of the blast furnace is not only because of the very high production rate but also because of the great degree of heat utilization that can be obtained in such furnaces. The degree of heat utilization is to an extent of 80 – 90 % (Jaroslav and Zdenka, 1988). This is possible because the blast furnace uses a counter-current heat exchange in the bosh and shaft.

Even so, the blast furnace process faces many problems such as lower flexibility in production capacity, emission of air pollutants and high investment cost (Yusfin and Pashkov, 2002). A 3 Mt blast furnace, for example, emits about 4 Mt of CO₂ per year and one steel plant may consist up to five blast furnaces (Gielen, 2002). According to Gielen (2002), previous studies have concluded that removal of the carbon dioxide from the blast furnace could cost about 35US\$/t CO₂. Hot blast stoves also release dust, nitrogen oxides, sulphur dioxide and carbon monoxide (Lungen, 2001). Lungen (2001) reported that the costs for realizing all demands to ensure environmental protections amounts to about 20% of the overall capital outlay for a new blast furnace and the operating cost of pollution control facilities to up to 18% of the total hot metal costs. The reason that the blast furnace offers poor production flexibility is due to the fact that once a blast furnace has been lit, production must be maintained at nearly a uniform level for 10 years. This implies that production cannot be halted and then restarted (Sasaki, 1998).

The current major problem, however, encountered by the blast furnace is the decrease in supplies of coking coal. The coal required for coke production must have rather special properties and is not plentiful. Coking coals must have low ash in lump form (i.e. low silica, silicates and carbonaceous shale) and low levels of volatile components like oxygen and hydrogen (Orhan, 1997). This requires the burning of coal in coking ovens to burn off the volatiles, which is not environmentally friendly (IARC, 1998). There are limited reserves of coking coals, including South Africa, with many countries having no reserves at all (Yusfin and Pashkov, 2002). Research conducted by the Department of Mechanical Engineering, University of Cape Town (Anon, 2001) confirms that only approximately 2% of the large coal reserves in South Africa, i.e. 55 billion tons, are suitable for coke making.

Due to the lack of good coking coal within South Africa, and dwindling supplies worldwide, new iron making processes are being developed to use cheaper coal supplies. The processes that produce a molten product, similar to blast furnace hot metal, directly from ore are classified as direct smelting processes. Processes that produce iron by reduction of iron oxide below the melting point of the metal produced are generally classified as direct reduction processes and the products referred to as direct reduced iron (**DRI**) (Feinman, 1999). DRI is the product, which has high metallization degree, obtained by reducing iron bearing materials with natural gas or non-coking coal in a reducing unit. The product, which is porous, is also known as sponge iron (Narcin, et. al., 1995). In 2001, the worldwide production of DRI amounted to 39 Mt, which constituted 4% of the world iron production (Moore, 2001). Yusfin and Pashkov (2002) have projected that the production of DRI will reach 53 Mt in 2005.

Current processes obtain iron oxide from natural reserves. These include hematite (Fe_2O_3) as well as magnetite (Fe_3O_4) reserves. In 1996, world resources were estimated to exceed 800 billion tons of crude ore containing more than 230 billion tons of iron (Kirk, 1997). Research carried out by the Department of Mechanical Engineering, UCT, indicated that South Africa has an abundance of natural resources, which includes 5.9 billion tons of iron ore, giving South Africa the 8th largest reserve in the world. South

Africa, therefore, ranks amongst the leading iron-making countries (others include the industrialized European Countries, Japan and the US).

Although iron ore is the primary source of iron oxide the existing reserves need not be utilised at the current rate. Replacing part of the iron concentrates with recycled steel scrap, iron containing dust and metal machining scrap, can reduce the use of natural resources (Jyrki Heino, et al., 2000). It was reported by Kirk (1997) that in 1997 ferrous scrap constituted up to 7% of the worldwide blast furnace burden. In 2001, steel scrap also constituted 37%, i.e. 362 Mt, of the world iron production (Moore, 2001). In South Africa, Phalaborwa Mining Limited as well as Foskor Limited produce magnetite as a by-product. The magnetite is accumulated in stockpiles consisting of 190Mt and 35Mt dumps respectively (Minerals Bureau, 2001). Richards Bay I&T also produces a low-manganese pig-iron by-product, which is transported to the Steelworks and Iron Foundries. It is, therefore, evident that the waste scrap and mining by-products can be utilized as burden material for the direct reduction process. Magnetite was used in this study as the waste burden material due to the large supplies of it in South Africa as well as worldwide.

Presently most direct reduction processes employ an excess of coal, which is much higher than the required stoichiometric addition. These processes are also run at temperatures in excess of 1000°C, which is higher than necessary for direct reduction to proceed; with the minimum being around 850°C (Gilchrist, 1980).

Iron-ore fed in the form of pellets are a common and novel type of charge material, which improve the efficiency of pig iron and steel manufacture significantly. When pre-reduced pellets are used, most of iron oxides are reduced to metal, in this instance, in the form of sponge iron. Pre-reduced pellets consist of a metallised core encased in a partially reduced oxide shell (Sharma, 1997). The direct reduction process was therefore greatly affected by the development of pelletizing, since pellets with a suitable composition are excellent materials for reduction processes. In 1998 the World pellet production of iron

ore was around 220 Mtpa and new DRI projects required more than 20Mtpa of pellets (ACTED Consultants, 1999).

Nascimento, et al. (1998), have reported that an alternate way of charging the iron ore and the coal to the reduction reactor is to agglomerate them together, as pellets. This results in self reducing pellets. By using mixed pellets of ore and coal it is hoped that a lowering of traditional furnace temperatures, to say 900°C, in addition to allowing indirect reduction, will initialise direct reduction. This would reduce coal use (as the product of direct reduction is carbon monoxide used both as fuel and in indirect reduction) and should reduce residence time of material in the furnace.

In this process lignobond, which contains lignosulphonate, is used as the pellet binder. Lignosulphonates are complex polymers derived from the pulping industry. The wood from trees is composed mainly of three components – cellulose, hemicellulose and lignin. In the sulphite pulping process, the lignins are sulphonated so they become water-soluble and thus can be separated from the cellulose. The soluble lignins are called lignosulphonates. Lignosulphonates are extremely versatile and are used in a wide variety of industrial applications, for example, as binders, dispersants and emulsifiers in a host of products such as gypsum board, animal feed pellets, coal briquettes and micronutrient systems. When compared to a more common binder used for iron oxide pellets, namely bentonite, lignosulphonates have the advantage of increasing carbon levels, which could be used as reducing agents. Bentonite, on the other hand, is a plastic clay, which contains a variety of minerals in addition to montmorillonite (Anon, 2003). These minerals (which may include quartz, feldspar, calcite and gypsum) only serve to increase slag levels. An added advantage of using lignosulphonates is that they are environmentally friendly. Toxicological tests carried out at the Stanford Research Institute International in California have confirmed that lignosulphonates are non-toxic and not irritating, not mutagenic or genotoxic, and safely used in animal and human food contact products (Lignin Institute, 1991).

The project thus seeks to develop a lower temperature, clean, low cost process for iron-making using fine iron ore and fine coal. By using mixed pellets of magnetite and coal, with an environmentally friendly binder, i.e. lignobond, and manipulating the furnace atmosphere it is hoped that high temperature contact will initialise direct reduction. This will reduce coal use because the product of direct reduction is carbon monoxide used in indirect reduction.

Chapter 2: Literature survey

2.1. Direct Reduction of Pellets

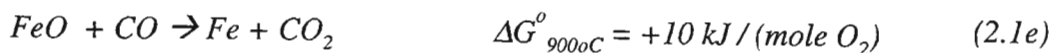
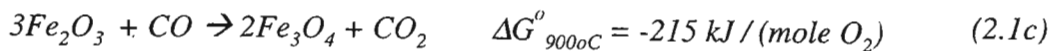
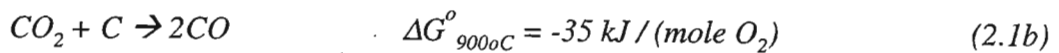
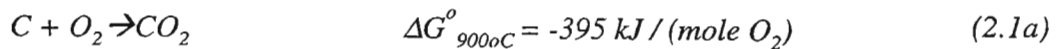
2.1.1 *Mechanism of Reduction of Iron Ore*

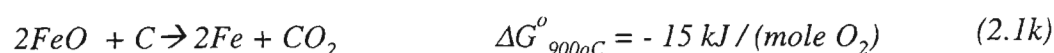
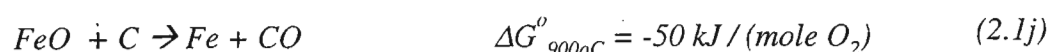
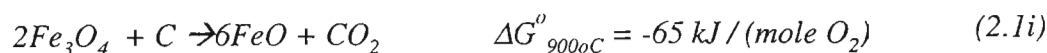
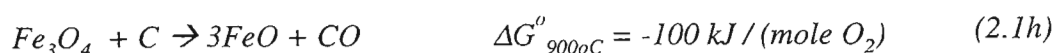
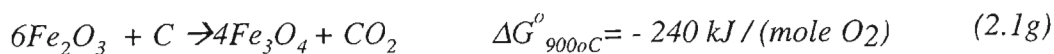
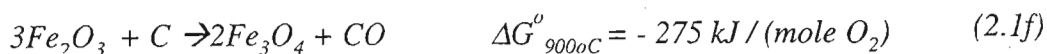
The factors that govern the mechanism of direct reduction of the iron oxides are the physical and chemical properties of the input iron oxide, the solid products that are formed, and conditions that exist during the reduction process (Gilchrist, 1980).

2.1.1.1 Direct and Indirect Reduction

Although the mechanism of Direct Reduction is considered in this study, Haque and Ray (1995) realised that it is doubtful if one can prevent indirect reduction completely. In fact they concluded from their experimentation that indirect reduction plays the major role in the reduction of iron oxide by coal. True direct reduction can only be studied when the gaseous products of reaction, namely, CO and CO₂, are removed from the system as soon as they are produced, which is quite doubtful.

During reduction of pellets, the following reactions may take place (Gilchrist, 1980):





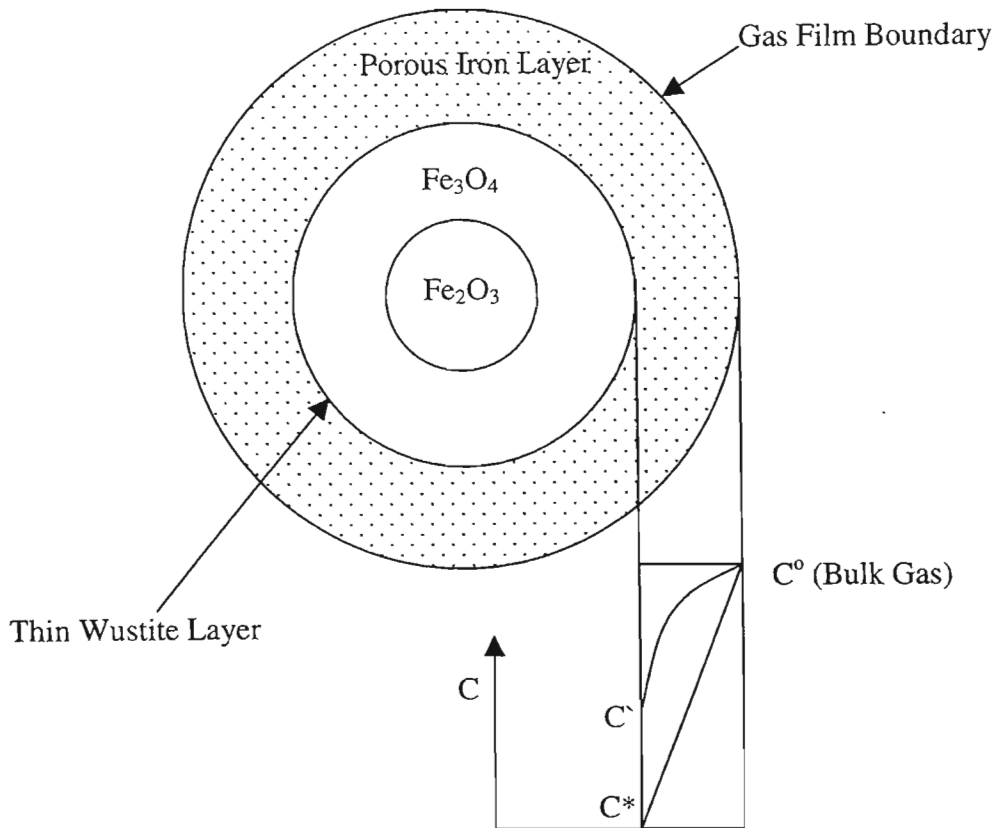
Reactions (2.1a) - (2.1e) depict indirect reduction due to the Carbon monoxide first being formed via the Boudouard reaction, i.e. 2.1a and 2.1b. The carbon monoxide then reduces the hematite to magnetite (2.1c), magnetite to wustite (2.1d) and then wustite to iron (2.1e). Reactions (2.2f) - (2.2k) depict direct reduction due to the Carbon reacting directly with iron ore. Reaction (2.1e) has an unfavourable free energy change at 900°C, implying that direct reduction is required for metal production, at a high P_{CO}/P_{CO_2} ratio.

It is evident that product gases evolved during direct reduction could be carbon dioxide, carbon monoxide or mixture of both. The carbon monoxide formed could then react indirectly with the iron oxide to produce iron. The Gibbs free energies that are included are obtained from Ellingham diagrams (Gilchrist, 1980) and serve to show that direct reduction should proceed effectively at 900°C.

2.1.1.2 Reaction Pathways in Pellet

In considering the reactions that occur during direct reduction (2.1(a) – 2.1(k)), Negri et al (1987), concluded from their comparison between one- and three-interface pellet models that one has to take into account the intermediate reduction steps (hematite → magnetite → wustite → iron). One-interface modeling implies an approach using global kinetics for the reduction of the iron oxide directly to iron, while three-interface model considers intermediate reduction steps found in the actual process.

The reduction sequence that a hematite pellet will undergo is given in the schematic below.



C^* = equilibrium concentration of CO at the given temperature
 C' = concentration of CO at the reaction interface

Fig. 2.1 Schematic diagram of the mode of gaseous reduction of a spherical sample of ferric oxide. Possible concentration gradients of the reducing gas across the iron layer are shown. (Biswas, 1981, fig. 2.5)

Metallographic examination of reduced iron oxide, comprising hard dense matter usually indicates a layered structure comprising a Fe_2O_3 core, surrounded by Fe_3O_4 , FeO , and finally Fe (as indicated in *Fig. 2.1*). In porous oxides, however, the reducing gas can penetrate faster than it can react at any oxide interface. Therefore, no distinct interfaces are observed, like the hard dense oxide, except a gradual transformation of Fe_2O_3 in the centre to Fe on the outside.

Hematite is generally reduced with a higher reaction rate than Magnetite. The rate of reduction is influenced by the stagnant boundary layer of gas that surrounds each oxide particle (the Nernst boundary layer). This factor is independent of the nature of the oxide but depends on the rate of flow of reducing gas past the oxide particle, i.e. it is a function of the design and operation of the apparatus used for reduction. Increasing the rate of flow of gas may eliminate the resistance of the boundary layer, but this way may not be economically feasible because unreacted gas will escape in the stack.

Fluidized Beds serve to eliminate the resistance of the boundary layer. In addition fluidised bed reactors offers the advantages of no feed agglomeration, uniform temperature in the reactor and excellent heat and mass transport. The reduction of iron oxide in a fluidised bed reactor proceeds through the following steps (Habermann et al, 2000; Strinivasan and Staffansson, 1990):

- i. Transport of gaseous reactants (CO) from the bubble phase of the fluidised bed into the emulsion phase.
- ii. Transport of the CO from the emulsion phase to the external surface of the iron ore particle.
- iii. Diffusion of the CO through the pores of the particle to the internal surface.
- iv. Chemical reaction between the CO and the unreacted oxide at the reaction interface and the generation of product gas.
- v. Diffusion of products (CO₂) from the pores of the particles to the external surface.
- vi. Transport of products from the external surface into the emulsion.
- vii. Transport of products from the emulsion phase into the bubble phase of the fluidised bed.

The reduction of iron ore particles proceeds through two phases with highly different rates of reduction. In the first, fast phase of reduction the rate is controlled by the transport of the reducing gas from the bubble phase of the fluidised bed to the iron ore particle and the transport of the product gas from the particle to the bubble phase. During the second, slow phase the rate of reduction is controlled by solid-state diffusion in the small grains of the iron ore particles.

It is evident that during direct reduction of iron oxide, using solid carbon as the reducing agent, steps i – iii do not play a major role. Although these are the fast phases of gaseous reduction and are not necessarily rate controlling, it would have no effect on the direct solid reduction process. If the product carbon monoxide is recycled, the reaction would then proceed via steps i – vii. This would only occur provided an inert atmosphere is used thereby partially fluidising the bed to allow the recycled CO to react with the oxide. If air at reaction temperature is used instead, carbon in coal will first form CO via Bourdard reaction (2.1a and 2.1b); thereafter reduction proceeds via steps i - vii.

Kang, et al (1996), concluded mechanisms for a coal and iron oxide system. Different mechanisms were concluded for a wustite/coal system compared to a hematite/coal system at temperatures of 1400°C.

For the wustite/coal system

- i. Combustion of coal
- ii. Melting of wustite and ash in char
- iii. Collision between particles
- iv. Agglomeration of molten wustite and unburnt carbon
- v. Direct reduction of molten wustite and unburnt carbon

For the hematite/coal system

- i. Combustion of coal

- ii. Thermal-decomposition of hematite into magnetite
- iii. Melting of magnetite and ash in char
- iv. Collision between particles
- v. Agglomeration of molten magnetite and unburnt carbon
- vi. Direct reduction of molten magnetite with unburnt carbon

It can be seen that this system is for the molten state reduction of magnetite or wustite. Seeing that such high temperatures are undesirable in this study, direct *solid* reduction of the magnetite or wustite is required instead of molten phase reduction. Direct solid reduction would therefore proceed via a combination of both steps (gaseous and solid), with direct solid reduction replacing molten phase reduction. A way of enhancing the direct reduction process would be to mix the coal and oxide as pellets. This would have the advantage of increasing the probability of contact between the different solid reagents. Reddy, et al (1991), reported that mixing the ore and coal (each having particle size less than 150 μ m) increases the rate of reaction.

2.1.1.3 Effect of Temperature on Iron Oxide Phases

Minimum temperatures required for direct reduction to proceed range between 800°C – 850°C. The reason that the current study is specific to temperatures in the range of 850°C - 900°C, is due to higher temperatures causes sintering and sticking of the iron ore (Weeda et al, 1990). This serves to show that current DRI processes run at higher temperatures than required; in the range of 1000°C – 1200°C (explained in greater detail in chapter 2.2). In addition, to maintain the higher temperatures, excess coal is used (much more than the stiochiometric addition) as the coal supplies the energy by combustion, in certain processes.

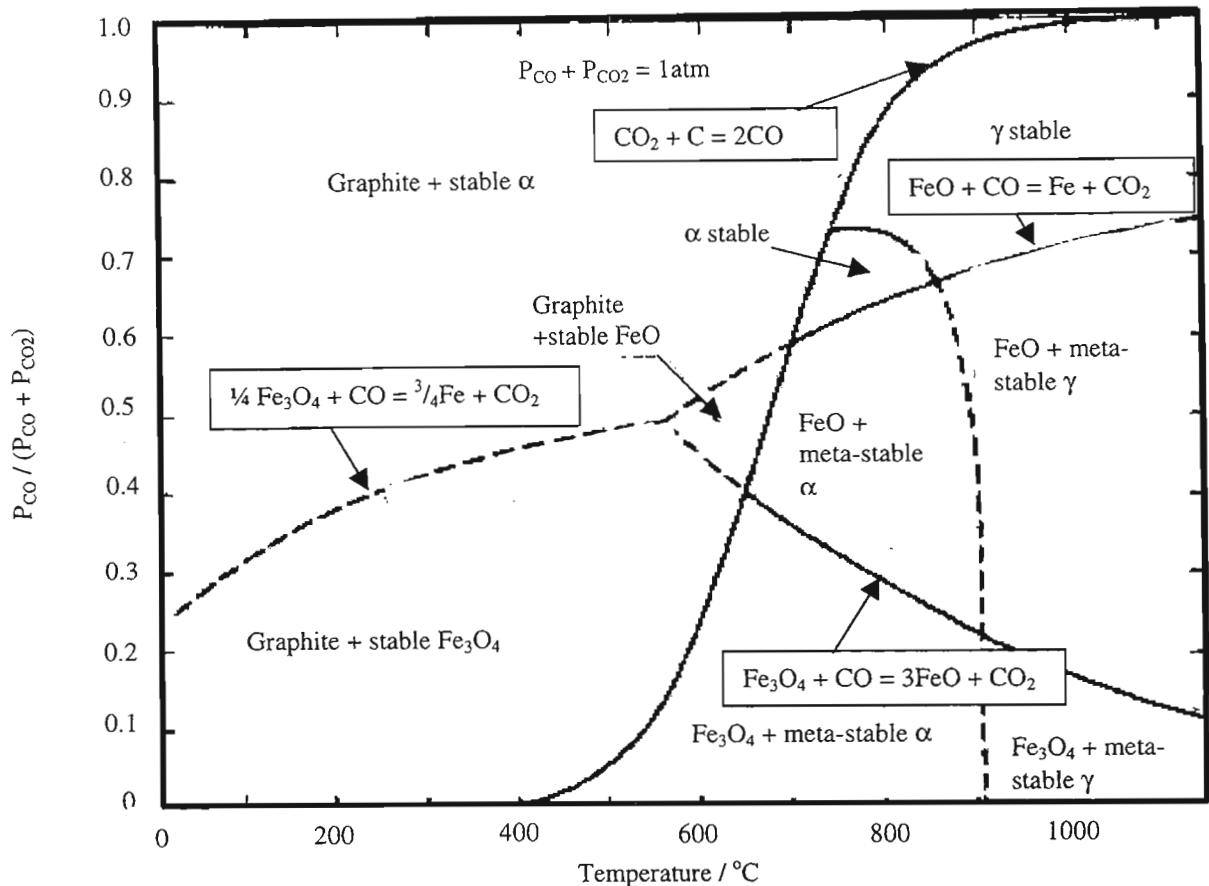
Complete reduction usually takes place between 950°C and 1000°C. Higher temperatures result in sintering of the particles, as mentioned above. At about 1200°C the presence of impurities causes a pasty porous mass to be formed. If reduction is carried out in the presence of carbon, the iron absorbs the carbon rapidly and the product begins to melt at

1300°C. Iron containing 4.5% carbon melts at 1125°C, which is far below the melting point of pure iron (1530°C) (Gilchrist, 1980). Swelling or shrinking may also accompany reduction of iron oxide. Swelling is due to the formation of whiskers, which in turn is related to the phenomena of nucleation and crystal growth. Shrinkage is due to the volume change when the oxide is reduced to metal as well as due to sintering. Both are influenced by impurities.

While investigating the mechanism of reduction, the phase changes of that the oxide undergoes at the different temperatures as well as different ratios of CO:CO₂, needs to also be noted. The changes can be observed from the Fe-O-C phase diagram shown in *graph 2.1*.

The different areas of stability of ferrite, austenite, wustite and magnetite can be seen. Ferrite or α -iron is a magnetic allotrope of iron and is stable below 906°C. γ -iron is the non-magnetic allotrope of iron that is the basis for austenite. γ -iron is stable between 906°C and 1403°C. Austenite is a non-magnetic solution of ferric carbide or carbon in iron and is used in making corrosion-resistant steel.

Graphite is used as the reducing agent in this case. The S-curve that is visible across the centre of the graph represents the Boudouard reaction.



Graph 2.1: Plot of $p_{CO}/(p_{CO} + p_{CO_2})$ versus temperature for pressure of 1 atm, showing areas of stability of ferrite, austenite, wustite, magnetite and graphite. (Esdaile and Motlagh, 1991)

In reduction processes, the presence of carbon drives the ratio of $p_{CO}/(p_{CO} + p_{CO_2})$ higher at higher temperatures. Therefore, if one concentrates on the region where $p_{CO}/(p_{CO} + p_{CO_2}) > 0.5$ and at a temperature around $900^{\circ}C$, the specified region indicates the stability of mainly α -iron, γ -iron and wustite. If the CO that is formed via direct reduction is recycled the pressure of CO will increase, resulting in more of the wustite reacting with CO to produce α -iron and γ -iron.

The experimental section of this study will, therefore, include reacting mixed coal and iron oxide pellets at temperatures around $900^{\circ}C$ in an induction furnace, with the product gases being recycled. Magnetite instead of hematite, which is not included in the phase

diagram, will be used as the iron oxide to be reduced. The metallic product should be in the region of stable α -iron and γ -iron.

2.1.2 Kinetic Rate Equations

2.1.2.1 Kinetics of Ore/Coal Systems

Reddy, et al (1991), proposed a kinetic rate equation for direct reduction of iron ore by non-coking coal in terms of molar concentrations of reactants, i.e. iron oxide and carbon in coal. The experimental procedure included isothermally reducing mixed iron ore-coal pellets (14mm) in a muffle furnace at five different temperatures ranging from 900 to 1100°C in 50°C increments. The crucibles, each containing one pellet, were taken from the furnace at regular intervals and the carbon left in the pellet was estimated.

It is evident that the kinetics expressed here will be, to a certain extent, representative of the kinetics of the current study. This is due to mixed ore-coal pellets also being used in the current study at temperatures around 900°C. The only difference is that Reddy, et al, use hematite as the iron oxide. However, from the mechanisms of reduction (Chapter 2.1.1), it is evident that magnetite follows a shorter reduction pathway to metallic iron as compared to hematite. The activation energies, therefore, obtained by Reddy, et al, can be a representation of the *maximum* time required for a specific conversion of magnetite to metallic iron.

The degree of reduction is calculated using the following equation,

$$\text{Degree of reduction, } \alpha = \frac{\text{weight of oxygen removed from iron ore}}{\text{Weight of removable oxygen}} \quad (2.1.1)$$

$$\begin{aligned} \text{Weight of oxygen removed} = & \text{total weight loss} - \text{weight loss due to volatile} \\ & \text{matter of coal} - \text{Weight loss due to} \\ & \text{combustion/gasification of fixed carbon} - \text{loss on} \\ & \text{ignition of iron ore} \end{aligned} \quad (2.1.2)$$

$$\begin{aligned} \text{Weight loss due to gasification of carbon} = & \text{total weight of fixed carbon in pellet} \\ & - \text{weight of carbon left in pellet} \\ & \text{after reduction} \end{aligned} \quad (2.1.3)$$

The reaction was assumed to be non-elementary and homogeneous therefore the following reaction was considered.



Rate Equation, assuming non-elementary homogenous reaction

$$-r_A = -dC_A/dt = kC_A C_B \quad (2.1.4)$$

where

$$C_A = \text{concentration of Fe}_2\text{O}_3, \text{ mol g}^{-1}$$

$$C_B = \text{concentration of carbon in coal (fixed carbon), mol g}^{-1}$$

$$-r_A = (\text{moles of Fe}_2\text{O}_3 \text{ disappearing}) / [(\text{unit time})(\text{unit weight})]$$

$$C_A = C_{A0} - C_{A0}X_A = C_{A0}(1 - X_A) \quad (2.1.5)$$

$$C_B = C_{B0} - C_{B0}X_B \quad (2.1.6)$$

$$C_{A0} = \text{initial concentration of Fe}_2\text{O}_3, \text{ mol g}^{-1}$$

$$C_{B0} = \text{initial concentration of carbon, mol g}^{-1}$$

$$X_A = \text{fractional conversion of Fe}_2\text{O}_3 = \% \text{ reduction}/100$$

$$X_B = \text{fractional conversion of carbon}$$

At any time, the amounts of Fe_2O_3 and carbon that have reacted are related, due to stoichiometry, as

$$1.5C_{A0}X_A = C_{B0}X_B \quad (2.1.7)$$

Substituting from equation (2.1.7) into equation (2.1.6)

$$\begin{aligned} C_B &= C_{B0} - 1.5C_{A0}X_A \\ &= C_{A0}(C_{B0}/C_{A0} - 1.5X_A) \\ &= C_{A0}(M - 1.5X_A) \end{aligned} \quad (2.1.8)$$

where

$$M = C_{B0}/C_{A0} \quad (\text{the ratio of initial concentrations of reactants})$$

Substituting from equations (2.1.8) and (2.1.5) into equation (2.1.4)

$$-r_A = -dC_A/dt = kC_{A0}^2(1 - X_A)(M - 1.5X_A) \quad (2.1.9)$$

Also from equation (2.2.18)

$$\begin{aligned} C_A &= C_{A0}(1 - X_A) \\ \Rightarrow -dC_A &= C_{A0}dX_A \end{aligned} \quad (2.1.10)$$

Therefore substituting equation (2.1.10) in (2.1.9) and rearranging gives

$$\int_0^{X_A} \frac{dX_A}{(1 - X_A)(M - 1.5X_A)} = C_{A0}k \int_0^t dt \quad (2.1.11)$$

Integrating gives

$$\frac{1}{C_{A0}(1.5 - M)} \ln \frac{M(1 - X_A)}{(M - 1.5X_A)} = kt \quad (2.1.12)$$

This equation is valid for $M > 1.5 X_A$.

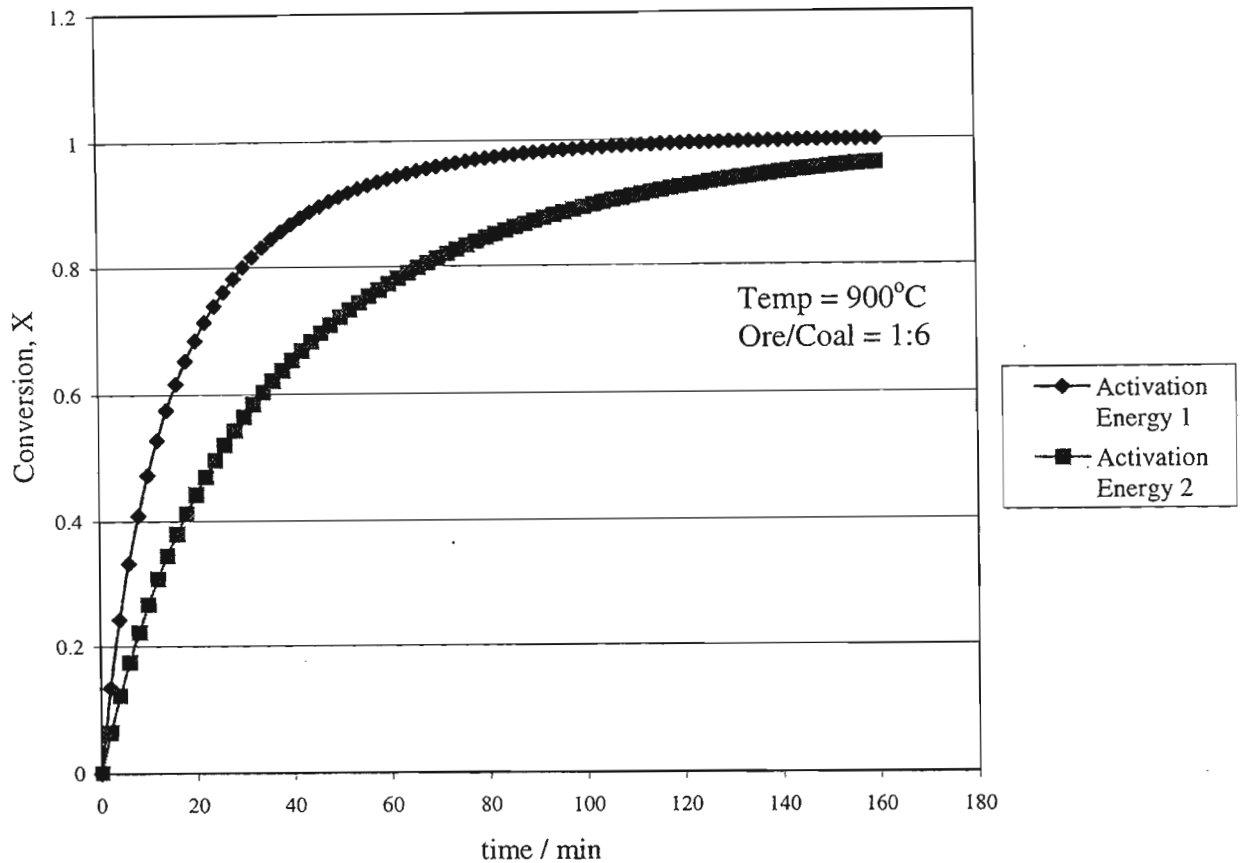
It can be seen that if the left hand side of equation (1.1.12) is plotted against reduction time a straight line should be obtained, the slope of which will be equivalent to the rate constant at the given temperature. This will valid only if the proposed equation represents the kinetics of reduction of iron ore by coal.

Results obtained showed that at each temperature the plot yielded a two part straight line, designated as k_1 and k_2 respectively. The slopes of $\ln k$ versus inverse temperature were determined to give activation energies of $E_1 = 108.15 \text{ kJ mol}^{-1}$ and $E_2 = 93.16 \text{ kJ mol}^{-1}$ respectively. The reason for the change in activation energies could be due to the fact in the reduction of iron ore by coal more than one parallel reaction takes place. In the initial stages one may dominate and as the reaction proceeds another reaction may become more dominant as the concentrations of intermediate products build up. Change in stoichiometry, due to formation of CO and also mass loss assumption, could be the cause of the change in stoichiometry. Reddy, et al concluded from the studies that the reduction by coal in a mixed system is not very temperature sensitive.

The reaction was also investigated at three more ratios of initial concentration of reactants. The proposed reaction was found to be valid in all cases. This implies that the direct reduction of iron ore by coal in a mixed system can be treated as a homogenous non-elementary reaction for the purpose of deriving a rate equation, though in fact the reaction may be heterogeneous.

Using the kinetics proposed by Reddy, et al for the system of concern in this study a conversion verses time graph can be plotted (see calculations in Appendix A). The conversions obtained for both the reported activation energies are plotted in *Graph 2.2*. The system of concern uses composite pellets of magnetite and coal mixed in a stoichiometric ratio.

Graph 2.2 Conversion of Magnetite to iron using Reddy et al (1991)
Kinetics



The above plot can be used to gauge the *minimum* time required to achieve a specific conversion of magnetite. This would therefore be useful in estimating the amount of magnetite converted to iron in an induction furnace operating at 900°C, after a certain length of time.

Sharma (1993), in a study that also included investigating composite pre-reduced pellets, used equation 2.1.1, i.e. degree of reduction (α), to obtain reduction kinetics for an ore coal mixture. It was concluded that the kinetic data fitted the first order reaction model,

$$-\ln(1 - \alpha) = kt \quad (2.1.13)$$

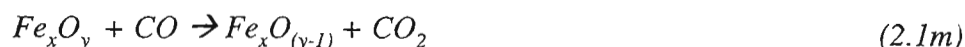
Sharma quoted an activation energy value of **68.52kJ/mol**.

Narscimento, et al. (1998) also investigated the reduction of agglomerated pellets, using wustite as the iron oxide, and quoted a reduction activation energy of **116kJ/mol**. This would represent the latter stage of the reduction process considered in this study due to wustite being used. In the case of Narscimento, et al., the activation energy is slightly higher due to the pellets being agglomerated in *stoichiometric* ratios of oxide and coal.

2.1.2.2 Kinetics of Fluidised Beds

To investigate the kinetics of iron ore reduction in a fluidised bed, Habermann, et al, (2000) set up a series of experiments so as to record the exhaust gas by FT-IR spectroscopy every 10 seconds, which detects all oxygen containing species.

The theory used to determine the rate of reduction proceeds as follows:



The number of oxygen atoms reduced from the iron ore by the above reaction can be evaluated by the following balance of the oxygen atoms:

$$O_{red} = O_{out} - O_{in} \quad (2.1.14)$$

Where

O_{red} = number of oxygen atoms reduced from the iron ore, mol

O_{out} = total number of oxygen atoms leaving the reactor in the form of H₂O, CO and CO₂, mol

O_{in} = total number of oxygen atoms entering the reactor, mol.

The actual rate of reduction is given by

$$dR/dt = O_{red,i} / (O_0 \cdot \Delta t) \quad (2.1.15)$$

Where

O_0 = total number of oxygen atoms initially present in the iron ore, mol

dR/dt = rate of reduction, l min⁻¹

Δt = time step.

The Fractional reduction can be obtained by:

$$R = \Delta O / O_0 \quad (2.1.16)$$

Where

R = Fractional reduction

ΔO = loss of oxygen, mol

ΔO is calculated by summarizing the number of oxygen atoms reduced from the iron ore (O_{red}) in each time step i :

$$\Delta O = \sum_{i=0}^t O_{red,i} \quad (2.1.17)$$

Thus the rate of reduction and the fractional reduction can be determined.

Habermann, et al (2000), concluded from the study that the rate of reduction increased strongly with decreasing sample weight. In this case silica sand was used as the excess weight. The rate of reduction increased with higher temperatures and higher molar flow of reducing gases, but was not affected by the absolute pressure in the reactor and small quantities of CH_4 in the reducing gas. Particles with a size of 0.5-4.0mm showed significantly lower rates of reduction than particles with a size between 0.125 and 0.5mm, but reached the same fractional reduction at the end of the reduction.

Haque, et al. (1991), in their study of fluidised Bed Reduction of iron ore fines by coal fines (fluidising medium being air) concluded that the kinetic data fitted equation (2.1.13). The degree of reduction (α) was calculated using the following equation,

$$\alpha = K [(\%Fe_T^{\tau} - \%Fe_T^i) / (\%Fe_T^{\tau} \cdot \%Fe_T^i)].100 \quad (2.1.18)$$

where

K = ratio of weight of iron to that of oxygen in the ore

$\%Fe_T^i$ = percentage of total iron in the initial ore

$\%Fe_T^r$ = percentage of total iron in the reduced mass.

The apparent activation energy value for the reduction reaction, which was estimated from the Arrhenius type plot (i.e. slope = $-E/R$), was found to be **155kJ/mol**. The value predicted is nearly half the value for the true CO₂ gasification of carbon by chemical reaction (**360kJ/mol**). It was, therefore, concluded that the reduction reaction is controlled by combination of carbon gasification and pore diffusion.

It should, however, be noted that Weeda, et al (1990) reported an activation energy of **250 kJ/mol** for the uncatalysed gasification of pure CO₂.

2.1.2.3 Thermogravimetric Methods to Calculate Reduction Kinetics

When analysing reaction kinetics via thermogravimetric methods, the studies of reduction of iron oxide by coal are complicated because the reduction of oxide and the oxidation of carbon both contribute towards the weight loss. Kinetics of reduction of ore-coal mixture is often described in terms of a pseudo-kinetic parameter ' f ', called the degree of the reaction. ' f ' is pseudo kinetic implying it is not proportional to the degree of oxygen removal, α . It should be noted however that, for a given ore-coal mixture there exists a relationship between the degree of reduction (α) and the fraction of reaction (f) (Anon, 1990). One can, therefore, plot a calibration curve between α and f using which one can undertake kinetic studies on the basis of weight loss measurement.

The theory required to develop a relationship between α and f proceeds by using the definitions of α and f .

$$\begin{aligned} \text{Degree of reduction, } \alpha &= \frac{\text{weight of oxygen removed in time } t}{\text{Weight of total removable oxygen, i.e. oxygen in iron oxides}} \\ &= \frac{\text{Oxygen removed}}{K_1 \cdot W_1} \end{aligned} \quad (2.1.19)$$

Where

K_1 = constant for a particular type of iron ore depending upon its chemical composition. It is defined as percent of oxygen (attached with iron only) in the ore. It is also assumed that other oxides present in the ore are not reducible.

W_1 = total weight of ore only

$$\text{Degree or fraction of reaction, } f = \frac{\text{Weight loss in time } t}{\text{Max. possible weight loss}} \quad (2.1.20)$$

$$\begin{aligned} \text{Or, } f &= \frac{\text{Oxygen removed from ore} + \text{Moisture, volatile matter and fixed carbon removed from coal}}{\text{Total oxygen in ore} + \text{Total moisture, volatile matter and fixed carbon in coal}} \\ &= \frac{\text{Oxygen removed from ore} + \text{Weight loss from coal}}{K_1 W_1 + K_2 W_2} \quad (2.1.21) \end{aligned}$$

Where

K_2 = constant (in %) for a particular type of coal, and is defined as percentage of moisture, volatile matter, and fixed carbon in coal

W_2 = total weight of coal in the mixture

From Equations (2.1.19) and (2.1.21)

$$\alpha = f [1 + (K_2 W_2 / K_1 W_1)] - \text{Weight loss from Coal} / (K_1 W_1) \quad (2.1.22)$$

From equation (2.1.22) it can be seen that there is no linear relationship between α and f unless the last term is negligible, e.g. low content of coal in ore-coal mixture. However, for a fixed ore-coal system, there should be a unique relationship between the two and one can use a calibration curve to obtain α values from f in a given system.

Swantantra and Hem (1990) employed the use of the variables α and f in their study to predict the reduction kinetics of iron ore under fluctuating temperature conditions. In the isothermal studies α was calculated using equation (2.1.18) and f was calculated using equation (2.1.20).

To evaluate the kinetic parameters of the reduction of iron ore by coal the fraction of reaction ' f ' and degree of reduction ' α ' were plotted against dimensionless time. Both the graphs showed the Ginstling-Brounshtein (G.B.) equation as the rate-determining model. The Ginstling-Brounshtein equation is applicable to reactions controlled by diffusion through a nonporous solid product (Habashi, 1969). Other models include the Jander Model and Spherical Symmetrical Model.

The Ginstling-Brounshtein Model is:

$$G(x) = 1 - \frac{2}{3}x - (1-x)^{2/3} \quad (2.1.23)$$

Where

$G(x)$ represents the G.B. Model

x represents the fraction reacted, i.e. f or α

The rate constants were determined from the G.B. plots and were fitted into an Arrhenius type plot. The activation values obtained were **90.9 kJ/mol** and **111.2 kJ/mol** for the f case and the α case respectively.

These activation energies were used as a comparative study of direct reduction of the mixed pellets in a thermobalance. (See Chapter 5)

2.1.3 Conclusion

From the mechanism of direct reduction it is evident that indirect reduction plays the major role in the reduction process. It is also apparent that stage reduction takes place, i.e. Hematite \rightarrow Magnetite \rightarrow Wustite \rightarrow Metallic Iron. Therefore when analysing for extent of reduction, all the different oxidative states of Iron have to be investigated. This can be done via X-Ray Diffraction, which gives a qualitative analysis of the pellet.

Most of the kinetic studies performed uses hematite as the iron ore. Due to magnetite following a shorter reduction pathway than hematite, the kinetic models obtained can be a representation of the minimum time required for a specific conversion. The models can therefore be used to approximate the time required for conversion of a set amount of magnetite in an induction furnace.

When one compares the activation energies of ore/coal systems to fluidised bed systems, it is evident that there is a significant decrease in activation energies. This could be attributed to the intimate contact between the ore and coal as well as a combination of direct and indirect reduction. Also finer particles increase the rate of reduction. Fluidised beds normally just have the reducing gas, viz. CO, H₂ or CH₄, passing through a bed of iron oxide. Some fluidised beds, however, have a bed of both ore and coal with the fluidising gas being air. This would induce the Boudouard reaction before actual reduction of the ore. In these fluidised beds the reaction is controlled by combination of carbon gasification and pore diffusion.

Reduction in an induction furnace having a bed of mixed iron oxide and coal pellets would incorporate both direct reduction between the oxide and coal, as well as a partial fluidised bed. The furnace provides external heat therefore high activation energies for combustion of coal would not be necessary. If air was used as the fluidising medium, this would correspond to fluidised beds mentioned above. Due to CO being a product, it could be recycled, together with the air, thereby enhancing the reduction process.

It can also be concluded that one can use weight loss of the pellet during reduction to evaluate kinetic parameters, i.e. activation energies, pre-exponential factors, etc. This is possible due to the fact that fraction of reaction ' f ' and degree of reduction ' α ' are related. ' f ' considers all reacting species, therefore it is a function of total weight loss of the pellet. ' α ' only considers only the reduction of iron oxide. Weight loss of mixed pellets can be recorded by using a thermobalance furnace.

2.2. Iron-Making Processes

2.2.1 *The Blast Furnace Operation*

The blast furnace is a counter current reactor in which the reducing gas is produced by coke gasification with the oxygen of the hot blast. The blast is injected via tuyeres in the lower part of the furnace. The reducing gas flows upwards, reducing the iron bearing materials charged at the top of the furnace (Lungen, 2001).

2.2.1.1 The Blast Furnace Set-up (Biswas, 1981)

A furnace is an apparatus used to conduct a reaction at high temperature. To prevent the loss of heat, it is usually lined with refractory bricks. In the design of a furnace, the method of heating is first taken into consideration. Consequently, provision is made for introducing the feed material, collecting the reaction products, measuring and controlling the temperature, as well as other auxiliaries. A furnace may be operated on a continuous or on a batch basis. The reactions may be gaseous, molten, or solid (Gilchrist, 1980).

A section of the blast furnace is shown in the *fig. 2.2*.

The cylindrical top portion is called the *throat* and below that the *stack* or *shaft* extends with increasing diameter up to the cylindrical belly or *bosh-parallel*. The furnace, thereafter, decreases in diameter, known as the *bosh*. The bosh connects with the bottom most portion, the hearth, where molten metal and slag accumulate.

The opening at the top is provided with a double bell for charging the burden, which has to travel downwards for more or less 25 metres in order to provide the ascending gases the opportunity to give up its sensible heat as well as to enable its reducing component CO (and H₂) to pre-reduce the iron oxides (indirect reduction). From the opening, the throat extends vertically downwards for a couple of metres or more. Thereafter, the stack

extends downwards to an extent of about 3/5 of the total height, its increasing diameter facilitating a uniform flow of the thermally expanding gases and burden materials.

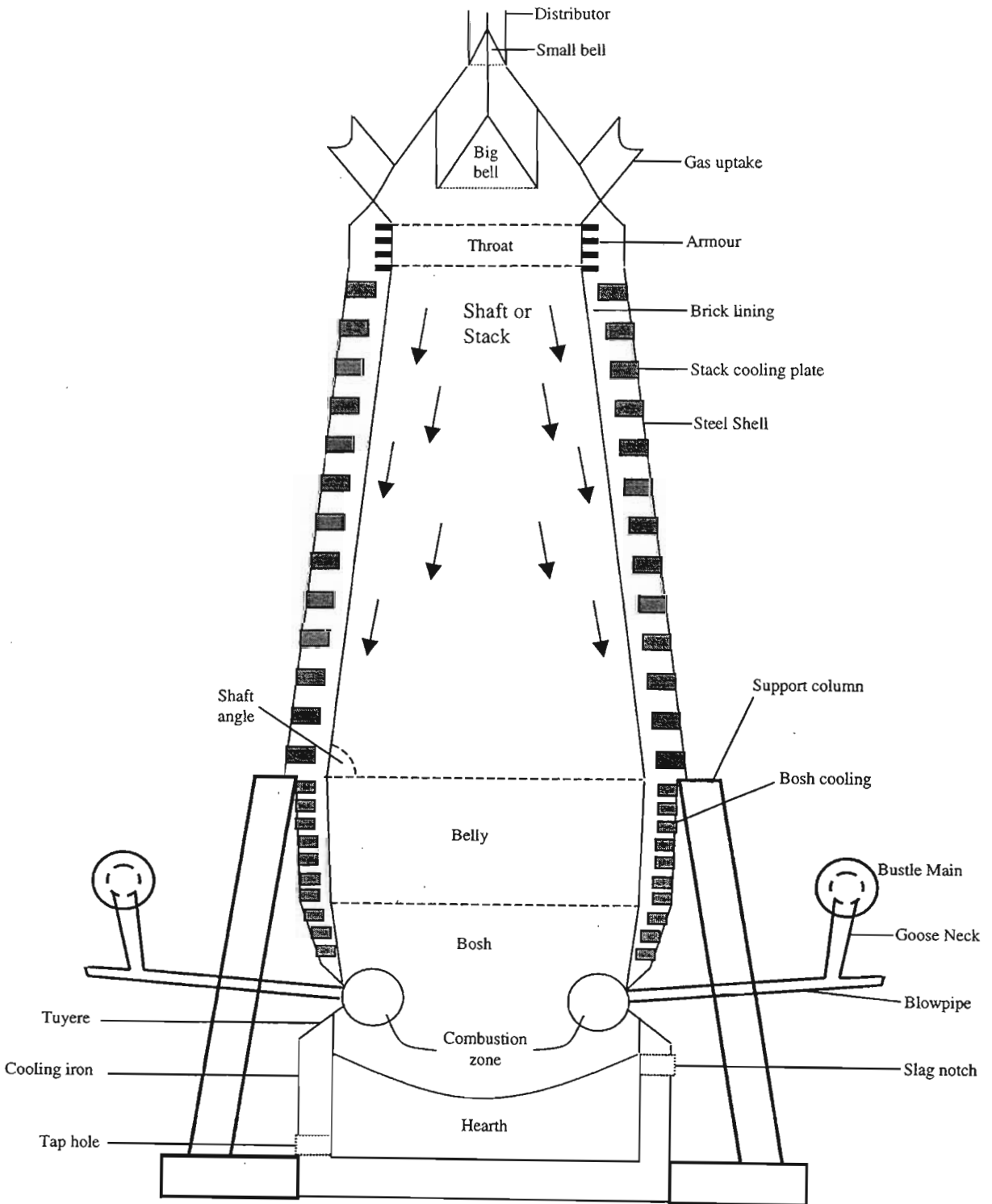


Fig. 2.2 Section of the Blast Furnace (Biswas, 1981)

The cylindrical belly has the largest diameter in the furnace and, normally, the fusion and consequent contraction of the slag and metal start in this region. The bosh has the shape of an inverted truncated cone, the base merging with the belly and the top with the top of the hearth. The blast is introduced through a series of equidistant water-cooled *tuyeres* around the hearth periphery about 40-60cm below its upper rim at a pressure of 1.5-2.5atm. gauge. The pressure used is to provide a jet of air which penetrates into the bed. The blast enters the hearth at a velocity of 150-300m/s.

The iron notch or *tap-hole* is situated about 50-150cm above the hearth bottom and the *slag notch* about 1m above the iron notch. The oxygen necessary for the burning of coke is supplied by air (blast). The cold blast from the turbo-blowers is carried through the hot regenerative stoves for preheating and subsequently distributed to the *tuyeres* from a *bustle pipe* or *ring main* around the furnace *goose-necks* and *blow pipes*.

At the top of the furnace there is a device for preventing the escape of the blast furnace gas as well as for proper distribution of the charge materials. The conventional furnace consists of a small and big bell; one remaining closed while the other discharges the materials on the big bell or into the furnace. The small bell rotates with a distribution hopper for delivering materials around the top of the large bell according to predetermined *charge cycle* or *sequence* and when the latter is full it is lowered to allow the materials to drop in the furnace. The materials or the stock or burden should be properly distributed for uniform distribution of the ascending gases. The distribution pattern at the top (stock-line) depends on the size and other physical characteristics of the materials as well as on the diameter and angle of the large bell of the materials from the large bell rim or *lip*.

The lining of the furnace consists usually of fire-clay bricks. The lower and hotter portions like the bosh and the belly should be lined with alumina-rich (40-50% alumina) high duty fire-clay bricks whereas in the upper stack they need only be resistant to abrasion. The thermally most susceptible portion is the hearth and its bottom which are lined with very high duty alumino-silicate or carbon bricks. The latter is highly

refractory but it is susceptible to attacks by low-carbon iron or oxidizers like ore and air. It is better to line the hearth base with a thick layer of carbon bricks with water or air cooling underneath. The life of the bricks is enhanced by cooling with water from the hearth to the top with the help of hearth bosh and stack cooling plates.

Figure 2.3 gives an indication of the temperature profile of the blast furnace. The gas isotherms shown in the figure were simulated using a blast furnace model proposed by Danloy, et al. (2002), which is in good agreement with industrial experience. The figure shown is for a specified charging pattern where the coke and ore are distributed in such a way to obtain a uniform distribution to gas flow.

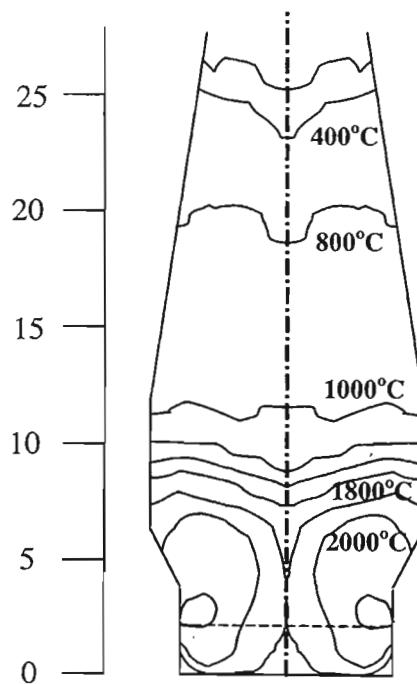


Fig. 2.3 *Simulated gas temperature map for typical Blast Furnace, (Danloy, et al.,2002), fig. 13.*

The hot blast of air entering through the tuyeres burns the coke carbon to CO_2 immediately in front of them. The intense heat produced gives a flame temperature (tuyere gas temperature) of $1800\text{--}2000^\circ\text{C}$, depending on the blast temperature. Since CO_2 is unstable in the presence of carbon above 1000°C , CO is produced according to

Boudouard Reaction (*Reaction 2.1a and 2.1b*). The tuyere gas, therefore, consists only of CO and nitrogen, their contents being about 35 and 65% respectively when dry blast is used. The coke does not fall continuously but only periodically into the tuyere zone from above. This reducing gas rises through the *active coke bed* to the bosh, belly and the shaft and reduces the iron oxides.

2.2.1.2 Role of Coke in the Blast Furnace

A typical analysis of the coke used in blast furnaces is given in *table 2.1*.

	%
C	90
SiO ₂	4.4
Fe	1.3
Mn	0.07
P	0.03
Al ₂ O ₃	2.8
CaO	0.3
MgO	0.2
S	0.9
H ₂ O	1.5

Coke generally plays a triple role in the blast furnace, i.e. physical, thermal and chemical role (Lungen, 2001).

I. Physical Role:

Due to reduction, softening and melting, ferrous materials change their chemical and physical properties when passing from the stock line to the hearth of the furnace. However, coke remains the only solid material below the melting zone of iron bearing

materials. The coke has to guarantee the furnace permeability in three parts of the furnace: for the furnace gas in the dry region above the cohesive zone, in the cohesive zone itself, and for gas and molten products in the hearth. The cohesive zone, where the softening and melting of iron bearing materials form impermeable layers, is separated by permeable coke layers or windows. The coke in the cohesive zone also forms a strong grid that supports part of the weight of the overlying burden.

II. Chemical Role:

The carbon needed for the production of reducing gases (CO) is supplied by the coke in the high temperature zone of the furnace. The carbon in coke also acts as a reductant for the direct reduction of iron oxides, including reduction of alloying elements like silicon and manganese. It is also responsible for the carburisation of the hot metal, which is necessary to reduce the melting temperature of iron.

III. Thermal Role:

The carbon of the coke and other possible carbon containing injectants supply approximately 80% of the heat required for the process. The remaining 20% is supplied by the hot blast.

It can therefore be evident that blast furnaces cannot be operated without coke. One has to only consider the physical reasons to reach this conclusion. On the other hand, coke is generally the most expensive charge material for blast furnaces. Therefore, an effort will always be made by blast furnace operators to try to reduce the coke consumption to the lowest possible technical levels. This is done by injecting coal, oil or other alternative reducing agents.

2.2.1.3 Other Raw materials and Products

- *Iron ores*

Iron ores are the most important raw material charged to blast furnace. High-grade ores contain 60 – 70% Fe, medium-grade 40 – 60% Fe, and low-grade < 40% Fe. The world's main supply of iron is obtained from ores containing hematite. Those containing magnetite supply only about 5% of the world's iron.

- *Limestone*

The function of limestone is to render the gangue in the ore and the ash of the coke easily fusible. The ash of the coke is mainly SiO₂ and Al₂O₃ that have high melting points. In the blast furnace, the limestone, which is used in pieces 5-10 cm in size, is decomposed starting at 800°C as follows:



- *Air*

Air for the blast furnace has to be preheated to 500°C - 1000°C and compressed to 200 – 300 kPa to burn the necessary amount of coke to furnish the required temperature for the reaction:



Air always contains a certain amount of moisture depending on the atmospheric humidity. Near the tuyeres, any moisture in the air will react with the coke as follows:



Since this reaction is endothermic, variation in atmospheric humidity greatly affects the balance of the furnace to such an extent that it would cause wide variation in the chemical composition of the iron produced. A unit could be installed to separate the moisture from the air by refrigeration before entering the furnace.

- *Pig iron*

The main product is pig iron, which is transferred in a molten state as hot metal or moulded in pig-machine. A typical analysis of pig iron is given in *table 2.2*. The hearth temperature influences the carbon content in pig iron.

Table 2.2: Typical Analysis of Pig Iron

	%
C	3.5 - 4.25
Si	~ 1.25
Mn	0.9 - 2.5
S	~ 0.04
P	0.06 - 3.00
Fe	~ 94

- *Slag*

Slag formed in the blast furnace serves to collect the impurities in the molten metal and to protect the metal from oxidation by the furnace atmosphere. About 1% of the slag containing about 60% Fe is recovered by magnetic separation and is returned to the blast furnace. Analysis of a typical blast furnace slag is given below.

Table 2.3: Typical Analysis of Blast Furnace Slag	%
SiO ₂	35
CaO	44
Al ₂ O ₃	15
MgO	3
FeO	1
MnO	1
S	1

- *Gas*

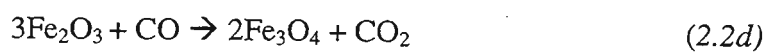
Gas coming out of the furnace top is more than that introduced at the bottom due to gasification of carbon. This is a result of excess coke being required to ensure that the conditions are sufficiently reducing so as to minimize the loss of iron to the slag as FeO. The coke reacts with CO₂ (Boudouard Reaction) forming CO. This reaction not only consumes coke but also consumes heat since it is endothermic. It is estimated that about 15 – 25% of the total fuel requirement is consumed in this manner. A typical analysis of the gas is given in the *table 2.4*.

Table 2.4: Typical analysis of Product Gas

	% Vol
CO	27
CO ₂	12
N ₂	60
H ₂	1
	100

- *Flue Dust*

Flue dust is composed of about 15% carbonaceous material, 15% gangue, and 70% Fe₂O₃ though only Fe₂O₃ may have been charged. The reason for this is the reaction at the top of the furnace:



Flue dust is collected as a mud in the venturi scrubbers and Cottrell precipitators. It contains about 40% solids.

Raw Materials	tons
Ore	1.7
Coke	0.5 - 0.65
Flux (Limestone)	0.25
Air	1.8 - 2.0
Products	
Pig Iron	1
Slag	0.2 - 0.4
Flue dust	0.05
Blast Furnace Gas	2.5 - 3.5

2.2.2 *Commercial Direct Reduction Processes*

Commercial Direct Reduction Processes that are in use today can be subdivided into gas-based processes, coal based processes and reduction smelting processes.

Some of the processes that are currently in operation can be seen below (Feinman, 1999).

Direct Reduction Processes – Gas Based Processes

- Shaft Processes
 - Midex
 - HYL Process
 - Danarex
- Fluidized Bed Processes
 - Fior/FINMET
 - Circored

Direct Reduction Processes – Coal Based Processes

- Rotary Kiln Processes
 - Krupp-CODIR
 - SL/RN
 - DRC
 - ACCAR/OSIL
- Shaft and Hearth Processes
 - Kinglor-Metor
 - Fastmet
 - INMETCO
- Fluidized Bed Processes
 - Circofer (Pilot Plant)

Reduction Smelting Processes

- COREX
- Direct Iron Ore Smelting (DIOS)
- HlSmelt
- Romelt

Some of the current processes shown in the tables above as well as some new processes will be reviewed in this chapter to give an indication of operating parameters.

2.2.2.1 Midrex Direct Reduction Process (Jones, 2001)

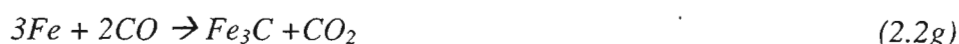
Gas based DRI processes are the world leaders when compared to carbon based DRI processes. Gas based processes share approximately 93% of the total DRI production, with in total 68% produced by the Midrex shaft furnaces (Lungen, 2001).

The Midrex Process, which has been proven at large scale, is based on shaft furnace processing with the feed being pelletised iron ore and natural gas (Cheeley, 1999). Midrex Direct Reduction Plants have processed iron oxide pellets and lump ores from over 50 sources around the world. Feed mixes have varied from 100 percent pellets to 100 percent lump ore, and numerous combinations.

In the Midrex Process reformed natural gas is used to reduce iron oxide pellets in a 60m high shaft furnace at 750°C. Gases leaving the furnace are first cooled and washed with water to remove the dust, then compressed before passing to the reformer where the following reactions take place:



The reformer is made up of special alloy tubes whose catalytic action makes the reforming reactions possible. The CO + H₂ mixture produced is first cooled before being injected in the lower part of the furnace. In the lower part of the furnace, the reduced pellets are gas cooled to 52°C. These pellets are porous and contain 0.8 to 1.4%C in the form of iron carbide, Fe₃C, as a result of the reaction:



Direct reduction is carried out continuously in a vertical shaft furnace. Iron oxide is fed to the top of the shaft, where it flows downward by gravity. It is discharged from the bottom in the form of direct reduced iron (DRI).

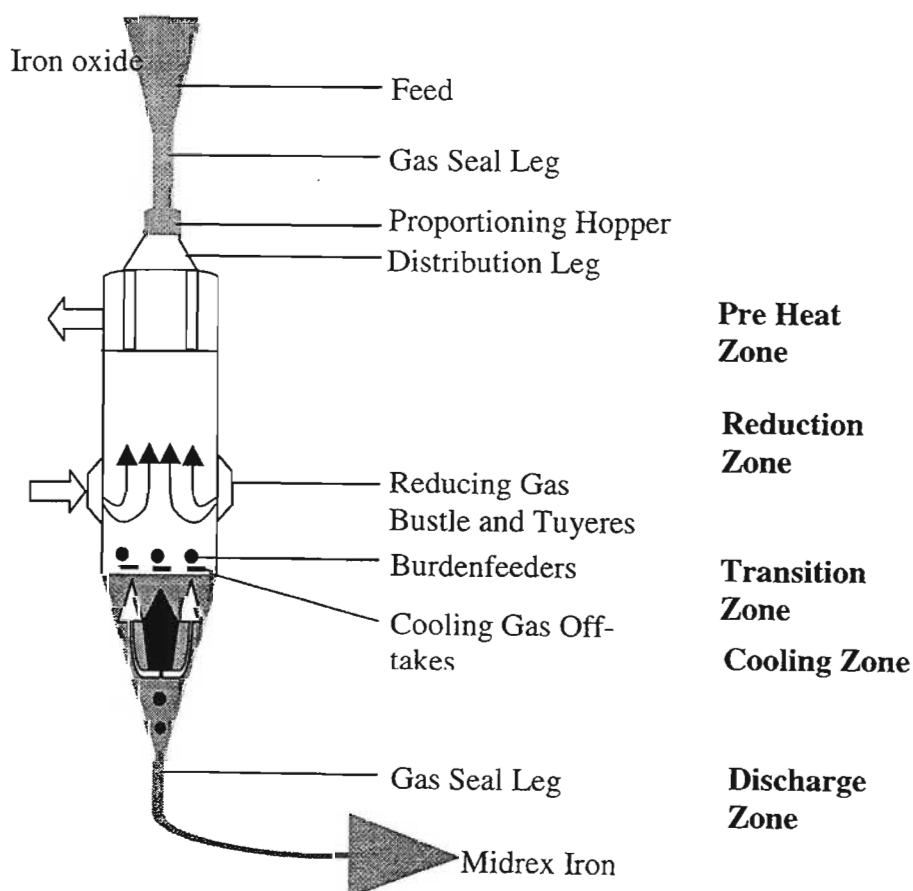


Fig 2.4 Shaft furnace detail (Cheeley, 1999)

The shaft furnace of a standard cold discharge plant has two independent zones. In the reduction zone, iron oxide is heated and reduced by hot counter flowing gas containing hydrogen and carbon monoxide, which is the reducing agent. In the cooling zone, a counter flowing gas cools the DRI and increases its carbon content.

2.2.2.2 Danarex Process (Martinis, et al., 2000)

The Danarex process was devised Danieli & Co.. The Danarex direct reduction process is characterized by process whereby the temperature of the reducing gas, with O₂ injection, is increased.

In the Danarex process, hematite is reduced to metallic iron by a reducing gas mix made up of CO, H₂ and CH₄. Fig. 2.5 shows the chemical reactions that occur in the Danarex reactor.

The overall reduction reactions are:



There is also a reduction given by the following reaction:



This reduction, which is part of the 'autoforming' reactions, occurs in the lower (wustite) zone). This reaction forms the basis for the increase in production given by the coupled reactions of reforming and reduction. Injecting a suitable amount of oxygen in the gas flow, which is responsible for partial combustion of CH₄, CO and H₂, develops the energy required for this endothermic reaction.

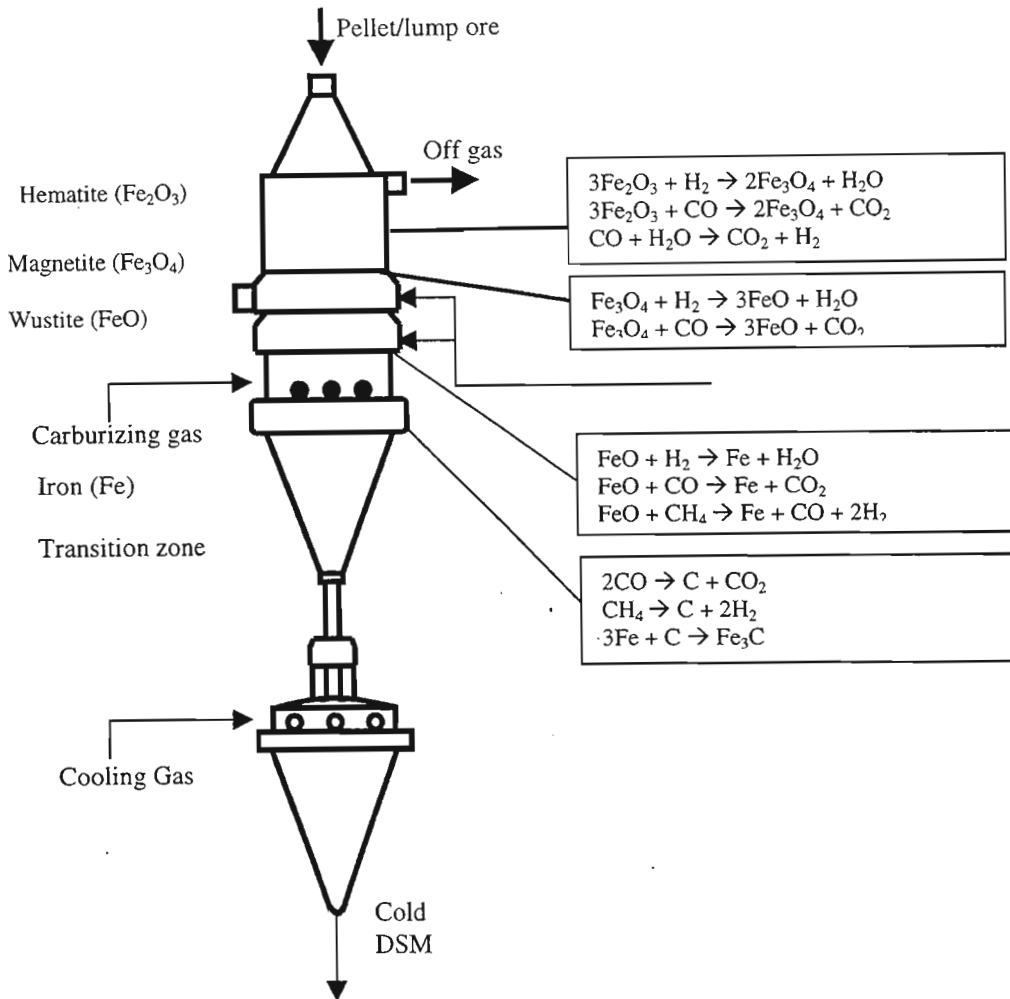


Fig 2.5 Chemical Reactions in the Danarex reactor (Matinis, et al., 2000)

Product carburation begins in the discharge cone through the following reactions:



The material remains in the reactor at 650 – 700°C for a suitable time so that the deposited carbon can fuse inside the iron matrix and form FeC, Fe₂C and finally Fe₃C. The Fe₃C layer makes the product stable, non-pyrophoric and easy to handle and store.

The high attainable metallization allows high metallic yield in the electric arc furnace, whilst the carbon content is calibrated to optimize the balance between chemical and electrical energy contribution. The oxide pellet and lump ore entering the furnace is coated with a solution of hydrated lime, bauxite or cement so as to make it possible to reach high temperatures in the reduction zone without any risk of sticking or clustering. Through the use of the autoreformer principle together with high reducing gas temperature decreases the time required to complete reduction, i.e. complete reduction occurs in less than three hours.

2.2.2.3 SL/RN Process (Jaroslaz and Zdenka, 1988)

The SL/RN process was devised by Lurgi in cooperation with the Steel Co. of Canada. The process deals with converting complex ferroginous raw materials into pre-reduced pellets.

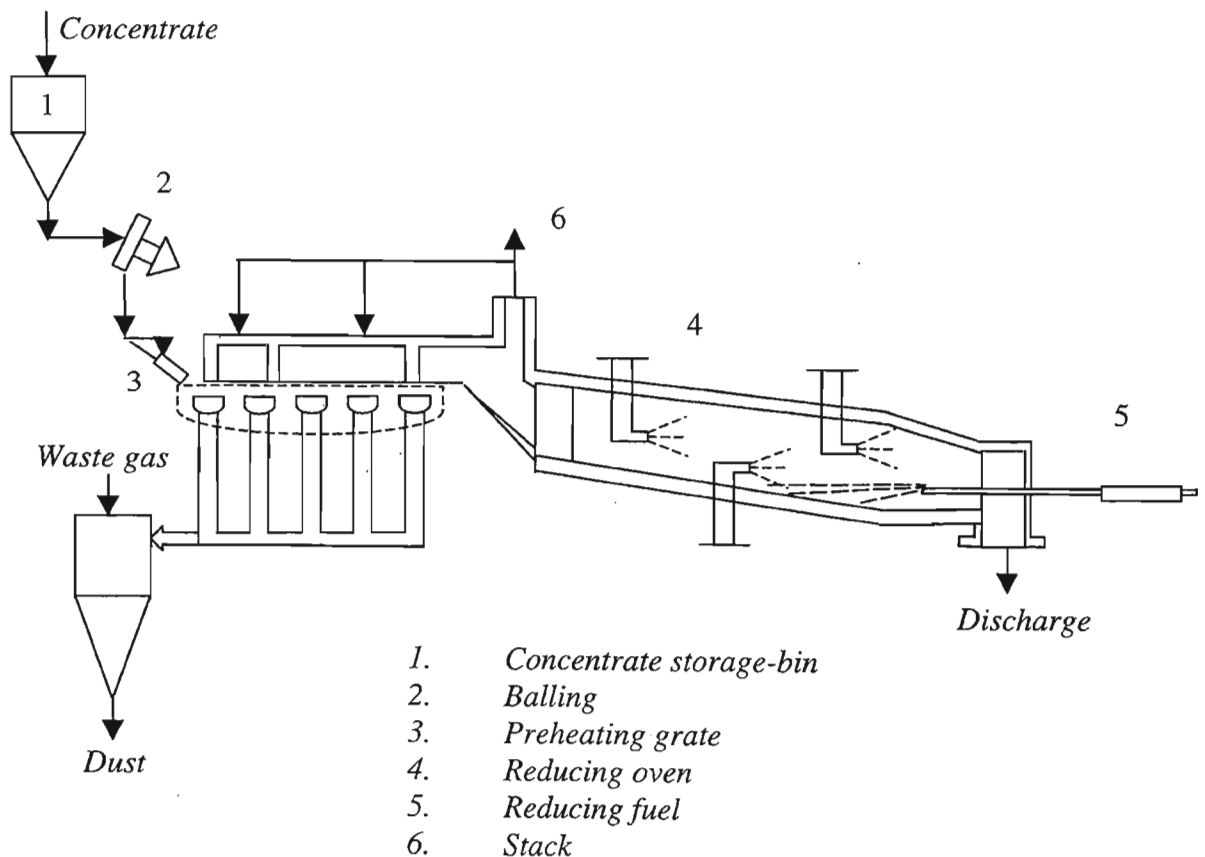


Fig. 2.6 The SL/RN process flow-sheet (Jaroslav and Zdenka, 1988)

The process flow consists of a rotary kiln, a cooling drum, a classifier and a magnetic separator. The kiln is fired at the discharge end by an axial gas or oil burner and auxiliary burners mounted coaxially in the kiln jacket at various intervals. The jacket can be partly or completely put on standby if a reductant high in volatile combustible matter is employed. The charge materials are pellets of 8 – 15mm and coke, anthracite or coal (<5mm sizes). The fuels are added as about 5% of the ore charge. The product is then cooled in a drum, screened in a 8mm screen, and magnetically separated. The pre-reduced pellets go straight to the blast furnace.

2.2.2.4 *Fastmet Process* (Fowkes, 1997; Tanaka, et al., 2002)

The Fastmet process, developed by the Midrex Corporation, is a direct coal based reduction process for producing iron from iron ore and scrap iron. The feed material includes oxide fines and/or steel mill wastes with the reductant being pulverized coal or other carbon bearing material, when necessary. The end product, DRI, can be hot briquetted, discharged as hot DRI into transfer containers, cooled if cold DRI is required, or directly charged to a melter (EIF) for production of ‘fast iron’. The process flow-sheet can be seen in *fig. 2.7*.

The coal and iron ore are ground to a pellet feed size (40 μ m) and then pelletizing the material together with a binder into spheres of diameter about 20mm. The pellets are then dried and fed into a rotary hearth furnace (RHF) in a single layer where reduction proceeds to completion at temperatures, hopefully, lower than the melting point of the feed and products. Gas, oil, or coal burners supply the heat for the furnace. Pellets are then removed and the furnace restocked.

In cases where steel mill wastes are the primary feed materials, the wastes can be briquetted and placed on the hearth in a single layer. Briquetting provides more flexibility in utilizing the waste materials, reduces much of the need for grinding feed materials and drying the green pellets.

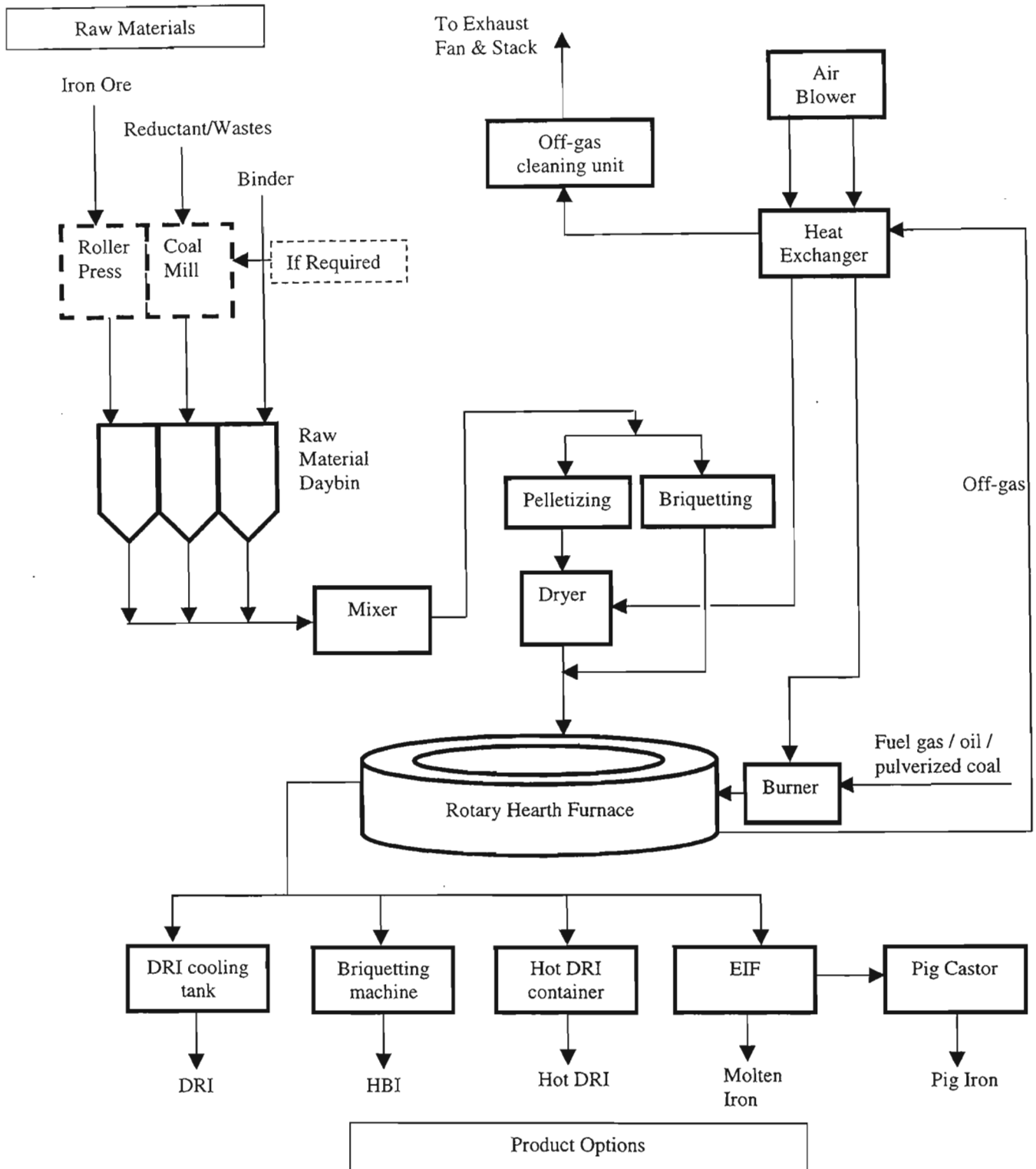


Fig. 2.7 Flowsheet of Fastmet Process (Tanaka, et al., 2002)

Reduction of the iron oxide occurs in the hearth, as it rotates. The flue gas leaving the RHF is fully combusted and partially quenched in the flue gas conditioner. Heat exchangers use thermal energy in the flue gas to preheat combustion air for the RHF burners. The flue gas is further cleaned in an SO₂ scrubber.

The chemistry occurring within pellets proceeds in essentially two stages:

1. CO being formed via bourdoudard reaction.
2. CO reducing hematite to magnetite, then magnetite to wustite, and finally wustite to iron. (See Reactions (2.1a) – (2.1k))

Blast furnaces, traditionally, have a reduction time of anything from 5 – 16 hours. The Fastmet process, on the other hand, has a reduction time of only about 6 – 12 minutes, depending on the feed material, with a 90 – 95% conversion. This is due to the more intimate contact between the reduction agents and iron ore in the pelletized material, the high reduction temperature and the high heat transfer rate.

The pellet mix used, i.e. 40% coal to 60% hematite, contains much more coal (by a factor of 5) than that required for stoichiometric conversion. It therefore seems unlikely that the availability of reducing gases limits the process.

2.2.2.5 Corex Process (Jones, 2001; Kawasaki Steel Foundation, 2001)

Corex, a smelting reduction process developed by the VAI group, produces hot metal of blast furnace quality, yet using non-coking coal as a direct reducing agent and energy source. The Corex process differs from the conventional blast furnace route in that the iron ore can be directly charged to the process in the form of lump ore or pellets, and the fact that non-coking coal is used. There is, therefore, no need for coke or coking plants. The Corex process flowsheet can be obtained from *fig. 2.8*.

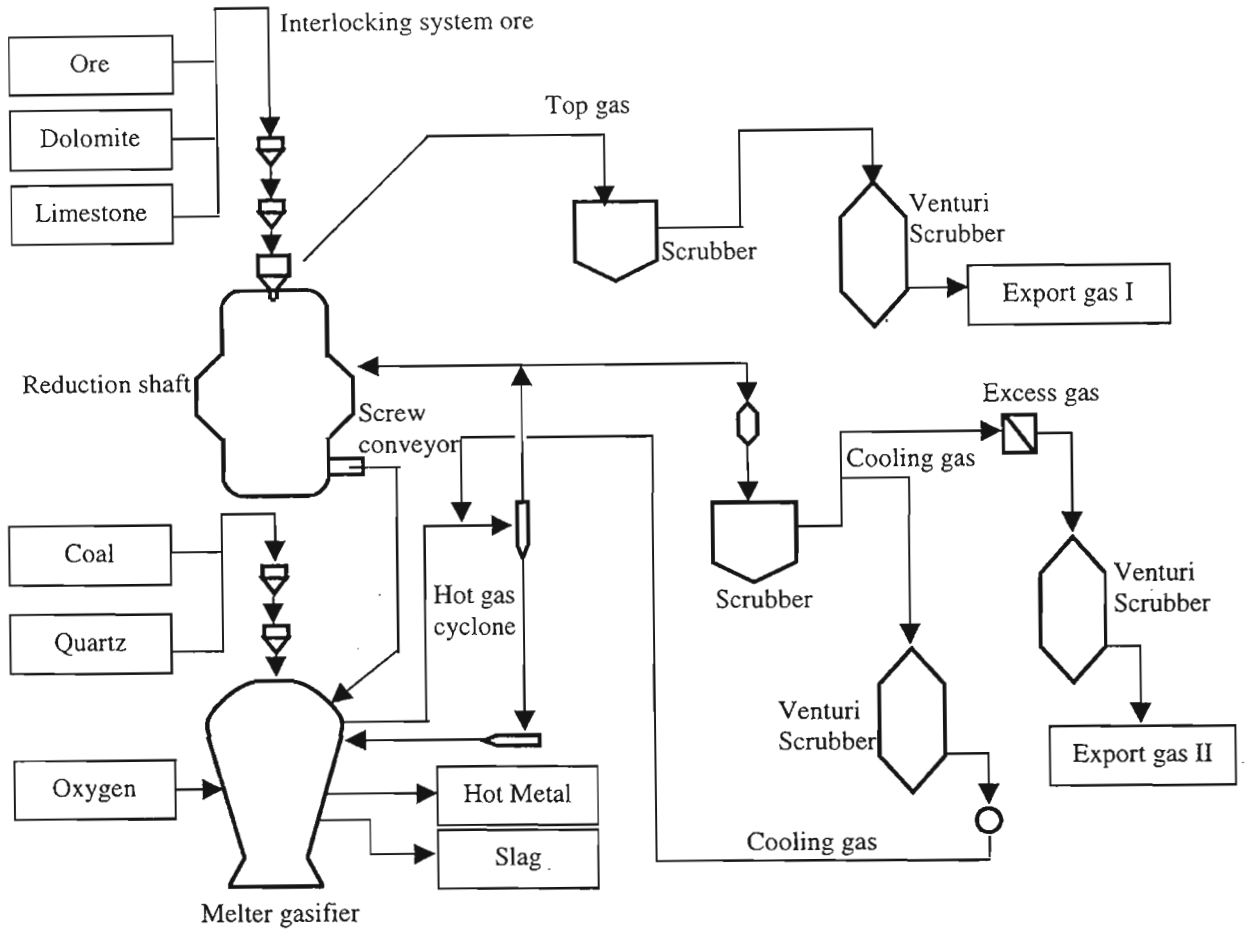


Fig. 2.8 Flowsheet of the Corex Process, (Kawasaki Steel, 2001)

In the Corex process, all metallurgical work is carried out in two separate process reactors, i.e. the reduction shaft and the melter gasifier.

Lump ore, sinter, pellets ore a mixture thereof are first charged to the reduction shaft via a lock hopper system where they are reduced to DRI. The gas required for reduction moves through in counterflow. Discharge screws convey the DRI from the reduction shaft into the melter gasifier where final reduction and melting takes place in addition to all other slag reactions.

Non-coking coal is directly charged into the melter gasifier via a lock hopper system. Due to the high temperatures sustained in the dome of the melter gasifier (in excess of

1000°C), the higher hydrocarbons released from the coal during devolatilization are immediately dissociated to carbon monoxide and hydrogen.

Undesirable by-products such as tars and phenols, etc., are destroyed and therefore cannot be released to the atmosphere. Combustion with oxygen injected into the melter gasifier results in the generation of a highly efficient reduction gas. The reduction gas exiting the melter gasifier mainly consists of CO and H₂ laden with fine coal, ash and iron dust. The dust is largely removed from the gas stream in a hot gas cyclone and is then recycled to the process. Through the addition of cooling gas the reduction gas temperature is adjusted to its optimum working range of 800 – 850°C. After leaving the hot gas cyclone the reduction gas is then blown into the reduction shaft via a bustle, reducing the iron ores in counterflow. The top gas is subsequently cooled and cleaned in a scrubber, after which it is available as a highly export gas which is suitable for a wide range of applications.

2.2.2.6 *The HIs melt Process* (Bates and Muir, 2000)

The HIs melt process converts iron ore to liquid pig iron through injection of non-coking coal and fine iron ore pellets into a molten iron bath. Because the process eliminates the need for sinter/pellet plants and coke ovens, HIs melt environmental impact is more favourable than traditional blast furnace technology.

The hearth of the HIs melt process consists of a vertical water-cooled Smelt Reduction Vessel (SRV) (see *Fig. 2.9*). The SRV, which has a refractory lined hearth and water-cooled panels, operates at a pressure around 100kPag. The metal is continuously tapped through a forehearth whilst the slag is batch tapped via a conventional water-cooled taphole. The metal temperature is easily controlled by the operator and can be varied depending on the requirement of the downstream BOF/EAF steelmaker.

In the HIs melt process the iron-bearing feeds and ground coal are reacted and smelted in the metal bath and not the slag (as occurs in some other processes). The solid feed materials including fluxes, are injected through water-cooled injection lances into the metal bath, which sits below the slag. This allows for very high reaction rates in the reduction of iron oxide and creates a large amount of turbulence in the bath. The carbon dissolved in the metal bath promotes the reduction of iron oxide, which results in the evolution of CO and H₂ from the bath.

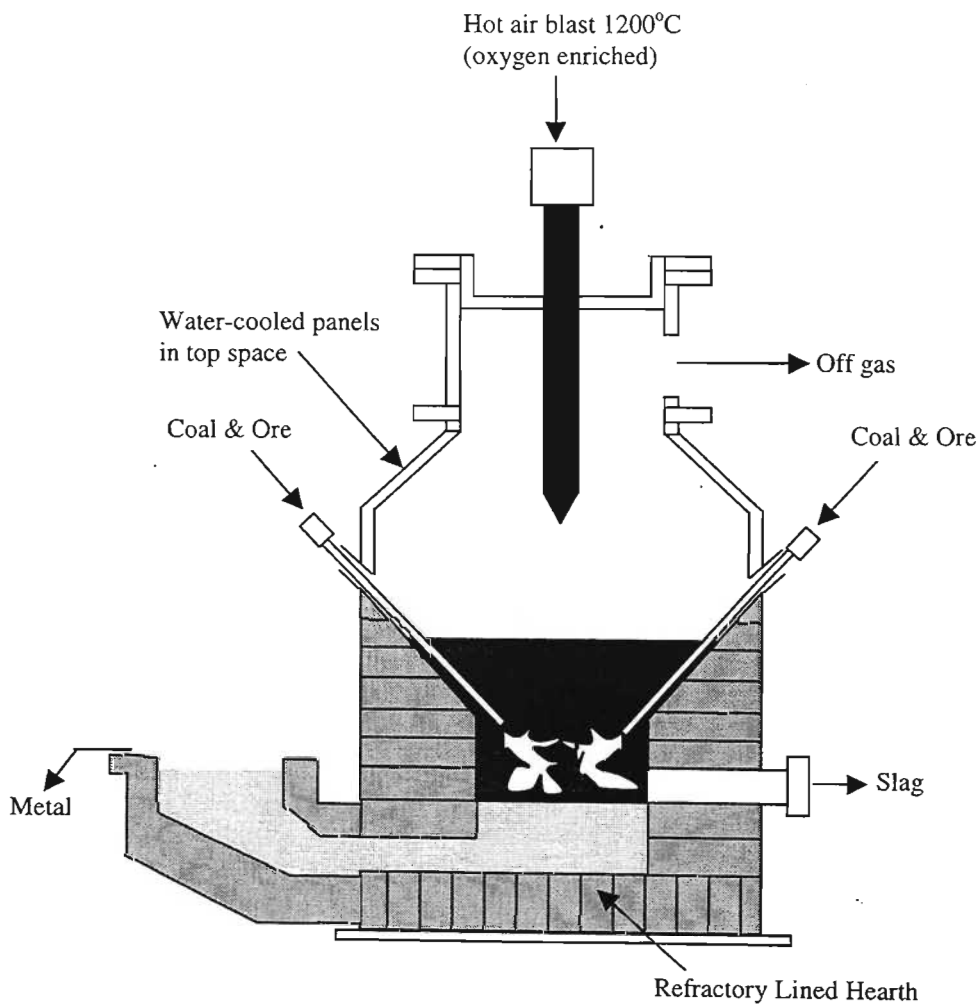


Fig. 2.9 *The Hismelt Smelt Reduction Vessel (SRV) (Bates and Muir, 2000)*

Preheated air at 1200°C, which may contain some oxygen enrichment, is injected through a water-cooled lance above the bath to 'post combust' the CO and H₂, coming from the

bath to CO₂ and H₂O. The significant amount of energy liberated can be used for smelting ore. The turbulent nature of the process has been found to be very effective at transferring this energy back to the metal bath, which greatly improves the efficiency of the process.

2.2.2.7 New Technologies

- The Comet Process (Munnix, et al., 1997)

The Comet process developed by CRM is an efficient coal-based direct reduction process. Fig. 2.10 shows a flow-sheet of the process.

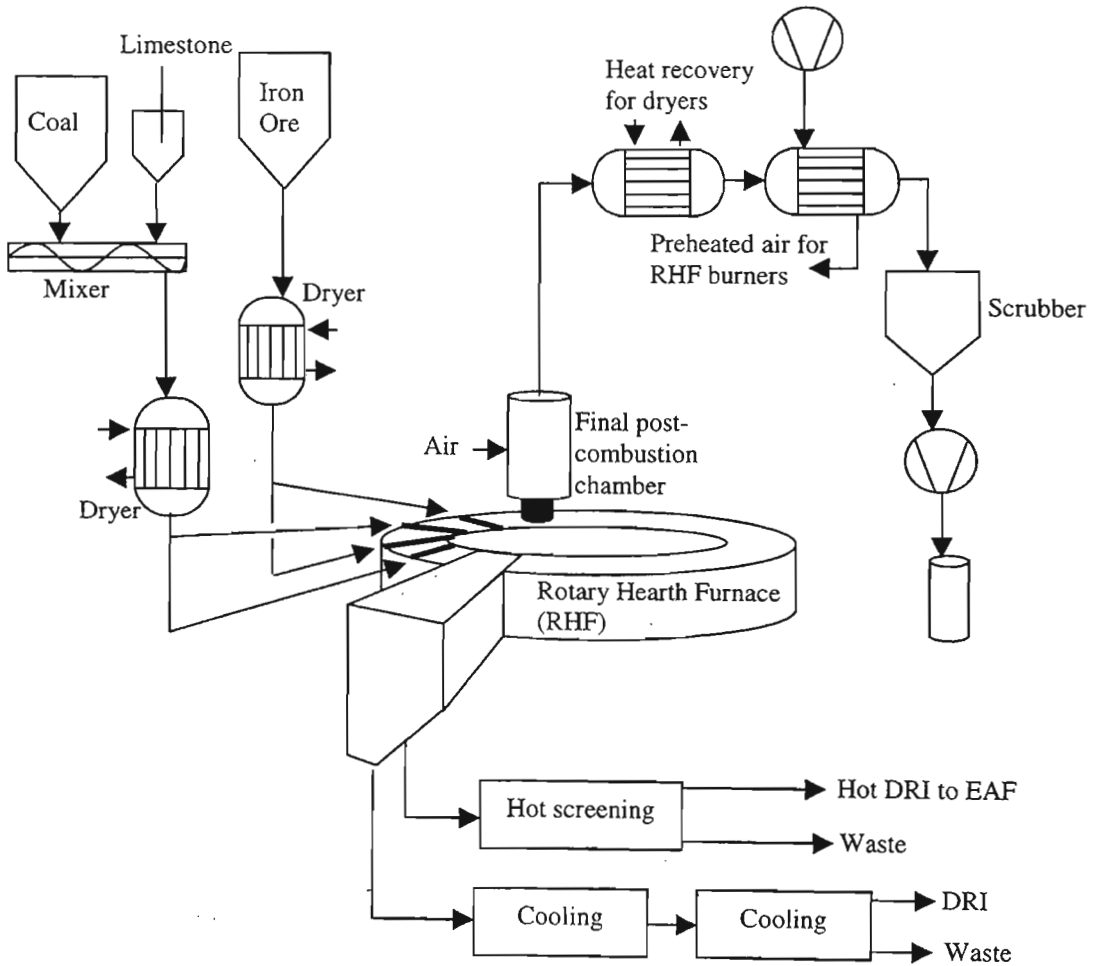


Fig. 2.10 Flow sheet of the Comet Process (Munnix, et al., 1997)

The basic equipment is a rotary hearth furnace, which moves inside an annular tunnel furnace and is continuously covered by alternate layers of crushed coal and iron ore fines. For desulphurizing purposes, the coal is mixed with a small amount of slaked lime or limestone.

Inside the furnace chamber, the temperature of the multi-layer bed is progressively increased from 25°C up to 1300°C. The raw materials first release their residual moisture and volatile matters. When the temperature is above 700°C, CO₂ and H₂O react with the carbon in the coal layers and generate the CO and H₂ required for reduction. The iron oxides are thus progressively reduced, from Fe₂O₃ to Fe₃O₄, then to FeO and finally to metallic iron. The sulphur released by the coal is fixed by the calcium, which is available in the reductant layers.

The heat required by the process is generated in the upper part of the furnace chamber, partly by fuel burners (using natural gas, coke oven gas, pulverized coal, etc.) and partly by preheated air injections in order to burn off the combustible gases released by the solids (volatile matters, excess CO and H₂).

The reduced iron layers at the exit of the furnace are sintered because of the high processing temperature. The residues of the reductant layers, however, remain powdery and are thus easy to separate by screening. The hot products are continuously discharged from the rotary hearth and can be handled in different ways, according to specific needs. One possibility is to cool down the products before screening while another possibility is to screen the products at high temperature and to charge the hot DRI into an electric arc furnace in order to take advantage of its heat content.

The off-gas flows counter-currently to the hearth rotation in the furnace and escapes through the chimney. In order to achieve total post combustion, additional air is injected into the exhaust gas. The sensible heat of the hot gas is then afterwards used in order to dry the raw materials and to preheat the combustion air for the rotary hearth furnace burners. After scrubbing, the waste gas is finally ejected at the stack.

Based on the laboratory results and on heat and mass balances of the Comet process, typical calculated consumption rates for the production of 1 ton of DRI are:

- 1 390 kg of Samarco pellet feed,
- 420 kg of Witbank coal,
- 8 kg limestone, and
- 2,8 GJ of fuel gas

A pilot installation with a design capacity of 100 kg DRI/h is in operation at CRM-Liege.

□ Direct Reduction of Metal Oxide Agglomerates (Innes, 1998)

This invention relates particularly to the production of metallic iron from iron oxides in the form of ores and partly reduced ores. Unlike the Midrex process, which reduces iron oxides in the form of pellets to metallic iron but is operated under conditions to avoid forming molten iron, this process operates deliberately under conditions to produce molten metal from the agglomerates. It should be noted however that solid reductants are used.

The method comprises passing gas at an elevated temperature through a bed of composite agglomerates that are formed from metal oxides and solid carbonaceous material and thereby reducing the metal oxides in the agglomerates to metal and melting the metal. Thereafter, the molten metal can be collected from the agglomerates.

The invention is based on the realization that composite agglomerates of metal oxides (such as iron oxide), carbonaceous material (such as coal), and flux material (such as lime or limestone) can be produced with suitable structural properties, e.g. porosity, strength and composition. This serves to enable the agglomerates to be formed into a bed of agglomerates, which results in an effective medium for the reduction of metal oxides in the agglomerates to metal and melting the metal in the presence of a gas at an elevated temperature. The term “elevated temperature” is understood to mean a temperature that is above the melting point of the metal formed by the reduction process. In the case of

iron oxides, the minimum elevated temperature is of the order of 1250/1300°C. The proportions of metal oxides, carbonaceous material, and flux should be 55%, 35%, and 10%, respectively, on a weight basis. It is also preferred that the agglomerates comprise a binder such as bentonite. The agglomerates should be in the form of pellets having a diameter in the range of 10 – 25 mm.

Fig. 2.11 illustrates one embodiment of the invention.

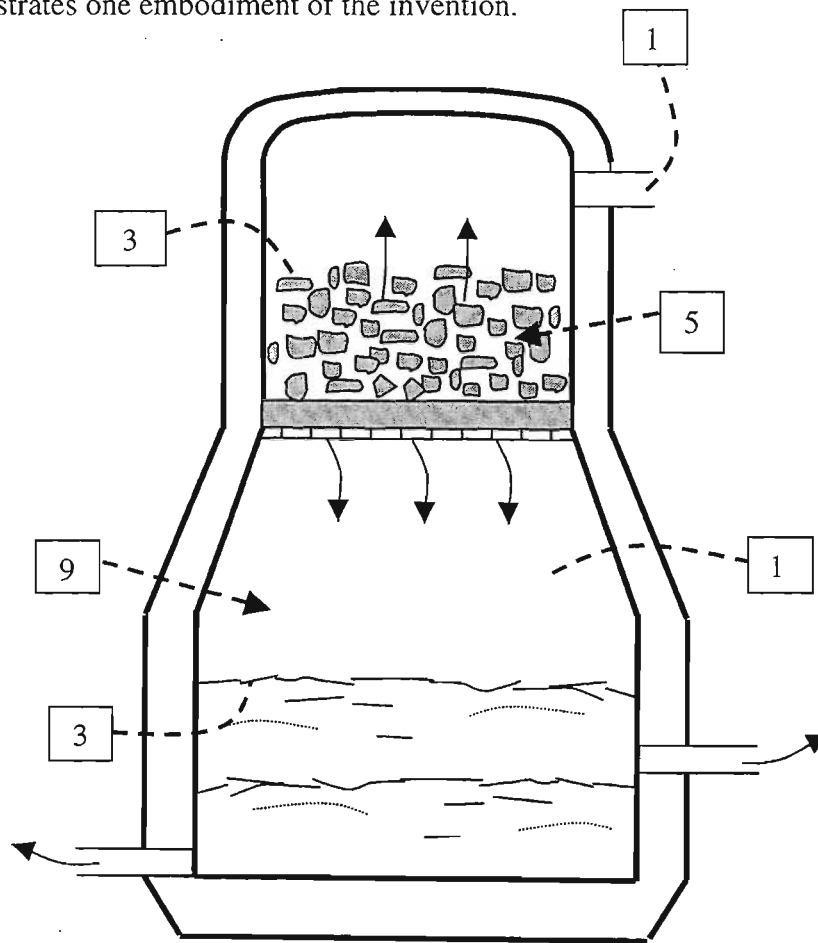


Fig. 2.11 *Apparatus for Direct Reduction of Metal Agglomerates (Innes, 1998)*

With reference to the above figure, agglomerates 3 of iron ore, soft coking coal, limestone/lime, and bentonite are supplied to a metallurgical vessel to form a packed bed 5 that is supported by means of a water cooled grid 7 above a bath 9 of molten iron and

slag in the vessel 11. In order to minimize the possibility of agglomerates falling through grid 7, a layer of pieces of ceramic material and/or coke that are larger than the agglomerates 3 may be positioned on 7. A suitable reducing gas (such as natural gas) and hot air injected into the space 13 in the vessel 11 that is between the molten bath 9 and grid 7. The hot air combusts a portion of the reducing gas and generates heat, which maintains metal and slag in the bath 9 in a molten state. A stream of off-gas at a temperature of the order of 1600°C flows upwardly from the gas space 13 through the grid 7 and in the bed 5 of agglomerates 3 to an off-gas outlet 15 in an upper section of the vessel 11. The off-gas is cooled to a temperature of the order of 800°C as it passes through the bed 5 of agglomerates 3. A portion of the off-gas is recycled to the gas space 13 between the bath 9 and grid 7.

The off-gas contacts the agglomerates with the result that:

- i. The coal reacts to provide a source of fuel and reductant;
- ii. The iron oxides are reduced by the off-gas and the reacted coal to metallic iron which then melts to form droplets; and
- iii. The limestone/lime reacts with impurities in the iron oxides to form a molten slag that coats the molten iron droplets and thereby inhibits oxidation of the iron.

2.2.2.8 Overview of Iron-making Processes

Table 2.6 gives an overview of the different process parameters.

If one considers the Gas-Based processes, the temperatures are quite low but the natural gas consumption is considerably high.

The coal based processes, which is of greater concern in this study, show much higher temperatures. The Fastmet Process, for instance operates at about 400°C above normal reduction temperatures (900°C). The coal consumption is also higher than normal

(0.23tCarbon / tFe, stoichiometry). The Circofer process, on the other hand, runs at temperatures of about 800 – 900°C but the addition of coal is almost 4 times excess than required.

The Smelting processes show a considerable excess of coal used, ranging from 3 to 5 times the stoichiometric addition, due mainly to the need for exothermic reaction with air or oxygen. A higher temperature is obviously required to reach the melting point of Fe.

Table 2.6: Process Parameters

Process	Metallization Ratio	Production rate	Temperature °C	Iron Ore	Coal Consumption	Natural Gas Consumption	Calorific Consumption ^(b)
Blast Furnaces ^(a)	> 90%	1.9 Mt HM / a	800 - 2000		0.6 t Coke / t HM		17.88 GJ / t HM ^(c)
Gas based processes							
Midrex	92 - 95%		750	1.45 t / tDRI		10.13 GJ / t DRI	10.13 GJ / t DRI
HyL	92 - 95%			1.45 t / tDRI		9.34 GJ / t DRI	9.34 GJ / t DRI
Danarex	92 - 94%	90 - 110 tDRI / h	650 - 860			290 m ³ / t DRI	11.54 GJ / t DRI
FINMET	92 - 95%	500 000 tDRI / a	550 - 800	1.55 t / tDRI		12.56 GJ / t DRI	12.56 GJ / t DRI
Circored	92 - 93%	500 000 tHBI / a	630	1.42 t / tHBI		11.72 GJ / t HBI	11.72 GJ / t HBI
Coal based processes							
Fastmet	92%	450 000 tDRI / a	1250 - 1350	1.34 t / tDRI	0.38 t / t DRI	80 -90 Nm ³ / t DRI	15.13 GJ / t DRI
Circofer (Pilot)	92 - 93%	500 000 tHBI / a	800 - 900	1.42 t / tHBI	0.8 t / t HBI		24.72 GJ / t HBI
Direct Smelting processes							
Corex		60 000 - 1 100 000 tHM / a	Above 1000	1.48 t / tHM	0.98 t / tHM		30.28 GJ / t HM
DIOS		500 tHM / day	800	1.485 t / tHM	1 t / tHM		30.90 GJ / t HM
HISmelt		100 000 tHM / a	850	1.54 t / tHM	0.63 t / tHM	22 Nm ³ / tHM	20.34 GJ / t HM
Romelt		50 000 tHM / a	1500 - 1800	1.6 t / tHM	1.1 t / tHM		33.99 GJ / t HM

a) Blast Furnace production rate reported by Lungen (2001) for average production per furnace, per year in 2000.

b) Calorific values for natural gas, coal and coke obtained from Anon (2001), "Estimated average gross calorific values of fuels in 2001".

c) Calorific value quoted does not include energy required for heating blast air to 2000°C.

2.2.3 Conclusion

It is evident that most industrial processes are either run at extremely high temperatures or require excess amounts of coal. Some processes require a combination of both. In addition, all the processes make use of iron ore, while the waste iron oxides from the steel industry are being stockpiled. This determines the cost of pig iron, which is the raw material of the steel industry. If one considers the use of coke as the reducing agent, this leads to environmental factors as well.

One way of reducing costs would be to consider a direct reduction process that reduces iron oxide fines (in this case magnetite), which can be obtained as by-products from mining industries as well as steel mill wastes. The magnetite can be fed as mixed pellets with the reducing agent being waste coal. Flotation of the coal would also be beneficial, as this would reduce the ash content of the coal, resulting in a cleaner process. This eliminates the need for coke as well as coking plants.

The pellet mix should allow for a more intimate contact between the oxide and coal. The pellet would consist of stoichiometric ratios of oxide and coal. If an induction furnace is used and run at temperatures around 900°C, the coal consumption would be reduced because coal would not be needed as fuel but purely as a reductant. The induction furnace has the added advantage of rapid heating times

The product pellets, which may still contain trace amounts of magnetite and coal (probably wustite as well), can be used as pre-reduced pellets for further processing. These pre-reduced pellets can be used as feed material for the blast furnace to produce pig iron. This would resemble the Corex process, which operates in two stages, viz. pre-reduction of lump ores and pellets in a shaft furnace followed by final reduction and melting to hot metal and slag in a melter gasifier unit. The process considered above would represent the former stage of the Corex process. The second stage would only be necessary for finalising reduction and melting the pre-reduced pellets to hot metal. This would considerably decrease the addition of reducing agents due to most of the pellet

already being reduced. Slag formation would also decrease, as the coal in the mixed pellet would have been floated.

The conditions that one can aim for to incorporate a more efficient pre-reduction process are listed as follows:

- Use of waste coal and mining by-products, i.e. magnetite.
- Flotation of coal to reduce ash content, thereby reducing slag formation.
- Mixing of pellet in stoichiometric ratios of magnetite and coal.
- Decrease in reduction temperature to 900°C.
- Use of induction furnace as heating apparatus.
- Use of product gas, CO, as a reducing agent.

Chapter 3: Pelletization

3.1. Pelletization Theory

The basic technological process whereby fines are transformed into agglomerates is termed balling. The wet agglomerates that are formed are known as green balls. In pelletizing, these agglomerates serve as an input material for further processing such as hardening by drying or firing. The pellets must therefore be of good quality to be acceptable for the requirements of the process technologies.

In theory (Jaroslav and Zdenka, 1988), when a fine-grained raw material is moisturized, a thin liquid film develops on the surface of each grain. Bridges are then formed at points where the moisturized particles contact each other. As shown in the figure below, the particles are rotated into balls and bonding forces develop gradually in the ball.

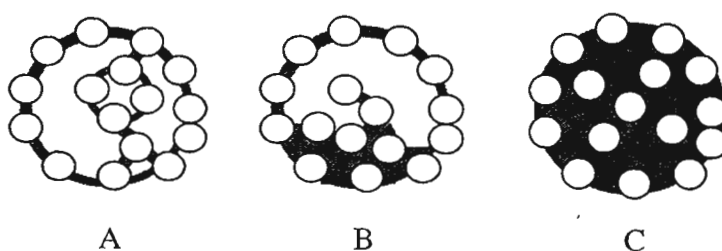


Fig. 3.1. Mechanism of ball formation (Jaroslav and Zdenka, 1988)

The initial bonding between the particles does not possess sufficient strength because it is actually a water-bridge or meniscus, *fig. 3.1A*. The addition of more liquid causes the liquid films on the particle surface to coalesce, although closed air-filled cavities remain between the grains, *fig. 3.1B*. A nucleus is formed and the ball grows as more moisturized particles are coated onto the nucleus. The bumping of the balls against each other and against the walls of the pelletizer produce mechanical forces, which expel the air enveloped in the balls, *fig 3.1C*. The liquid fills the free space between the particles.

In the balling process the material particles are moved by rotation, moisturized, and agglomerated into round balls. There are two phases of balling, which is a continuous process, viz. (i) formation of nuclei, and (ii) ball growth. Capillary forces are predominant in the first phase; as the balls grow, forces due to motion take over.

The nuclei begin to form when the material is sprayed with a liquid, which wets the particles not quite uniformly. The underlying factor for the nucleus to form is the degree to which the particles are moisturized. This in turn depends on whether the liquid droplet randomly hits a particle as it is rotated in the balling device. Frequent collisions of particles and droplets produce a variety of combinations of bonding. A weak nucleus may be destroyed by the incoming impacts and the disintegrated particles go on to produce a new nucleus elsewhere.

Ball growth is a stage in which the particles envelop the nucleus. The simultaneous rotation and frequent collisions and impacts make the growing ball compact thus causing the ball to assume a regular globular shape.

Mechanical properties of the pellet such as resistance to abrasion, good compression strength, and shatter strength are essential for good ball properties. This is due to the fact that balls undergo considerable mechanical loading during shipping, storage, drying and high temperature hardening. The properties will differ for balls that are a final product and for balls intended for further processing. Pellets intended to constitute a portion of a blast furnace burden are made in equipment, which is able to impart suitable green balls, i.e. balls that are still wet and have not been processed further.

Granulometric composition is also of particular importance. The ball size is normally tailored to further use of the product. There are three basic groups:

- a) small balls, or micro-balls, with a diameter of 3 - 8mm, intended for sintering or hydrometallurgical processing;

- b) normal balls with a diameter of 10 - 15mm, which is a standard size for blast-furnace pellets;
- c) large balls with a diameter of 20 - 30mm, intended for steelmaking pellets, fluorite pellets and raw materials for cement manufacture.

3.2. Pellet Manufacture

3.2.1 Properties of fines

According to Jaroslav and Zdenka (1988), the main property of the fines intended for balling is ballability, i.e. *ability to produce balls* with satisfactory compression strength.

The fines of concern in this study comprise coal as well as magnetite. The magnetite used was obtained from Phalaborwa mines, which was supplied by Martin and Robson Ltd. in Middelburg. The coal used was waste coal normally used as fuel for boilers; therefore the ash content of the coal was very high. Due to the coal not being in the form of fines, the coal had to be milled in a rod mill and then floated to reduce the ash content. The flotation of coal comprised using paraffin as the activator and pine oil as the collector as well as frother (Orhan, 1997).

A scanning electron microscope (SEM) was used to investigate the elemental analysis of the magnetite, un-floated coal and floated coal. *Table 3.1* shows the SEM analysis. (SEM images can be viewed in Appendix G.)

Table 3.1 Elemental Analysis of Feed Material

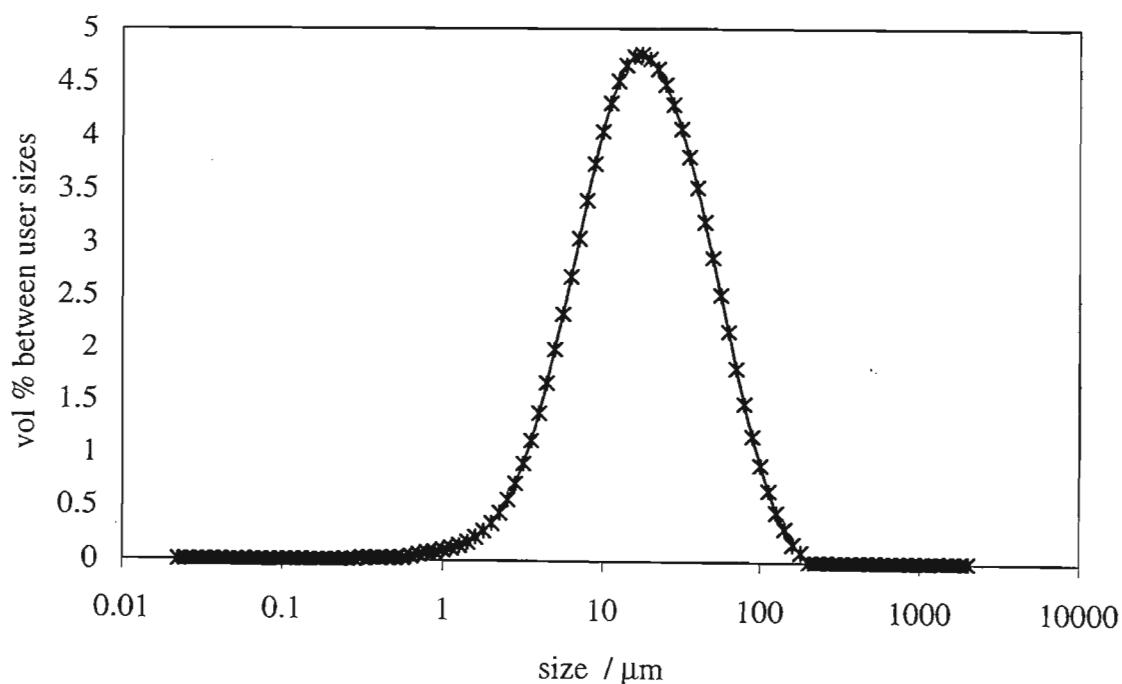
	Mass %		
	Magnetite	Un-floated Coal	Floated Coal
C	7.54	65.16	71.77
O	17.43	24.80	23.50
Mg	0.83	0.00	0.04
Al	0.27	3.83	1.50
Si	0.23	4.29	2.21
P	0.00	0.26	0.00
S	0.05	0.41	0.27
K	0.00	0.39	0.05
Ca	0.54	0.17	0.00
Ti	0.71	0.32	0.12
Cr	0.03	0.00	0.00
Mn	0.00	0.00	0.00
Fe	72.37	0.37	0.54

It is evident from the analysis that the magnetite is reasonably pure with traces of slag material. There is a definite reduction in the ash content of the coal due to flotation. The carbon purity of the coal rose by almost 7%. The high oxygen content of the coal is due to the presence of carbonates and slag forming oxides, e.g. MgO, Al₂O₃, SiO₂, etc.

Other ash tests were also performed on the floated and un-floated coal. These involved burning the coal off at 500°C. The ash content of coal was initially 25% on a mass basis and was reduced to 18% by flotation. This can be compared with the pellets produced by Sharma (1997) for his experimentation, which consisted of 18.26% ash. Although the ash just goes to the slag, when the ash is exposed to high enough temperatures it acts as glue in agglomeration thereby increasing the strength of the pellet (Benson et al., 1995).

The size distribution of the magnetite, which was already in the form of fines, was measured using a Malvern analyser. Graph 3.1 shows the size distribution.

Graph 3.1: Malvern Size Analysis of Magnetite



Graphs 3.2 and 3.3 show the size distribution of two sets of coal milled for different lengths of time in a rod mill, specifically for 30 and 15 minutes respectively. This was done so as to obtain a coarse coal and fine coal, with different specific surface areas so as to investigate the effect of coal particle size on the reduction process. The particle size would also have an effect on pelletizing.

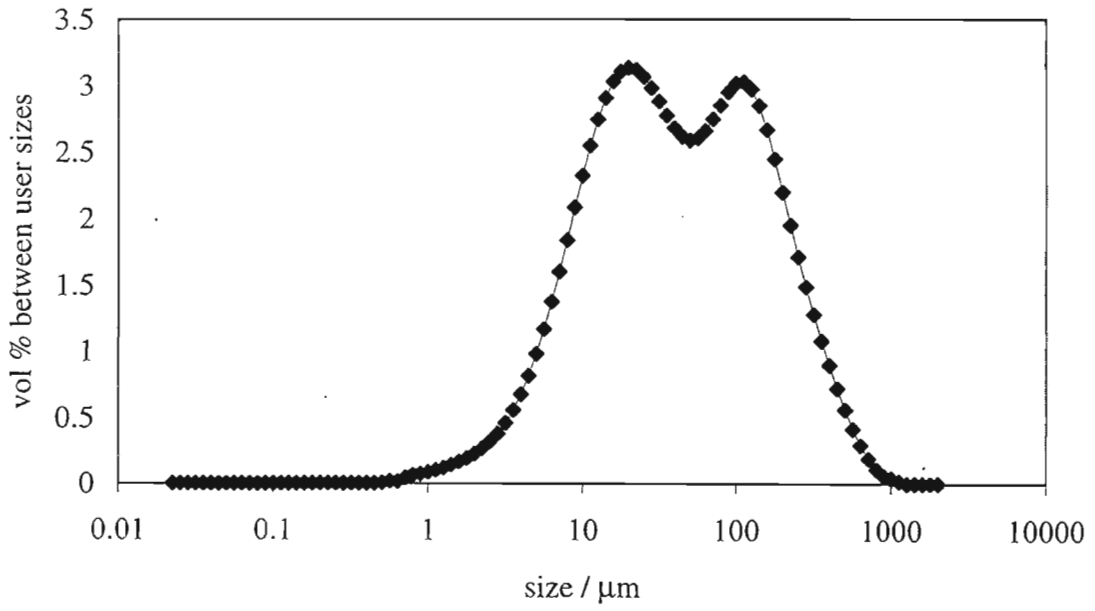
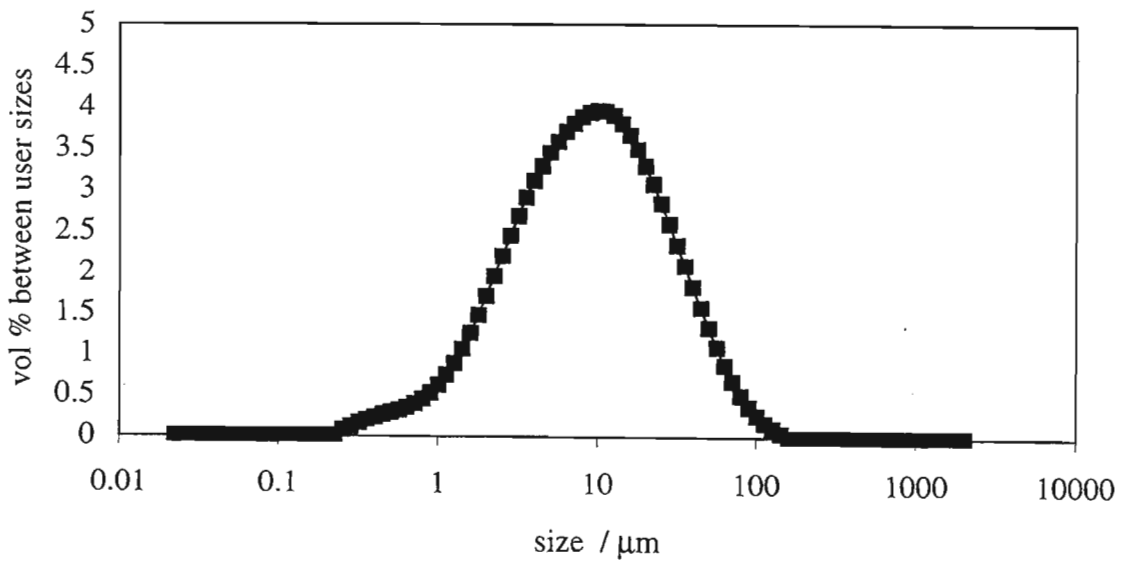
The table below compares the specific surface area and the volume weighted average size of the different feed material.

Table 3.2 Surface Areas and Size of Feed Material

	Magnetite	Coarse Coal	Fine Coal
specific surface area / m^2/g	0.56	0.37	1.44
volume weighted mean / μm	25.85	81.71	14.40

The coarser coal will be referred to as coal $< 100\mu\text{m}$, while the finer coal will be referred to as coal $< 20\mu\text{m}$.

The particle sizes of the feed material are comparable with the material used for pellets in the Fastmet Process, which are around $40\mu\text{m}$. It should be noted however that iron ore and coal fines less than 0.15mm can be balled satisfactorily (Pandey and Sharma, 1999).

Graph 3.2: Malvern Size Analysis of Coarser Coal*Graph 3.3: Malvern Size Analysis of finer coal*

Dried lignosulphonate powder was used as the pellet binder. It is recovered from the sulphite pulping industry and is environmentally friendly and non-toxic (Lignin Institute, 1991). The lignobond used for experimentation was obtained from Lignotech SA and referenced as Lignobond. The elemental analysis can be seen in *table 3.3*.

Table 3.3 Elemental Analysis Lignobond

	Mass %
C	43.88
O	47.32
Mg	0.07
S	4.45
K	0.15
Ca	4.12

Lignosulphonates have been previously used as a coal pellet binder (Burchill et al., 1994). Other commercially used binders include bentonite, lime, and cements. Ripke and Kawatra (2000) noted that bentonite might result in “slag bonding” that improves the strength of the fired pellet. In the case of lignobond, a likely bonding enhancement would be the creation of ‘hot-spots’ between particles of slag and iron oxide causing point melting and fusing them together. Also bentonite is normally added in the range of 0.5 – 1% by mass. A maximum of 1% lignobond binder was therefore added to increase pellet strength. Excess lignobond will only result in increased slag production, which is undesirable.

Another advantage of lignobond is that it is hydrophilic thereby rendering the material to be pelletized wettable. Wettability is an important factor that greatly affects ballability and ball strength. Lignobond can therefore be very useful because coal is naturally hydrophobic.

3.2.2 Pelletization Experimental Set-up

The rotating disc pelletizer was used, as it had been selected for tests on the use of Lignobond. It has an advantage due to its ability of combining balling and screening in one operation. This is due to the balls which discharges over the disc lip have very close size tolerances making screening unnecessary. Another advantage is that changing different parameters of the disc pelletizer can control the quality of product, viz. disc inclination angle, revolutions per minute, point of feed and wetting of raw material (Jaroslav and Zdenka, 1988).

A photograph of the disc pelletizer used in this study can be viewed in Appendix E. (Photograph E1).

The motion of the fines can be seen in *fig. 3.2*. Variations of the movement depend on the amount of feed to the pelletizer and on the revolutions per minute. The rpm is the main factor influencing the quality of the process. It is expressed in terms of a fraction of the *critical rpm*, i.e. the rpm at which the material in the pelletizer ceases to ball and at which does not fall under the action of centrifugal force. The generally accepted optimal number of revolutions per minute is expressed as $n_{opt} = 0.75n_{crit}$.

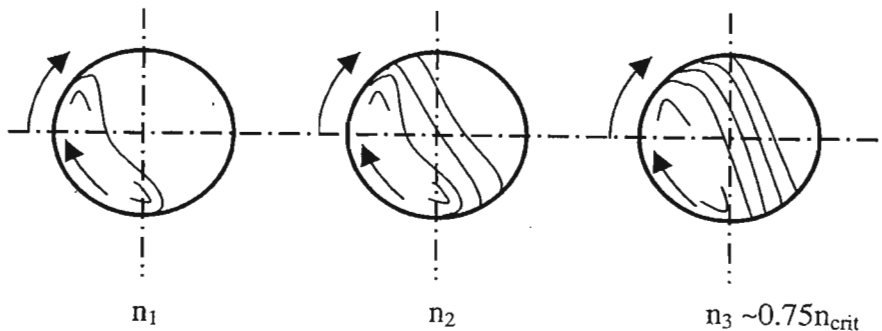


Fig 3.2. Motion of Material in a disc pelletizer revolving at various speeds

$(n_1 < n_2 < n_3)$ [Jaroslav and Zdenka, 1988, fig. 35]

An equation that can be used to determine the critical revolutions which includes the effect of the disc inclination angle, α , is

$$n_{crit} = (42.3 / D^{0.5}) (\sin \alpha)^{0.5} \quad (3.2.1)$$

Where D is the disc diameter (m).

The pelletizer of concern in experimentation has a diameter of $D = 0.61$ m. Using a disc inclination angle of 60° to the horizontal, equation (3.2.1) gives $n_{crit} = 47.2 \text{ min}^{-1}$ and $n_{opt} = 35.4 \text{ min}^{-1}$.

The agglomeration of pellets produced in the pelletizer depends on the manner in which the raw materials are fed, and on the wetting system, in addition to the main parameters such as disc diameter, inclination, and revolutions. The basic arrangements of feed and wetting systems to allow for different size pellets can be seen in *fig.3.3*.

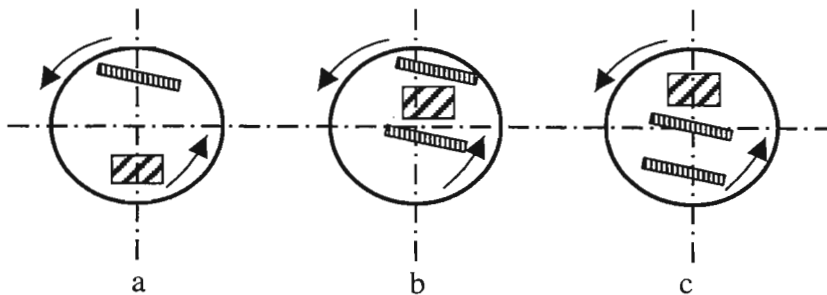

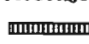


Fig 3.3. Typical arrangements of feeding and spraying in a disc pelletizer [Jaroslav and Zdenka, 1988, fig. 36]

 – feed  – water

- a) for 20-30mm balls
- b) for 10-20mm balls
- c) for 1-10mm balls

The size of the pellets required to range between 10 – 20mm, therefore option (b) in *Fig 3.2* was employed.

The pellets required for direct reduction testing in the furnace were pelletized mixtures of magnetite and floated coal fines, including a 1% solid lignobond binder. The production of pellets was conducted batch-wise, using 500g of feed material with gradual addition of water. Each run lasted 15 – 30 minutes, with the speed and the angle being 20 rev.min⁻¹ and 60 – 70° respectively, to ensure that the pellets were between 10 – 20mm in diameter.

Although the speed is much less than n_{opt} , i.e. 35.4 min⁻¹, this was necessary to prevent pellets from falling off the pelletizer. It should be noted that n_{opt} was calculated for a continuous system where the pellets accumulate and fall of the disc.

The experimentation thereafter involved feeding the pellets to the muffle furnace and subsequently testing the strength of pellets with a strength tester.

3.3 Evaluation of Pellets

Standard test methods from Biswas (1984) were used to evaluate pellets.

3.3.1 *Ball Size*

It was initially observed that pellets produced comprising coal < 20 μm were mostly less than 10 mm. This could be attributed to the extreme fineness of the coal. Another reason could also be that two *different* types of material were agglomerated together, each having different properties. For example, while the particle sizes were quite comparable, the densities were significantly different (ρ_{coal} is approximately 1350 kg/m^3 , while $\rho_{\text{magnetite}}$ is approximately 5200 kg/m^3) (Perry and Green, 1997). One can therefore assume that all the magnetite particles and the coal particles agglomerate separately forming partially mixed pellets. Due to the initial mixture being well mixed, the probability of one magnetite particle finding another magnetite particle (or 2 coal particles agglomerating) was quite small. This resulted in small pellets being produced. Further pelletization and addition of water resulted in different balls sticking together forming irregular shaped pellets.

Pelletizing a mixture of coal < 100 μm and iron oxide produced balls which fell in the size range 10 – 20 mm, which is sufficient for industrial purposes. A possible reason for this could be that the coal particles are large enough to trap the smaller magnetite particles whilst agglomerating with other coal particles. This resulted in a more homogenous batch of pellets.

3.3.2 *Compression Strength*

The compression strength of pellets was analyzed by subjecting pellets to uniform loading between two parallel plates until the ball is ruptured. The apparatus (strength tester) used to test the strength can be seen in *fig. 3.4*.

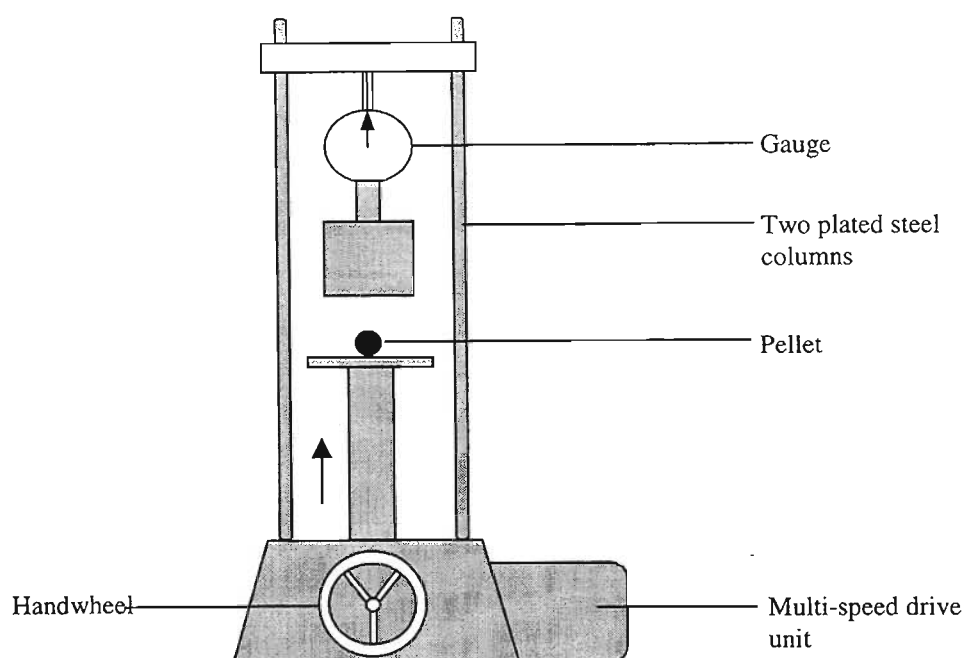
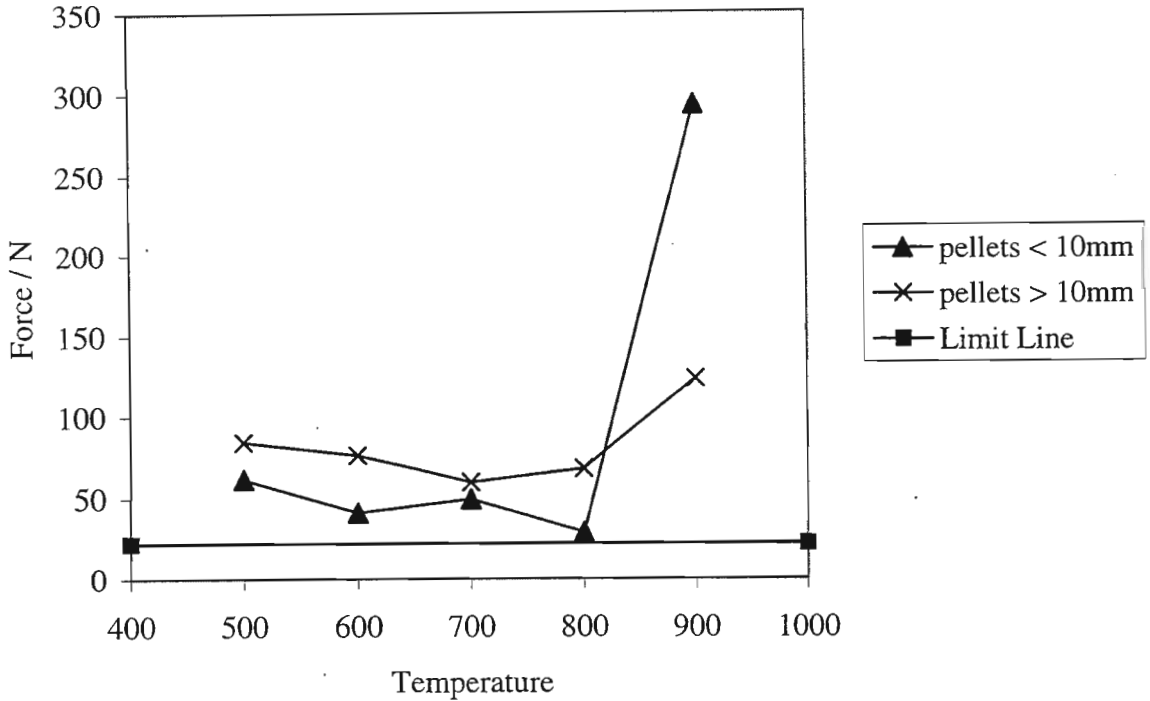


Fig. 3.4. Strength Tester

The pellet was placed on a support and was gradually raised until it pushed against the upper plate and the dial on the gauge moved. The hand-wheel was then locked and the multi-speed drive unit started pushing the pellet upwards. At the first sign of pellet failure the gauge reading was noted and converted to Force units using a calibration chart. (Calibration chart can be seen in Appendix F1).

It was required that the pellets should not fail under furnace conditions, therefore, the pellets were tested at high temperatures. The mixed magnetite and coal pellets (added in stoichiometric ratio) with a 1% lignobond binder were therefore heated in a muffle furnace for 30 minutes, at temperatures ranging from 500 – 900°C. Both particle sizes of coal were tested, i.e. coal < 20 μm and coal < 100 μm , or pellets < 10 mm and pellets > 10 mm.

Results can be seen in *graph 3.4*.

Graph 3.4 Strength of Magnetite/Coal Pellets

Ripke and Kawatra (2000) quoted that the industrially acceptable strength of magnetite pellets is 22N; hence the limit is shown in *graph 3.4*. The first noticeable trend was that both sets of pellets were above the acceptable limit. The larger pellets initially showed a higher strength but above 800°C this trend seemed to change. The extreme increase in strength of the pellets < 10 mm at 900°C could have been due to partial sintering of the pellet at reduction temperature. The pellets > 10 mm also showed a significant increase in strength at this temperature, although it was not so pronounced. Reasons for this could have been due to the actual reduction of the pellets, which will be investigated in *Chapter 6*.

It should also be considered that Jaroslav and Zdenka (1988) reported 20 and 50 N for balls 14mm in diameter. Therefore the strength of the pellets produced for this study was sufficient for industrial purposes.

3.3.3 *Drop Strength*

The drop strength was measured by means of letting a ball hit a steel plate repeatedly from a specified height. The resultant value was expressed as the drop number, which was indicated by the number of drops the ball was able to withstand without observable damage. A total of 10 balls of average size were tested. On completion of the test the material was subjected to screen analysis after the end of the drop test.

Dutta et al. (1997) tested the drop strength of iron ore pellets (with a cement binder) by dropping from a height of 46 cm on a steel plate. The drop strength of the green pellets (wet pellets which have recently been pelletized) mostly lay between 4 to 6. The same procedure was incorporated in this study for the sake of comparison. Drop strengths obtained ranged from 5 to 8 for both types of pellets. The drop strengths obtained showed considerable strength but it should be noted that some values recorded were as low as 3 while others were as high as 10. Pellets dried at 200°C showed an increase in drop strength to an average of 8.

3.3.4 *Resistance to Abrasion*

This test was done on dry balls and was measured on a vibratory screen. The charge was approximately 500g and lasted 15 - 20 minutes. The resistance to abrasion was stated in wt.% of the undersize smaller than 0.1mm.

Pandey and Sharma (2000) quoted an abrasion index (+6.3 mm surviving) of 90% for double-layered iron ore and non-coking coal pellets. These pellets, however, were made by hand rolling therefore a pellet size of 8-10 mm could be maintained.

The abrasion index obtained for the pellets in this study can be seen in *table 3.4*.

Table 3.4. Abrasion Index of Mixed Magnetite/Coal Pellets

Screen Size	Pellet < 10 mm		Pellet > 10 mm	
+ 500 μm	94.48	%	82.30	%
- 500 + 106 μm	2.19	%	16.25	%
- 106 μm	3.33	%	1.45	%

3.3.5 *Moisture Content*

The moisture content of green balls was found to be 8-10% by mass. This was found to be equivalent to the moisture content stated by Sharma and Pandey (2000). The moisture content of pellets prepared by Dutta et al. (1997), lay in the range of 5.5 to 8.5%, which was also quite comparable.

3.3.6 *Tests with Bentonite*

Tests using bentonite as a binder were also performed, as a basis of comparison, and similar results were obtained.

3.4 Conclusion

From batch pelletizing of mixtures, it was evident that smaller size particles of pellets result in smaller size pellets being produced. Using coal $< 100 \mu\text{m}$ resulted in pellets which fall in industrially acceptable size limits, i.e. 10 mm – 20 mm. It was also observed that one could alleviate this problem of minute pellets by adding more water and increasing pelletizing times. This, however, resulted in larger pellets of irregular shapes.

Strength test evaluations of the two types of pellets showed that the pellets retained sufficient strength for furnace processing. Both types of pellets were above the industrially acceptable limits. Drying at 200°C resulted in an increase in pellet strength. At reduction temperatures the pellets showed significant increase in strengths, which could be attributed to partial sintering of the pellet.

Drop strength tests, resistance to abrasion tests, and moisture content tests, compared favourably with literature values.

Lignobond, therefore, revealed the desired effect as a pellet binder. The pellet obtained met all industrial requirements and was adequate for reduction testing.

Chapter 4: Reduction in Tube Furnace

4.1 Experimental Set-up

The aim of conducting the initial experiments was to observe if reduction occurs at 900°C. It was also intended to investigate the efficiency of using mixed pellets of ore and waste coal in a furnace. To this end, mixed pellets comprising magnetite and coal, ratio of 1:1 on a mass basis, were pelletized inclusive of a 1% binder addition. It should be noted that the coal addition was in excess to that required for direct reduction. Two types of pellets were employed consisting of lignobond binder and bentonite binder respectively.

The furnace that was used for preliminary experimentation was referred to as the tube furnace due to it having a quartz tube through centre to hold the pellet sample. *Fig 4.1* shows a schematic for the experimental set-up of the reduction testing.

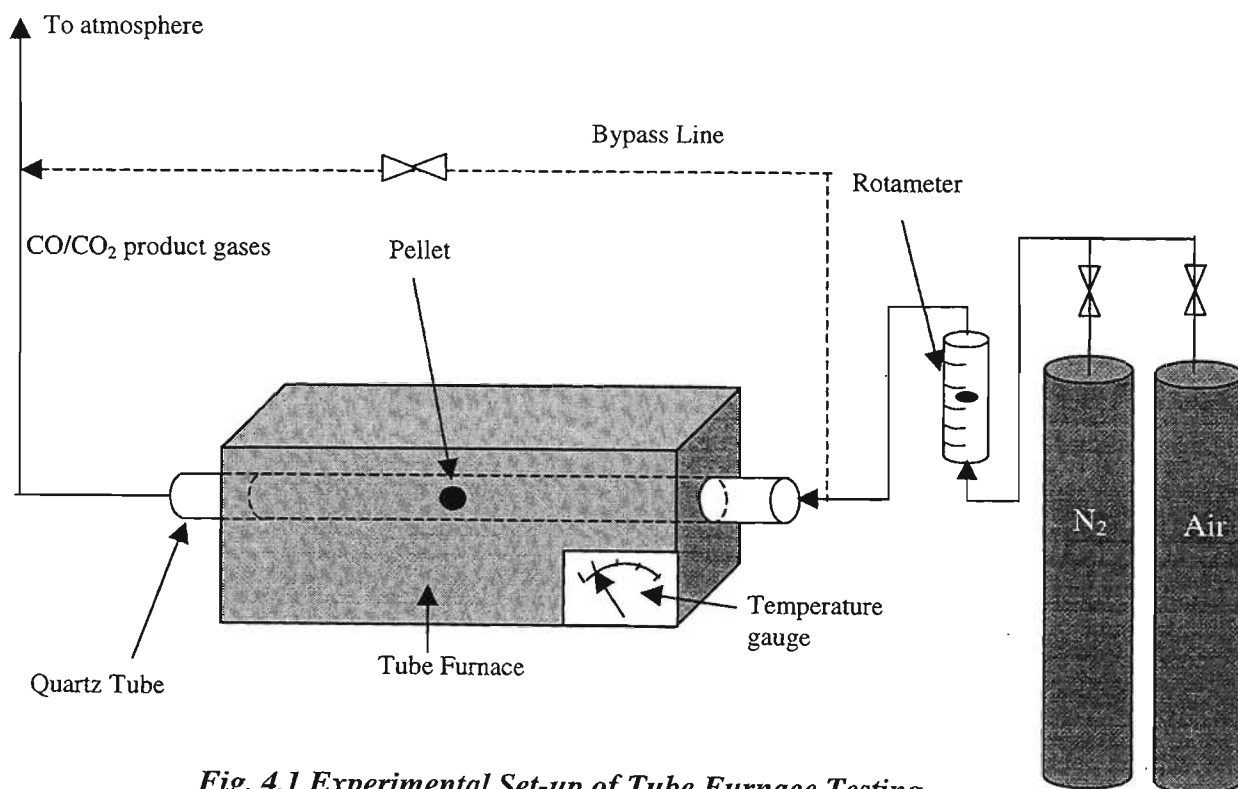


Fig. 4.1 Experimental Set-up of Tube Furnace Testing

The maximum attainable temperature in the quartz tube furnace was found to be 1 200°C; therefore the furnace was adequate for a working temperature of 900°C. The temperature controller controls the temperature inside the tube furnace. The entering gases, the flow-rates of which were controlled by a rotameter, were initially compressed air and, thereafter, nitrogen. The product gases, i.e. CO and CO₂, were vented to the atmosphere. It was later evident that a bypass stream for the nitrogen was necessary; hence it is shown in the Fig. 4.1.

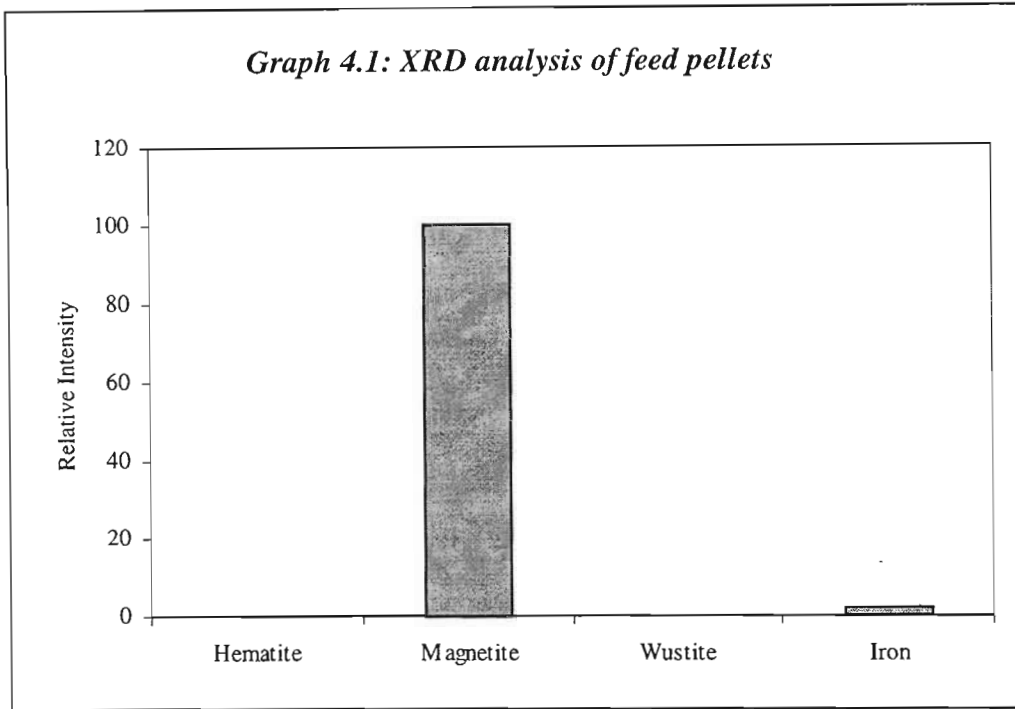
The experiments conducted included initially placing a few mixed feed pellets (approximately 30 grams) inside the tube and setting the furnace temperature at 900°C. The inlet gas was immediately introduced. It was observed that the furnace took approximately 15 – 20 minutes to reach reaction temperature. Experiments were conducted with increasing residence times of 1, 2 and 3 hours respectively to gauge the optimum time required for reduction.

The product pellets were then analysed via X-ray diffraction (XRD), which gives relative intensities of hematite, magnetite, wustite and pure iron respectively (A review of XRD analysis can be seen in Appendix B). XRD analysis was also used by Purwanto, et al. (2001) to detect for hematite, magnetite and iron in briquettes undergoing direct reduction. Although XRD is a qualitative analysis and not quantitative i.e. exact percentages on a mass basis could not be achieved, it gives an indication of the extent of the reaction.

4.2 Results of Tube Furnace Tests

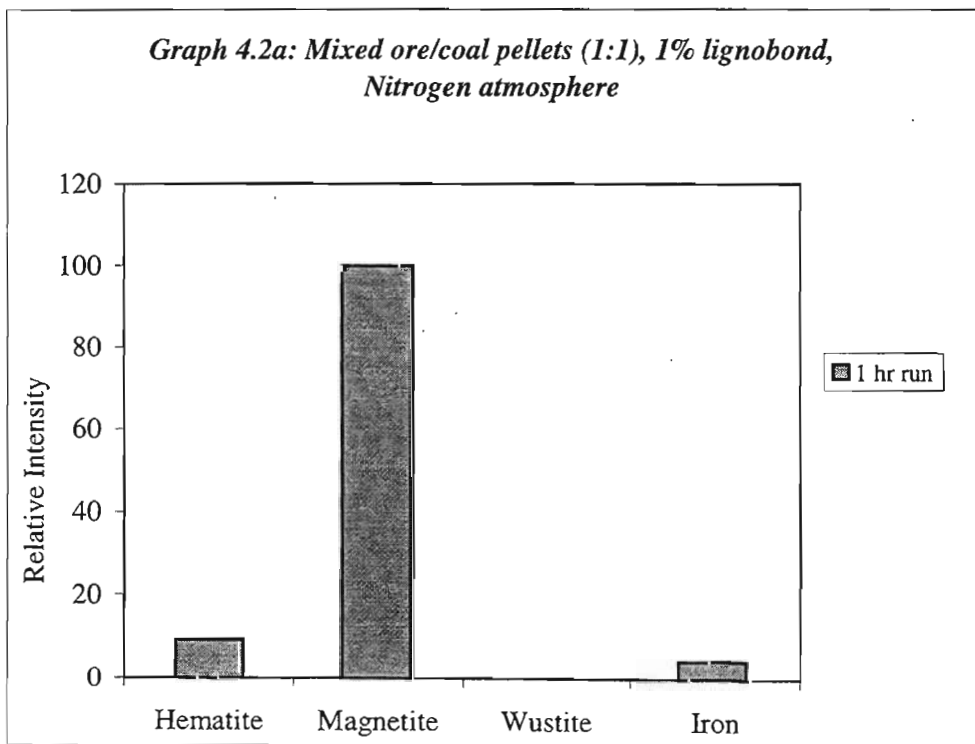
The initial set of experimentation was investigated using an inert atmosphere of nitrogen gas to induce mainly direct reduction by removing most of the carbon monoxide and carbon dioxide from the reaction tube.

Feed pellets were also analysed using XRD as a comparison of the degree of reduction.

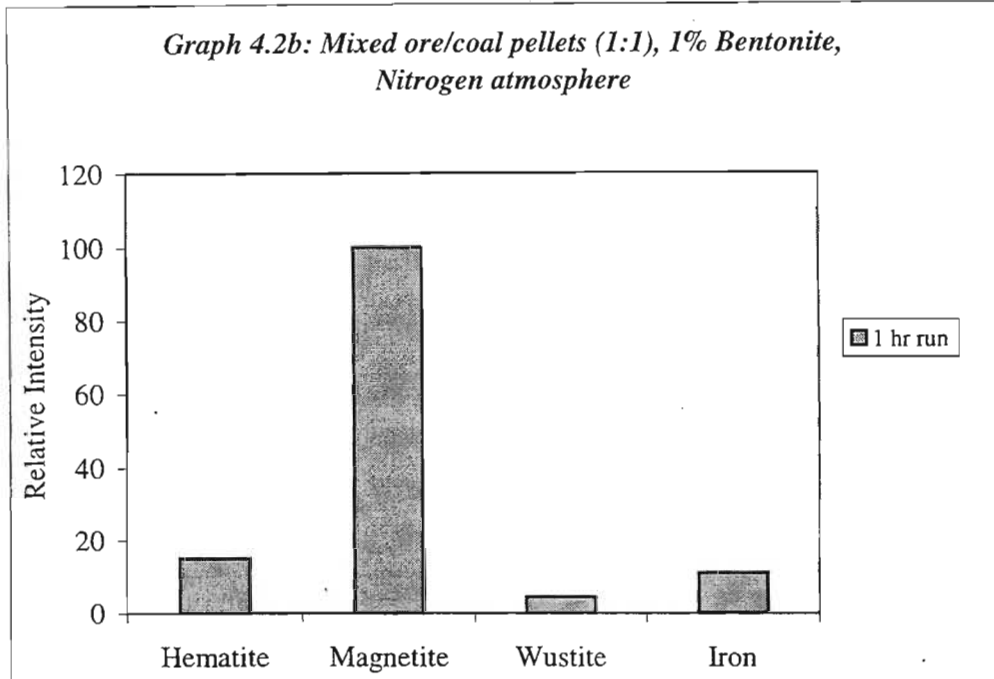


Appendix H, rc10

Graphs 4.2a and b show the relative intensities of the different oxides of the lignobond and bentonite pellets respectively, after 1 hour at 900°C.



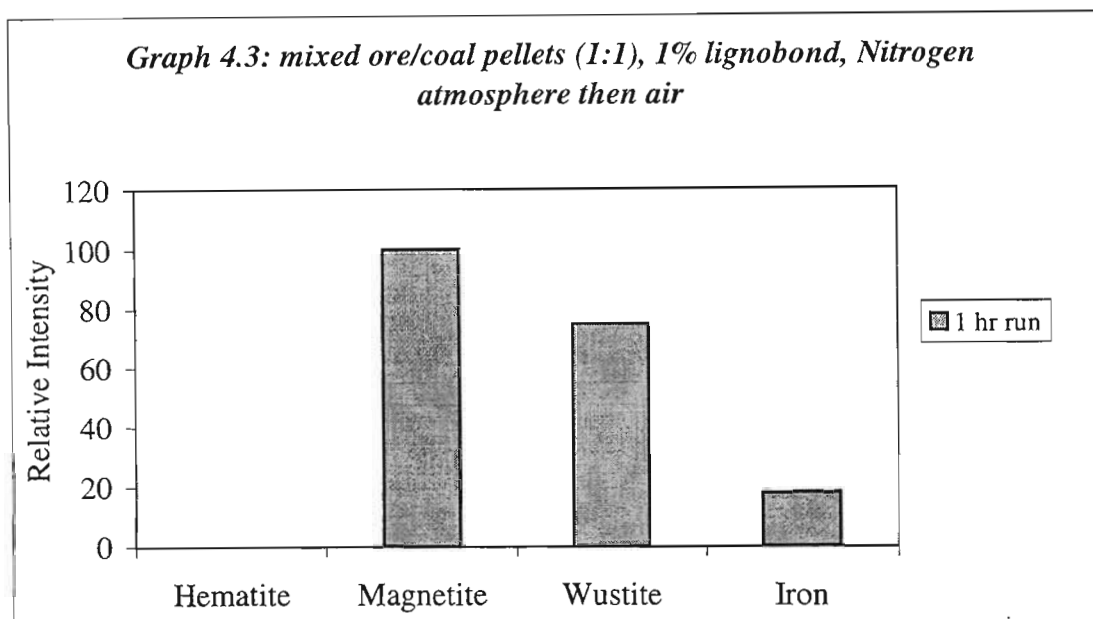
Appendix H, rc3



Appendix H, rc2

The first noticeable trend is that, although an excess amount of coal needed for reduction was used, in both cases very little reduction occurred when compared to the feed pellets. Although slightly more reduction did occur in the bentonite pellets, there was no significant difference. The hematite that formed could have been due to the exposure of the product pellets to the atmosphere during grinding for subsequent XRD analysis. It was concluded that a combination of direct and indirect reduction needed to be implemented, to enhance the Fe production.

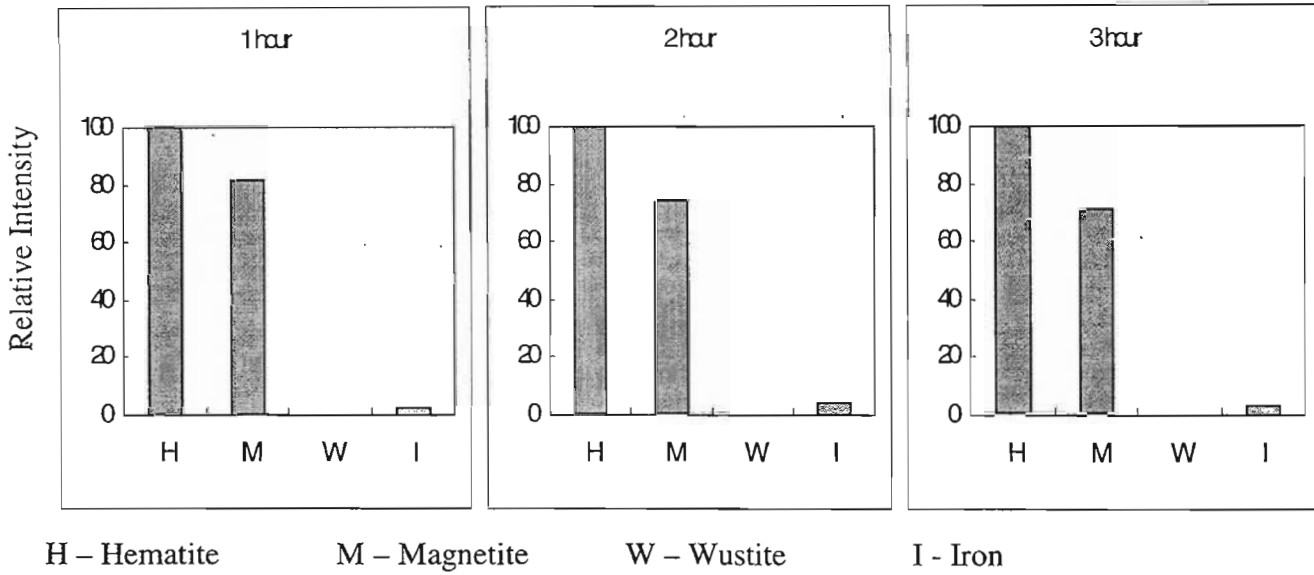
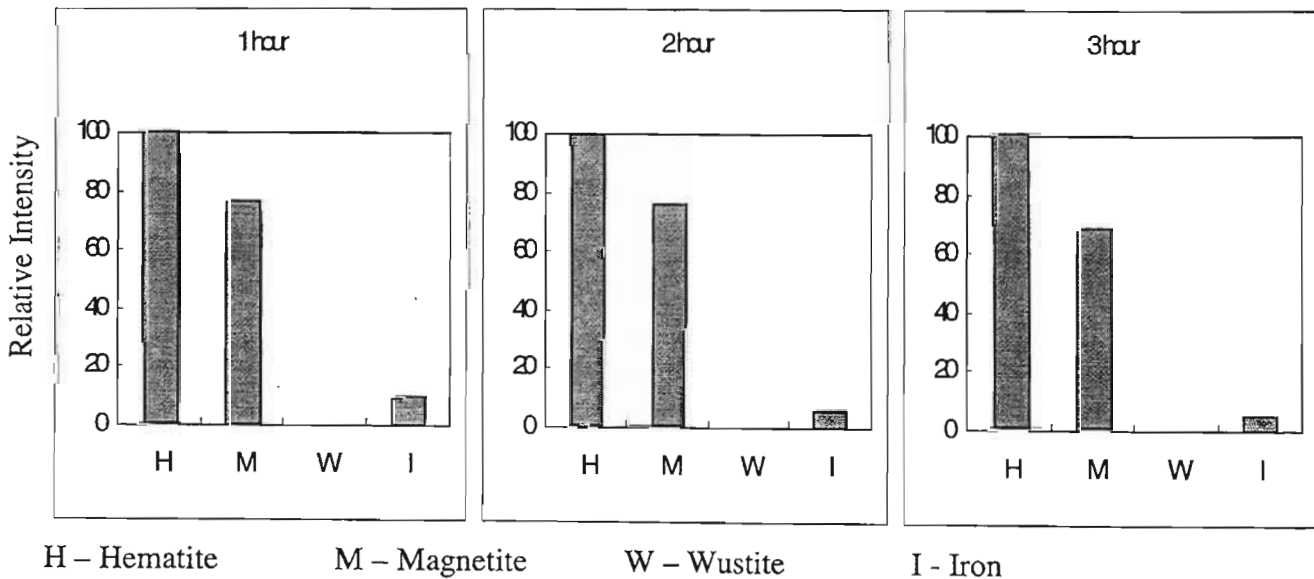
This led to allowing the temperature of the lignobond pellets to rise to reduction temperature in an inert atmosphere (so that no oxidation of ore occurs) then changing the environment to air. The oxygen in air thus induces carbon monoxide formation, which in turn reacts with the iron oxide forming iron indirectly. Results produced can be seen in *Graph 4.3*.



Appendix H, r

The introduction of indirect reduction along with direct reduction shows a definite increase in the production of iron.

The increase in reduction products at atmospheric pressure promoted the reducing of pellets at only atmospheric pressure without the inclusion of an inert atmosphere stage. It was also necessary in this case to increase residence times of the process. Two different experiments were conducted; one employing lignobond pellets while the other employing bentonite pellets. Each experiment was conducted at three different residence times of 1, 2 and 3 hrs respectively. Results obtained can be seen in *Graph 4.4a and b*.

Graph 4.4a: mixed ore/coal pellets (1.1), 1% lignobond, air atmosphere**Graph 4.4b: mixed ore/coal pellets (1.1), 1% bentonite, air atmosphere**

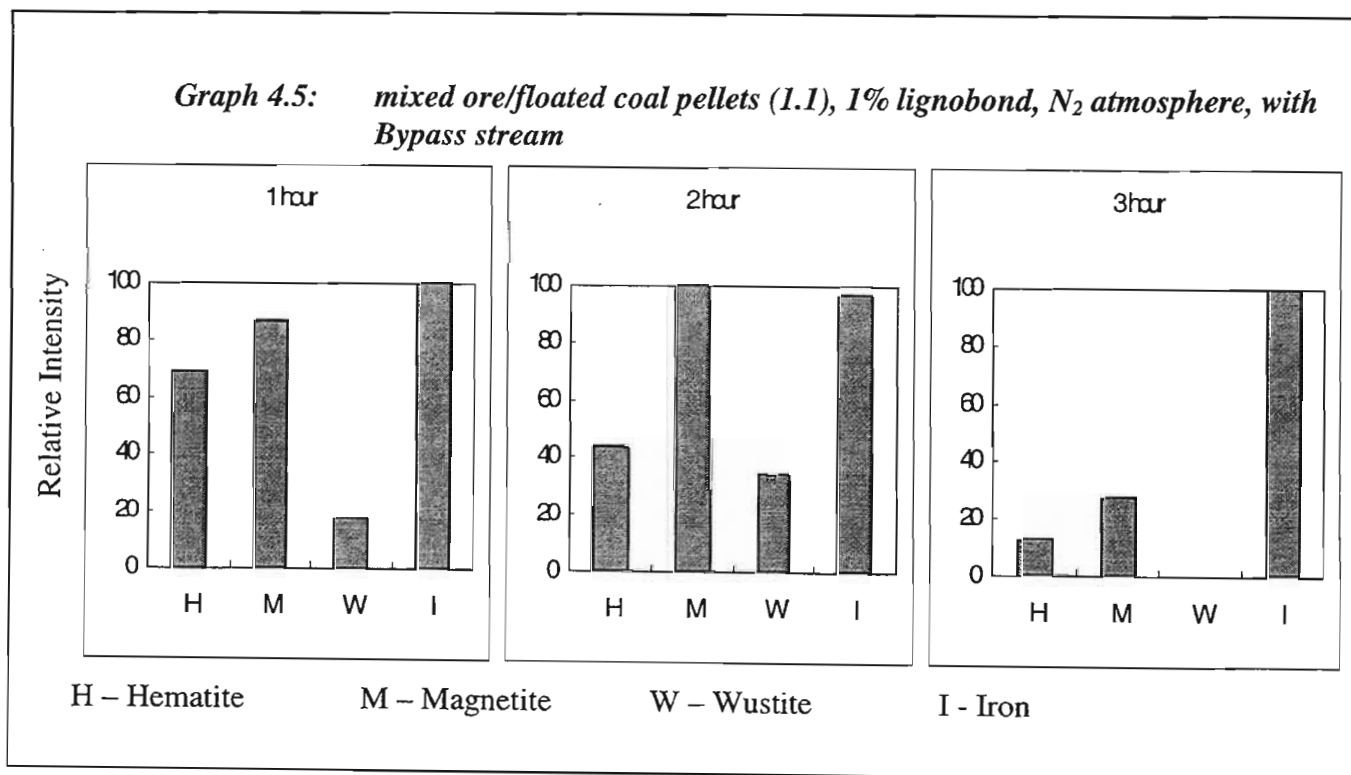
Graph 4.4a: 1 hour – Appendix H, rc4
 2 hour – Appendix H, rc5
 3 hour – Appendix H, rc6

Graph 4.4b: 1 hour – Appendix H, rc7
 2 hour – Appendix H, rc8
 3 hour – Appendix H, rc9

It is quite evident that, in both cases, the air sent in promoted the oxidation of magnetite to hematite instead of indirect reduction of the magnetite to iron.

It was noted that the lignobond pellets gave almost the same reduction results when compared to the bentonite pellets, and that lignobond was an efficient binder for pellets. All charge pellets, for further experimentation, were therefore only bonded with lignobond.

The last set of experimentation involved adding a bypass stream to the system so that no oxygen enters the system (through inlet and outlet) and the entering nitrogen does not dilute the unreacted CO to a great extent. Flotation of coal was also necessary for the following experimentation. Results can be viewed in *graph 4.5*.



Graph 4.5: 1 hour – Appendix H, run1rc
 2 hour – Appendix H, run3rc
 3 hour – Appendix H, run2rc

4.3 Discussion of Tube Furnace Tests

From the first set of experimentation (*Graphs 2a & b, and Graph 3*), it is evident that indirect reduction plays a major role in reduction of iron ore. Haque and Ray (1995) also arrived at the same conclusion. It is also apparent that a large percent of wustite was formed. Given enough residence time the wustite that was formed would reduce completely to iron. It has to, although, be mentioned that the production of iron is much less than that noted in commercial reduction techniques used.

Due to the presence of air enhancing indirect reduction and to increase the conversion of magnetite, the pellets were reduced in an air atmosphere. This resembled the blast furnace process whereby air is blasted in at reduction temperature. The presence of air, however, had the adverse effect of oxidizing the magnetite to hematite. The carbon present in the *unfloated* coal was not sufficient to induce direct reduction. It can also be seen that the longer the pellet was exposed to air, more magnetite oxidized to hematite. It was concluded that no indirect reduction occurred as the air displaced all the CO and CO₂ that did form.

From the experiments thus far concluded, it seemed apparent that indirect reduction needed to be included to get a higher percentage of iron formation. Introducing air into the reaction system, however, could not do this, as the oxygen in air invoked oxidation of the magnetite. It was, therefore, necessary to use a N₂ atmosphere. However, constant flow of nitrogen diluted unreacted CO and extracted it from the system. A bypass line was therefore introduced, which was only open (using the bypass valve) after nitrogen purged the system of air. This allowed most of the nitrogen to exit the reaction zone without interference, whilst maintaining that oxygen does not enter the system. The CO that formed during direct reduction therefore reduced unreacted iron oxide. The combination of direct and indirect reduction in addition to the coal being richer in carbon content, i.e. floated coal, increased the amount of product iron to a great extent as predicted.

An increase in the residence time, from 1 to 2 hours, allowed more of the magnetite to be reduced to wustite. A further increase in time, to 3 hours, allowed most of the wustite formed to reduce to iron, which was in agreement with mechanisms predicted by Negri et al (1987) (see page 7). The effect of residence on the reduction process is due the reduction activation energies predicted by Reddy et al (1991). Using the predicted activation energies, a conversion graph shows the conversion of magnetite to metallic iron gradually increases to a maximum of 90 – 100%, after 3 hours (see *graph 2.2*). Although XRD is a qualitative analysis, *graph 4.5* shows definite increase in conversion of magnetite to metallic iron with an increase in time.

4.4 Conclusion

From the preliminary tube furnace experimentation a number of conclusions can be made to help in setting parameters for further reduction experimentation, e.g. induction furnace testing.

- Firstly, reduction occurs quite effectively at 900°C, although indirect reduction plays the major role.
- Lignobond is an efficient pellet binder for the reduction process. Comparison with a commercially used binder, viz. bentonite shows no significant changes.
- Re-oxidation of iron oxide or reduced iron can be avoided by using an inert atmosphere initially, to remove all oxygen present.
- Increasing the residence time of the mixed pellet allows the intermediate iron oxides, e.g. wustite, to reduce further to metallic iron.

Chapter 5: Reduction in Thermobalance

5.1 Experimental Set-up

The thermobalance is an apparatus used to measure loss of mass of constituents placed inside the thermobalance furnace, when subjected to high temperature. An indication of the extent of reduction is the loss of mass encountered by the pellet over time at a specific temperature. This method was therefore used like other authors, e.g. Reddy et al. (1991), Swantantra and Hem (1990), to calculate reduction kinetics.

The experimental set-up is given in *fig. 5.1*. A photograph of the Thermobalance can be viewed in Appendix E (Photograph E2).

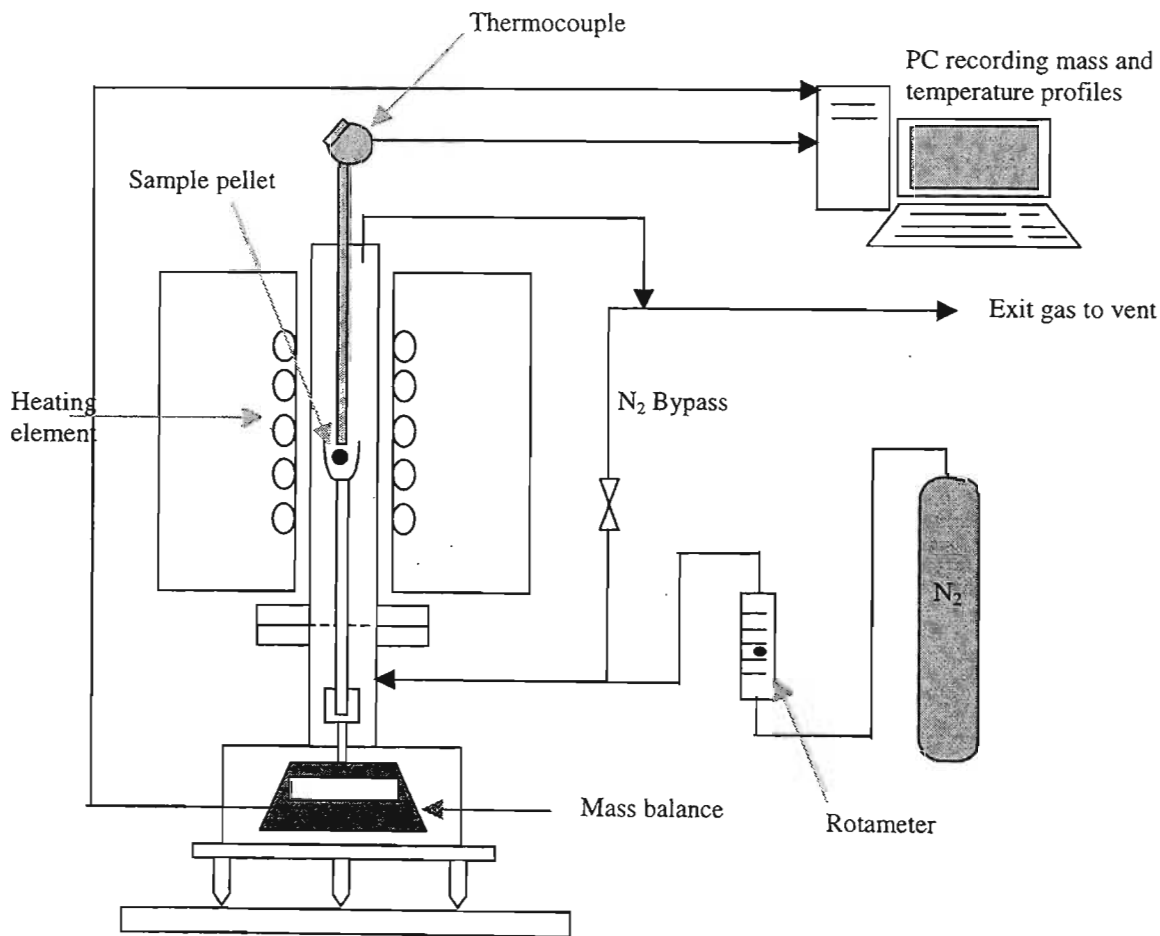


Fig. 5.1 Thermobalance Experimental Set-up

The pellet that was placed inside the thermobalance furnace was a mixture of floated coal and magnetite (stoichiometric ratio), with the binder being lignobond. The pellet was placed on a support, which in turn rested on a mass balance so that changes in mass of the pellet could be recorded. The temperature of the pellet was measured using a thermocouple. All data was logged to a computer, as shown in *fig. 5.1*.

As was concluded from the tube furnace testing that an initial inert atmosphere was the optimum set-up for initiating direct as well as indirect reduction, therefore, a similar set-up was employed in this case. The N₂ flow-rate was maintained at 200 ml/min via a rotameter (see Appendix F1 for calibration chart).

The actual running of experiments involved heating the pellet to reaction temperature in the thermobalance whilst constantly recording mass of the pellet and temperature. The pellet was allowed to remain in the furnace until the mass remained constant, i.e. no loss of mass.

To calculate activation energies, reduction experiments had to be conducted at 3 different temperatures, viz. 800°C, 900°C and 1000°C. Results of the experimentation can be viewed in *chapter 5.2*.

5.2 Results of Thermobalance Tests

The mass of the pellet and temperature of the furnace for the 3 runs, i.e. 1000°C, 900°C and 800°C, were recorded against time. (All graphs can be viewed in Appendix C)

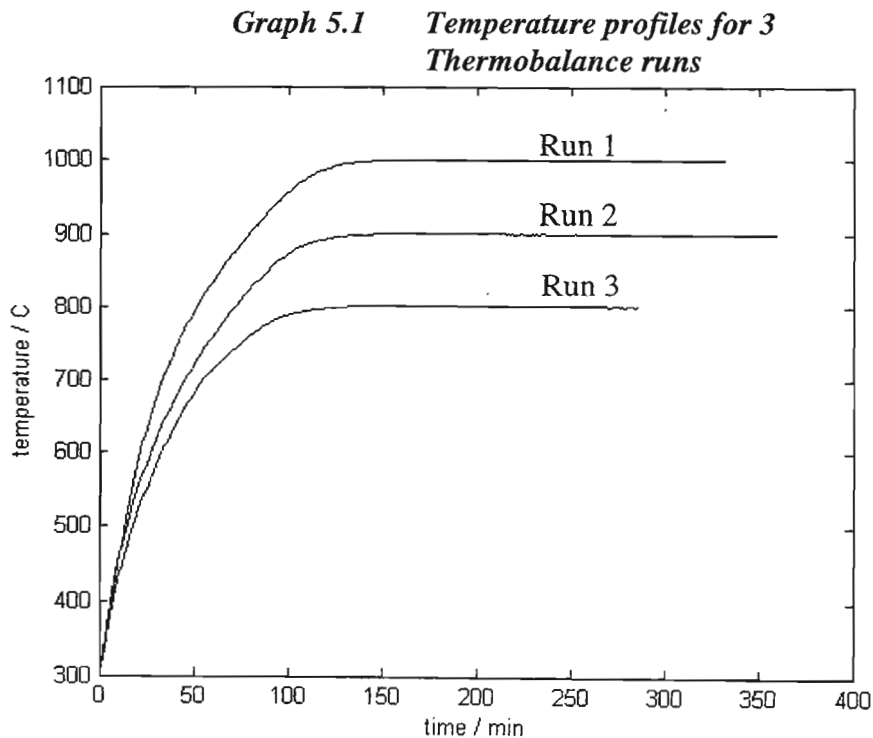
The fraction of reaction, f , was then calculated using *equation 2.1.20*, as it gives an indication of the degree of reduction, α (Anon, 1990).

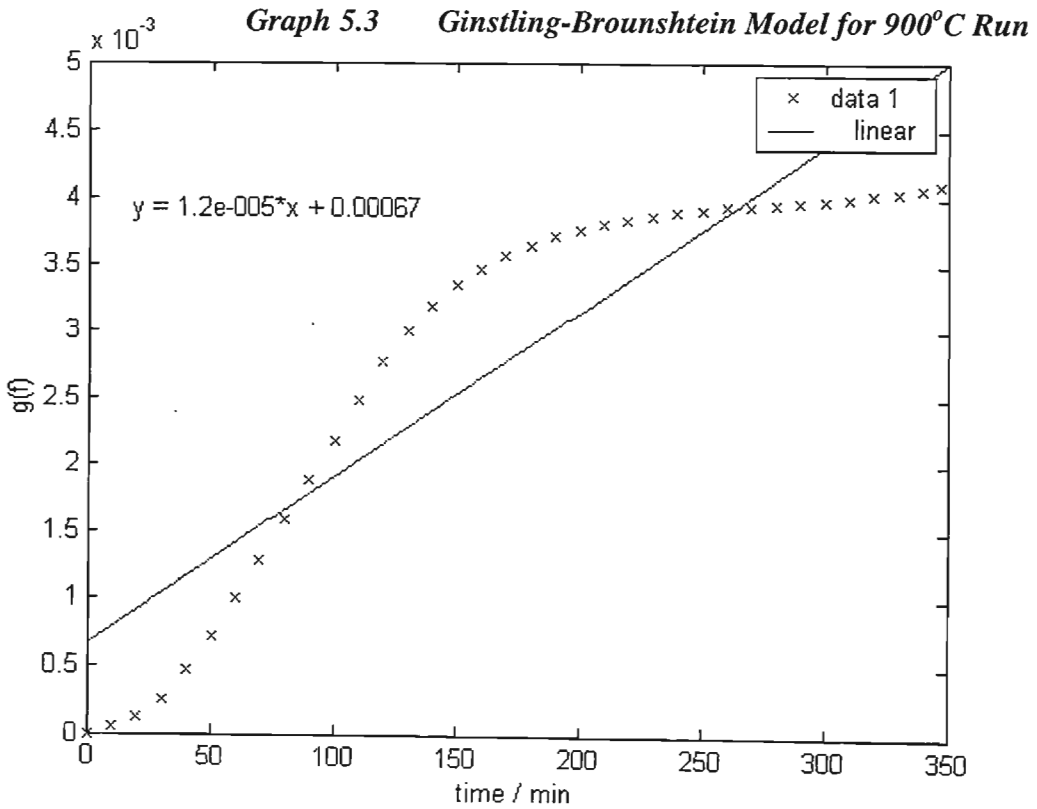
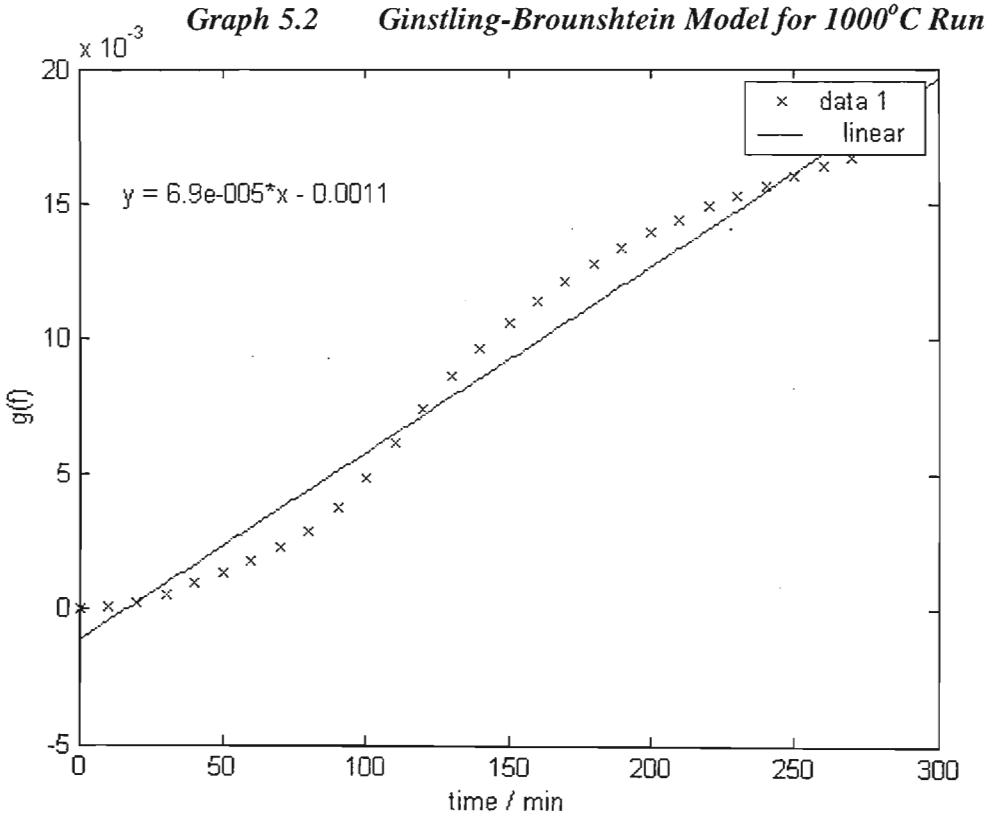
$$\text{Fraction of reaction, } f = \frac{\text{Weight loss at time } t}{\text{Max. possible weight loss}}$$

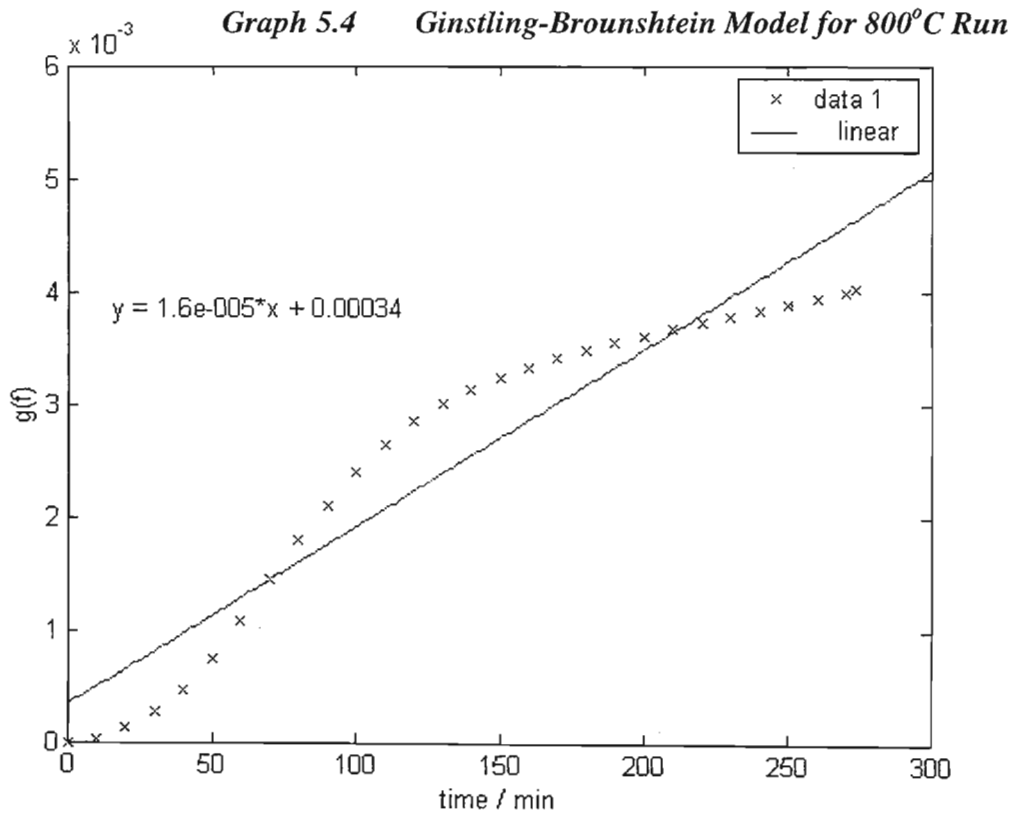
One can calculate kinetic rate constants, k , for the different temperatures using the Ginstling – Brounshtein equation (Habashi, 1969), which is applicable to reactions controlled by diffusion through a nonporous solid product as the rate-determining model, i.e.

$$g(f) = 1 - \frac{2}{3}f - (1-f)^{2/3} \quad (2.1.23)$$

The graphs below show the respective plots that were obtained.







Estimating the straight line equations, to obtain $y = kx$, gives:

1. $y = 6.9 \times 10^{-5} x$, at 1000°C.
2. $y = 1.2 \times 10^{-5} x$, at 900°C.
3. $y = 1.6 \times 10^{-5} x$, at 800°C.

Using the respective k -values, one can plot the Arrhenius equation, i.e.

$$k = Ae^{-E/RT} \quad (5.1)$$

or $\ln(k) = -E/RT + \ln(A)$ (5.2)

where k = reaction rate constant [min⁻¹]

A = pre-exponential factor [min⁻¹]

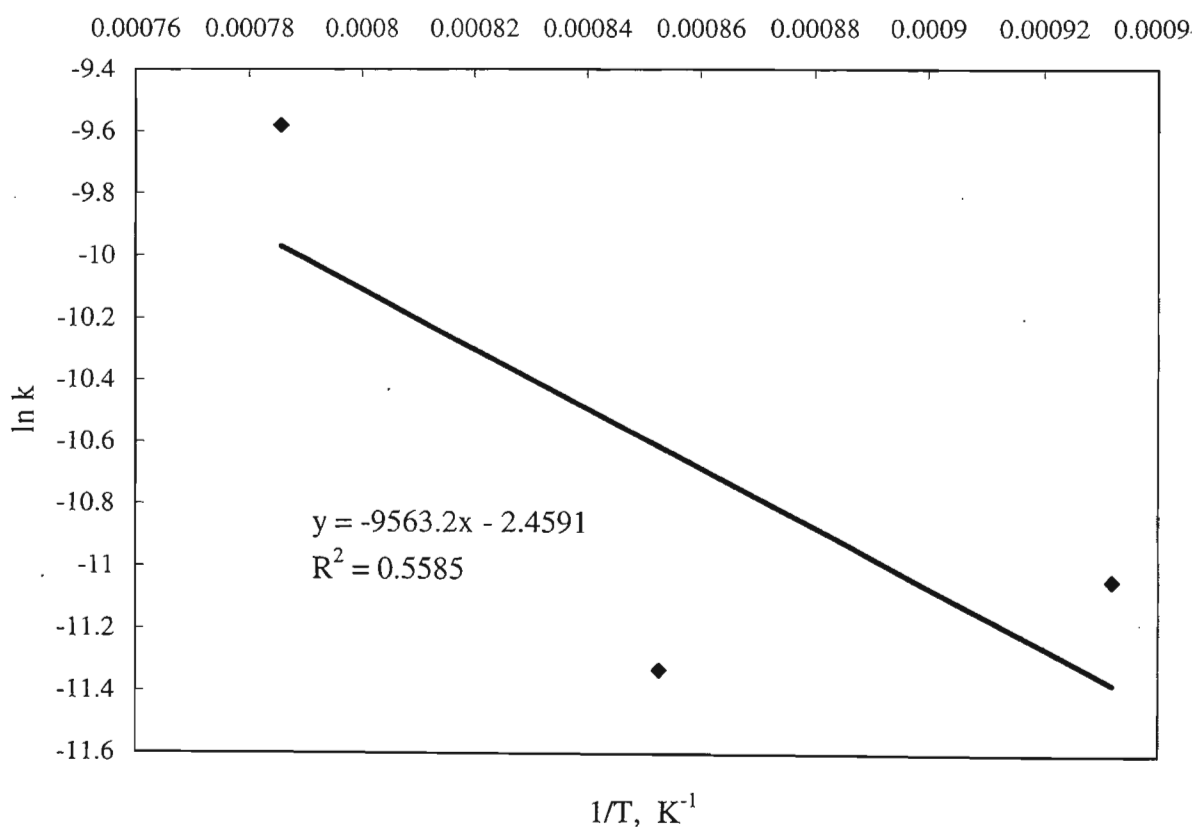
E = activation energy [kJ/kmol]

R = gas constant = 8.314 [kJ/kmol/K]

T = temperature [K]

The Arrhenius plot of $\ln(k)$ vs. $1/T$ can be seen in *graph 5.5*.

Graph 5.5 Arrhenius Plot



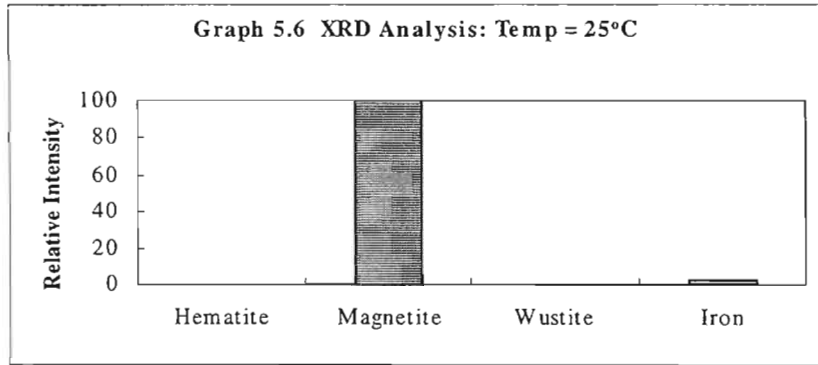
It is evident that the Arrhenius plot is inconclusive, i.e. a straight line is not obtained.

Force fitting a straight line gives,

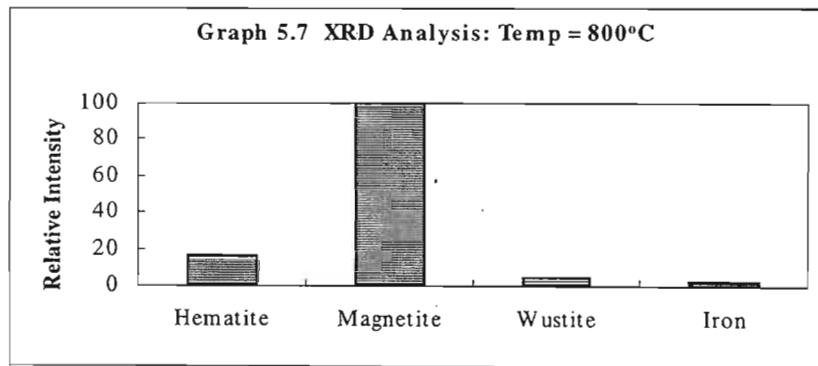
$$E = -9563.2 \times R = 80 \text{ kJ/mol}$$

$$A = \exp(2.4591) = 0.09 \text{ min}^{-1}$$

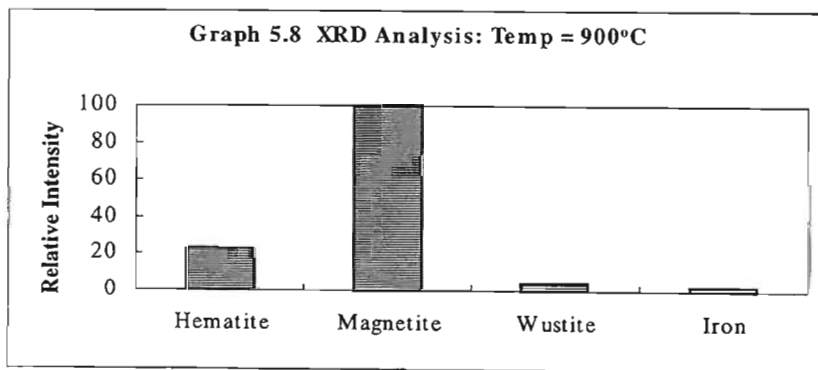
XRD analysis of the respective pellets can be seen in *graphs 5.6 – 5.9*. Elemental analysis of the pellets can be seen in *Table 5.1*.



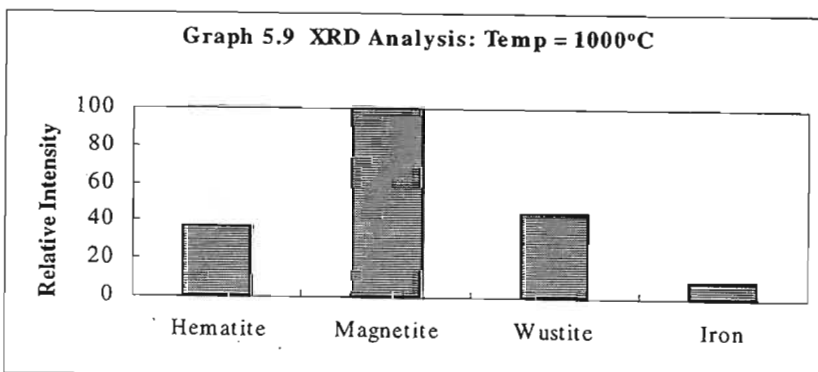
Appendix H,
rc10



Appendix H,
UNDR4



Appendix H,
UNDR3



Appendix H,
UNDR2

Table 5.1 *Mass Percent of Elements in Reduced Pellet*

	<i>1000°C</i>	<i>900°C</i>	<i>800°C</i>
C	36.79	33.91	38.91
O	17.31	17.66	19.64
Mg	0.62	0.64	0.67
Al	0.74	0.71	0.85
Si	0.93	0.85	1.01
P	0.00	0.00	0.04
S	0.19	0.15	0.17
K	0.00	0.00	0.01
Ca	0.57	0.51	0.47
Ti	0.39	0.39	0.39
Cr	0.06	0.08	0.06
Mn	0.08	0.00	0.00
Fe	42.32	45.10	37.77

5.3 Discussion of Thermobalance Tests

Thermobalance tests were performed to gain an indication of the time required for reduction of magnetite to metallic iron. The kinetics of the reaction needed to therefore be studied. To this end, the Swatantra (1990) thermogravimetric method was employed.

The fraction of reaction, f , was calculated for 3 different runs, i.e. 800°C, 900°C and 1000°C. Although the Ginstling – Brounshtein equation, i.e. the rate-determining model, did not produce straight lines, the different reaction rate constants, k 's, were estimated (*Graphs 5.2 – 5.4*). The Arrhenius plot (*Graph 5.5*) also proved inconclusive. If one had to force fit a straight line to the Arrhenius plot, an activation energy and pre-exponential factor of **80 kJ/mol** and **0.09 min⁻¹** respectively were obtained. This gives a k -value of **2.46 x 10⁻⁵ min⁻¹**, which is very low when compared to Swatantra (1990) who quotes a value of **3.33 x 10⁻⁴ min⁻¹** for an ore/coal system.

From the kinetic evaluation, it was evident that very little reduction took place. This was confirmed by XRD analysis (*Graphs 5.6 – 5.9*), which showed very little metallic iron being formed. The most significant amount of iron including wustite was obtained in the 1000°C run, which was expected. The other two runs, viz. 800°C and 900°C did not show much difference. The hematite that formed indicates the presence of oxygen. This could be the result the nitrogen being closed off after the experiment, but combustion and re-oxidation of the pellet continuing.

The elemental analysis (*Table 5.1*) obtained from Scanning Electron Microscope (SEM) also serves to confirm the fact that reduction progressed at a very slow rate. The oxygen content is high indicating significant amounts of hematite, magnetite and wustite being present.

The inconclusive results obtained from the Thermobalance and poor conversions of magnetite shown by the XRD and SEM analysis, indicates the pellet may not have been

at reaction temperature. Although the furnace temperature was maintained at the respective temperatures, the nitrogen entering the furnace could have hampered heat transfer to pellet. From *graph 5.1*, one could note that the furnace took approximately 2.5 hours to reach reaction temperature. Although this residence time is in itself quite long, the pellet could have taken longer to heat up. Another hindering fact could be that the pellets were inside a crucible made of refractory material, which has a very low heat transfer coefficient.

A way of reducing heating times could be to use an induction heater (to be discussed in greater detail in Chapter 6). Due to an oscillating magnetic field the heat can be concentrated to the pellet. The magnetic iron oxide would heat up via the changing magnetic field and would not be hampered by flow of inert gas. Heating times would be substantially decreased. If a susceptor were used, e.g steel, conduction and convection effects would also be induced to heat the pellet.

5.4 Conclusion

Thermogravimetric methods, viz. Swatantra (1990), were used in an attempt to establish kinetic parameters for the magnetite/coal system under study. Results proved inconclusive due to a long heating up period and possible ingress of oxygen while the sample was cooling. The mass loss occurred during the period in which the sample was heating up, making the model fitting meaningless.

The activation energy and pre-exponential factor of **80 kJ/mol** and **0.09 min⁻¹** respectively did not compare with Swatantra (1990) kinetics, i.e. activation energy and pre-exponential factor of **90.9 kJ/mol** and **2.76 sec⁻¹** respectively.

XRD and SEM analysis confirmed that very little reduction took place.

Chapter 6: Reduction in an Induction Furnace

6.1 Theory of Induction Heating

The simplified theory of induction heating states that a varying or changing current in a primary circuit can induce a current in a closed or secondary circuit (Khan, et al, 2000). The induced currents are used for heating of the components that act as a secondary circuit. Therefore, if a metal object is being supplied with an alternating current, a magnetic field is created, which in turn creates an induced current. This induced current heats the metal through its internal resistance (Vanderlinde and Su, 2002).

Fig. 6.1 shows the principle of induction heating.

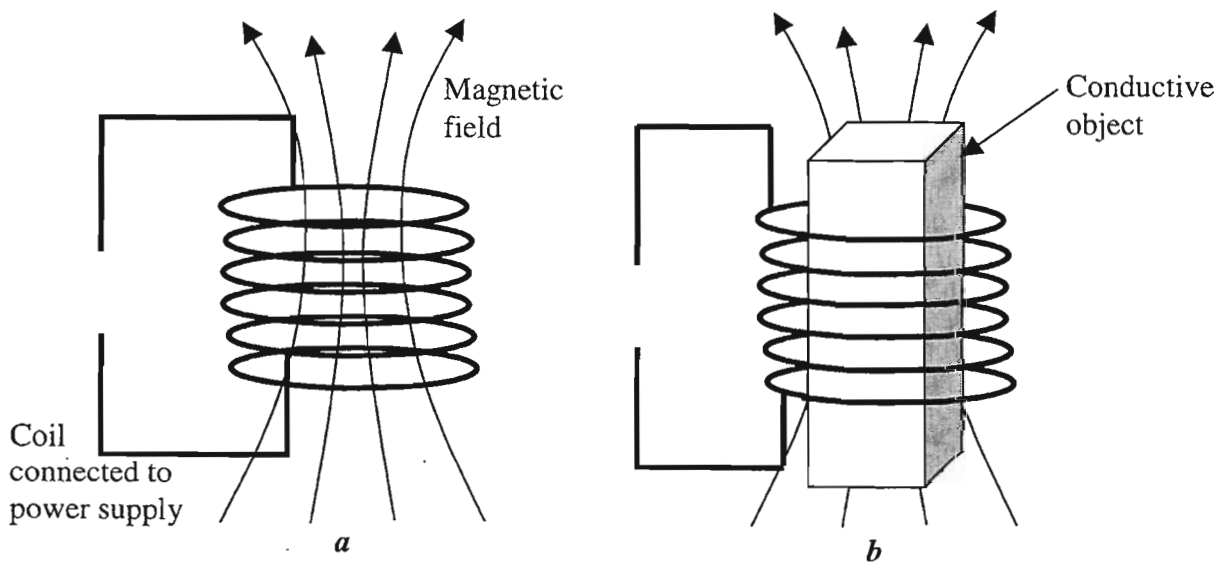


Fig. 6.1 Principle of Induction Heating (Khan, 2000, fig. 2)

When the coil is connected to a power supply, a varying magnetic field is generated by the current flow (fig. 6.1a). If an electrically conductive object is placed inside the coil (fig. 6.1b), the magnetic field induces an e.m.f. which creates an electric current in the object that flows opposite to that in the coil. By flowing against the resistance of the object, these eddy currents dissipate energy and produce heat (Khan, 2000).

The density of the induced current is greatest at the surface and reduces as it penetrates the surface. This is known as the penetration depth or skin depth of the induced current. The penetration depth depends upon the frequency of the alternating current being used.

Power supplies for the induction heater are frequency changers converting a.c. frequency to the desired single-phase power at the required frequency. Power supplies are often referred to as converters, invertors or oscillators but they are normally a combination of these. The converter converts the a.c. line input frequency to the direct current, and the invertors or oscillators change the direct current to single-phase alternating current.

6.2 Advantages of Induction Heating

Induction heating is an established process for heat treatment of ferrous alloys (Khan, 2000). It is commonly used for transformation hardening, tempering and annealing of steels and cast irons. The general advantages are summarized below (Anon, 2003).

- **Improved Quality** - contact-free process induces heat in the product without touching it, therefore, heat can be concentrated in a localized region. This implies that the metallurgical characteristics of the heated region are changed without affecting the rest of the material to a great extent.
- **Economically Viable** - energy efficient process converts up to 80% of the expended energy into useful heat to save costs. Although energy cost and capital cost may be higher for induction heating compared to oil or gas-fired furnaces, induction heating methods are more economical, more profitable per unit weight of the heated product. Due to fossil fuels becoming increasingly scarce in the future, electricity could become the major source of industrial energy.
- **Rapid Heating** - instantaneous heat allows for increased production and reduced distortion.

- **Environmentally Sound** - clean, non-polluting process produces no smoke, waste heat, noxious emissions, or noise. Induction heating is also more environmentally advantageous than traditional heating. Induction type electric furnaces radiate a lower level of heat than conventional furnaces.

- **Elimination of Contamination** – work-piece can be isolated in an enclosed chamber with a vacuum, inert or reducing atmosphere.

- **Process Repeatability** - if the temperature is accurately controlled uniform results are consistently achieved.

When considering the current process, from the tube furnace experimentation it was concluded that reduction of iron ore to iron does take place at 900°C in a mixed pellet of waste coal concentrate and fine magnetite, albeit a single pellet sample was used. Using the same environment as the tube furnace, i.e. inert atmosphere with a recycle stream of product gases, the reduction of the pellets needed to be scaled up to accommodate a batch of pellets. From the thermobalance experimentation, it was evident that the pellet took a long time to heat up to reduction temperature. Given enough time, i.e. more than 3 hours, a greater percentage of iron would have been produced.

An induction furnace would drastically reduce time taken to heat the pellet as it induces changing magnetic fields within the susceptor, i.e. a steel casing, which would result in rapid heating of the casing. The casing would in turn heat the mixed pellets to required temperature. The induction furnace would also allow for batch heating of an increased number of pellets.

6.3 Induction Furnace Set-up

A schematic of the induction heater is shown in *fig 6.2*. (The Induction Furnace can be seen in more detail in Appendix D1)

The Induction furnace to be used is the Mapham Induction Heater which supplies a maximum output power of 2.5 kW to the heating coils. The cooling water should have a maximum temperature of 26°C and a minimum flow-rate of 1.5 l/min (maintained via a rotameter, Calibration chart in Appendix F1), so as to cool the coils. The glass tube has a high temperature refractory lining so that the pellets, whilst being heated, would not be in contact with the glass tube. A distributor plate, which allows efficient flow of N₂, supports the pellets within the induction zone, during reduction. (N₂ rotameter calibration chart in Appendix F1)

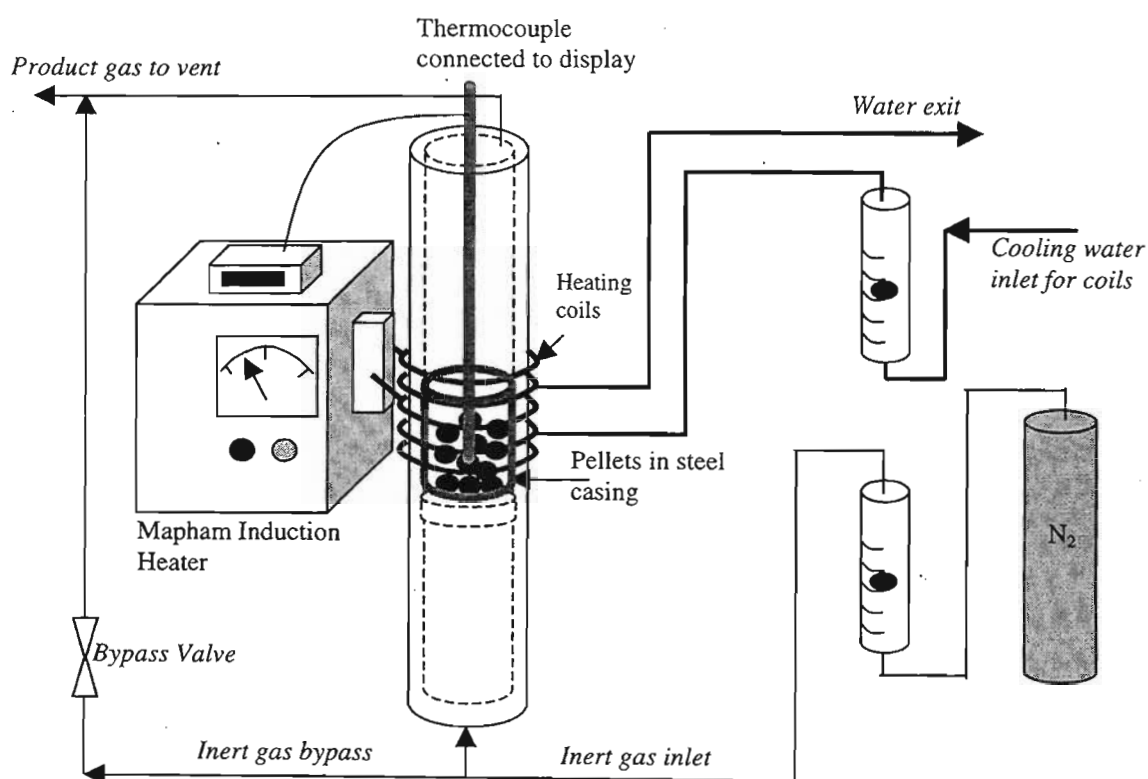


Fig. 6.2 Induction Furnace Experimental Set-up

The pellets used were mixed floated coal and magnetite fines, with a lignobond binder. The pellets were mixed in specific ratios of coal:magnetite depending on the experimental parameter being varied. A batch of around 500g of pellets was used in each run.

The furnace was maintained at a temperature of 900°C; therefore calibration of the equipment was firstly required (Heating rates can be seen in Appendix F2). This was done with the aid of a thermocouple, and gave an indication of time required for the pellet to reach reduction temperature. It was found that the optimum power of 1.2 kW heated the batch of pellets (500g) in a minimum time of approximately 20 minutes.

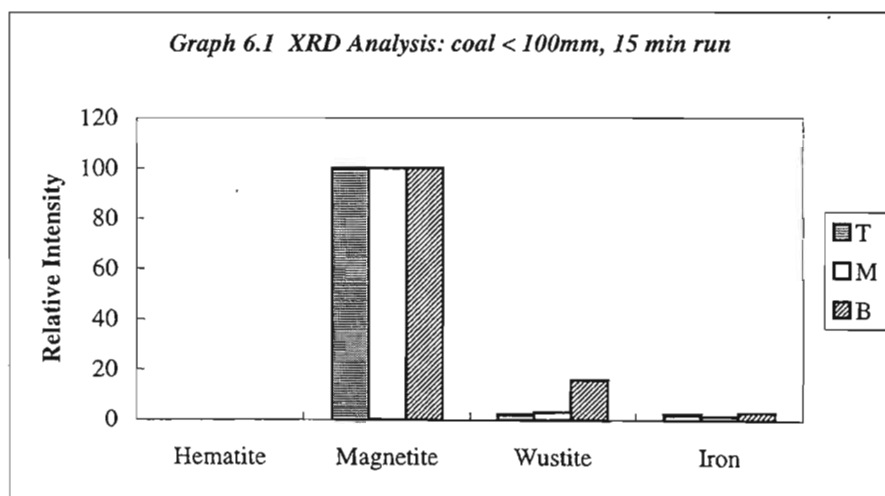
After each run 3 samples of pellets were analysed by XRD, for traces of hematite, magnetite, wustite and iron. SEM analysis was also performed and averaged for the 3 samples to acquire amounts of carbon and oxygen remaining.

(The Experimental procedure can be seen in Appendix D2.)

6.4 Results and Discussion of Induction Furnace Testing

6.4.1 Reduction of Pellets containing coal < 100 μm

The first set of experiments that were performed gave a standard indication for comparison with other experimentation. With reference to *graphs 6.1 – 6.3*, the coal used was of a coarser nature, i.e. < 100 μm (finer coal < 20 μm). The magnetite/coal ratio was 6:1, i.e. stoichiometric ratio. *T*, *M*, and *B* in the key indicate pellets taken from the *top*, *middle*, and *bottom* of induction heater respectively. These 3 samples were taken so as to gain an indication of the extent of reduction at the three different points, due to some pellets being heated at different rates.

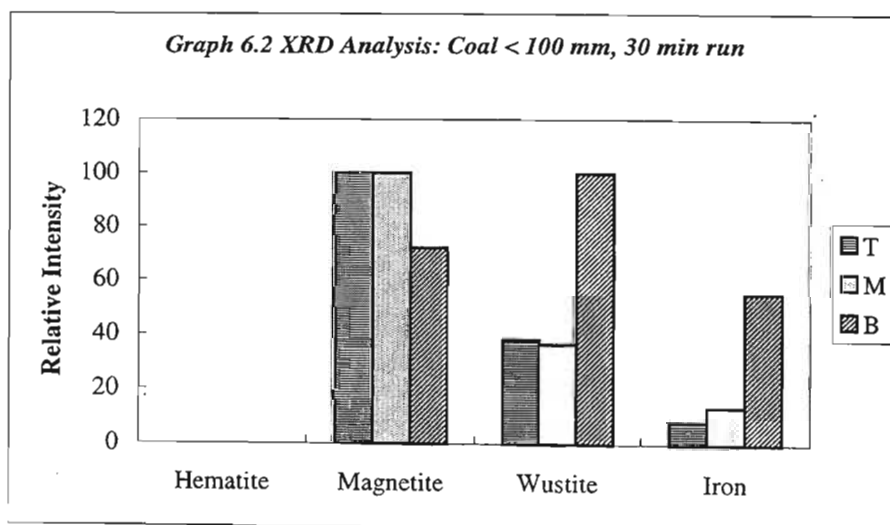


Appendix H,

T – UND1D4A

M – UND1D4B

B – UND1D4C



Appendix H,

T – UND1D5B

M – UND1D5C

B – UND1D5A

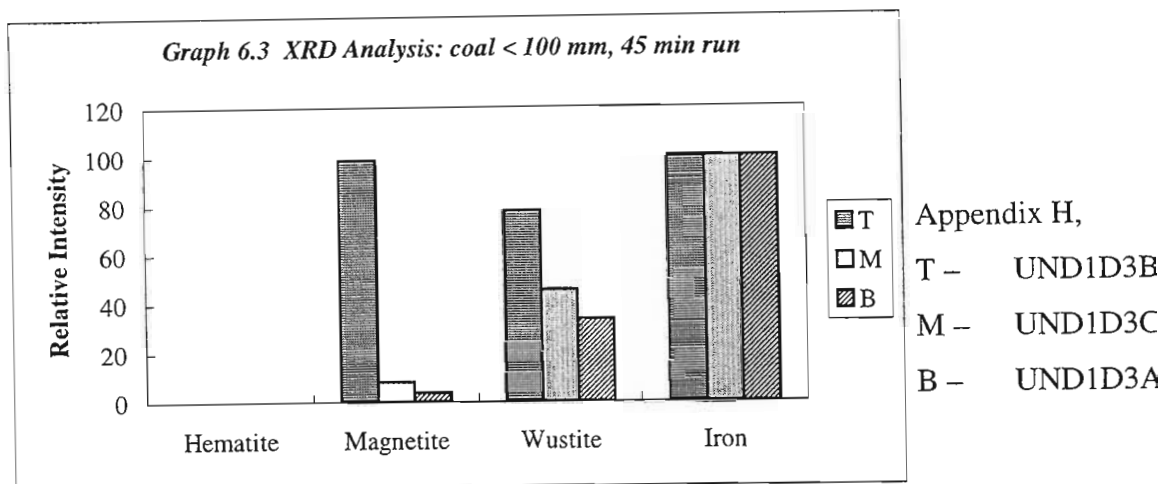


Table 6.1 SEM Elemental analyses of reduced pellets containing coal < 100 μ m

	Mass percent	
	15 min run	45 min run
C	26.58	23.26
O	17.50	14.09
Mg	0.72	0.73
Al	0.64	0.72
Si	0.72	0.80
P	0.00	0.00
S	0.13	0.14
K	0.00	0.00
Ca	0.58	0.64
Ti	0.62	0.70
Cr	0.00	0.00
Mn	0.00	0.00
Fe	52.51	58.93

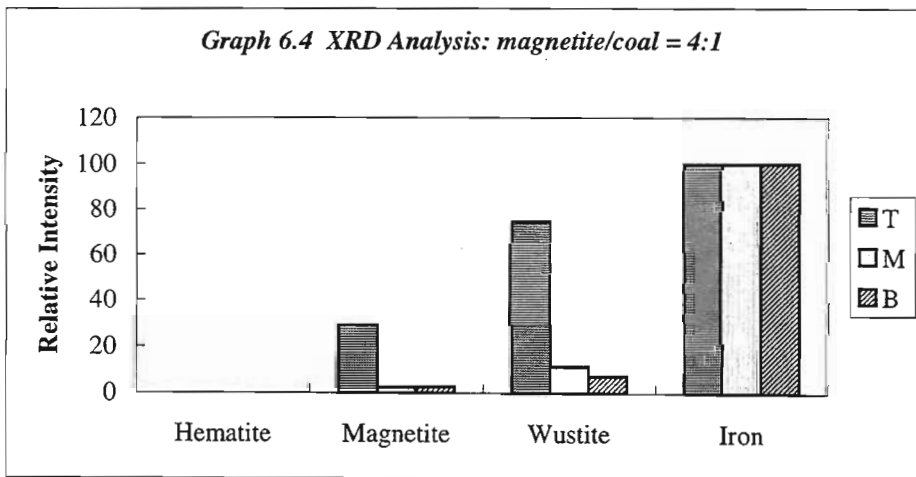
From the graphs it could be seen that very little reduction took place in the initial 15 minutes. However with time, reduction proceeds showing more wustite in the 30 minute run and more metallic iron in the 45 minute run. This length of time was not sufficient however, as indicated by the magnetite and wustite still present in the 45 minute run.

If one concentrated on the individual sampling points, it was apparent that the bottom sample always indicated the greatest degree of reduction. *Graph 6.2* shows an increase in wustite from top to bottom, implying more magnetite was being reduced to wustite from

top to bottom respectively, after 30 minutes. Graph 6.3 shows a decrease in wustite from top to bottom, implying more wustite is being converted to metallic iron, after 45 minutes. This was possibly due to the bottom sample being in contact with the steel susceptor while the top sample was furthest from the susceptor. The bottom sample, therefore, reached reaction temperature first resulting in the longest duration for conversion of magnetite.

The insufficient residence time was also indicated by the SEM elemental analysis (*table 6.1*), which shows substantial amounts of carbon still present, even in the 45 minute run.

6.4.2 Effect of Varying Magnetite/Coal Ratios

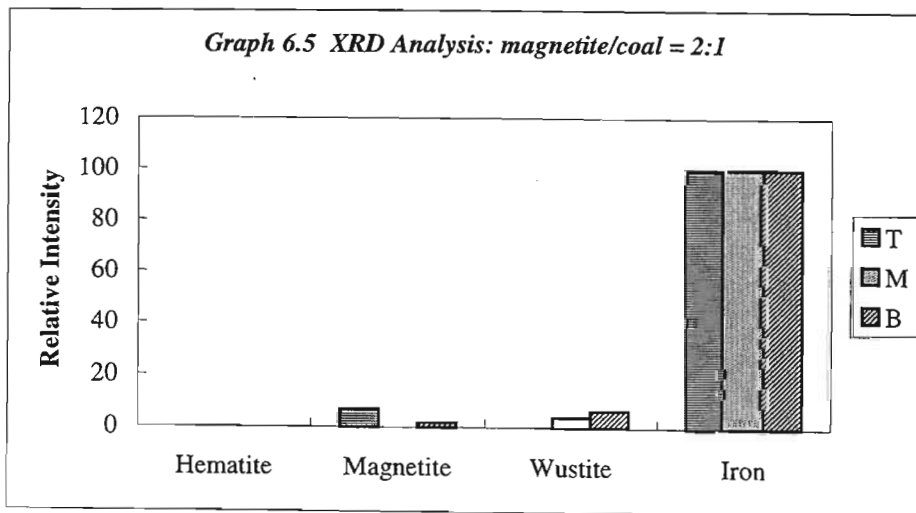


Appendix H,

T – UND1D7A

M – UND1D7E

B – UND1D7C



Appendix H,

T – UND1D6A

M – UND1D6E

B – UND1D6C

Table 6.2 SEM Elemental analyses of reduced pellets, magnetite/coal = 2:1

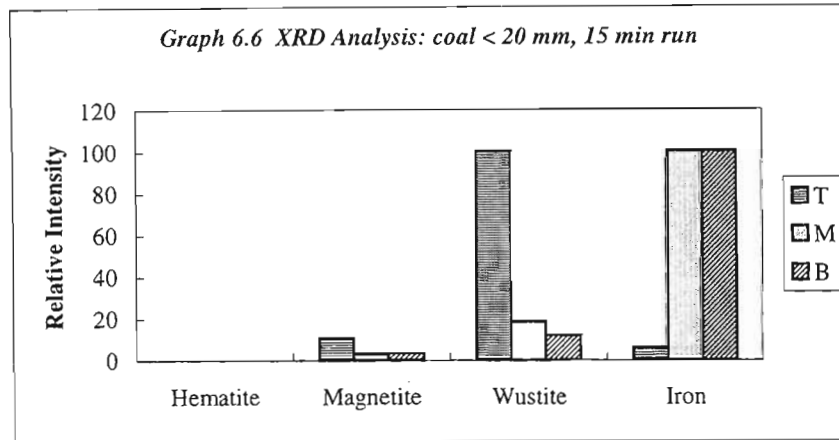
	Mass Percent
C	47.48
O	13.55
Mg	0.98
Al	1.55
Si	1.70
P	0.05
S	0.16
K	0.02
Ca	0.54
Ti	0.85
Cr	0.07
Mn	0.14
Fe	32.92

Graphs 6.4 and *6.5* show the effect of varying the feed ratios on the reduction process, i.e. magnetite/coal = 4:1 and 2:1 respectively. Both experiments were run for 15 minutes, with the coal < 100 μm and flow of nitrogen being 200 ml/min.

If one compared *graph 6.4* to *graph 6.1* (also 15 minute run), it could be seen that the conversion of magnetite increased considerably. The reason for this could be the excess amount of coal available increased the probability of magnetite being in intimate contact with the carbon in coal for direct reduction as well as maintenance of a high CO/CO₂ ratio. As expected the pellet sample furthest from the steel susceptor showed the most magnetite and wustite being present.

Addition of more coal into the reacting system (*graph 6.5*) increased the conversion of magnetite and wustite that formed. The graph shows that this system possessed the most potential for reduction of magnetite. The magnetite remaining and wustite formation were at a minimal. The elemental analysis (*table 6.2*), however, indicates that this system could be optimised further. The oxygen content of the pellets signified that magnetite and wustite were still present in the pellet. The carbon content of the pellet was expected due to the excess carbon used and the run only lasting 15 minutes.

6.4.3 Effect of Varying Coal Particle Size

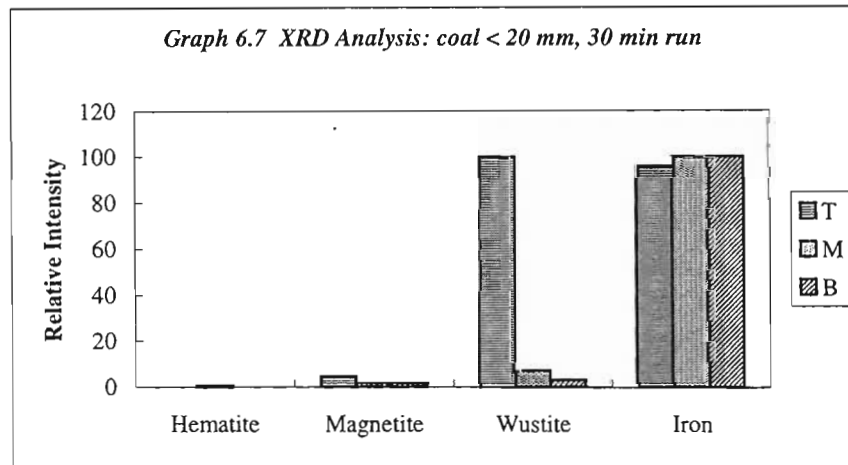


Appendix H,

T – id2t

M – id2m

B – id2b



Appendix H,

T – id1t

M – id1m

B – id1b

Table 6.3 SEM Elemental analyses of reduced pellets containing coal < 20 μm

	Mass Percent, 30 min run
C	21.34
O	12.73
Mg	2.27
Al	1.07
Si	1.14
P	0.08
S	0.16
K	0.00
Ca	0.95
Ti	1.11
Cr	0.53
Mn	0.00
Fe	58.61

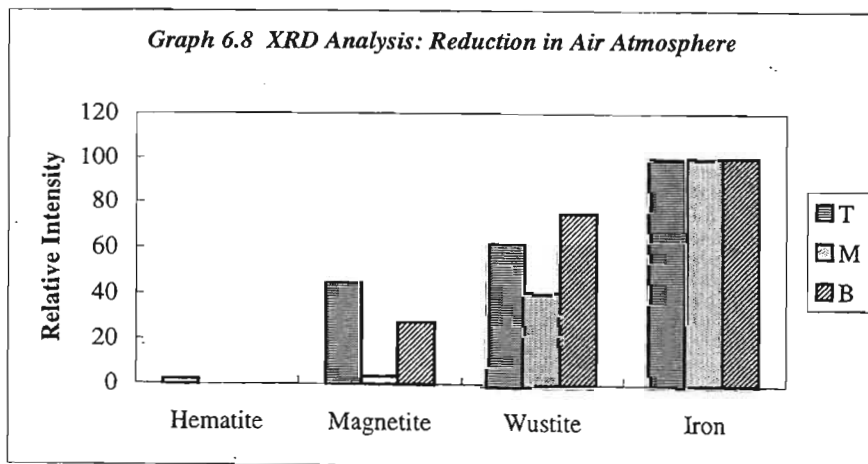
Graphs 6.6 and 6.7 show the effect of varying the coal particle size on the reduction process, i.e. coal < 20 μm . Both experiments were run for 15 and 30 minutes respectively, with the magnetite/coal = 6:1 and flow of nitrogen being 200 ml/min.

Comparing graph 6.6 to graph 6.1 (coal < 100 μm), it was observed that the conversion of magnetite was increased substantially. This was undoubtedly due to the difference in size of the coal particles because all other experimental parameters are the same. The coal < 100 μm and the coal < 20 μm have specific surface areas of 0.37 m^2/g and 1.44 m^2/g respectively (Chapter 3.2). This significant increase in surface area of the coal < 20 μm allows for a larger reacting surface to contact the magnetite.

Graph 6.7, showing a 30 minute run, indicates a typically greater conversion. Considering kinetics reported by Reddy, et al (1991) a magnetite conversion of 70 – 80 % was expected after 30 minutes, compared to a conversion of 40 – 50 % after 15 minutes.

The elemental analysis (table 6.3) indicates that the reaction did not proceed to completion. However, the carbon and oxygen present in the pellet for the 30 minute run for coal < 20 μm (C = 21.34, O = 12.73), was less than that present in the pellet for the 45 minute run for coal < 100 μm (C = 23.26, O = 14.09). This signified that a better reducing agent was obtained with a finer coal source.

6.4.4 Effect of Using Air Atmosphere



Appendix H,
 T – UND1D8A
 M – UND1D8B
 B – UND1D8C

Table 6.4 SEM Elemental analyses of pellets reduced in air atmosphere

	Mass Percent
C	18.48
O	14.82
Mg	0.95
Al	0.74
Si	0.78
P	0.02
S	0.11
K	0.00
Ca	0.74
Ti	1.00
Cr	0.03
Mn	0.17
Fe	62.15

Graph 6.8 shows the effect of using air instead of nitrogen on the reduction process. The experiment was run for 15 minutes, with the magnetite/coal = 6:1. Coal < 20 μm was used as it was found to be a better reducing agent than coal < 100 μm (*Chapter 6.4.3*).

The current set-up resembled the blast furnace process, whereby air at reaction temperature is blasted into the furnace. It was intended that the oxygen in air would promote combustion of carbon to carbon dioxide, and consequently the boudouard reaction producing carbon monoxide, i.e reaction of CO_2 with C (*Reactions 2.1a and b*). The carbon monoxide would then reduce magnetite via indirect reduction. This set-up was investigated due to indirect reduction playing the major role in reduction of iron oxide by coal (Haque and Ray, 1995).

However, comparing *graph 6.8* to *graph 6.6* (same parameters except for air atmosphere instead of nitrogen), it can be seen that although reduction did proceed, the presence of oxygen in air induced re-oxidation of metallic iron to wustite and subsequently magnetite. The temperature of the coal was not sufficient to promote the instantaneous combustion to CO_2 , and thereafter the boudouard reaction, as is observed in the blast furnace. It should be noted that the air entering the blast furnace is blasted in at around

1800°C (Biswas, 1981), while the current induction heater is only run at 900°C. This temperature, however, is sufficient for the re-oxidation of the iron.

A comparison of *table 6.4* with *table 6.3* shows that the mass percent of carbon remaining in the pellets reduced in an air atmosphere was less than the carbon in the nitrogen atmosphere. Also *table 6.3* and *table 6.4* indicate mass percentages for a 30 and 15 minute run, respectively. A reason for the decrease in carbon content could be due to combustion of coal. However, the CO₂ that was formed could have left the system without converting to CO, due to the much lower temperature of 900°C. The increase in oxygen level was expected due to re-oxidation of the metallic iron.

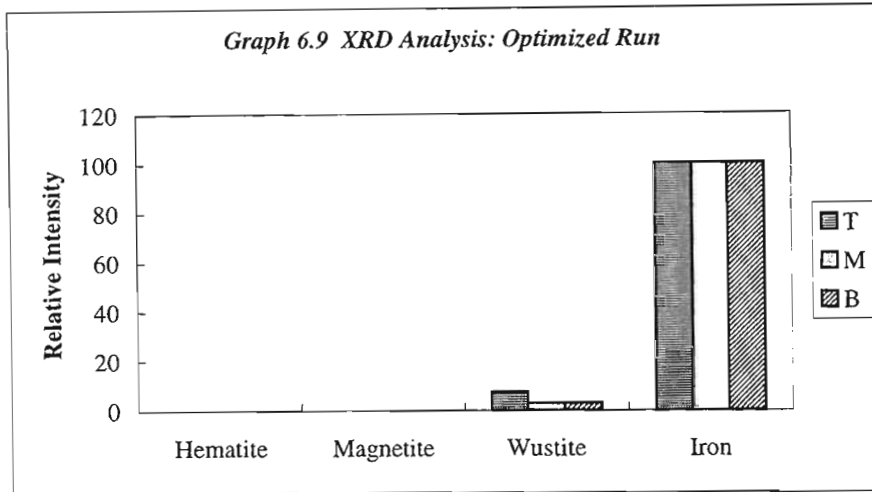
6.5 Optimising Reduction in Induction Furnace

6.5.1 Parameters for Optimised Run

From the induction experimentation thus far completed, an optimised run could be achieved using the following parameters for a 500g batch of pellets:

- Power Input = 1.2 kW (to reach 900°C after 20 minutes; thereafter periodic power input for temperature control at 900°C)
- Residence Time = 1 hour (after 20 minutes of heating time)
- Magnetite/Coal ratio = 2:1, on a mass basis
- Particle size of coal < 20 µm
- Initial purging of induction heater with Nitrogen.

6.5.2 Results and Discussion of Optimised Run



Appendix H,
 T – UND1D9A
 M – UND1D9B
 B – UND1D9C

Table 6.5 SEM Elemental analyses of pellets for Optimised Run

	Mass Percent
C	3.95
O	3.50
Mg	0.00
Al	2.69
Si	3.31
P	0.00
S	0.33
K	0.00
Ca	1.36
Ti	1.11
Cr	0.00
Mn	0.23
Fe	83.53

The optimised run showed significant improvement to the reduction process, compared to results previously achieved. The XRD analysis (*Graph 6.9*) shows traces of wustite present and no magnetite present. Due to a solid product being formed containing large amounts of reduced metallic, the product will now be referred to as DRI. (SEM images can be viewed in Appendix G.)

Using the elemental analysis (*Table 6.5*), an approximate mass balance could be performed to get the mass percent of DRI produced. This could be done because the oxygen available could be in wustite (FeO) or in the slag oxides (SiO₂, Al₂O₃, CaO, etc). If one assumes that *all* the oxygen was either wustite or in the slag, this gives the lower and upper limits of the percentage conversion respectively. This calculation procedure could not, however, be used in the previous experimentation, due to both wustite and magnetite being present in uncertain ratios. (Calculations can be viewed in Appendix D3.)

Assuming that all the oxygen was in the slag phase, a percentage conversion of magnetite to DRI of approximately 100% was gained. This was, however, improbable as the XRD analysis show traces of wustite present. Assuming that all the oxygen was in the wustite (FeO) phase, the calculated ratio of FeO:DRI was 0.15:0.85. This was also improbable due to oxygen certainly being present in the slag phase. The actual ratio of FeO:DRI was therefore between the limits of 0.15:0.85 and 0:1.

Therefore, a single pellet comprised approximately 75 – 80% metallic iron, 5 – 15% wustite, 5 – 10% slag, and 4% carbon. This compares well with the composition of pig iron, which contains up to 5% carbon (Pearcy and Davenport, 1979). Even though excess coal was fed to the system, most of the carbon was used up with the increase in residence time. The excess of coal used implies that carbon does not limit the process.

The residence time of 1 hour, however, does not compare well with some DRI processes, viz. the Fastmet Process, which has a residence time of 6 – 12 minutes. It should be considered, though, that the Fastmet mixed pellets contains 5 times more than the stoichiometric amount required, while the current process contains a reduced amount of 3 times stoichiometric requirement.

6.5.3 Slag Formation

Using the elemental analysis (*table 6.5*) the percentage slag present can be calculated. It was assumed that the FeO:DRI ratio of the pellets were 0.1:0.9 on average. To gain an indication of maximum possible slag present, all the oxygen was assumed to be in the slag phase. (Calculations can be viewed in Appendix D3.) The slag was calculated to be **0.17 ton / ton DRI**.

If one compares this to conventional blast furnaces, i.e. 0.2 – 0.4 tons / ton DRI, a cleaner process is apparent. It should, however, be considered that in the blast furnace process, limestone is deliberately added as flux. This allows for efficient removal of slag from the iron phase. The molten slag also serves to cover the molten iron produced, thereby protecting it against re-oxidation.

6.5.4 Energy Consumption of Induction Furnace

A direct comparison of the feasibility of the current reduction process to other DRI processes is the energy consumption.

As reported in *Chapter 6.3*, a power output of 1.2 kW heated the batch of pellets (500g) in a minimum time of approximately 20 minutes. Including a residence of 1 hour, the energy consumption of the induction heater was found to be **9.94 GJ / ton DRI**. It should be noted that after 20 minutes, the induction heater had to be manually operated so as not to overshoot the operating temperature. This implied that the heater had to be switched off during certain periods. Therefore, this value is based on 20 minutes to heat to operating temperature of 900°C and 30(approximate value) minutes of heating time. However, if one considers the primary energy that is required to generate electricity in the first instance, thereby taking into account the efficiency, the actual energy consumption is undoubtedly higher. Due to the energy value required for heating of DRI processes not being available in literature, this value cannot adequately be compared. Heat losses in small-scale tests are also more significant. It should be noted, however,

that the current process runs at a lower temperature as compared to most DRI processes, i.e. 900 – 1200°C.

Using a coal calorific value of 30.9 GJ / ton (Anon, 2001), the coal energy consumption was found to be **23.71 GJ / ton DRI**. (Calculations can be viewed in Appendix D4.) From *Table 2.6*, the blast furnace calorific consumption amounts to approximately 17.9 GJ / ton Hot Metal. This value is based only on coke consumption, and does not consider energy consumed for heating the furnace to around 1800°C, i.e. almost double the temperature of the current process. Even though, the coal consumption maybe higher, coke is more expensive and in short supply compared to waste coal. The calorific consumptions of coal based processes for production of DRI range between 15 and 25 GJ / ton DRI. These values are also only based on consumption of coal and do not include heating to operating temperature. The coal consumption of the induction process under consideration may, therefore, compare favourably to current DRI processes.

The induction process cannot be compared fairly to direct smelting processes, as these processes obviously require substantially large amounts of energy to reduce the iron oxide as well as melt it. The fuel required is greater than 30 GJ / ton Hot Metal, not considering energy required to melt the metal.

6.5.5 *Advantages of the DRI Processes*

From the discussions above, it is apparent that this invention has certain advantages over other DRI processes. It would be most suitable to relatively small and flexible applications.

As seen above (Chapter 6.2), the induction heat has a number of advantages over conventional heating techniques. The use of the induction heater in the current invention reduces amount of coal fed in, as coal is not needed as a fuel but solely as a reducing agent. The heater provides all energy required to heat pellets to reduction temperature.

Due to the operating temperature being only 900°C, excessive quantities of high temperature refractory material is not needed as in blast furnace processes, i.e. processes run in excess of 1400°C. This would reduce cost of refractory material to a great extent. The current process, for example, uses a silica tube as the casing with a refractory lining (thickness = 10mm) capable of withstanding a temperature of 1200°C.

If the current invention was to be scaled-up for industrial applications, the capacity of the induction heater could be modified, by manufacturers, to handle industrial amounts of feed. For example, Lepel manufactures (Anon, 2003), which offers one of the widest selections of induction heating power supplies in the industry, can provide power supplies with output power ranging from 500 W to 2500 kW at frequencies ranging from 10 kHz to 30 MHz. The coils and refractory casing could also be custom-designed for optimum penetration depth and design capacity, respectively. It should be noted that the Mapham Induction Heater provides a maximum power output of 2.5 kW at 3 kHz. Only 1.2 kW was required for a 500g sample.

6.5.6 *Uses of the DRI Process*

Due to the product being a solid DRI of about 75 - 80% purity, further processing is obviously required to produce a molten hot metal like the blast furnace product pig iron. This process, in effect, produces a pre-reduced pellet.

This process could therefore be used as pre-reduction step before final reduction and melting of the finished product. The Corex and Fastmet processes both have similar pre-reduction steps, albeit reduction of the pellets occurs in a shaft and rotary hearth furnace respectively. In fact, reduction via induction heating, as in this process, if proven on an industrial scale could provide a more easily controlled, lower temperature process.

As with both the commercial processes, a melter can thereafter be used to produce hot metal. Due to the already significant amount of metallic iron already present in the feed to the melter, a minimal amount of coal could be used to reduce un-reacted iron oxides.

6.6 Conclusion

The Mapham Induction heater supplying a power output of 1.2 kW was sufficient to heat 500g of mixed pellets to 900°C in 20 minutes. XRD and SEM analysis reported the following conclusions:

- A better reducing agent was obtained when a smaller particle size of coal was used, of the order $< 20 \mu\text{m}$.
- Increasing the coal/magnetite feed ratio, in this case from 1:6 to 1:2, increases the degree of reduction. Depletion of carbon would therefore not limit the process.
- Reduction in an air enhances the re-oxidation of reduced iron.

Setting optimum parameters, an optimized run gave a product DRI comprising approximately 75 – 80% metallic iron, 5 – 15% wustite, 5 – 10% slag, and 4% carbon.

Energy consumption based on coal usage amounted to 23.71 GJ/ton DRI, which compares with the calorific consumptions of most coal-based processes. Energy consumed during induction heating amounted to 9.94 GJ/ton DRI, based on output power from induction heater only and not considering the efficiency of the primary energy to generate electricity.

The DRI process encompassing induction heating showed industrial potential. If scaled up and proven on a pilot scale, this process could produce pre-reduced pellets, which could be used as feed for smelting processes. These pre-reduction stages are common in DRI processes, e.g. Corex and Fastmet.

Chapter 7: Conclusion and Recommendations

7.1 Conclusion

A new low temperature process for iron-making, using mixed pellets of fine waste iron oxide and fine domestic coal, with a natural carbonaceous binder (lignobond), was investigated.

The pellet suitability to the reduction process was initially investigated to observe the effectiveness of the lignobond binder. Strength test evaluations of the two types of pellets, viz. pellets comprising coal <100 μ m and coal < 20 μ m, showed that the pellet strength was above the minimum limit of 22N for industrial blast furnaces. Higher temperatures resulted in increase in pellet strength. Drop strength tests, resistance to abrasion tests, and moisture content tests, also compared favourably with literature values. Lignobond, therefore, revealed the desired effect as a pellet binder.

From the preliminary tube furnace it was evident, upon pellet analysis by X-Ray Diffraction, that reduction of the magnetite occurred at 900°C, provided oxygen was purged from the system. This allowed the CO to further reduce unreacted magnetite, seeing that indirect reduction plays the major role in the reduction process. Upgrading of waste coal by flotation, to remove gangue material, increased the conversion of magnetite, due to increased levels of carbon. Mixing of the pellets also allowed for more intimate contact between the coal and magnetite. It was noticed that, increasing the residence time of the mixed pellet allows the intermediate iron oxides, e.g. wustite, to reduce further to metallic iron.

Thermogravimetric methods were used to establish kinetic parameters for the magnetite/coal system under study. Results proved inconclusive due to the activation energy and pre-exponential factor of approximately 80 kJ/mol and 0.09 min⁻¹ respectively did not compare with Swatantra (1990) kinetics, i.e. activation energy and pre-exponential factor of 90.9 kJ/mol and 2.76 sec⁻¹ respectively. It was concluded that the pellet took extremely long to heat up and, in effect, was not at

reduction temperature. XRD and SEM analysis confirmed that very little reduction took place.

Induction heating was found to solve the problem of slow heating times. The Mapham Induction heater supplying a power output of 1.2 kW was sufficient to heat 500g of mixed pellets to 900°C in 20 minutes. Induction furnace testing, upon pellet analysis by XRD and SEM illustrated the following:

- A better reducing agent was obtained when a smaller particle size of coal was used, of the order < 20 µm as compared to coal < 100 µm.
- An increase in the coal/magnetite feed ratio, from 1:6 to 1:2, increased the degree of reduction. Although the coal consumption was 3 times more than the stoichiometric requirement, it was still less than coal consumption of some DRI processes, e.g. Fastmet.
- Reduction in an air atmosphere induces the re-oxidation of reduced iron.

Optimization of the induction process gave a product DRI comprising approximately 75 – 80% metallic iron, 5 – 15% wustite, 5 – 10% slag, and 4% carbon.

Energy consumption based on coal usage amounted to 23.71 GJ/ton DRI, which compares with the calorific consumptions of most coal-based processes, i.e. coal consumption between 15 and 25 GJ/ton DRI. Energy consumed during induction heating amounted to 9.94 GJ/ton DRI, as electricity. Larger-scale tests should result in significant reductions in power consumption.

The use of the induction heater has a number of advantages over conventional heating methods. Coal consumption would be significantly decreased as it is used only for reduction purposes and not as a fuel. Cost of refractory material would also be reduced as the process is run at a lower temperature.

The DRI process encompassing induction heating showed industrial potential, and if proven on a pilot scale could produce pre-reduced pellets, which could be further

processed to pig iron. This process is in effect a pre-reduction stage, which is common in DRI processes, e.g. Corex and Fastmet.

7.2 Recommendations

It is initially recommended that modifications be made to the laboratory induction heater set-up and process parameters to further optimise the process. These include:

- Replacing the tube with higher temperature material so that experimentation at higher temperatures could be performed. This may serve to reduce reduction times.
- A temperature control unit could be attached to the thermocouple and display unit to allow for automatic control of the temperature.
- Seeing that coal consumption is 3 times the stoichiometric requirement, the waste feed coal could be re-floated a few times to increase carbon content. This should also reduce slag formation.
- Reduction of hematite could also be tested.
- The induction heater could be set-up to accommodate a continuous process.

Thereafter, scale-up of the process to pilot plant scale needs to be implemented to test the efficiency of the process industrially.

References

- ACTED Consultants, (1999), "Direct Reduced Iron and Iron Ore", Chemlink Pty Ltd, www.chemlink.com.au/
- Anon, (1990), "The Relationship between the Degree of Reduction (α) and the Fraction of Reaction (f) during Reduction of Ore-Coal Mixture", *ISIJ International*, Vol. 30, No 11, p 997 – 999.
- Anon, (2001), "Estimated average gross calorific values of fuels in 2001", www.dti.gov.uk/energy/inform/calvalues.pdf.
- Anon, (2001), "Preliminary Energy Outlook for South Africa", Energy Research Institute, Dept of Mechanical Engineering, UCT, Rondebosch, www.dme.gov.za/energy/iep.pdf.
- Anon, (2003), "Bentonite", EUBA – The European Association of the Bentonite Producers, IMA – Europe, Belgium, www.ima-eu.org/euba.html.
- Anon, (2003), "Induction Heating", Lepel, <http://inductionheating.com/>.
- Bates P., Muir A., (2000), "HIs melt – Low Cost Iron Making", Gorham Conference June 2000, Commercialising New Hot Metal Processes – Beyond the Blast Furnace, HIs melt Corporation Australia.
- Benson S.A., Sondreal E.A., Hurley J.P., (1995), 'Status of coal ash behaviour research', *Fuel Processing Technology*, Vol. 44, p 1 – 12.
- Biswas A.K., (1981), "Principles of Blast Furnace Ironmaking", Cootha Publishing House, Brisbane.
- Burchill P., Hallam G.D., Lowe A.J., Moon N., (1994), "Studies of colas and binder systems for smokeless briquettes", *Fuel Processing Technology*, Vol. 41, p 63 – 77.

-
- Burgo J.A., (1999) "The Manufacture of Pig Iron in the Blast Furnace", Chapter 10, AISE Steel Foundation, Pittsburgh, www.aise.org/newpubs/ironchap%2010.pdf.
- Cheeley R.B., (1999), "Gasification and the Midrex Direct Reduction Process", Midrex 3rd Quarter, Midrex Direct Reduction Corporation, www.midrex.com.
- Danloy G., Mignon J., Munnix R., Dauwels G., Bonte L., (2002), " A Blast Furnace Model to Optimize the Burden Distribution", Centre for Research in Metallurgy, Belgium.
- Dutta D.K., Bordoloi D., Bororthakur P.C., (1997), "Investigation on reduction of cement binder in cold bonded pelletization of iron ore fines", *Int. J. Miner. Process.*, Vol. 49, p 97 – 105.
- Els J., (2001), Chapter: "Next Generation Developments in the Ferrous Industry", " School Pyrometallurgy: Current Issues and Future Trends", The South African Institute of Mining and Metallurgy, Mintek, Randburg.
- Esdale J. D., Motlagh M., (1991), "Calculation of equilibrium diagrams for direct reduction of iron ore", *Ironmaking and Steelmaking*, Vol. 18, No 6, p 423 – 429.
- Feinman J., (1999), "Direct Reduction and Smelting Process", Chapter 11, AISE Steel Foundation, J. Feinman and Associates, Inc., Pittsburgh, www.aise.org/newpubs/ironchap%2011.pdf
- Fowkes N., (1997), "The reduction of iron ore pellets in the Fastmet process", Mathematics Department, University of Western Australia, Australia.
- Gielen D., (2002), "CO₂ removal in the iron and steel industry", National Institute for Environmental Studies, Japan.
- Gilchrist J.D., (1980), "Extraction Metallurgy", Second Edition, Pergamon Press, UK.

-
- Habashi F., (1969), “ Principles of Extractive Metallurgy”, Vol. 1, Gordon and Breach Science Publishers, Inc., p 148 – 164.
- Habermann A., Winter F., Hofbauer H., Zirngast J., Schenk J.L., (2000), “An Experimental Study on the Kinetics of Fluidised Bed Iron Ore Reduction”, *ISIJ International*, Vol. 40, No. 10, p 935 – 942.
- Haque R., Ray H.S., (1995), “Role of Ore/Carbon Contact and Direct Reduction in the Reduction of Iron Oxide by Carbon”, *Metallurgical and Materials Transactions. B*, Vol. 26B, p 400-401.
- Haque R., Ray H.S., Mukherjee A., (1991), “Fluidized Bed Reduction of Iron Ore Fines by Coal Fines”, *ISIJ International*, Vol. 31, No. 11, p 1279 – 1285.
- Innes J.A., (1998) World Intellectual Property Organization (WIPO), Patent No. WO9827239A1: “Direct reduction of metal agglomerates”.
- International Agency for Research on Cancer (IARC), (1998), “Coke Production”, France, www.iarc.fr.
- Jaroslav SRB., Zdenka R., (1988), “Pelletization Of Fines”, Elsevier Science Publishers, New York.
- Jones R. T., (2001), “Iron and Steel”, www.science.murdoch.edu.au
- Jyrki Heino, Hannu Makkonen, Leena Laitila, Jouka Hatkki, Esko Poylio, (2000), “Recycling or utilisation of dust, scales and sludge from steel industry”, www.cc.jyu.fi/helsie/pdf/heino.pdf
- Kang S.M., Joo S., Min D-J., Lee I-O., (1996), “Simultaneous Behaviour of Pulverized Coal Char Combustion and Fine Oxide Reduction by Injecting the Mixture of Coal Char and Iron Oxide”, *ISIJ International*, Vol. 36, No.2, p 156 – 163.
- Kawasaki Steel 21st Century Foundation, (2001), “An Introduction To Iron and Steel Processing”, Chapter 6, www.kawasaki-steel-21st-cf.or.jp.

-
- Khan S., Ahamed M., Khan M.A., ul-Haq A., (2000), "Innovative Applications of Induction Heating for Selective Heat Treatment", *Quarterly, Science Vision*, Vol. 5, No. 4, p 14 - 19.
- Kirk W.S. (1997), "Iron Ore – Magnetite", U.S. Geological Survey, Mineral Commodity Summaries.
- Lignin Institute, (1991), www.lignin.info.
- Lungen H.B., (2001), "State of the Art and Future of the Blast Furnace", Paper presented at the 35th Meeting of the IPIS, Berlin, www.pig-iron.com/Informationen/images/Luengen.pdf.
- Martinis A., Bueno H., Benedetti G., (2000), "The Danarex high kinetic direct reduction process", *MPT international*, Vol. 23, No. 2, p 40 – 44.
- Minerals Bureau, (2001), "Producers of Iron Ore", Directory D8/2001, www.dme.gov.za/publications/pdf/project_research/minerals/d8_2001/d8_2001-02.pdf
- Moore C., (2001), "120 Years in Pig Iron", 60th Electric Furnace Conference, International Pig Iron Secretariat, Dusseldorf, Germany.
- Munnix R., Borlee J., Steyls D., Economopoulos M., (1997), "Comet – a new coal-based process for the production of DRI", *Metallurgical plant and technology international*, Vol. 20, No. 2, p 50 –61.
- Narcin N., Aydin S., Sesen K., Dikec F., (1995), "Reduction of iron ore pellets with domestic lignite coal in a rotary tube furnace", *Int. J. Miner. Process.*, Vol. 43, p 49 - 59.
- Nascimento R.C., Mourao M.B., Capocchi J.D.T., (1998), "Reduction-Swelling behaviour of pellets bearing iron ore and charcoal", *Canadian Metallurgical Quarterly*, Vol. 37, No. 5, p 441 – 448.
- Negri E.D., Alfano O.M., Chiovetta M.G., (1987), "Direct reduction of hematite in a moving bed. Comparison between one- and three-interface pellet models", *Chemical Engineering Science*, Volume 42, Issue 10, p 2472-2475.

-
- Orhan E. C. (1997), "Coal Flotation", Mineral Processing Site, Hacettepe University, Turkey, www.geocities.com/CapeCanaveral/Hangar/5555/coalflot.htm
- Pandey B.K., Sharma T., (2000), "Reducing agents and double-layered iron ore pellets", *Int. J. Miner. Process.*, Vol. 59, p 295 - 304.
- Peacey J. G., Davenport W.G., (1979), "The Iron Blast Furnace - Theory and Practice", Pergamon Press.
- Perry R.H., Green D.W., (1997), "Perry's Chemical Engineers' Handbook", Seventh Edition, McGraw-Hill, USA, p 2-12 – 2-14.
- Purwanto H., Shimada T., Takahashi R., Yagi J., (2001), "Reduction of cement bonded laterite briquette with CO-CO₂ gas", *ISIJ International*, Vol. 41, pp S31 – S35.
- Reddy G. V., Sharma T., Chakravorty S., (1991), "Kinetic rate equation for direct reduction of iron ore by non-coking coal", *Ironmaking and Steelmaking*, Vol. 18, No 3, p 211-215.
- Ripke S.J., Kawatra S.K., (2000), "Can fly-ash extend bentonite binder for iron ore agglomeration?", *Int. J. Miner. Process.*, Vol. 60, p 181 – 198.
- Sasaki N., (1998), "Direct iron-making process using fusion reduction(DIOS)", ICETT, Japan, www.icett.or.jp/techinfo.nsf.
- Sharma T, (1997), 'Reduction of double layered iron ore pellets', *Int. J. Miner. Process.*, Vol. 49, p 201 – 206.
- Sharma T., (1993), "Non-coking coal quality and composite pre-reduced pellets", *Int. J. Miner. Process.*, Vol. 39, p 299 – 311.
- Srinivasan N.S. and Staffansson L.I., (1990), "A theoretical analysis of the fluidized-bed process for the reduction of iron ores", *Chemical Engineering Science*, Volume 45, Issue 5, p 1253-1265.

-
- Swantantra P., Hem S. R., (1990), "Prediction of Reduction Kinetics of Iron Ore under Fluctuating Temperature Conditions", *ISIJ International*, Vol. 30, No. 3, p 183 – 191.
- Tanaka H., Sugiyama T, Harada T., Sugitatsu H., (2002), "FASTMET Dust Pellet Reduction", Operations report on the First Fastmet Waste Recovery Plant, KOBE STEEL, Ltd.
- VanderLinde K., Su T.E., (2002), "Induction Heating", <http://stuweb.ee.mtu.edu/~mtromble/induction/induction.html>
- Weeda M., Tromp P.J.J., Moulijn J.A., (1990), "The potential of coal gasification in a novel iron oxide reduction process", *Chemical Engineering Science*, Vol. 45, Issue 8, p 2721-2728.
- Yusfin Y., Pashkov N., (2002), "Non-Blast Furnace Steel: alternative or Supplement?", *Eurasian Metals, National Review*, en.eurasmets.ru/online/2002/1/science&tech.html.

Appendix A

Kinetic Analysis of Reduction as presented by Reddy et al (1991)

Reaction :



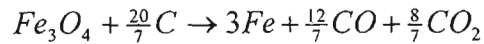
Carbon balance: $z = x + y$

Oxygen balance: $4 = x + 2y$

CO/CO₂: $\frac{3}{2} = \frac{x}{y}$ (not uncommon in traditional blast furnaces)

=> $x = \frac{12}{7}, y = \frac{8}{7}, z = \frac{20}{7}$

Reaction Stoichiometry:



Sample used: **Coal and Magnetite** (stoichiometric addition) => Carbon:Magnetite = 2.86:1

molar mass carbon = $12 \text{ g}\cdot\text{mol}^{-1}$

molar mass Fe₃O₄ = $232 \text{ g}\cdot\text{mol}^{-1}$

therefore, carbon:magnetite = 34.32g : 232g

Assuming 86% Carbon in Coal, on mass basis, (14% Ash, volatiles are not considered)

=> coal : magnetite = 40g : 232g

initial concentration of Fe₃O₄, $C_{A0} = 1/(40+232) = 3,68\text{E-}03 \text{ g}\cdot\text{mol}^{-1}$

initial concentration of Carbon, $C_{B0} = 2.86/(40+232) = 1,05\text{E-}02 \text{ g}\cdot\text{mol}^{-1}$

Ratio of initial concentrations of reactants, $M = C_{B0}/C_{A0} = 2,86$

Value of k using Arrhenius Equation

$$k = A e^{\frac{-E}{RT}}$$

R has the value of 0,00831 kJ mol⁻¹K⁻¹

k values (Reddy et al., 1991):	k ₁ / g mol ⁻¹ min ⁻¹	k ₂ / g mol ⁻¹ min ⁻¹	T / K
	35,71	12,86	1373,00

Activation Energy: E₁ = 108,15 kJ g⁻¹ mol⁻¹
 E₂ = 93,16 kJ g⁻¹ mol⁻¹

$$\begin{aligned} \text{therefore, } A_1 &= k_1 / e^{-E_1/RT} = 4,65E+05 \\ A_2 &= k_2 / e^{-E_2/RT} = 4,50E+04 \end{aligned}$$

$$\begin{aligned} \text{therefore, } k_{1(900)} &= 7,10 \text{ g mol}^{-1} \text{ min}^{-1} \\ k_{2(900)} &= 3,20 \text{ g mol}^{-1} \text{ min}^{-1} \end{aligned}$$

Kinetic Equation:

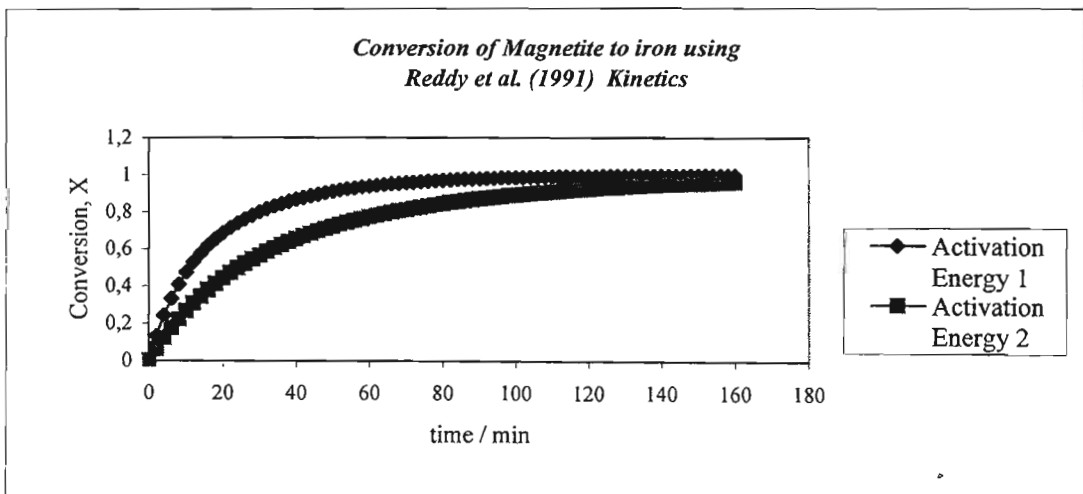
$$\frac{1}{C_{A0}(1.5-M)} \ln \frac{M(1-X_A)}{M-1.5X_A} = kt \quad \text{valid fo } M > 1.5X_A$$

(X_A = fractional conversion of magnetite)

rearranging kinetic equation:

$$X_A = \frac{M(e^{ktC_{A0}(1.5-M)} - 1)}{1.5e^{ktC_{A0}(1.5-M)} - M}$$

Conversion equation gives the graph below:



Appendix B

X-Ray Diffraction (Whittingham, 1997)

The discovery of X-rays enabled scientists to probe crystalline structure at the atomic level. X-rays, which are electromagnetic radiation of wavelength about 1 \AA (10^{-10} m), are about the same size as an atom.

X-ray diffraction is one of the most important tools used to determine the size and the shape of the unit cell for any compound. Each crystalline solid has its unique characteristic X-ray pattern, which may be used as a "fingerprint" for its identification. Once the material has been identified, X-ray crystallography may be used to determine its structure, i.e. how the atoms pack together in the crystalline state and what the inter-atomic distance and angle are, etc. Therefore, X-ray diffraction serves a two-fold purpose; for the characterization of crystalline materials, using its fingerprint, and the determination of their structure.

The reflection of x-rays when they hit the surface of a crystal can be seen in the figure below.

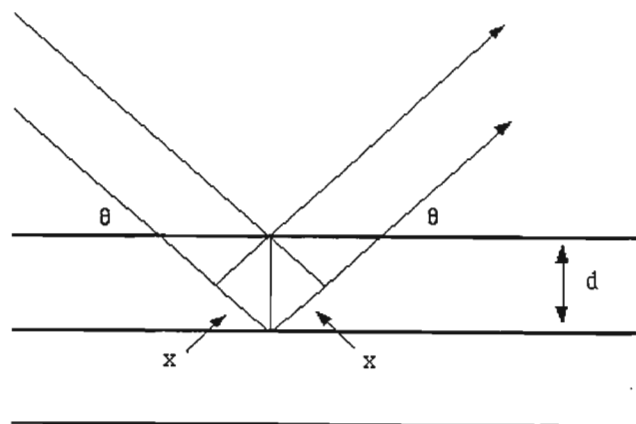


Fig. B1 Reflection of x-rays from two planes of atoms in a solid.
(Whittingham, 1997)

The path difference between two waves:

$$2 \times \text{wavelength} = 2d \sin \theta$$

b1.1

For constructive interference between these waves, the path difference must be an integral number of wavelengths:

$$n \times \text{wavelength} = 2x$$

b1.2

This leads to the Bragg equation:

$$n \times \text{wavelength} = 2d \sin \theta$$

b1.3

The X-ray diffractometer is the equipment used to conduct an X-ray diffraction experiment.

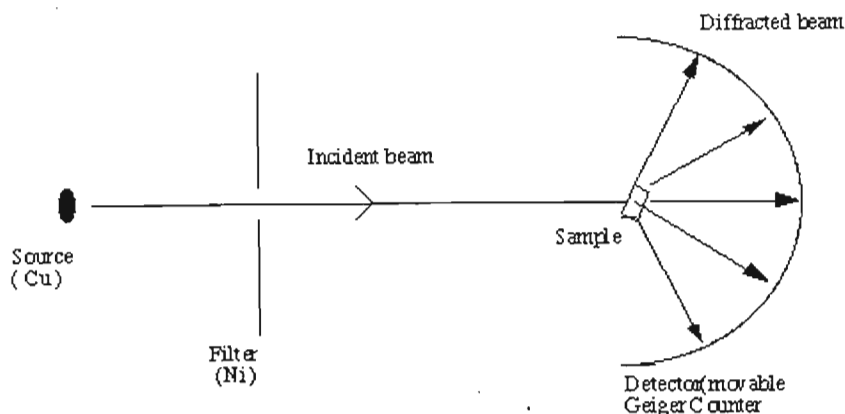


Fig B2. X-Ray Powder Diffractometer (Whittingham, 1997)

When the incident beam strikes a powder sample, diffraction occurs in every possible orientation of 2θ . The diffracted beam may be detected by using a moveable detector such as a Geiger counter, which is connected to a chart recorder.

The detector records relative intensities at each angle (2θ). The d-spacing is calculated from the Bragg Equation using the specified wavelength (K-Alpha). Seeing that each crystal structure has its own d-spacing, the different compounds in the sample can be identified.

The pages that follow show typical analysis obtained from an X-ray Diffractometer. The d-spacing for the different iron oxides, viz. hematite, magnetite, wustite and metallic iron were obtained from literature.

=====
 eology Department

=====
 University of Durban Westvill

Sample identification: und1d3a
 Data measured at: 7-Mar-2003 11:42:00

Diffractionmeter type: PW3710 BASED
 Tube anode: Co
 Generator tension [kV]: 40
 Generator current [mA]: 40
 Wavelength Alpha1 [Å]: 1.78896
 Wavelength Alpha2 [Å]: 1.79285
 Intensity ratio (alpha2/alpha1): 0.500
 Divergence slit: 1/4°
 Receiving slit: 0.1
 Monochromator used: YES

Start angle [°2θ]: 5.000
 End angle [°2θ]: 70.000
 Step size [°2θ]: 0.020
 Maximum intensity: 542.8900
 Time per step [s]: 1.000
 Type of scan: STEP

Peak positions defined by: Top of smoothed peak
 Minimum peak tip width: 0.00
 Maximum peak tip width: 1.00
 Peak base width: 2.00
 Minimum significance: 0.75
 Number of peaks: 12

Angle [°2θ]	d-value α1 [Å]	d-value α2 [Å]	Peak width [°2θ]	Peak int [counts]	Back. int [counts]	Rel. int [%]	Signif.
1.170	4.8694	4.8800	0.240	4	2	0.7	1.40
1.305	3.5361	3.5438	0.320	3	3	0.6	1.04
1.4960	2.9779	2.9844	0.240	8	3	1.4	1.39
1.6140	2.8838	2.8900	0.400	5	4	0.9	1.21
1.7090	2.8124	2.8185	0.480	4	4	0.7	1.29
1.1290	2.5370	2.5425	0.200	19	5	3.6	1.13
1.2280	2.4802	2.4856	0.120	85	5	15.6	2.07
1.5000	2.3374	2.3425	0.120	6	4	1.2	1.08
1.9245	2.1469	2.1516	0.200	182	5	33.6	7.79
2.4450	2.0242	2.0286	0.160	543	5	100.0	6.12
0.705	1.7701	1.7740	0.480	4	3	0.7	1.34
1.6890	1.6230	1.6265	0.480	3	3	0.6	1.68

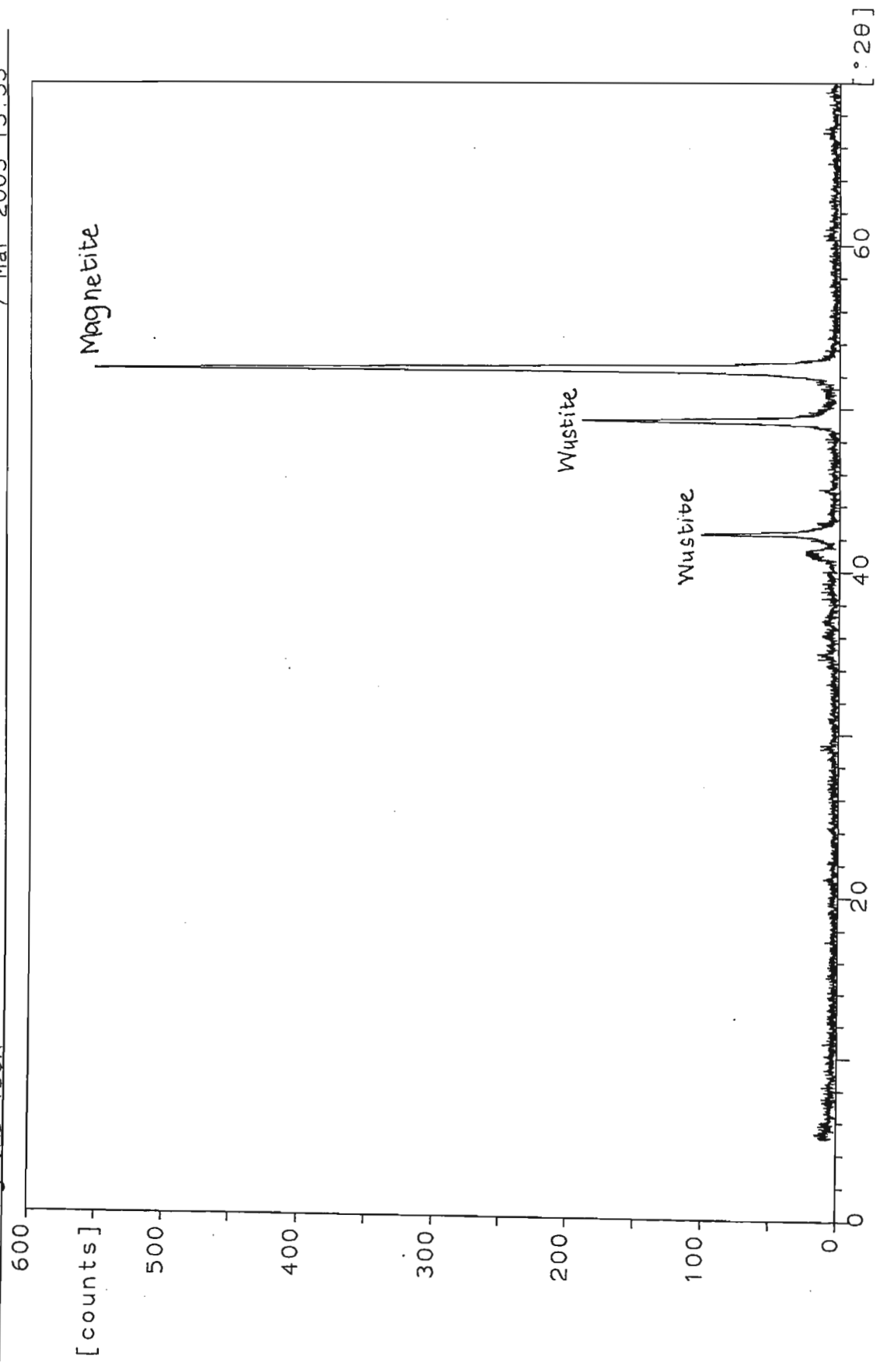


Table B1: D -Spacing of Respective Compounds

<u>Hematite</u>					
d	2.69	1.69	2.51	3.66	(d-spacing)
I/I ₁	100	60	50	25	(relative intensity)
<u>Magnetite</u>					
d	2.53	1.49	2.97	4.85	
I/I ₁	100	40	30	8	
<u>Wustite</u>					
d	2.15	2.49	1.52	2.49	
I/I ₁	100	80	60	80	
<u>Iron</u>					
d	2.03	1.17	1.43	2.03	
I/I ₁	100	30	20	100	

(ref.: "Mineral Powder Diffraction file", Search Manual, JCPDS Internation Centre for Diffraction Data, America, USA, 1980.)

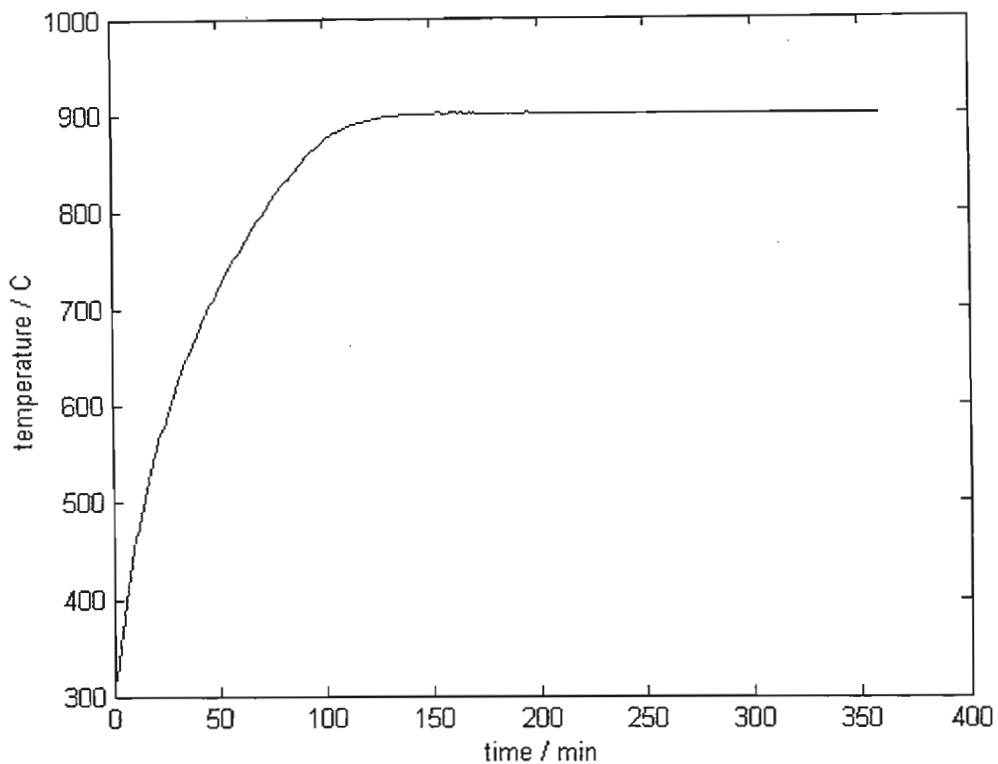
Appendix C

Kinetic Evaluation of Reduction Process using Thermobalance Data

Run 1: Temperature = 900°C

Temperature profile of Run 1 can be seen below.

Graph C1.1 Temperature Profile of Run1



Mass loss observed in Thermobalance can be seen in graph C1.2.

$$\text{Fraction of reaction, } f = \frac{\text{Weight loss at time } t}{\text{Max. possible weight loss}}$$

Ratio coal : iron oxide = 1:6 (Stoichiometric addition)

Weight of pellet in thermobalance = 23.6g

Weight of coal in pellet = $(1/6 \times 23.6)$ g = 3.94g

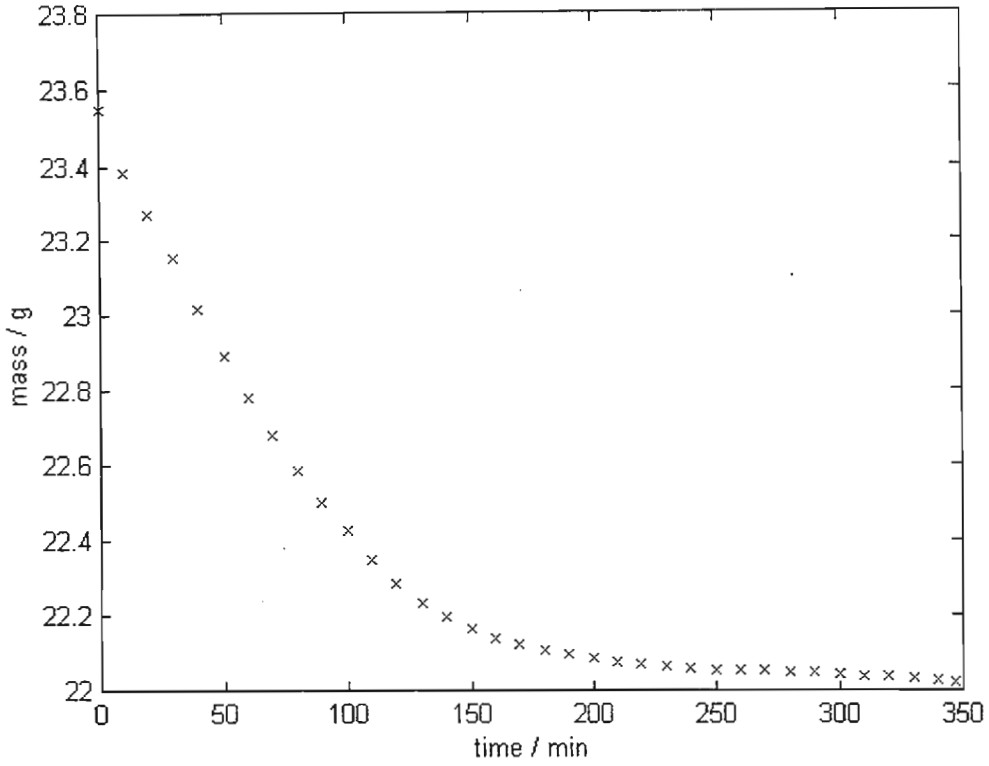
Weight loss from Carbon in coal = 0.72×3.94 g = 2.83 (72% C in coal)

Weight loss from oxygen in iron oxide = $64/232 \times (23.6 - 3.94)$ g = 5.43g

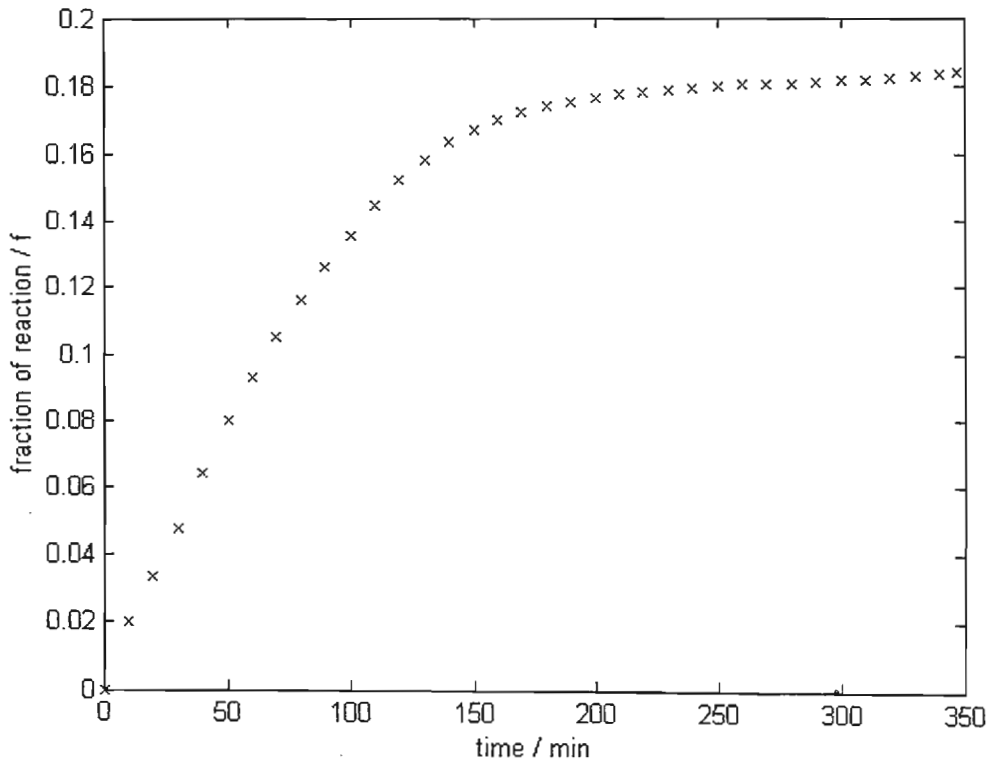
therefore, max. weight loss = 5.43g + 2.83g = 8.26g

Graph C1.3 shows the fraction of reaction, f , for Run 1.

Graph C1.2 *Mass of Pellet during Run 1*



Graph C1.3 *Fraction of Reaction During Run 1*



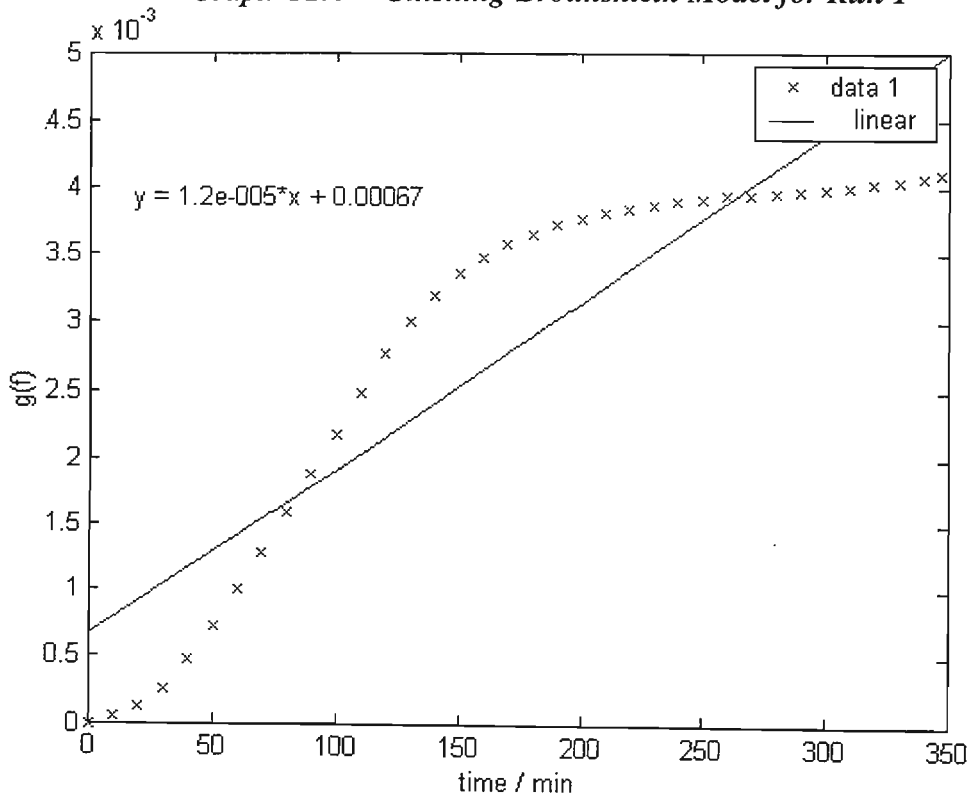
According to Swantantra and Hem (1990), the normal f-curves show the Ginstling-Brounshtein (G.B.) equation as the rate curve. The Ginstling – Brounshtein equation, which is applicable to reactions controlled by diffusion through non-porous solid product, was also compared to other applicable models, viz. Jander Model and Spherical Symmetrical Model (Habashi, 1969).

Ginstling Brounshtein: $g(f) = 1 - \frac{2}{3}f - (1-f)^{\frac{2}{3}}$

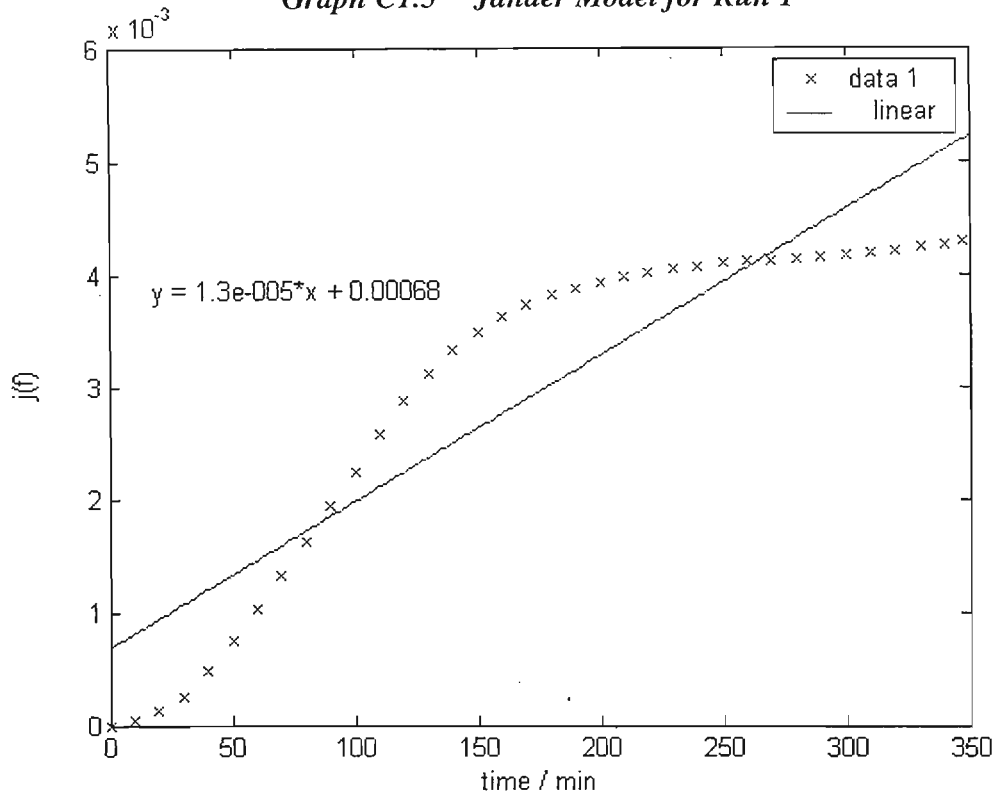
Jander: $j(f) = (1 - (1-f)^{\frac{1}{3}})^2$

Spherical Symmetrical: $s(f) = 1 - (1-f)^{\frac{1}{3}}$

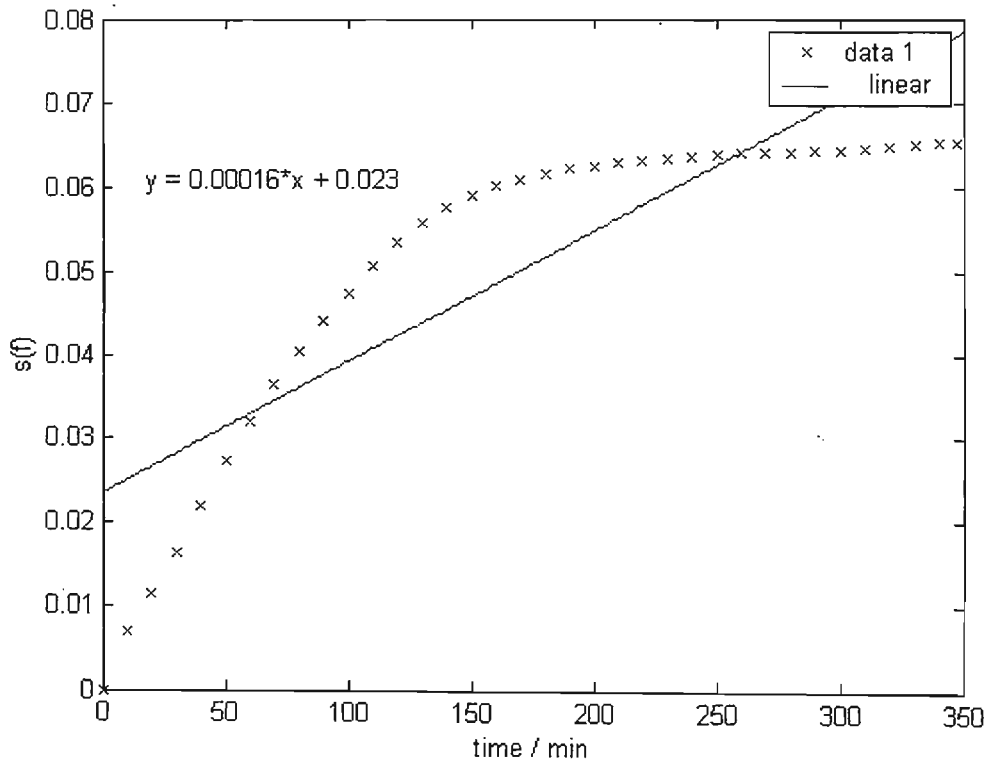
Graph C1.4 Ginstling-Brounshtein Model for Run 1



Graph C1.5 Jander Model for Run 1



Graph C1.6 Spherical Symmetrical Model for Run 1

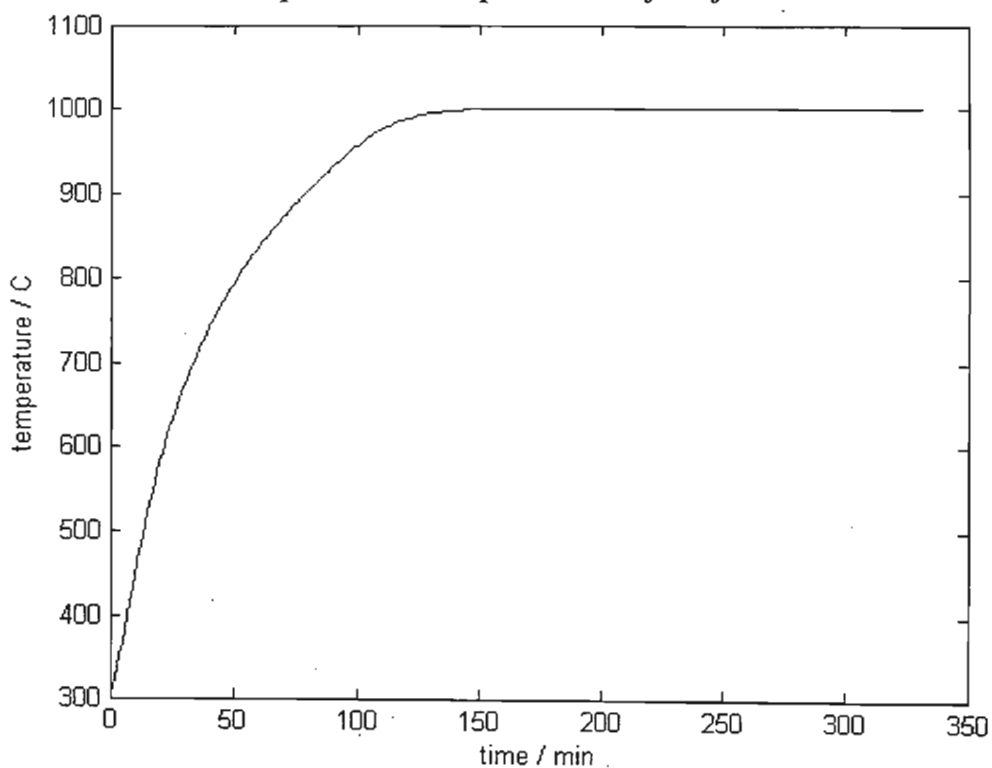


It was evident from graphs C1.4, C1.5 and C1.6 that although the G.B. Model does not depict a straight line, it is the closest when compared to the other two plots. The G.B. equation was therefore taken as the rate-determining model and used for runs 2 & 3, with temperatures 1000°C and 800°C respectively.

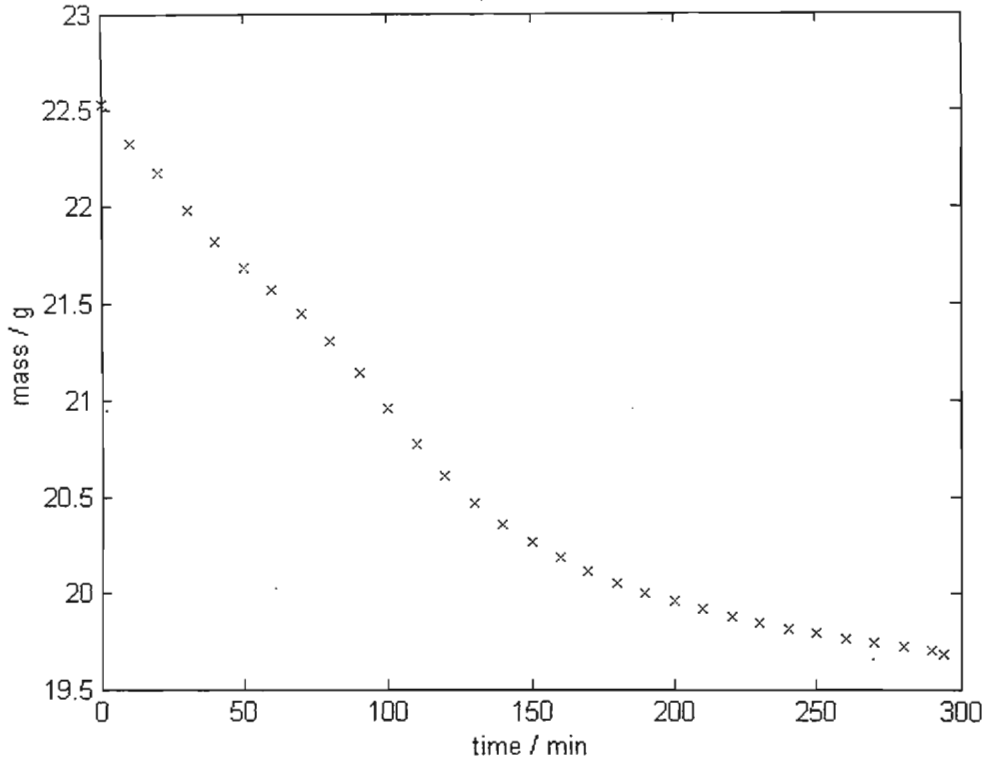
Calculations for runs 2 & 3 were the same as for run 1, with maximum weight losses being 7.93g and 8.25g respectively. Corresponding graphs can be seen below.

Run 2: Temperature = 1000°C

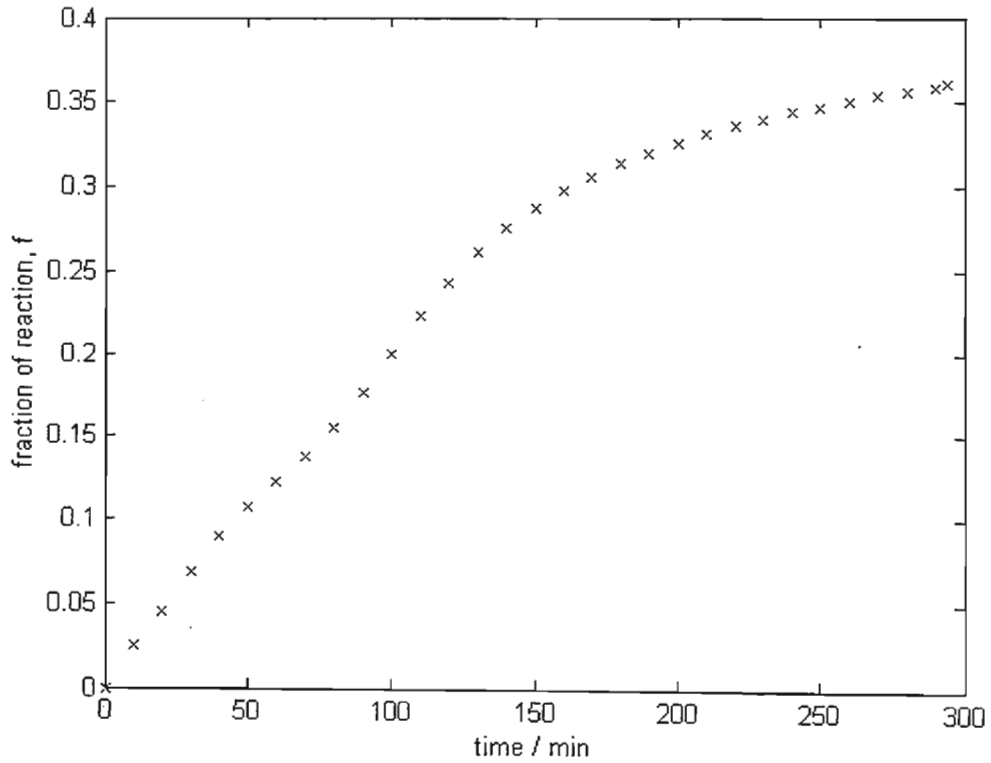
Graph C2.1 Temperature Profile of Run 2



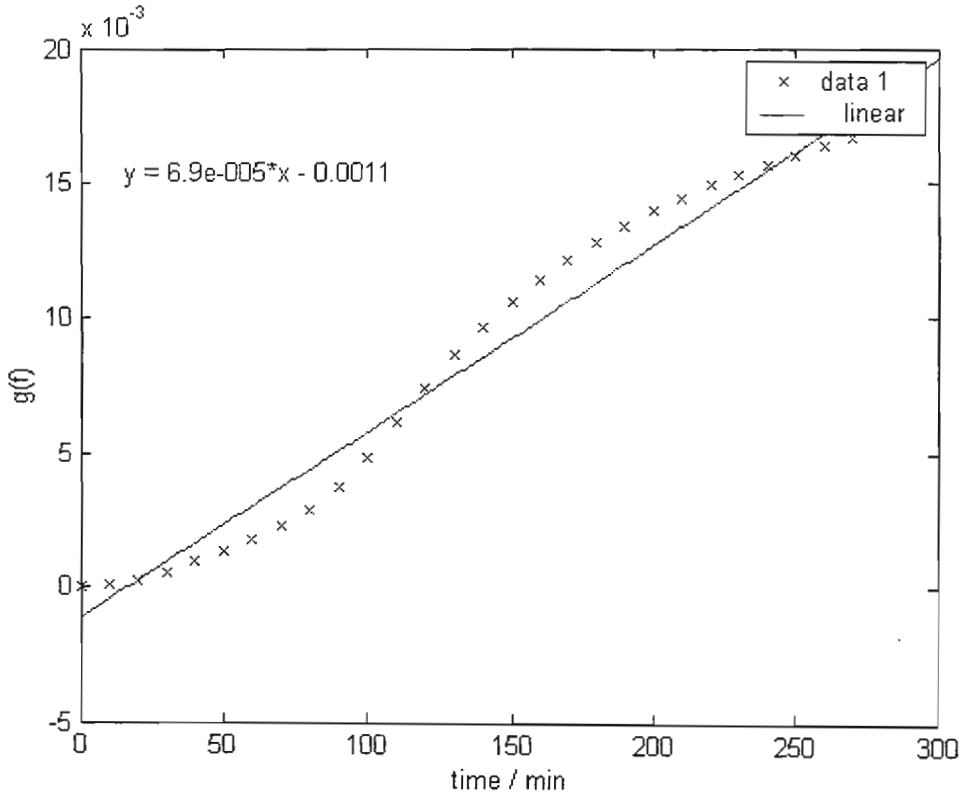
Graph C2.2 *Mass of Pellet during Run 2*



Graph C2.3 *Fraction of Reaction During Run 2*

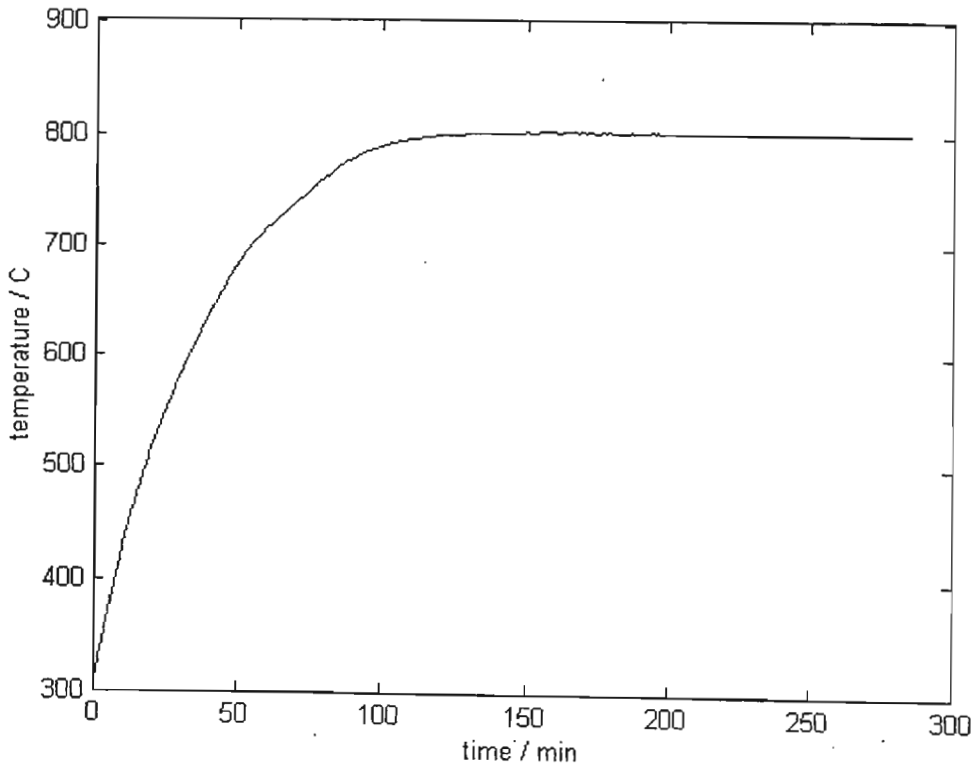


Graph C2.4 Ginstling-Brounshtein Model for Run 2

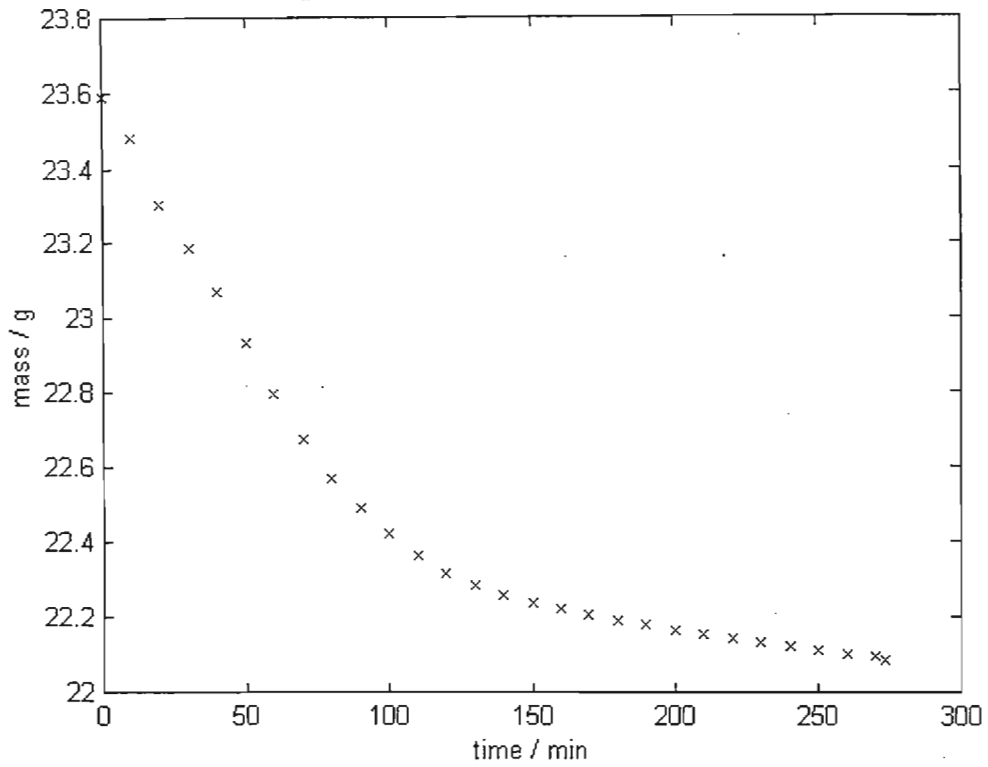


Run 1: Temperature = 800°C

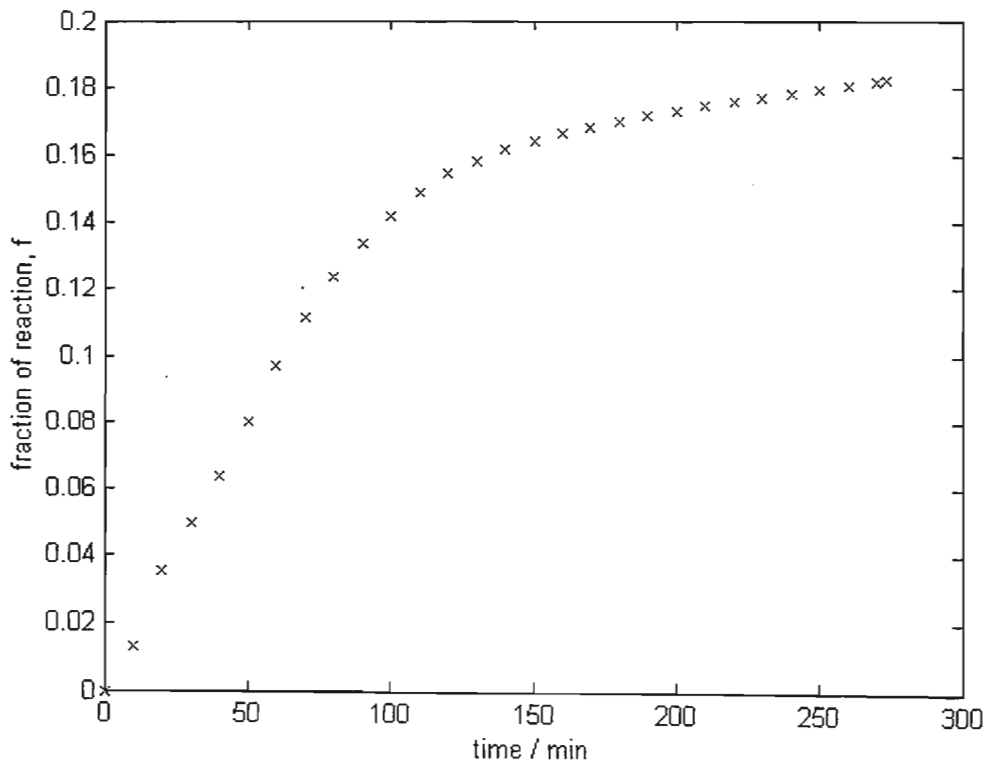
Graph C3.1 Temperature Profile of Run 3



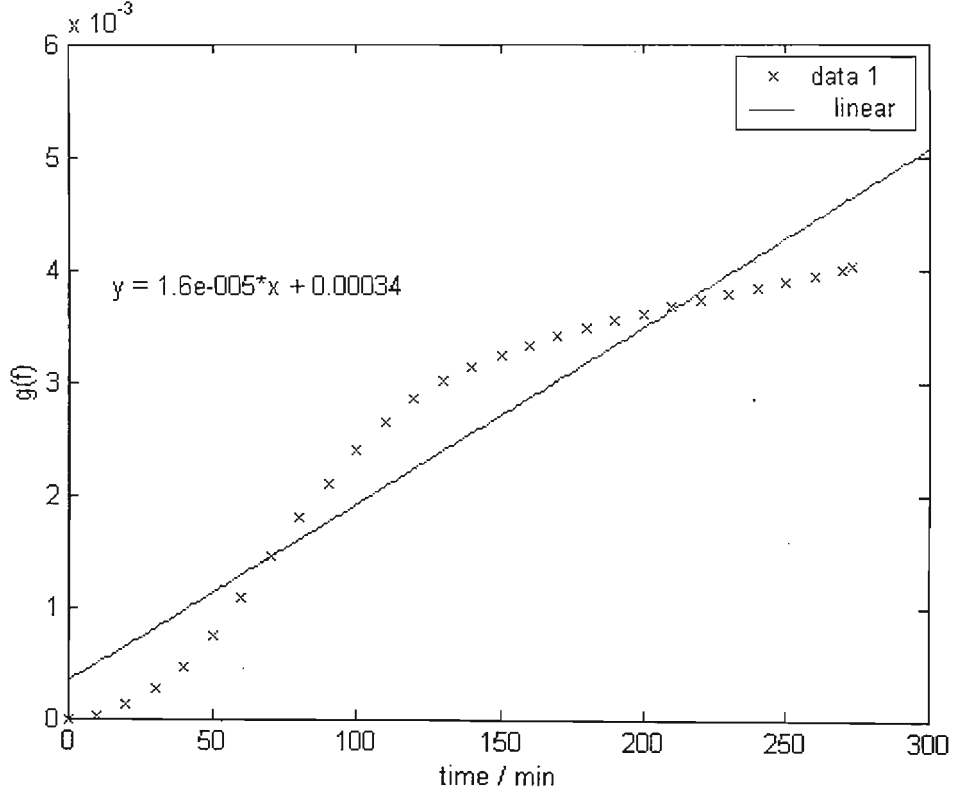
Graph C3.2 *Mass of Pellet during Run 3*



Graph C3.3 *Fraction of Reaction During Run 3*

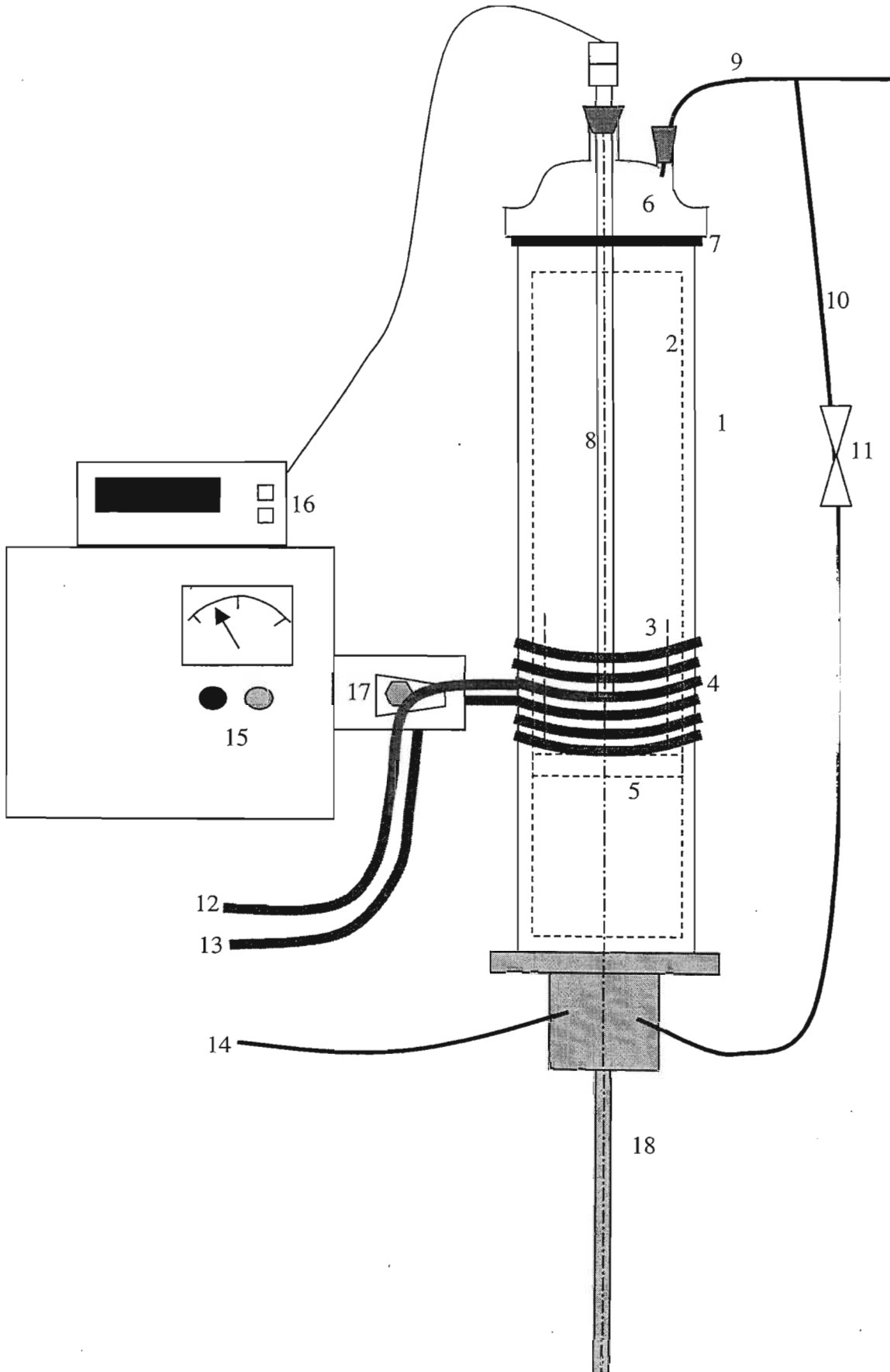


Graph C3.4 Ginstling-Brounshtein Model for Run 3



Appendix D1

Detail of Mapham Induction Heater



1. Glass Tube Reactor $L = 720\text{mm}$, $OD = 120\text{mm}$, $Thickness = 5\text{mm}$
2. High Temperature Refractory Lining $Thickness = 10\text{mm}$
3. Steel Casing $L = 200\text{mm}$, $OD = 77\text{mm}$, $Thickness = 0.5\text{mm}$
4. Copper Coil $L = 140\text{mm}$, $OD = 140\text{mm}$, $Thickness = 7\text{mm}$
5. High Temperature Distributor Plate $D = 8\text{mm}$
6. Glass Top
7. Washer
8. Thermocouple $L = 630\text{mm}$
9. Product Gas Vent
10. Product Gas Recycle
11. Recycle Valve
12. Inlet Coolant water inside copper coil
13. Outlet Coolant water inside copper coil
14. Inlet Nitrogen Gas
15. Mapham Induction Heater Controls
16. Temperature Display Unit
17. Busbars
18. Furnace support

Appendix D2

Induction Heating Experimental Procedure

1. Ensure main circuit breaker on the side of Mapham Induction Heater is *off*. Consequently whenever circuit breaker is *on*, then busbar protruding from the side of the cabinet and coil MUST BE REGARDED AS LIVE.
2. Remove glass top from the furnace and feed 500g pellets inside the steel casing of the furnace. Seal glass lid of furnace using silica seal.
3. Insert k-type thermocouple into reacting zone. Connect thermocouple to display unit.
4. Open Nitrogen gas cylinder. Set N₂ rotameter to 200ml/min. Ensure recycle valve is opened.
5. Open coolant water tap. Temperature of water should be around 26°C in order for coil water not to exceed 46°C. Set water rotameter to 2 l/min. (Minimum = 1.5 l/min)
6. Switch main circuit breaker on. Control panel light comes on. Switch on green 'Power On' button, which will liven the bus and coil nut will not yet cause the inverter to oscillate.

The power control potentiometer should be turned down to zero. This multi-turn control knob may be locked in any position. Do not force the knob if locked.

Press the 'Heat On Button' to cause the inverter to oscillate. The Power is controlled by the power control knob and indicated by the power meter.

Set the Power output to 1200 W. (max power output = 2500W)
7. The temperature display unit will indicate heating rate.
8. When pellets reach reaction temperature, control power supply to the coils to ensure that reaction temperature is maintained for duration of experiment.
9. When experiment is concluded, switch the red 'Heat Off' button followed by the 'Power Off' button.
10. Allow for cooling of pellets. When pellets have reached appropriate handling temperature turn coolant water as well as nitrogen flow off.
11. Remove pellet samples to analyze.

Appendix D3

Calculation of Percent Metallic Iron Produced

Table D3.1: Atomic Masses of Elements

Element	Atomic Mass	Oxide Molecules
C	12.011	
O	15.999	
Mg	24.305	MgO
Al	26.982	Al ₂ O ₃
Si	28.086	SiO ₂
P	30.974	P ₂ O ₅
S	32.065	
K	39.098	K ₂ O
Ca	40.078	CaO
Ti	47.867	TiO ₂
Cr	51.996	Cr ₂ O ₃
Mn	54.938	MnO
Fe	55.845	Fe ₂ O ₃ , Fe ₃ O ₄ , FeO

Table D3.2: Mass Percent of Elements in pre-reduced pellet

	Mass Percent
C	3.95
O	3.50
Mg	0.00
Al	2.69
Si	3.31
P	0.00
S	0.33
K	0.00
Ca	1.36
Ti	1.11
Cr	0.00
Mn	0.23
Fe	83.53
	100.00

Assuming Oxygen in slag

Oxygen Balance:

$$\begin{aligned} \text{O in Fe} = & \text{Total O} - (\text{O in MgO}) + (\text{O in Al}_2\text{O}_3) + (\text{O in SiO}_2) + (\text{O in P}_2\text{O}_5) \\ & + (\text{O in K}_2\text{O}) + (\text{O in CaO}) + (\text{O in TiO}_2) + (\text{O in Cr}_2\text{O}_3) + (\text{O in MnO}) \end{aligned}$$

O in Fe = -4.01 % Assume 0%

percentage Metallic Iron = 100% (compared to FeO, Fe₃O₄, Fe₂O₃)

Assuming Oxygen in Wustite (FeO)

No of moles O = 0.22 moles
No of moles Fe : 1.50 moles
Ratio of Fe:O = 1:1 => No of Moles FeO = 0.22 moles
Therefore, No of moles Metallic Iron = 1.28 moles

=> Mass Metallic Iron = 71.32 g

percentage Metallic Iron = $71.32/83.53 \times 100 = 85.38$
(compared to FeO, Fe₃O₄, Fe₂O₃)

Slag Formation

Assume all Oxygen in the slag.

Assume FeO:DRI = 0.1:0.9

Total Slag = 12.52 g

Mass Slag = $12.52 / (0.9 \times (83.53)) = 0.17$ tons / ton DRI

Appendix D4

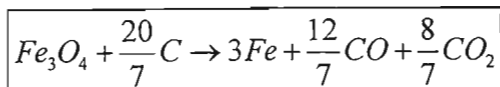
Calculation of Energy Consumption of Process

Amount Fe Produced in Induction furnace

Ratio Magnetite/coal = 2:1

=> for 500g pellet, magnetite = 333 g
coal = 167 g

Reaction Stoichiometry:



assuming CO/CO₂ = 3/2

molar mass Fe = 56 g.mol⁻¹

molar mass Fe₃O₄ = 232 g.mol⁻¹

Therefore, assuming 90% conversion of Fe₃O₄

amount Fe in produced in pellet = $0.9[333\text{g} \times 3(56)] / 232 = 217 \text{ g}$

Energy Consumption : Induction Furnace

Induction heater took 20 minutes to heat to operating temperature of 900°C. To maintain operating temperature for 1 hour, the heater had to be manually operated so as not to overshoot the temperature limit. This required the heater to be on for approximately 30 minutes

$$E = \frac{1.2\text{kW}}{217\text{g}} * 30\text{min} * \frac{60\text{s}}{1\text{min}} * \frac{1\text{GJ}}{1000000\text{kJ}} * \frac{1000000\text{g}}{1\text{ton}}$$

therefore E1 = 9,94 GJ / ton DRI

Energy Consumption: Coal

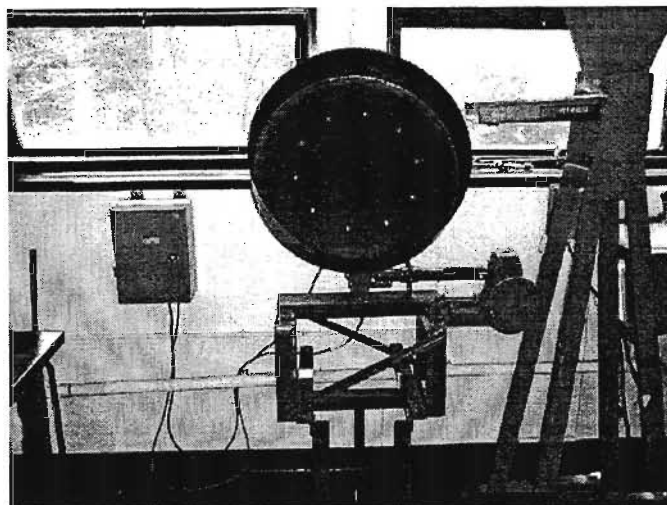
Calorific Value for Coal = 30,9 GJ / ton

E2 = $167\text{g} / 217\text{g} \times 30.9 \text{ GJ / ton} = 23,71 \text{ GJ / ton DRI}$

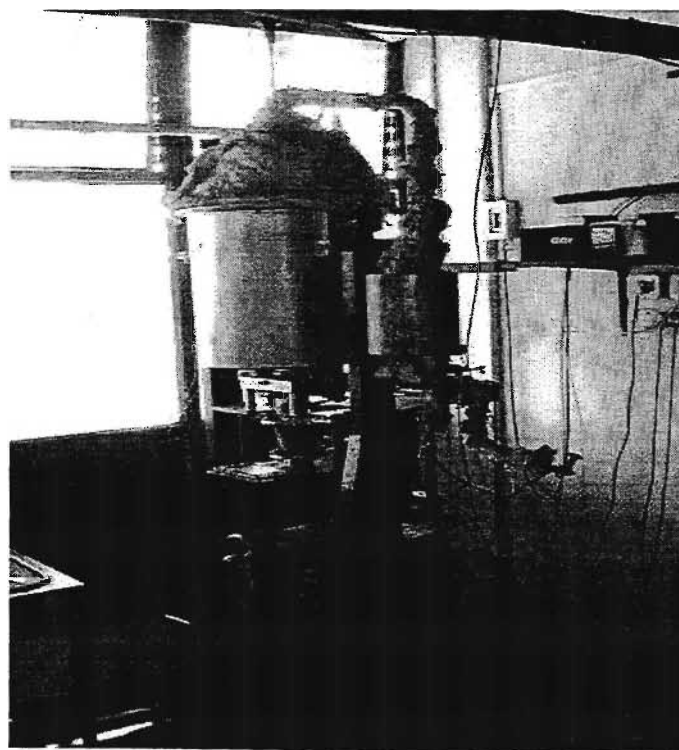
Total Energy Consumption = E1 + E2 = 33,65 GJ / ton DRI

Appendix E

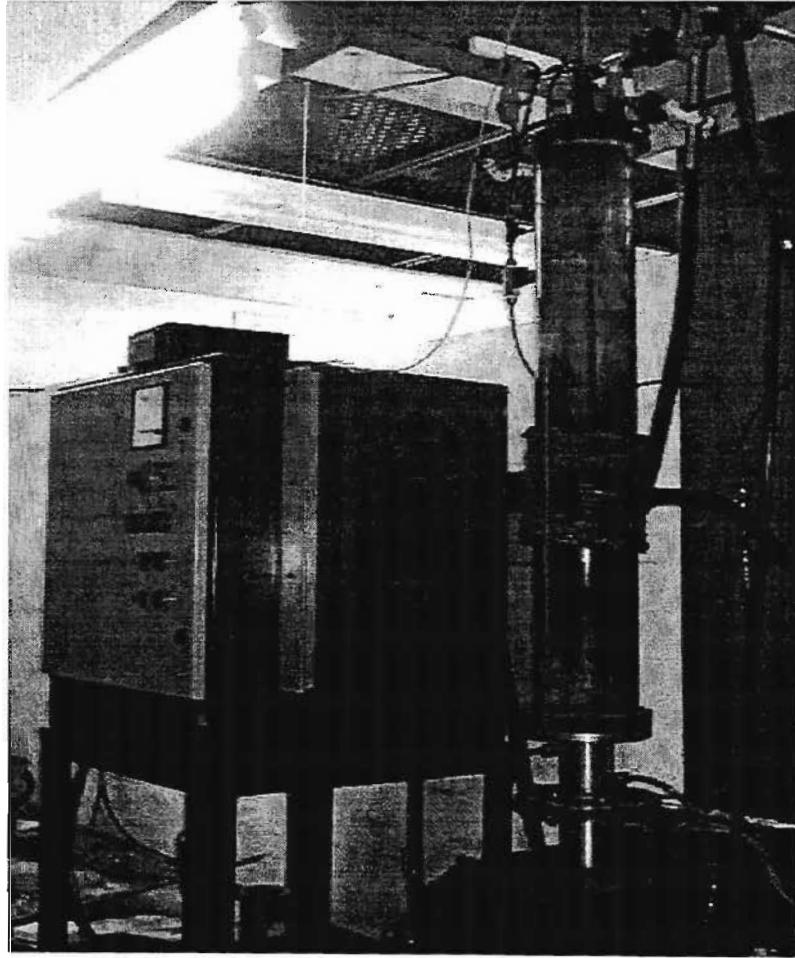
Equipment Pictures



Photograph E1 The Rotating Disc Pelletizer



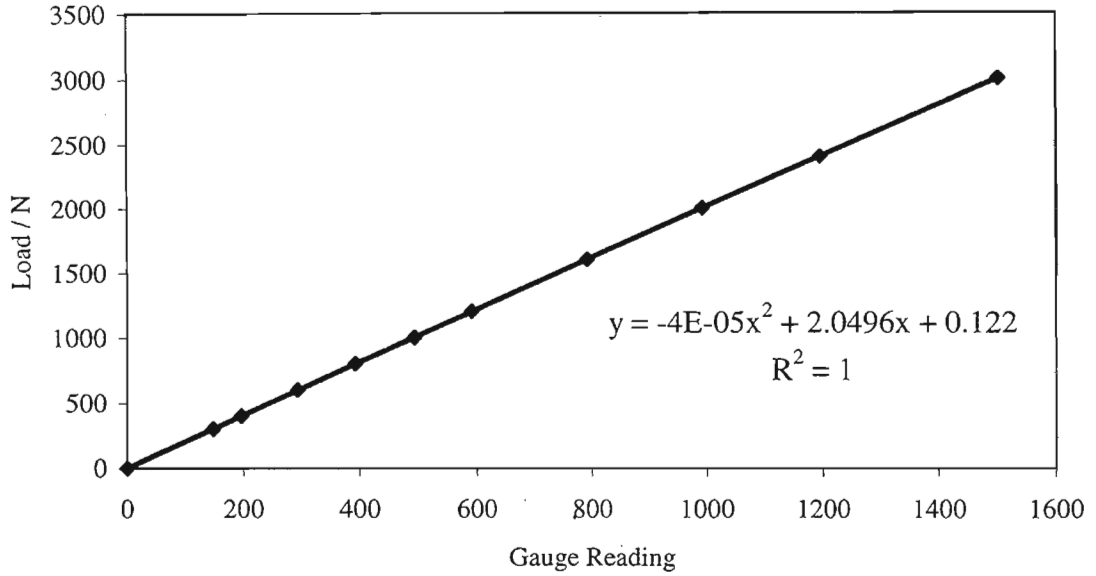
Photograph E2 The Thermobalance



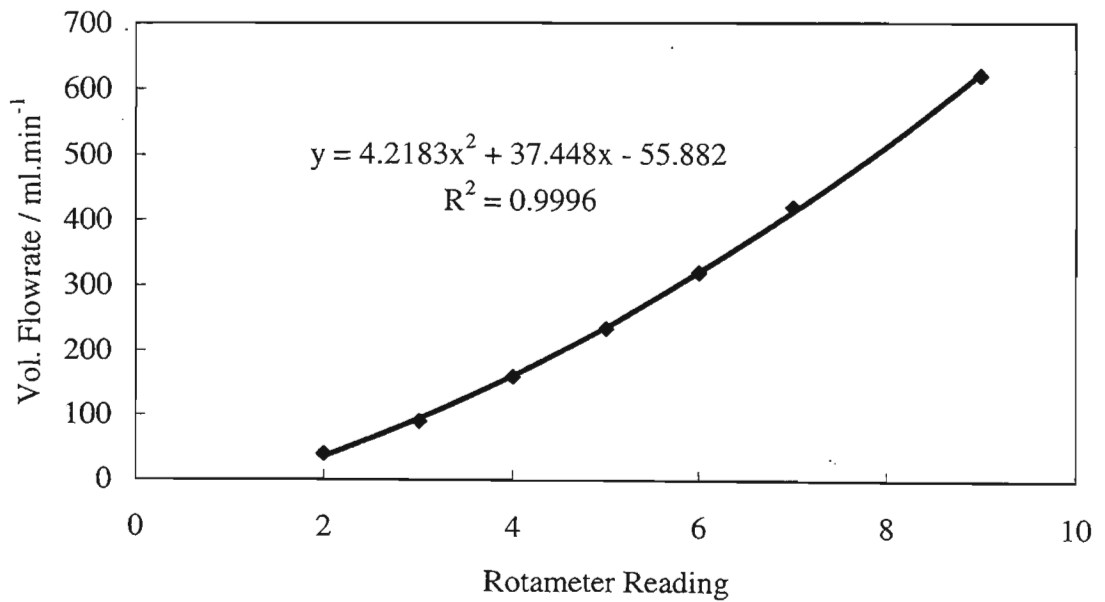
Photograph E3 The Mapham Induction Heater

Appendix F1

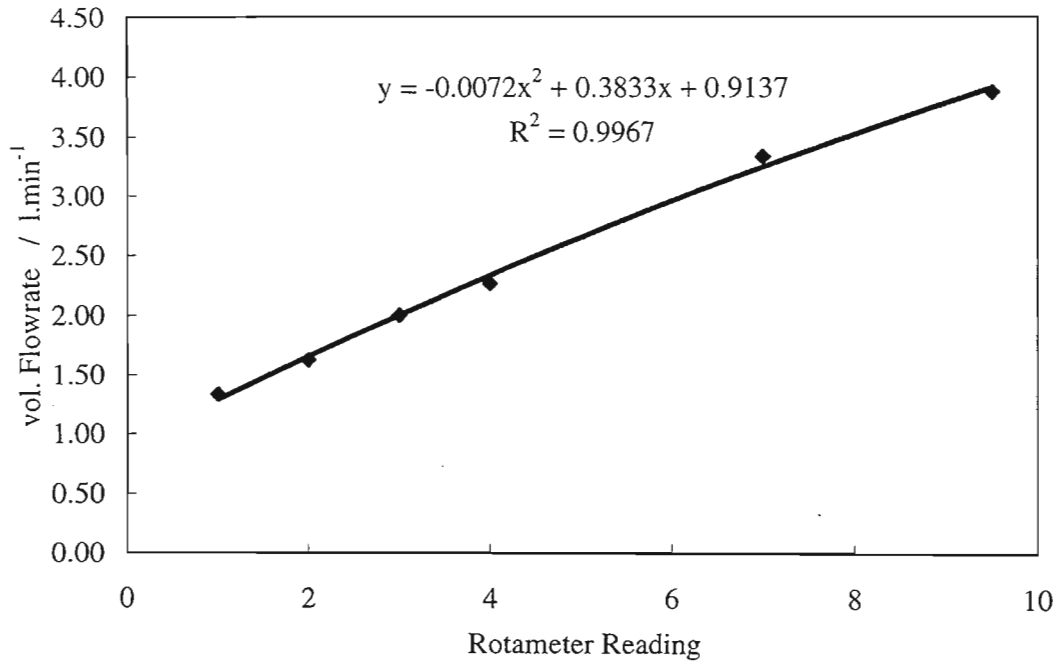
Graph F1.1: Strength Tester Calibration Curve



Graph F1.2: Calibration chart for N₂ Rotameter



Appendix F1.3: Calibration Chart for Water Rotameter

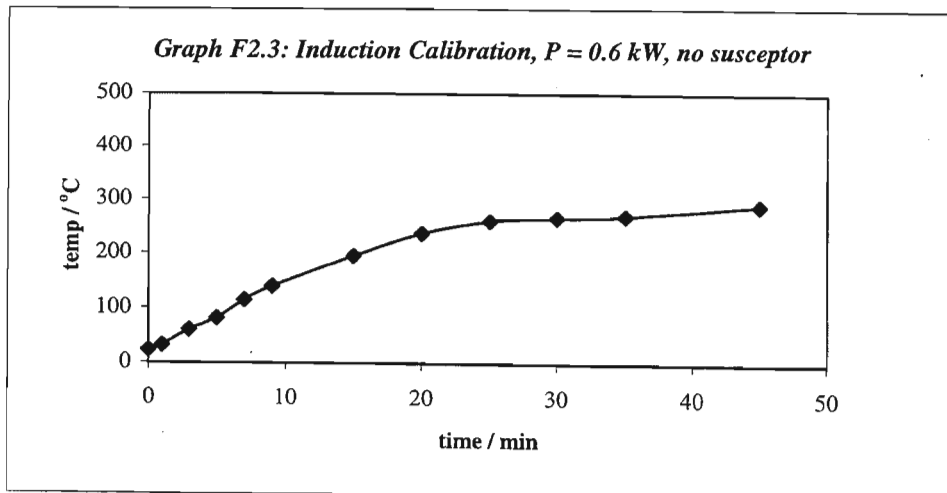
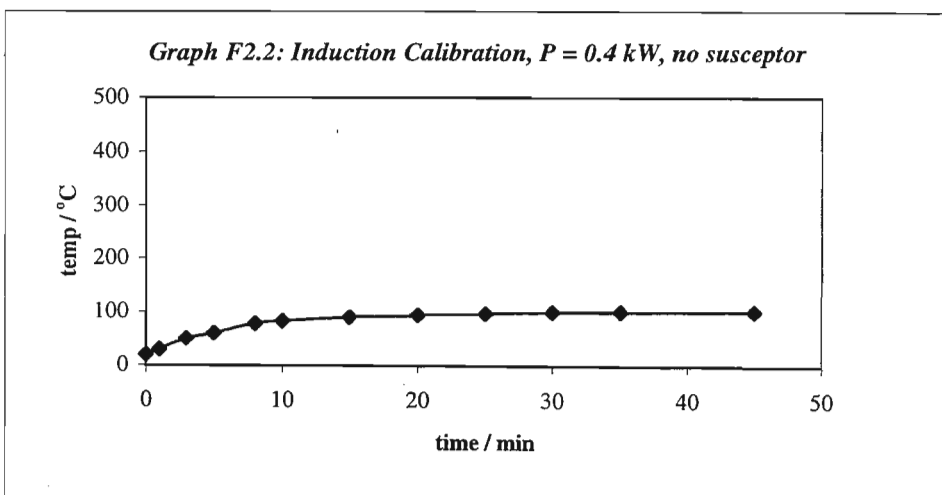
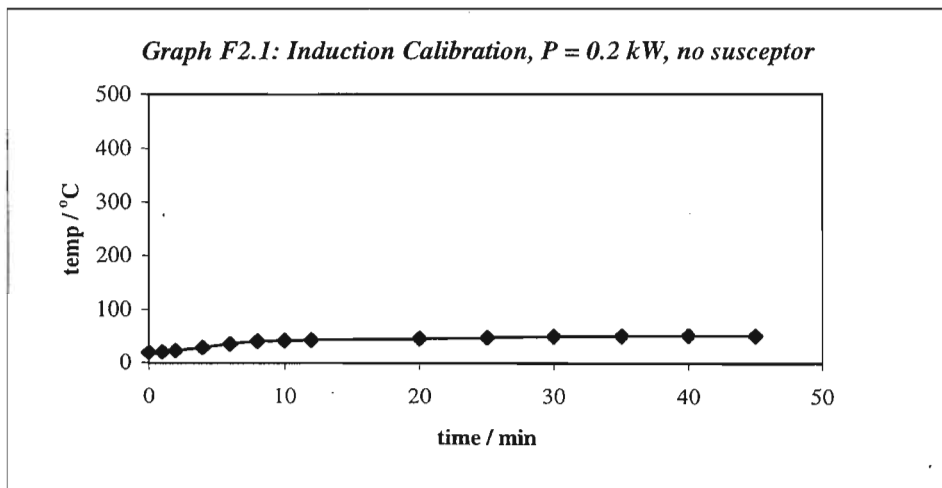


Appendix F2

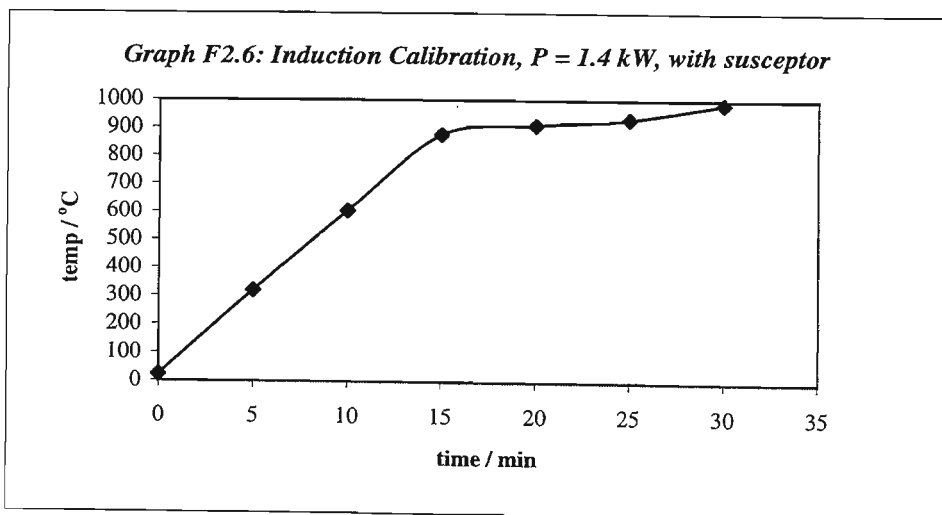
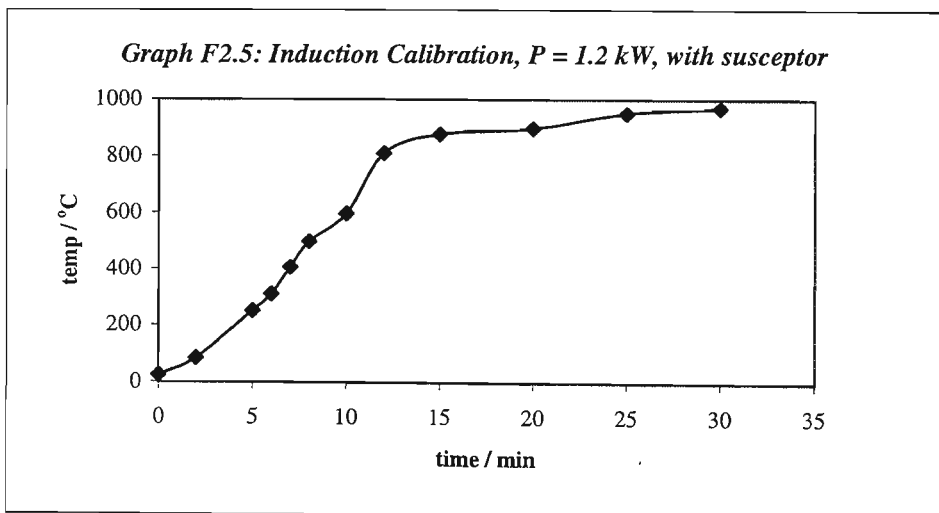
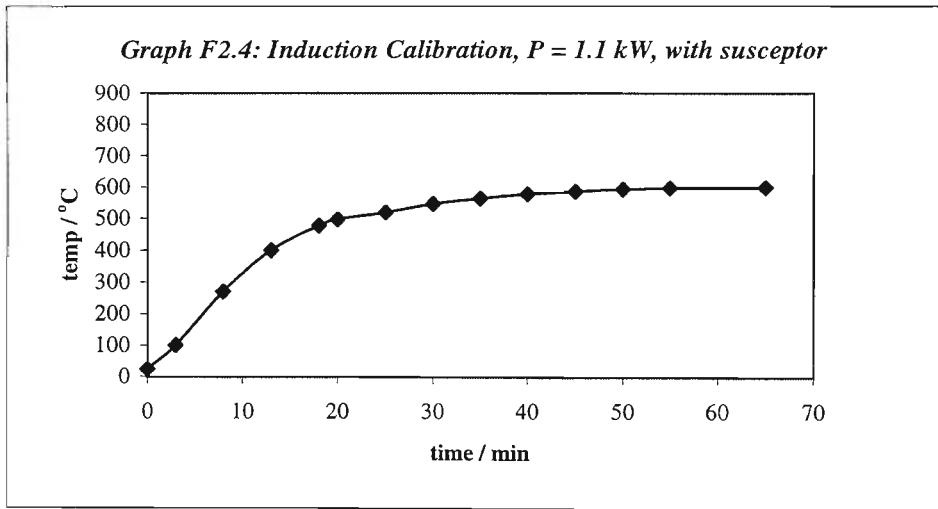
Induction Furnace Heating Rate

Calibration tests for heating rates of the mixed pellets in the induction furnace are given below. Graphs F1.1 - F1.3 show heating rates for the pellets without using a steel susceptor.

It was assumed that the iron oxide in the pellets would be able to heat up via an induced magnetic field.



It is evident that the heating rates are not sufficient for the pellets to reach reaction temperature in a reasonable period of time. A steel casing was therefore introduced into the system as a susceptor. Graphs F1.4 - F2.6 Show the heating periods obtained



Appendix G

SEM Images

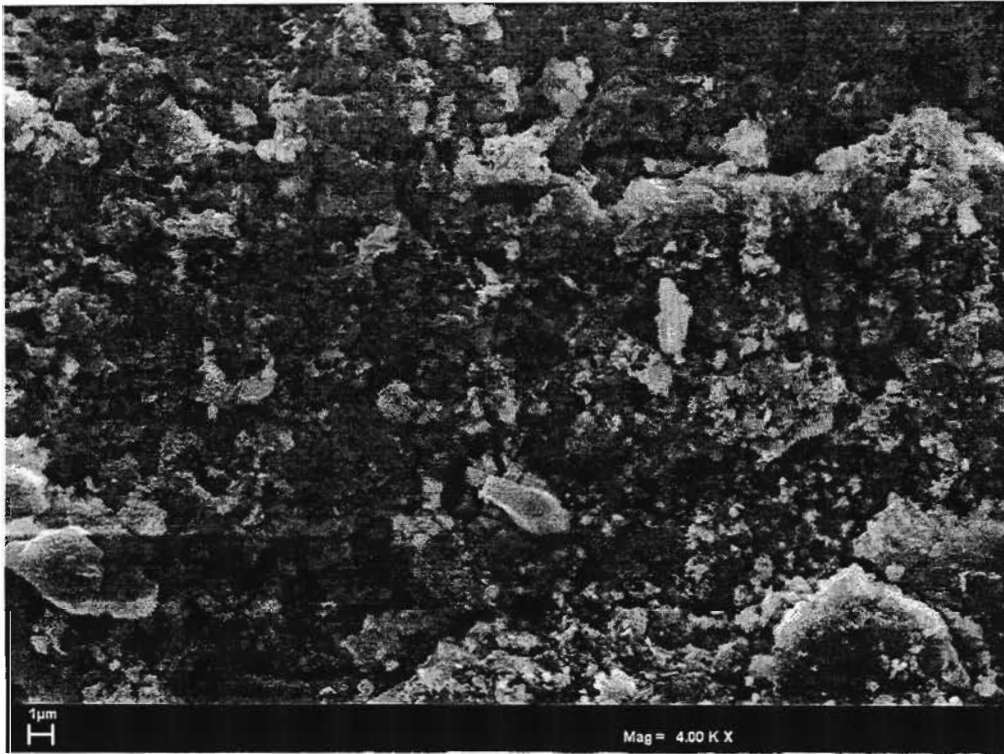


Image 1: Unfloated Coal



Image 2: Floated coal

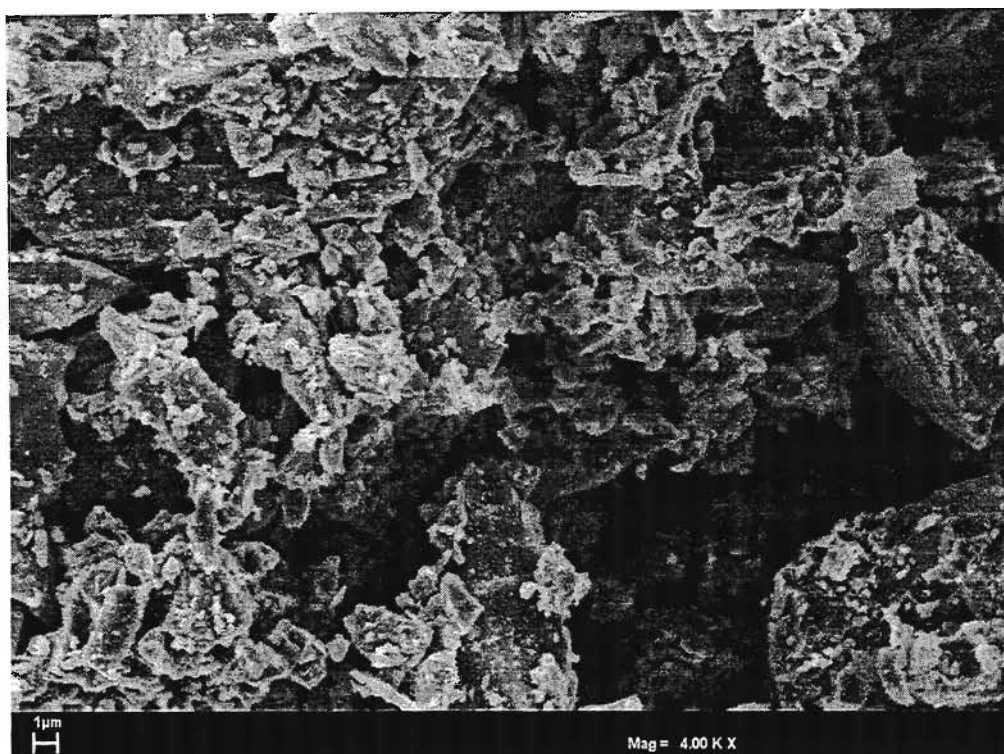


Image 3: Magnetite

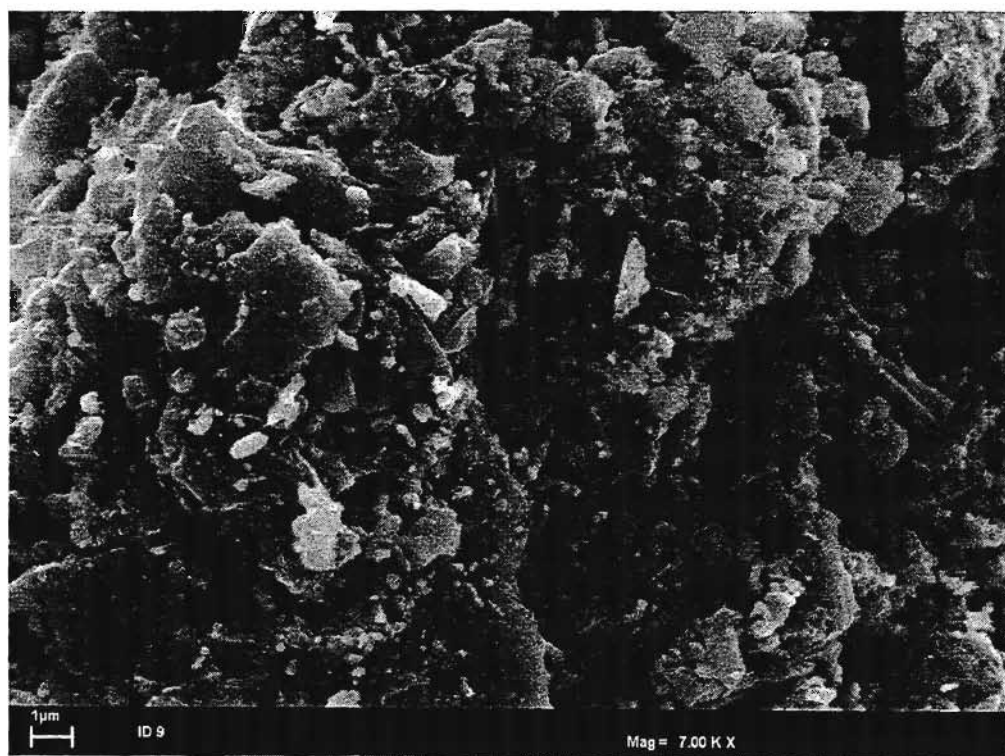


Image 4: Pre-reduced pellet produced in Induction heater

Appendix H

XRD Analytical Data

- *XRD Analysis of Pellets Reduced in Tube Furnace*
rc1 – rc10
run1rc – run3rc

- *XRD Analysis of Pellets Reduced in Thermobalance*
UNDr2 – UNDr4

- *XRD Analysis of Pellets Reduced in Induction Furnace*
UND1d1 – UND1d9

Description:
RC/1

Original scan: rc1
Date: 10/16/2001 09:36
Description of scan:
RC/1

Used wavelength: K-Alpha
K-Alpha1 wavelength (Å): 1.78897
K-Alpha2 wavelength (Å): 1.79285
K-Alpha2/K-Alpha1 intensity ratio: 0.50000
K-Alpha wavelength (Å): 1.78897
K-Beta wavelength (Å):

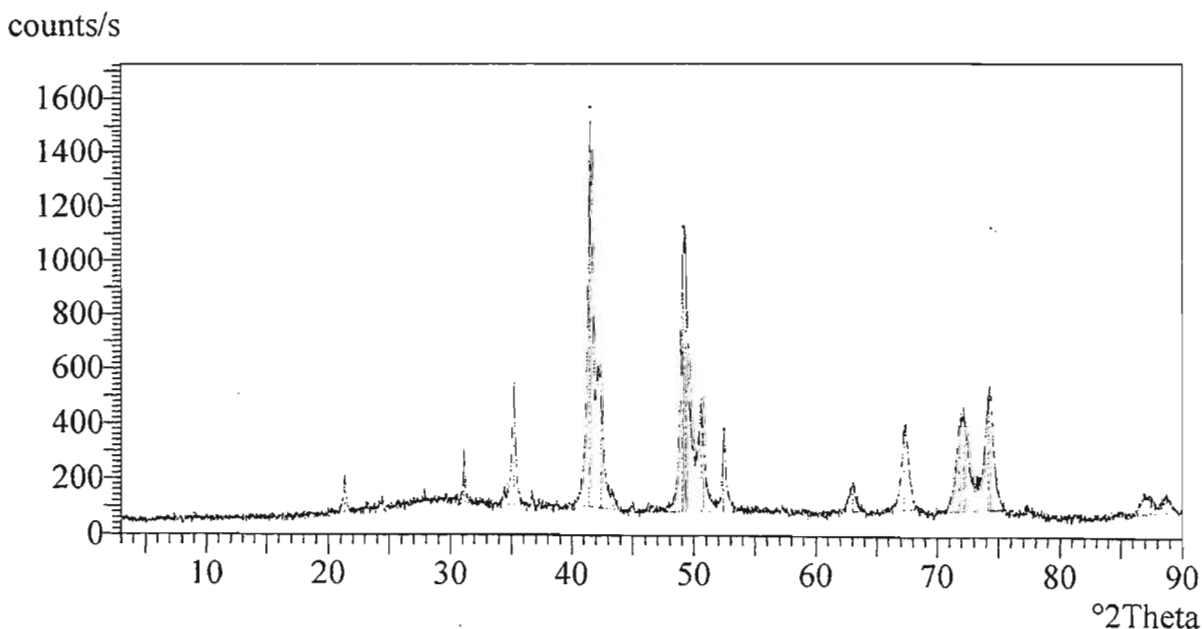
Peak search parameter set: As Measured Intensities
Set created: 04/28/1999 12:06
Peak positions defined by: Minimum of 2nd derivative
Minimum peak tip width (°2Theta): 0.00
Minimum peak tip width (°2Theta): 1.00
Peak base width (°2Theta): 2.00
Minimum significance: 0.60

d-spacing (Å)	Relative Intensity (%)	Angle (°2Theta)	Peak Height (counts/s)	Background (counts/s)	Tip Width (°2Theta)	Significance
6.39123	0.31	16.09045	4.16	58.22	0.24000	0.61
5.08115	0.86	20.27828	11.40	73.50	0.20000	0.70
4.83451	10.17	21.32463	135.12	78.84	0.10000	1.06
4.46513	1.23	23.11210	16.39	88.10	0.24000	0.79
4.23521	2.23	24.38552	29.61	94.86	0.12000	0.93
3.71744	1.44	27.84601	19.11	116.71	0.32000	0.62
3.33957	14.38	31.07194	191.12	117.06	0.10000	1.77
3.02775	2.77	34.36638	36.82	103.53	0.20000	1.10
3.042.96113	33.46	35.16447	444.54	104.67	0.16000	4.60
2.84958	2.01	36.38879	26.71	103.22	0.20000	1.61
2.52984	100.00	41.41194	1328.67	100.24	0.14000	4.05
2.47598	31.47	42.35567	418.12	95.61	0.44000	11.57
2.42141	4.35	43.35800	57.74	90.70	0.32000	0.84
2.33788	2.18	44.99023	28.94	84.21	0.20000	1.09
2.27597	1.49	46.32716	19.77	82.76	0.48000	0.61
2.15813	74.83	48.97200	994.25	83.72	0.10000	1.24
2.14739	73.77	49.23324	980.21	83.82	0.16000	1.70
2.09490	27.61	50.55217	366.82	84.30	0.12000	0.80
2.02835	18.00	52.33417	239.10	84.95	0.08000	0.85
1.93281	1.04	55.13438	13.81	85.97	0.32000	0.62
1.71245	8.32	62.97873	110.53	86.00	0.24000	1.65
1.61642	21.79	67.19733	289.51	93.12	0.16000	1.04
1.52655	23.12	71.74038	307.19	90.50	0.20000	1.15

d-spacing (Å)	Relative Intensity (%)	Angle (°2Theta)	Peak Height (counts/s)	Background (counts/s)	Tip Width (°2Theta)	Significance
6.39123	0.31	16.09045	4.16	58.22	0.24000	0.61
5.08115	0.86	20.27828	11.40	73.50	0.20000	0.70
4.83451	10.17	21.32463	135.12	78.84	0.10000	1.06
4.46513	1.23	23.11210	16.39	88.10	0.24000	0.79
4.23521	2.23	24.38552	29.61	94.86	0.12000	0.93
3.71744	1.44	27.84601	19.11	116.71	0.32000	0.62
3.33957	14.38	31.07194	191.12	117.06	0.10000	1.77
3.02775	2.77	34.36638	36.82	103.53	0.20000	1.10
3.042.96113	33.46	35.16447	444.54	104.67	0.16000	4.60
2.84958	2.01	36.38879	26.71	103.22	0.20000	1.61
2.52984	100.00	41.41194	1328.67	100.24	0.14000	4.05
2.47598	31.47	42.35567	418.12	95.61	0.44000	11.57
2.42141	4.35	43.35800	57.74	90.70	0.32000	0.84
2.33788	2.18	44.99023	28.94	84.21	0.20000	1.09
2.27597	1.49	46.32716	19.77	82.76	0.48000	0.61
2.15813	74.83	48.97200	994.25	83.72	0.10000	1.24
2.14739	73.77	49.23324	980.21	83.82	0.16000	1.70
2.09490	27.61	50.55217	366.82	84.30	0.12000	0.80
2.02835	18.00	52.33417	239.10	84.95	0.08000	0.85
1.93281	1.04	55.13438	13.81	85.97	0.32000	0.62
1.71245	8.32	62.97873	110.53	86.00	0.24000	1.65
1.61642	21.79	67.19733	289.51	93.12	0.16000	1.04
1.52655	23.12	71.74038	307.19	90.50	0.20000	1.15

X'Pert Graphics & Identify
Graph: rc1

User-1
10/16/2001 14:05



Description:
RC/2

Original scan: rc2
Description of scan:
RC/2

Used wavelength: K-Alpha
K-Alpha1 wavelength (Å): 1.78897
K-Alpha2 wavelength (Å): 1.79285
K-Alpha2/K-Alpha1 intensity ratio: 0.50000
K-Alpha wavelength (Å): 1.78897
K-Beta wavelength (Å):

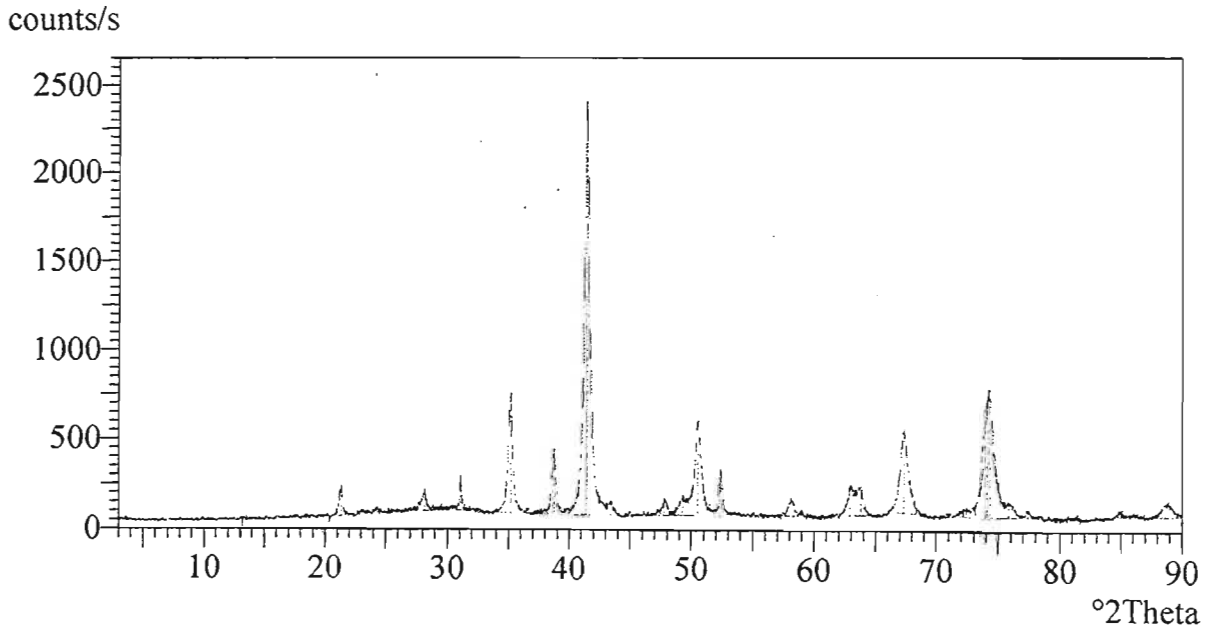
Peak search parameter set: As Measured Intensities
Set created: 04/28/1999 12:06
Peak positions defined by: Minimum of 2nd derivative
Minimum peak tip width (*2Theta): 0.00
Minimum peak tip width (*2Theta): 1.00
Peak base width (*2Theta): 2.00
Minimum significance: 0.60

d-spacing (Å)	Relative Intensity (%)	Angle (*2Theta)	Peak Height (counts/s)	Background (counts/s)	Tip Width (*2Theta)	Significance
11.44431	0.00	8.96557	0.00	44.78	0.12000	0.69
9.58013	0.06	10.71485	1.47	46.62	0.56000	0.73
7.85895	0.17	13.07083	3.88	49.33	0.04000	0.88
7.73477	0.42	13.28158	9.81	49.81	0.08000	0.69
4.84012	7.49	21.29961	173.95	71.39	0.10000	1.23
4.47852	0.81	23.04201	18.90	82.16	0.24000	0.61
4.25779	1.26	24.25427	29.36	89.65	0.16000	0.84
3.67951	5.02	28.13899	116.64	100.59	0.16000	1.35
3.34356	8.67	31.03401	201.28	102.73	0.16000	4.99
2.96225	27.96	35.15075	649.18	89.74	0.20000	7.67
2.85214	1.00	36.55481	23.18	87.78	0.24000	0.87
2.69769	15.04	38.72862	349.32	84.76	0.06000	0.81
2.52867	100.00	41.45202	2322.02	81.00	0.18000	9.99
2.42085	3.07	43.36846	71.31	78.31	0.32000	1.24
2.34007	1.15	44.94567	26.66	77.26	0.16000	0.67
2.21069	3.66	47.73429	85.03	80.18	0.16000	0.77
2.14752	4.49	49.22991	104.22	81.78	0.16000	0.71
2.09863	22.23	50.45610	516.16	83.10	0.28000	7.23
2.02710	11.06	52.36882	256.89	85.15	0.12000	1.96
1.83487	2.70	58.35175	62.80	80.10	0.14000	0.75
1.81832	1.23	58.93478	28.51	79.22	0.24000	1.04
1.71544	6.77	62.85635	157.22	85.15	0.20000	1.28
1.69305	6.58	63.78492	152.87	85.63	0.16000	0.68

d-spacing (Å)	Relative Intensity (%)	Angle (*2Theta)	Peak Height (counts/s)	Background (counts/s)	Tip Width (*2Theta)	Significance
1.61466	20.24	67.28022	469.90	99.35	0.40000	11.64
1.51565	1.66	72.17170	38.48	80.27	0.48000	0.74
1.48606	26.83	74.01454	623.02	78.21	0.16000	0.91
1.48228	30.16	74.23461	700.43	77.97	0.16000	1.11
1.45646	3.46	75.77996	80.38	76.24	0.56000	2.55
1.43174	1.74	77.52821	40.42	74.52	0.32000	1.36
1.37267	0.69	81.33036	15.97	67.30	0.96000	2.18
1.32470	1.18	84.94491	27.50	80.76	0.56000	2.49
1.27656	2.76	88.96575	64.19	87.68	0.40000	1.29

X'Pert Graphics & Identify
Graph: rc2

User-1
10/16/2001 14:07



Description: RC/3
 Original scan: rc3 Date: 10/16/2001 12:46
 Description of scan: RC/3
 Used wavelength: K-Alpha
 K-Alpha1 wavelength (Å): 1.78897
 K-Alpha2 wavelength (Å): 1.79285
 K-Alpha2/K-Alpha1 intensity ratio: 0.50000
 K-Alpha wavelength (Å): 1.78897
 K-Beta wavelength (Å):

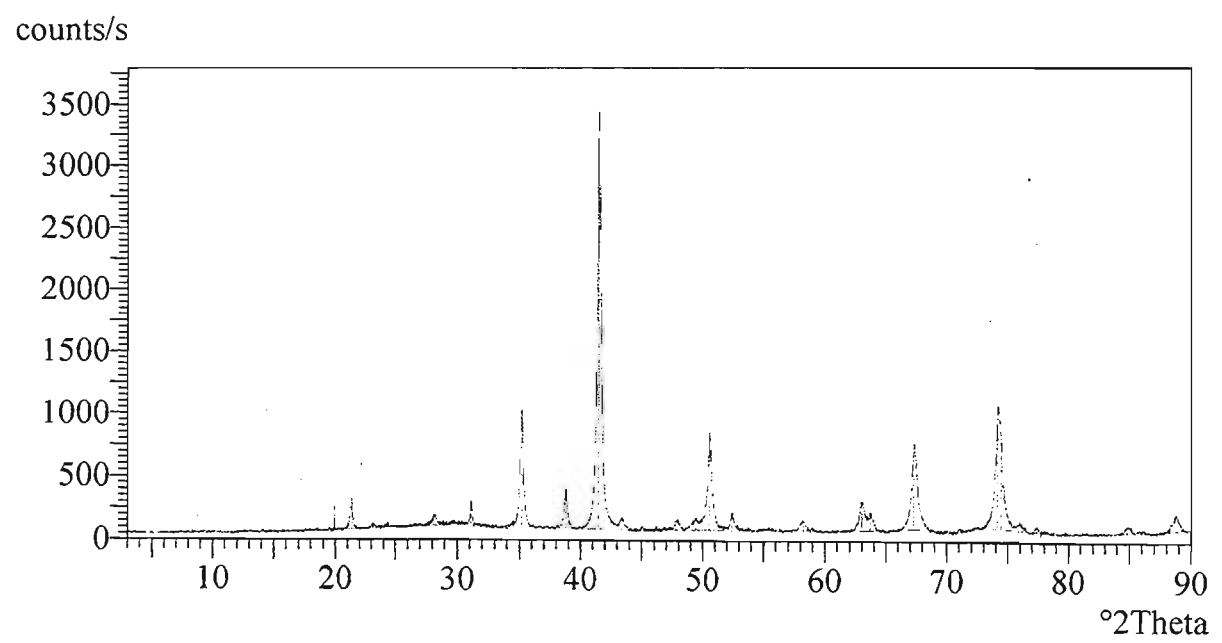
Peak search parameter set: As Measured Intensities
 Set created: 04/28/1999 12:06
 Peak positions defined by: Minimum of 2nd derivative
 Minimum peak tip width (°2Theta): 0.00
 Minimum peak tip width (°2Theta): 1.00
 Peak base width (°2Theta): 2.00
 Minimum significance: 0.60

d-spacing (Å)	Relative Intensity (%)	Angle (°2Theta)	Peak Height (counts/s)	Background (counts/s)	Tip Width (°2Theta)	Significance
1.61521	19.46	67.25449	653.59	94.38	0.24000	6.23
1.54093	0.48	70.96900	16.14	82.18	0.12000	0.72
1.48466	26.11	74.09608	876.97	100.26	0.10000	1.41
1.47985	21.50	74.37751	722.32	98.40	0.12000	1.00
1.45110	1.70	76.11011	57.03	86.89	0.12000	0.64
1.43150	1.22	77.34506	40.85	78.70	0.16000	0.60
1.37133	0.39	81.42666	13.19	67.74	0.40000	0.85
1.32685	1.50	84.77515	50.40	71.84	0.24000	0.78
1.30944	0.60	86.17282	20.30	73.55	0.48000	1.41
1.27931	3.40	88.72465	114.35	92.46	0.20000	1.19

d-spacing (Å)	Relative Intensity (%)	Angle (°2Theta)	Peak Height (counts/s)	Background (counts/s)	Tip Width (°2Theta)	Significance
5.72323	0.31	17.98321	10.38	66.67	0.06000	0.61
5.18114	4.66	19.88294	156.51	73.63	0.06000	4.01
4.83035	7.18	21.34323	241.22	80.48	0.16000	5.43
4.47151	0.74	23.07865	24.76	88.98	0.32000	0.94
4.24932	1.06	24.30335	35.73	95.50	0.12000	0.86
3.68533	2.67	28.09361	89.54	108.42	0.24000	2.32
3.59485	1.28	28.81577	42.92	107.68	0.06000	0.64
3.34223	4.92	31.04667	165.22	105.38	0.12000	3.44
2.96349	28.06	35.13565	942.54	99.25	0.22000	18.02
2.69600	9.17	38.75387	308.08	92.23	0.16000	4.26
2.52762	100.00	41.45011	3359.37	86.55	0.20000	23.47
2.42228	2.81	43.34156	94.49	82.57	0.28000	2.94
2.33836	0.90	44.98045	30.14	79.93	0.12000	0.96
2.21048	2.38	47.73905	79.92	79.21	0.16000	0.60
2.14064	2.76	49.39872	92.86	78.82	0.28000	1.61
2.09746	22.91	50.48629	769.57	78.56	0.08000	0.93
2.02714	4.42	52.36783	148.43	78.12	0.24000	4.01
1.98170	0.49	53.66349	16.40	77.82	0.32000	0.72
1.92284	0.54	55.44469	18.11	77.40	0.48000	0.65
1.83939	2.30	58.19460	77.38	76.75	0.20000	0.89
1.81714	0.73	58.97669	24.67	76.57	0.24000	0.77
1.71260	6.66	62.97255	223.59	80.99	0.28000	3.80
1.69538	3.72	63.68695	124.83	81.53	0.20000	1.18

X'Pert Graphics & Identify
 Graph: rc3

User-1
 10/16/2001 14:08



Description:
RC/4

Original scan: rc4 Date: 11/06/2001 10:31
Description of scan:
RC/4

Used wavelength: K-Alpha
K-Alpha1 wavelength (Å): 1.78897
K-Alpha2 wavelength (Å): 1.79285
K-Alpha2/K-Alpha1 intensity ratio: 0.50000
K-Alpha wavelength (Å): 1.78897
K-Beta wavelength (Å):

Peak search parameter set: As Measured Intensities
Set created: 04/28/1999 12:06
Peak positions defined by: Minimum of 2nd derivative
Minimum peak tip width (*2Theta): 0.00
Minimum peak tip width (*2Theta): 1.00
Peak base width (*2Theta): 2.00
Minimum significance: 0.60

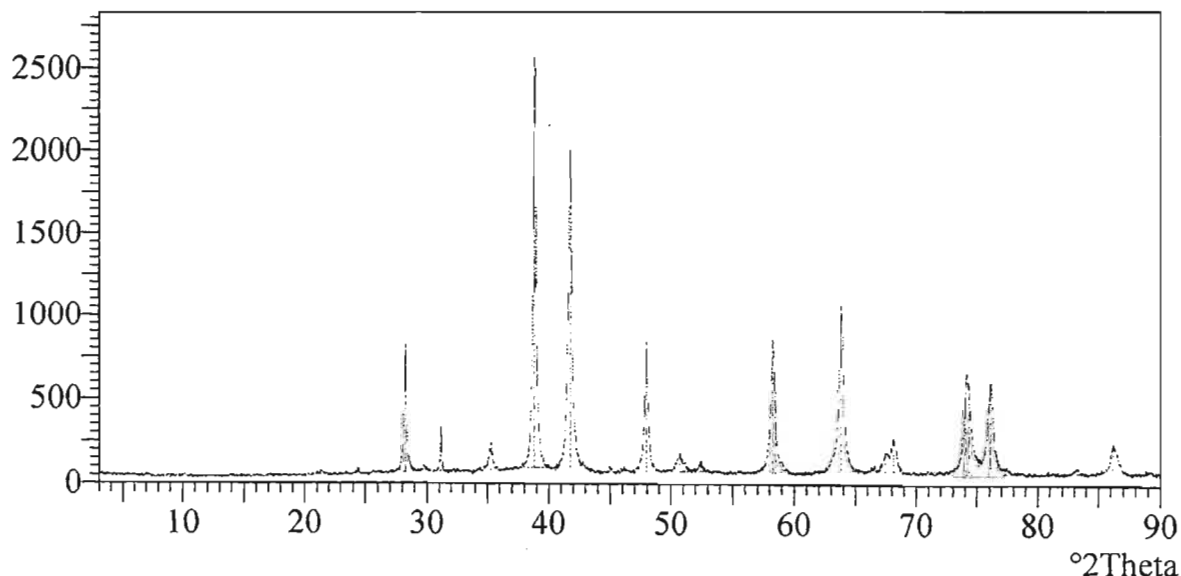
d-spacing (Å)	Relative Intensity (%)	Angle (*2Theta)	Peak Height (counts/s)	Background (counts/s)	Tip Width (*2Theta)	Significance
9.64601	0.56	10.64145	13.23	37.18	0.06000	0.60
6.70850	0.33	15.32524	7.68	39.18	0.20000	0.68
4.83342	1.03	21.32951	24.14	47.59	0.16000	0.61
4.24055	1.62	24.35439	38.12	54.89	0.10000	0.75
3.66956	31.35	28.21840	737.90	64.56	0.16000	10.25
3.48022	1.06	29.78647	24.96	67.18	0.32000	0.92
3.33478	10.57	31.11773	248.72	69.40	0.10000	2.24
2.95136	7.26	35.28471	170.83	76.89	0.10000	0.94
2.69455	100.00	38.77558	2353.68	92.05	0.20000	26.78
2.57729	0.73	40.61553	17.19	93.52	0.10000	0.70
2.51154	81.61	41.72774	1920.80	94.67	0.20000	17.69
2.34179	1.59	44.91088	37.41	66.63	0.10000	0.96
2.29593	0.59	45.85851	13.88	67.01	0.08000	0.65
2.27982	0.68	46.20139	16.05	67.16	0.48000	1.28
2.20099	32.01	47.95768	753.48	67.95	0.16000	6.57
2.09101	4.69	50.65289	110.38	69.16	0.24000	1.87
2.02555	2.21	52.41212	52.05	69.95	0.24000	1.91
1.83879	33.81	58.21530	795.79	67.59	0.10000	1.86
1.83199	21.29	58.45228	501.04	67.36	0.06000	0.68
1.81610	2.66	59.01382	62.55	66.82	0.20000	1.18
1.69523	41.42	63.77728	974.86	84.46	0.08000	1.30
1.61121	4.49	67.44368	105.80	77.33	0.28000	1.53
1.59783	7.98	68.08546	187.88	74.66	0.16000	1.05

d-spacing (Å)	Relative Intensity (%)	Angle (*2Theta)	Peak Height (counts/s)	Background (counts/s)	Tip Width (*2Theta)	Significance
1.53880	0.44	71.08202	10.46	66.27	0.40000	0.82
1.53213	0.18	71.43908	4.53	66.15	0.08000	0.63
1.48575	21.97	74.03257	517.03	65.09	0.08000	0.71
1.48075	19.79	74.32461	465.73	64.98	0.08000	0.81
1.45248	22.19	76.03467	522.30	64.30	0.08000	0.65
1.43241	1.44	77.28486	35.89	65.80	0.40000	0.61
1.37303	0.34	81.30459	8.11	63.33	0.48000	0.92
1.34700	1.31	83.21954	30.93	64.74	0.32000	0.92
1.31052	7.15	86.10120	165.38	67.73	0.24000	2.62

X'Pert Graphics & Identify
Graph: rc4

User-1
11/07/2001 07:15

counts/s



Description:
RC/5

Original scan: rc5 Date: 11/06/2001 11:47
Description of scan:
RC/5

Used wavelength: K-Alpha

K-Alpha1 wavelength (Å): 1.78897
K-Alpha2 wavelength (Å): 1.79285
K-Alpha2/K-Alpha1 intensity ratio: 0.50000
K-Alpha wavelength (Å): 1.78897
K-Beta wavelength (Å):

Peak search parameter set: As Measured Intensities
Set created: 04/28/1999 12:06
Peak positions defined by: Minimum of 2nd derivative
Minimum peak tip width (°2Theta): 0.00
Minimum peak tip width (°2Theta): 1.00
Peak base width (°2Theta): 2.00
Minimum significance: 0.60

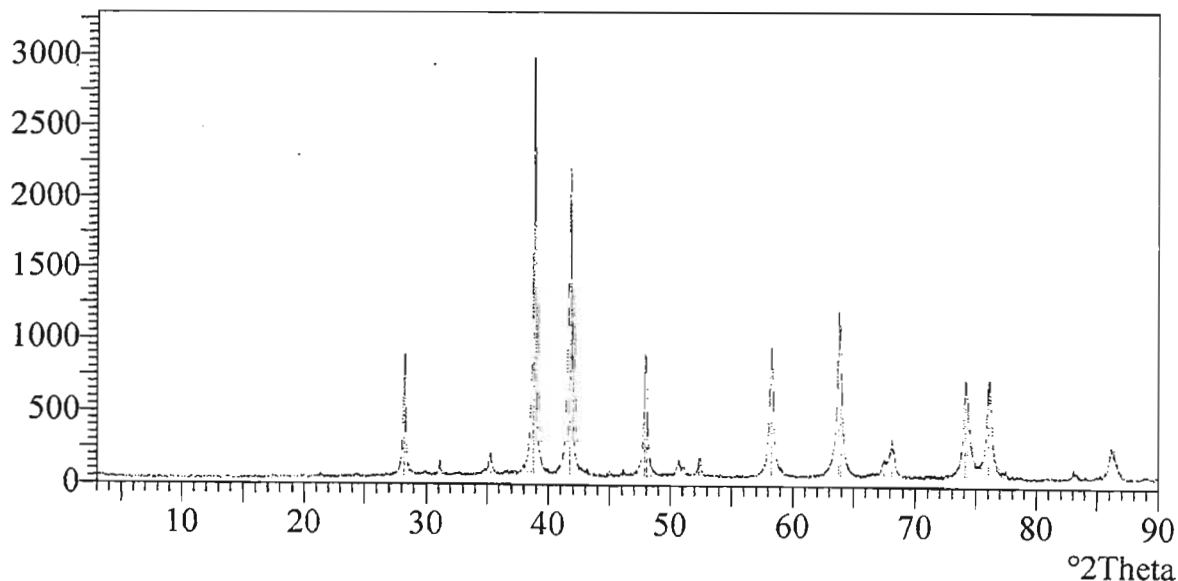
d-spacing (Å)	Relative Intensity (%)	Angle (°2Theta)	Peak Height (counts/s)	Background (counts/s)	Tip Width (°2Theta)	Significance
12.58391	0.29	8.15221	8.23	33.70	0.10000	0.91
9.16872	0.42	11.19714	11.88	33.39	0.06000	0.86
5.18018	0.12	19.88664	3.39	41.12	0.32000	0.62
4.83111	0.57	21.33983	16.15	43.48	0.24000	0.82
4.24228	0.49	24.34430	13.87	48.97	0.24000	1.15
3.67193	29.25	28.19821	835.55	58.40	0.16000	12.29
3.47168	0.80	29.86152	22.77	60.24	0.24000	0.61
3.13653	3.52	31.10102	100.67	61.62	0.12000	2.13
3.19180	0.33	32.54956	9.54	63.22	0.48000	1.07
2.95248	4.47	35.27086	127.58	70.40	0.08000	0.61
2.69492	100.00	38.77000	2856.59	81.05	0.20000	31.95
2.51352	73.99	41.69333	2113.52	71.66	0.18000	16.21
2.37342	0.38	44.28057	10.81	63.44	0.10000	0.66
2.34025	1.07	44.94206	30.56	62.78	0.12000	0.68
2.28512	0.89	46.08804	25.32	63.14	0.24000	1.30
2.20576	26.22	47.84764	749.02	63.74	0.08000	0.92
2.19913	22.37	48.00101	639.12	63.79	0.08000	0.72
2.09320	3.27	50.59627	95.53	64.67	0.24000	2.60
2.02887	4.29	52.31962	122.43	65.25	0.10000	0.99
1.83986	30.85	58.17820	881.38	74.27	0.18000	8.26
1.69412	39.52	63.73964	1128.84	75.98	0.12000	3.14
1.68963	28.28	63.92935	807.81	75.85	0.06000	0.61
1.63799	0.50	66.19789	14.35	74.35	0.48000	0.82

d-spacing (Å)	Relative Intensity (%)	Angle (°2Theta)	Peak Height (counts/s)	Background (counts/s)	Tip Width (°2Theta)	Significance
1.61135	3.96	67.43722	113.04	73.53	0.08000	0.70
1.59795	9.19	68.07964	262.50	73.10	0.08000	0.83
1.48530	22.59	74.05871	645.26	77.39	0.08000	1.58
1.48211	18.26	74.24462	521.58	76.99	0.16000	0.73
1.45312	22.57	75.98521	644.77	73.24	0.28000	9.60
1.45269	1.00	77.26699	28.64	70.49	0.32000	0.63
1.34839	1.58	83.11472	45.06	65.42	0.16000	0.69
1.31011	7.03	86.11801	200.81	66.77	0.16000	1.06
1.27751	0.50	88.88194	14.30	66.39	0.56000	1.85

X'Pert Graphics & Identify
Graph: rc5

User-1
11/07/2001 07:16

counts/s



Description:
 RC/6

Original scan: rc6
 Date: 11/07/2001 07:36
 Description of scan:
 RC/6

Used wavelength: K-Alpha

K-Alpha1 wavelength (Å): 1.78897
 K-Alpha2 wavelength (Å): 1.79285
 K-Alpha2/K-Alpha1 intensity ratio: 0.50000
 K-Alpha wavelength (Å): 1.78897
 K-Beta wavelength (Å):

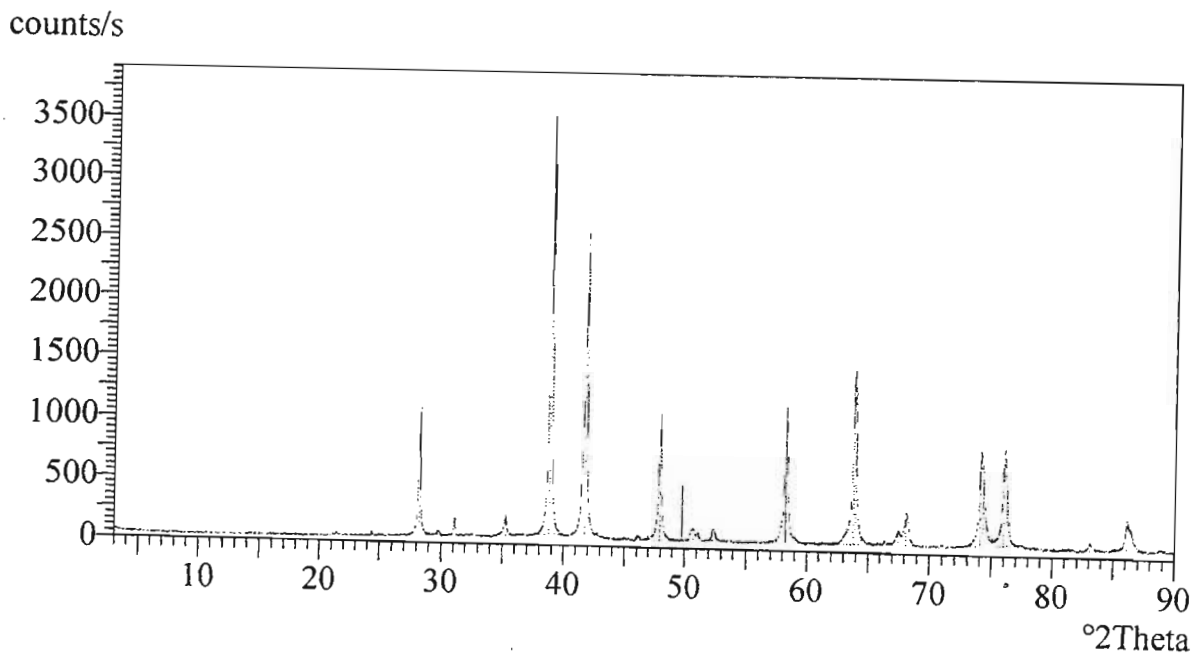
Peak search parameter set: As Measured Intensities
 Set created: 04/28/1999 12:06
 Peak positions defined by: Minimum of 2nd derivative
 Minimum peak tip width (*2Theta): 0.00
 Minimum peak tip width (*2Theta): 1.00
 Peak base width (*2Theta): 2.00
 Minimum significance: 0.60

d-spacing (Å)	Relative Intensity (%)	Angle (*2Theta)	Peak Height (counts/s)	Background (counts/s)	Tip Width (*2Theta)	Significance
4.82450	0.55	21.36940	18.56	40.68	0.32000	1.08
4.24076	0.79	24.35311	27.28	46.80	0.16000	1.26
3.66784	29.90	28.23033	1038.30	55.61	0.14000	11.62
3.48443	1.80	29.74964	62.58	58.35	0.12000	0.83
3.33606	4.24	31.10553	147.38	60.80	0.10000	2.42
2.95414	4.63	35.25047	160.77	67.24	0.06000	2.00
2.69390	100.00	38.78530	3472.33	81.32	0.18000	31.62
2.51296	70.21	41.70306	2437.84	80.20	0.16000	16.29
2.33926	0.35	44.96224	12.02	58.80	0.48000	1.35
2.28909	0.80	46.00345	27.80	59.41	0.12000	0.72
2.20403	29.27	47.88747	1016.19	60.56	0.16000	10.99
2.12667	13.01	49.74529	451.69	61.69	0.06000	1.06
2.08925	2.78	50.69860	96.66	62.28	0.32000	4.19
2.07560	1.82	51.05589	63.22	62.49	0.12000	1.55
2.02668	3.15	52.38058	109.40	63.30	0.24000	4.05
1.83950	31.83	58.19066	1105.08	65.33	0.12000	4.91
1.83605	23.06	58.31062	800.69	65.36	0.10000	0.85
1.73015	0.74	62.26214	25.69	66.20	0.06000	0.70
1.69355	37.74	63.76364	1310.56	65.78	0.10000	2.92
1.68926	28.88	63.94478	1002.85	65.73	0.06000	0.61
1.63678	0.71	66.25293	24.59	65.09	0.20000	0.82
1.61164	3.05	67.42347	105.95	64.76	0.32000	2.14
1.59814	7.80	68.07050	270.71	64.58	0.10000	1.24

d-spacing (Å)	Relative Intensity (%)	Angle (*2Theta)	Peak Height (counts/s)	Background (counts/s)	Tip Width (*2Theta)	Significance
1.54017	0.43	71.00943	15.07	65.14	0.24000	0.78
1.48371	20.41	74.03500	708.73	77.90	0.14000	4.56
1.48170	17.32	74.26860	601.25	78.56	0.08000	0.67
1.45280	22.72	76.00480	789.04	83.49	0.12000	2.41
1.44967	14.35	76.19867	498.43	84.04	0.08000	1.57
1.34877	1.64	83.08640	57.05	57.30	0.16000	0.77
1.31052	7.09	86.08452	246.28	57.30	0.16000	1.70
1.27877	0.65	88.77145	22.63	57.30	0.24000	0.84

X'Pert Graphics & Identify
 Graph: rc6

User-1
 11/07/2001 10:33



Description:
RC77

Original scan: rc7 Date: 11/07/2001 09:16
Description of scan:
RC77
Used wavelength: K-Alpha
K-Alpha1 wavelength (Å): 1.78897
K-Alpha2 wavelength (Å): 1.79285
K-Alpha2/K-Alpha1 intensity ratio: 0.50000
K-Alpha wavelength (Å): 1.78897
K-Beta wavelength (Å):

Peak search parameter set: As Measured Intensities
Set created: 04/28/1999 12:06
Peak positions defined by: Minimum of 2nd derivative
Minimum peak tip width (°2Theta): 0.00
Minimum peak tip width (°2Theta): 1.00
Peak base width (°2Theta): 2.00
Minimum significance: 0.60

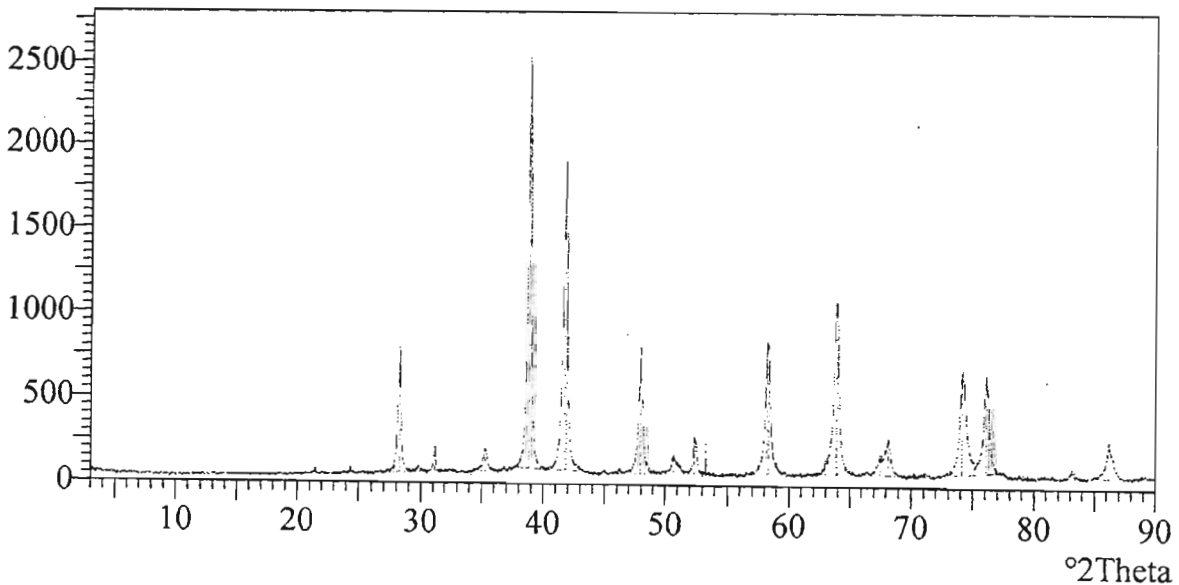
d-spacing (Å)	Relative Intensity (%)	Angle (°2Theta)	Peak Height (counts/s)	Background (counts/s)	Tip Width (°2Theta)	Significance
1.61052	3.90	67.47659	92.98	72.78	0.32000	0.99
1.59736	8.99	68.10798	214.12	70.45	0.16000	1.20
1.59207	4.38	68.36556	104.39	69.49	0.12000	0.62
1.53992	0.45	71.02273	10.63	65.59	0.48000	1.22
1.48492	24.05	74.05067	572.86	77.25	0.20000	2.87
1.45278	23.51	76.00632	559.98	85.76	0.12000	1.10
1.44905	17.96	76.23676	427.72	84.54	0.12000	1.53
1.37681	0.25	81.03454	6.76	61.99	0.96000	0.65
1.34828	1.80	83.12290	42.94	62.62	0.32000	1.33
1.31013	8.71	86.11679	207.37	65.21	0.16000	1.64

d-spacing (Å)	Relative Intensity (%)	Angle (°2Theta)	Peak Height (counts/s)	Background (counts/s)	Tip Width (°2Theta)	Significance
31.06118	0.68	3.30040	16.14	40.40	0.96000	0.70
8.39730	0.23	12.22953	5.57	34.53	0.12000	0.65
4.81897	0.78	21.39419	18.47	44.56	0.32000	1.05
4.24485	1.61	24.32933	38.26	49.40	0.12000	1.49
3.66836	30.67	28.22622	730.37	58.65	0.10000	2.51
3.48451	1.33	29.74902	31.66	60.02	0.24000	0.63
3.32944	6.86	31.16887	163.42	61.31	0.20000	6.03
3.19784	0.45	32.48636	10.70	62.51	0.64000	0.76
2.95466	5.30	35.24402	126.19	71.05	0.20000	2.10
2.69076	100.00	38.83232	2381.60	89.00	0.22000	26.85
2.51329	76.30	41.69737	1817.22	79.16	0.16000	7.59
2.50475	49.42	41.84624	1176.91	78.65	0.06000	0.76
2.33994	0.87	44.94834	20.65	61.24	0.32000	0.96
2.28283	0.94	46.13680	22.49	61.24	0.20000	0.84
2.20302	30.64	47.91073	729.80	61.25	0.12000	2.56
2.08926	4.28	50.69831	101.92	61.21	0.32000	3.26
2.02859	9.70	52.32758	230.97	61.21	0.06000	1.13
1.99674	7.80	53.22710	185.75	61.20	0.06000	2.76
1.83969	32.33	58.18418	769.96	67.39	0.06000	1.23
1.83584	29.46	58.31765	701.51	67.39	0.12000	1.87
1.71351	2.77	62.93536	66.03	72.82	0.10000	0.61
1.69198	42.08	63.82991	1002.25	73.62	0.10000	1.26
1.68919	33.50	63.94792	797.82	73.75	0.10000	0.82

X'Pert Graphics & Identify
Graph: rc7

User-1
11/07/2001 10:38

counts/s



Description:
 RC/8

Original scan: rc8 Date: 11/07/2001 10:49
 Description of scan:
 RC/8

Used wavelength: K-Alpha

K-Alpha1 wavelength (Å): 1.78897
 K-Alpha2 wavelength (Å): 1.79285
 K-Alpha2/K-Alpha1 intensity ratio: 0.50000
 K-Alpha wavelength (Å): 1.78897
 K-Beta wavelength (Å):

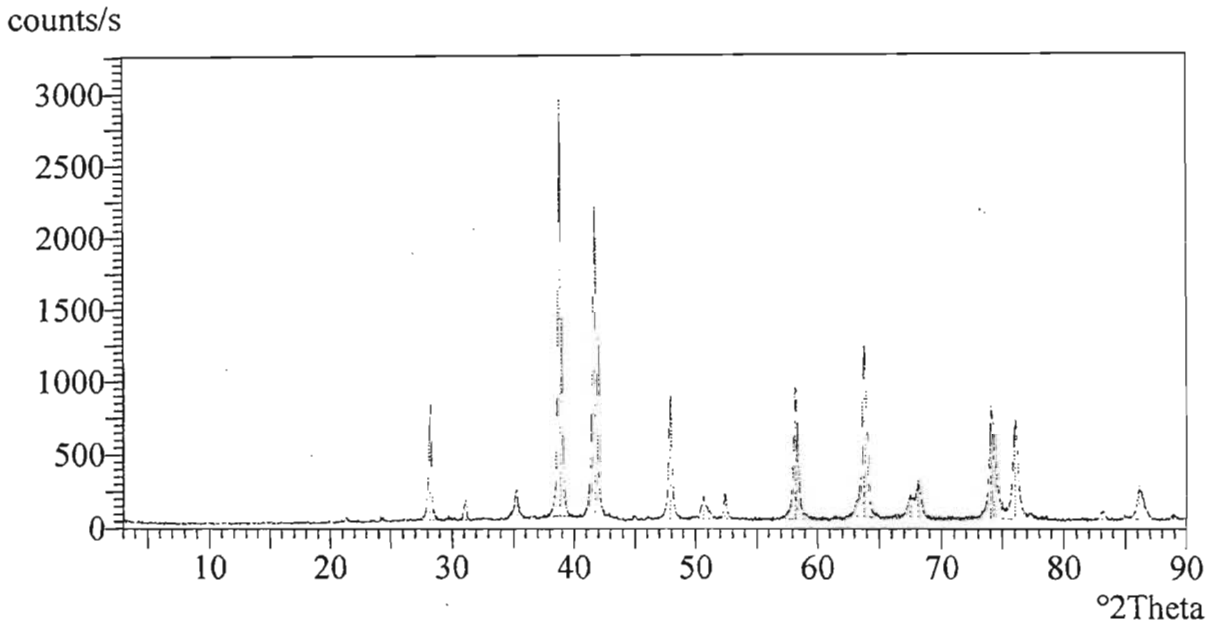
Peak search parameter set: As Measured Intensities
 Set created: 04/28/1999 12:06
 Peak positions defined by: Minimum of 2nd derivative
 Minimum peak tip width (°2Theta): 0.00
 Minimum peak tip width (°2Theta): 1.00
 Peak base width (°2Theta): 2.00
 Minimum significance: 0.60

d-spacing (Å)	Relative Intensity (%)	Angle (°2Theta)	Peak Height (counts/s)	Background (counts/s)	Tip Width (°2Theta)	Significance
6.86061	0.22	14.98304	6.22	35.12	0.48000	0.61
6.45425	0.19	15.93232	5.40	35.77	0.80000	0.79
4.82466	1.26	21.36870	35.38	43.41	0.12000	1.14
4.27774	1.05	24.13940	29.30	48.04	0.08000	0.88
3.67555	28.65	28.16990	803.14	55.30	0.20000	16.86
3.48654	1.30	29.73125	36.38	56.37	0.06000	0.70
3.32756	3.58	31.18701	100.30	57.36	0.08000	0.94
3.19812	0.26	32.48338	7.38	58.24	0.96000	0.87
2.95135	6.63	35.28492	185.75	66.25	0.10000	1.23
2.69226	100.00	38.80991	2803.31	80.95	0.24000	40.28
2.51260	75.52	41.70940	2116.92	83.62	0.24000	28.55
2.34378	1.13	44.87074	31.79	58.67	0.16000	0.69
2.28388	0.72	46.11441	20.17	59.29	0.24000	1.61
2.20374	29.26	47.89429	820.35	60.17	0.16000	6.82
2.09296	5.40	50.60232	151.39	61.51	0.20000	2.30
2.02762	5.93	52.35449	166.15	62.37	0.20000	3.71
1.84059	28.97	58.15295	812.01	62.84	0.10000	1.95
1.83590	24.70	58.31558	692.31	62.95	0.10000	0.91
1.69536	42.20	63.77165	1183.02	78.57	0.08000	1.04
1.61184	5.27	67.41387	147.85	73.05	0.20000	1.45
1.59816	8.49	68.06959	238.04	71.73	0.08000	0.65
1.48585	23.69	74.02671	664.06	71.91	0.08000	0.66
1.48160	21.17	74.27439	593.52	71.37	0.12000	1.96

d-spacing (Å)	Relative Intensity (%)	Angle (°2Theta)	Peak Height (counts/s)	Background (counts/s)	Tip Width (°2Theta)	Significance
1.45301	24.05	75.99171	674.22	67.67	0.16000	3.91
1.43140	1.45	77.34952	40.68	64.74	0.24000	0.94
1.41262	0.63	78.57432	17.58	62.11	0.16000	0.67
1.34805	2.01	83.14050	56.40	62.44	0.24000	1.36
1.31079	7.07	86.06296	198.10	62.34	0.10000	0.92
1.27690	1.11	88.93600	31.14	62.28	0.32000	0.90

X'Pert Graphics & Identify
 Graph: rc8

User-1
 11/07/2001 13:17



Description:
RC9

Original scan: rc9 Date: 11/07/2001 12:01
Description of scan:
RC9

Used wavelength: K-Alpha

K-Alpha1 wavelength (Å): 1.78897
K-Alpha2 wavelength (Å): 1.79285
K-Alpha2/K-Alpha1 intensity ratio: 0.50000
K-Alpha wavelength (Å): 1.78897
K-Beta wavelength (Å):

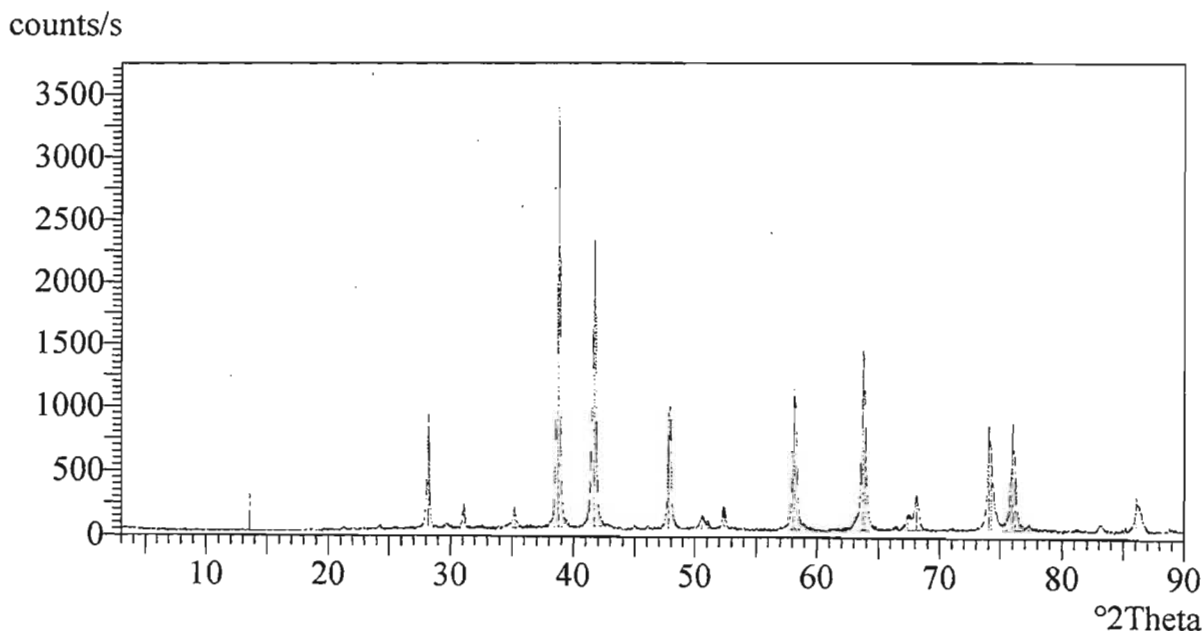
Peak search parameter set: As Measured Intensities
Set created: 04/28/1999 12:06
Peak positions defined by: Minimum of 2nd derivative
Minimum peak tip width (°2Theta): 0.00
Minimum peak tip width (°2Theta): 1.00
Peak base width (°2Theta): 2.00
Minimum significance: 0.60

d-spacing (Å)	Relative Intensity (%)	Angle (°2Theta)	Peak Height (counts/s)	Background (counts/s)	Tip Width (°2Theta)	Significance
1.61328	3.20	67.34575	106.70	64.01	0.20000	1.49
1.59830	8.30	68.06289	276.56	65.55	0.14000	1.91
1.54033	0.46	71.00054	15.38	64.12	0.32000	0.70
1.48604	23.35	74.01568	778.25	67.16	0.14000	5.32
1.48266	18.64	74.21288	621.39	67.06	0.10000	1.05
1.45342	24.85	75.96707	828.16	66.20	0.16000	6.95
1.44992	13.94	76.18316	464.61	66.09	0.12000	0.65
1.43263	1.26	77.27112	42.02	65.56	0.24000	2.38
1.37441	0.39	81.20548	13.08	60.07	0.32000	0.63
1.34932	1.50	83.04500	50.14	59.53	0.24000	1.14
1.31106	8.18	86.04053	272.75	59.25	0.06000	0.61
1.27775	0.67	88.86159	22.28	59.25	0.32000	0.87

d-spacing (Å)	Relative Intensity (%)	Angle (°2Theta)	Peak Height (counts/s)	Background (counts/s)	Tip Width (°2Theta)	Significance
7.59318	8.54	13.53039	284.70	35.31	0.04000	9.74
4.84832	0.68	21.26317	22.81	43.57	0.20000	0.77
4.25539	0.88	24.26811	29.42	48.67	0.12000	0.86
3.88387	0.30	26.63027	10.07	51.52	0.40000	0.71
3.67513	26.60	28.17321	856.50	53.38	0.22000	24.24
3.48051	1.21	29.78399	40.36	55.53	0.28000	1.22
3.35698	5.19	31.10530	172.87	56.92	0.12000	2.50
3.18787	0.50	32.59079	16.53	58.72	0.24000	0.82
2.95584	4.31	35.22902	143.68	63.49	0.12000	1.40
2.85950	0.38	36.45743	12.56	66.10	0.48000	0.81
2.69502	100.00	38.76849	3333.22	71.02	0.20000	38.01
2.51494	67.78	41.66869	2259.41	77.20	0.18000	19.87
2.34056	0.94	44.93589	31.40	58.65	0.12000	0.68
2.28856	0.63	46.00838	21.09	58.95	0.32000	1.04
2.20743	26.02	47.80905	867.42	59.50	0.12000	3.80
2.09361	3.17	50.53380	105.56	60.32	0.24000	1.97
2.07679	2.01	51.02459	67.02	60.47	0.12000	1.03
2.02981	5.22	52.29359	174.00	60.86	0.12000	1.40
2.02542	4.22	52.41562	140.66	60.89	0.08000	0.64
1.84131	32.68	58.12792	1089.39	64.68	0.14000	6.12
1.69461	40.73	63.71914	1357.65	66.31	0.20000	13.65
1.69039	26.39	63.89692	879.49	66.20	0.10000	0.84
1.63526	0.72	66.32264	24.10	64.66	0.24000	1.28

X'Pert Graphics & Identify
Graph: rc9

User-1
11/07/2001 13:18



Description:
RC/10

Original scan: rc10
Description of scan:
RC/10

Date: 11/07/2001 13:23

Used wavelength: K-Alpha
K-Alpha1 wavelength (Å): 1.78897
K-Alpha2 wavelength (Å): 1.79285
K-Alpha2/K-Alpha1 intensity ratio: 0.50000
K-Alpha wavelength (Å): 1.78897
K-Beta wavelength (Å):

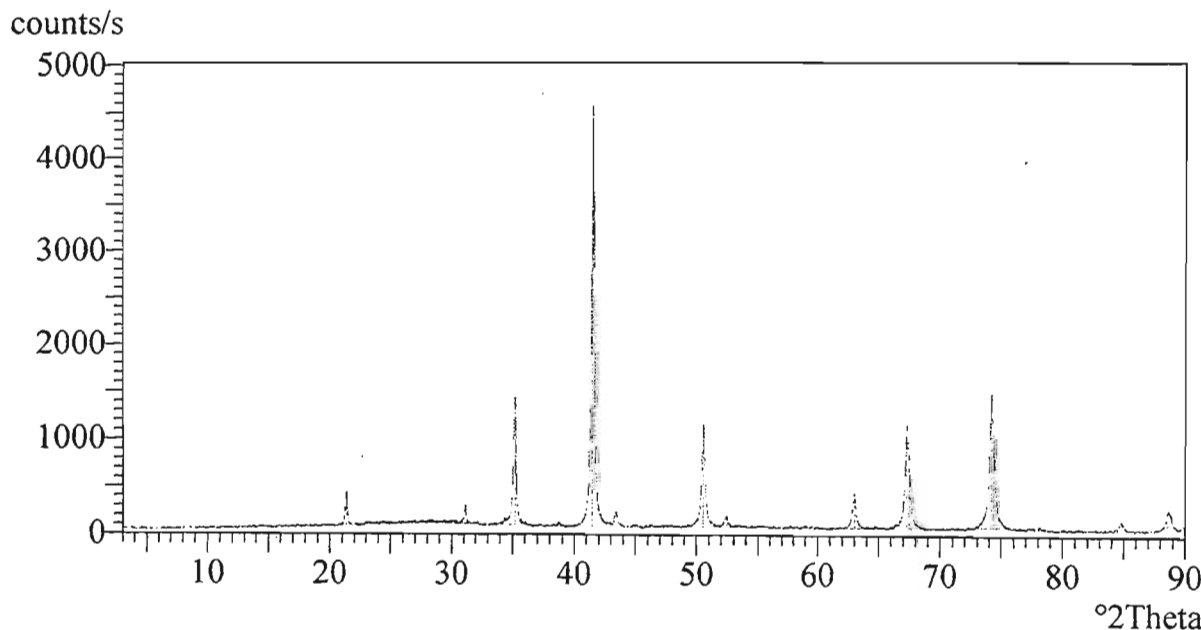
Peak search parameter set: As Measured Intensities
Set created: 04/28/1999 12:06
Peak positions defined by: Minimum of 2nd derivative
Minimum peak tip width (°2Theta): 0.00
Minimum peak tip width (°2Theta): 1.00
Peak base width (°2Theta): 2.00
Minimum significance: 0.60

d-spacing (Å)	Relative Intensity (%)	Angle (°2Theta)	Peak Height (counts/s)	Background (counts/s)	Tip Width (°2Theta)	Significance
32.45877	0.22	3.15826	9.82	43.62	0.24000	0.86
4.82919	8.23	21.34840	368.86	89.54	0.10000	3.10
4.25158	0.51	24.29023	22.75	104.29	0.28000	1.13
3.65021	0.51	28.36952	22.70	116.79	0.48000	0.85
3.33375	4.26	31.12759	190.98	105.66	0.08000	1.25
3.23866	0.44	32.06580	19.65	101.88	0.32000	0.80
2.96105	30.34	35.16552	1360.54	94.35	0.18000	15.15
2.87694	0.47	36.22867	20.89	89.01	0.06000	0.77
2.7694	0.51	38.76200	23.03	85.53	0.20000	0.80
2.69546	100.00	41.44908	4484.09	83.39	0.22000	47.05
2.52768	3.57	43.40225	160.25	81.93	0.20000	3.50
2.41906	0.54	44.94277	24.27	80.78	0.40000	1.51
2.34022	0.47	46.25418	20.96	80.75	0.24000	0.69
2.27756	0.31	47.81314	13.92	81.59	0.64000	0.64
2.20726	23.67	50.49821	1061.55	83.02	0.16000	9.47
2.09699	2.23	52.41880	100.04	84.05	0.24000	2.88
2.02531	0.30	55.51158	13.30	84.00	0.48000	0.73
1.92071	0.45	58.99902	20.18	81.46	0.24000	1.44
1.81652	7.95	63.00377	356.58	79.17	0.08000	1.15
1.71184	0.38	64.72713	17.03	78.94	0.16000	0.64
1.67102	25.02	67.25861	1122.09	78.60	0.16000	5.32
1.61512	16.26	67.43438	728.91	78.58	0.08000	1.74
1.61141	0.14	71.13443	6.35	77.45	0.64000	0.75

d-spacing (Å)	Relative Intensity (%)	Angle (°2Theta)	Peak Height (counts/s)	Background (counts/s)	Tip Width (°2Theta)	Significance
1.48557	32.46	74.15945	1455.71	85.45	0.14000	5.61
1.48037	21.56	74.34679	966.99	85.23	0.12000	1.54
1.43083	0.32	77.38643	14.27	73.96	0.32000	0.72
1.41985	0.69	78.09810	30.86	70.46	0.16000	0.65
1.37246	0.19	81.34549	8.57	66.06	0.48000	0.71
1.32754	1.90	84.72024	85.25	66.83	0.24000	1.75
1.28071	4.20	88.60224	188.18	71.07	0.24000	2.84
1.27753	3.51	88.88098	157.46	71.07	0.12000	0.61

X'Pert Graphics & Identify
Graph: rc10

User-1
11/07/2001 14:41



Description:
 RUN 1 RC
 Original scan: run1rc Date: 01/30/2002 10:56
 Description of scan:
 RUN 1 RC

Used wavelength: K-Alpha
 K-Alpha1 wavelength (Å): 1.78897
 K-Alpha2 wavelength (Å): 1.79285
 K-Alpha2/K-Alpha1 intensity ratio: 0.50000
 K-Alpha wavelength (Å): 1.78897
 K-Beta wavelength (Å):

Peak search parameter set: As Measured Intensities
 Set created: 04/28/1999 12:06
 Peak positions defined by: Minimum of 2nd derivative
 Minimum peak tip width (°2Theta): 0.00
 Minimum peak tip width (°2Theta): 1.00
 Peak base width (°2Theta): 2.00
 Minimum significance: 0.60

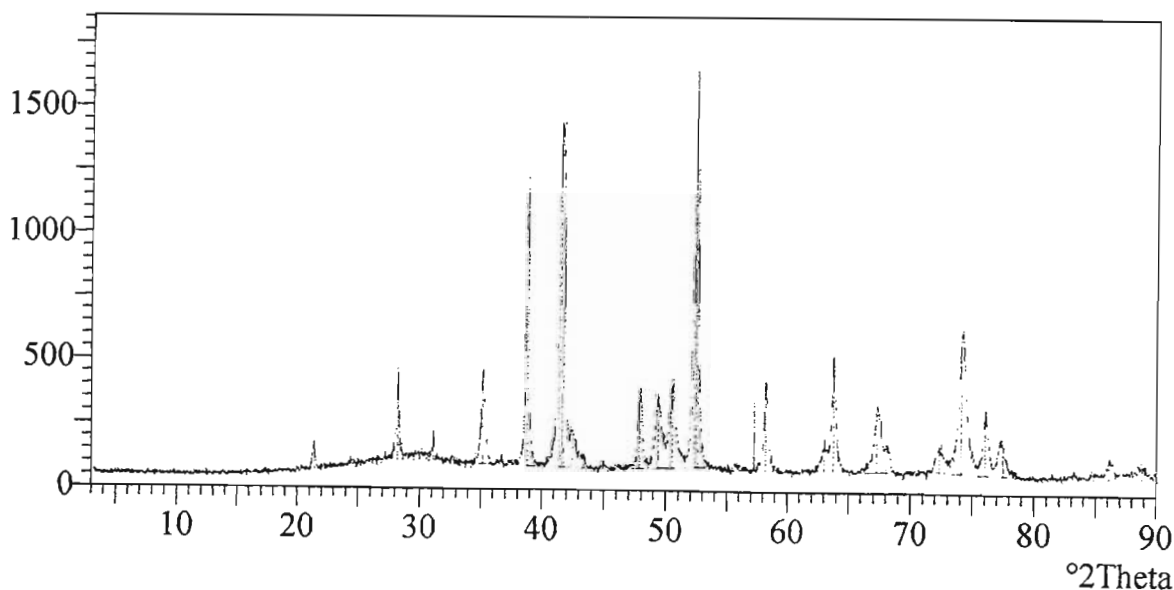
d-spacing (Å)	Relative Intensity (%)	Angle (°2Theta)	Peak Height (counts/s)	Background (counts/s)	Tip Width (°2Theta)	Significance
4.82509	7.51	21.36676	114.37	72.75	0.06000	0.68
4.24843	1.16	24.30848	17.74	89.25	0.24000	0.79
3.67284	23.97	28.19110	365.15	109.41	0.12000	2.95
3.33929	7.51	31.07469	114.38	108.04	0.08000	0.80
2.96363	24.69	35.13383	376.07	96.52	0.10000	1.22
2.83998	2.97	36.71684	45.30	93.83	0.08000	0.74
2.69412	69.27	38.78198	1055.18	90.33	0.18000	12.31
2.52695	86.46	41.46148	1317.05	85.78	0.18000	6.20
2.51142	65.91	41.72994	1003.98	85.32	0.12000	2.36
2.47224	9.56	42.42288	145.70	84.14	0.24000	3.25
2.42084	3.14	43.36869	47.77	82.54	0.24000	1.06
2.34111	1.98	44.92477	30.18	80.03	0.12000	0.86
2.28516	0.73	46.08709	11.18	80.03	0.32000	0.69
2.20628	19.28	47.83566	293.64	82.47	0.12000	2.02
2.14242	18.02	49.35512	274.49	84.60	0.32000	6.34
2.09755	20.56	50.48399	313.25	86.17	0.28000	6.51
2.02626	100.00	52.39231	1523.26	88.84	0.18000	11.48
2.02080	77.66	52.54463	1182.91	89.05	0.06000	1.22
1.91159	1.08	55.79946	16.38	82.56	0.32000	1.24
1.86763	17.62	57.23253	268.36	81.04	0.06000	0.86
1.84055	21.52	58.15432	327.78	80.07	0.14000	2.85
1.71198	6.38	62.99822	97.24	83.76	0.24000	0.77
1.69380	29.09	63.75326	443.12	83.89	0.10000	1.59

d-spacing (Å)	Relative Intensity (%)	Angle (°2Theta)	Peak Height (counts/s)	Background (counts/s)	Tip Width (°2Theta)	Significance
1.61517	16.98	67.25637	258.59	78.24	0.20000	1.91
1.59944	7.22	68.00740	109.94	77.89	0.10000	0.65
1.51655	7.00	72.23879	106.69	81.64	0.28000	1.26
1.48542	33.88	74.05184	516.10	78.17	0.32000	8.31
1.45300	15.72	75.99246	239.41	74.34	0.08000	0.67
1.42990	7.80	77.44570	118.84	71.47	0.16000	0.62
1.34889	1.20	83.07754	18.35	62.92	0.64000	1.17
1.32658	1.58	84.79578	24.06	62.92	0.48000	0.64
1.31068	5.38	86.07206	81.95	62.92	0.16000	0.73
1.27803	3.33	88.83239	50.72	62.92	0.56000	1.59

X'Pert Graphics & Identify
 Graph: run1rc

User-1
 01/30/2002 13:53

counts/s



Description:
 RUN 2 RC

Original scan: run2rc Date: 01/30/2002 12:19
 Description of scan:
 RUN 2 RC

Used wavelength: K-Alpha
 K-Alpha1 wavelength (Å): 1.78897
 K-Alpha2 wavelength (Å): 1.79285
 K-Alpha2/K-Alpha1 intensity ratio: 0.50000
 K-Alpha wavelength (Å): 1.78897
 K-Beta wavelength (Å):

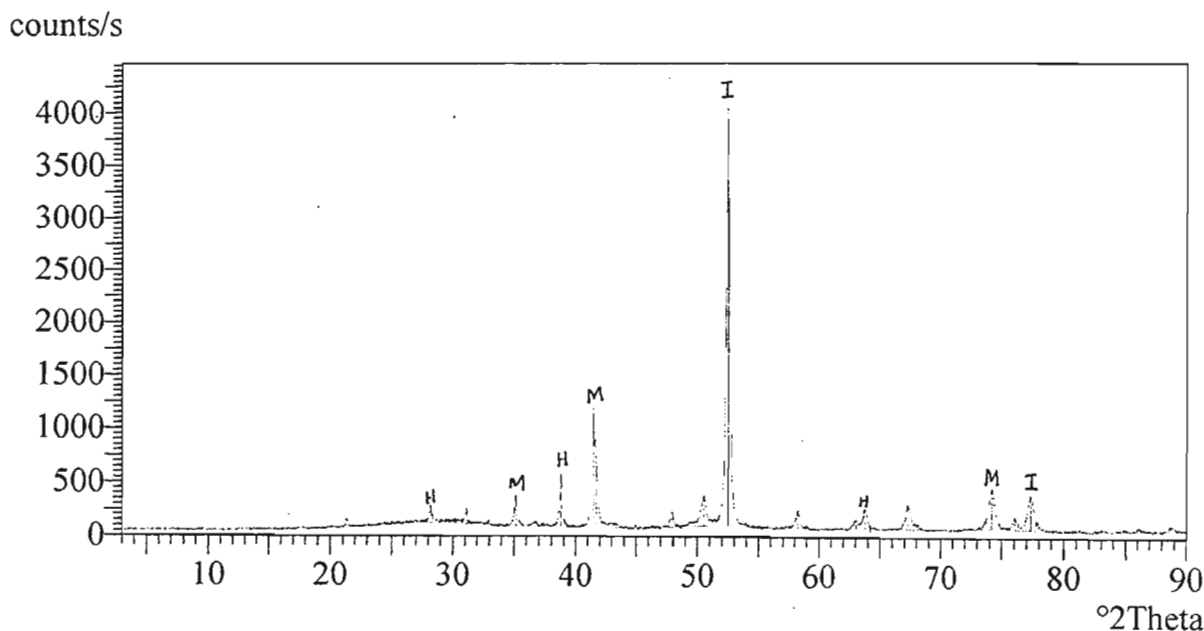
Peak search parameter set: As Measured Intensities
 Set created: 04/28/1999 12:06
 Peak positions defined by: Minimum of 2nd derivative
 Minimum peak tip width (°2Theta): 0.00
 Minimum peak tip width (°2Theta): 1.00
 Peak base width (°2Theta): 2.00
 Minimum significance: 0.60

d-spacing (Å)	Relative Intensity (%)	Angle (°2Theta)	Peak Height (counts/s)	Background (counts/s)	Tip Width (°2Theta)	Significance
30.79944	0.06	3.32845	2.49	50.41	0.48000	0.70
11.38454	0.00	9.01250	0.00	51.40	0.10000	0.66
5.57233	0.29	18.47442	11.39	66.35	0.10000	0.62
4.83747	1.72	21.31141	67.93	81.36	0.16000	1.31
4.24578	0.64	24.32392	25.42	101.74	0.12000	0.62
3.67358	4.01	28.18529	158.72	118.17	0.08000	0.78
3.33882	3.91	31.07916	154.99	106.19	0.08000	0.87
3.16027	0.85	32.88345	33.70	98.72	0.10000	0.84
2.96313	7.96	35.14000	315.18	93.37	0.08000	0.79
2.83981	1.03	36.71921	40.80	90.69	0.24000	1.67
2.69644	12.45	38.74724	492.98	87.26	0.24000	17.70
2.52776	27.89	41.44759	1104.12	82.69	0.10000	2.76
2.51463	15.34	41.67412	607.53	82.30	0.10000	1.16
2.43401	0.91	43.12213	35.97	79.85	0.64000	1.41
2.34131	0.52	44.92065	20.78	77.88	0.16000	0.90
2.28549	0.18	46.08012	7.16	80.22	0.64000	0.68
2.20133	2.91	47.94980	115.08	86.65	0.10000	0.61
2.09767	7.10	50.48090	281.14	95.35	0.36000	9.82
2.02604	100.00	52.39837	3959.23	101.94	0.16000	14.21
1.92251	77.89	52.49667	3083.70	102.28	0.12000	2.39
1.84004	4.20	55.17183	166.19	81.22	0.10000	0.91
1.81700	0.65	55.98172	25.58	79.97	0.24000	0.86
1.71214	2.06	62.79162	81.54	81.52	0.24000	1.94

d-spacing (Å)	Relative Intensity (%)	Angle (°2Theta)	Peak Height (counts/s)	Background (counts/s)	Tip Width (°2Theta)	Significance
1.69429	4.66	63.73267	184.52	81.18	0.16000	1.38
1.61535	5.86	67.24789	231.94	77.66	0.24000	3.76
1.59777	1.23	68.08850	48.81	76.73	0.16000	0.64
1.56388	0.20	69.77429	7.89	74.85	0.64000	0.65
1.48425	9.64	74.11957	381.80	84.17	0.36000	11.24
1.45332	2.80	75.97293	111.01	78.61	0.20000	1.81
1.43250	7.87	77.29223	311.79	74.65	0.40000	10.83
1.34839	0.26	83.11492	10.34	65.26	0.64000	0.97
1.32751	0.42	84.72293	16.54	66.35	0.32000	0.61
1.31153	0.92	86.09245	36.46	67.22	0.20000	0.85
1.27955	1.00	88.70311	39.42	72.52	0.40000	1.69

X'Pert Graphics & Identify
 Graph: run2rc

User-1
 01/30/2002 13:54



Description:
RUN 3 RC

Original scan: run3rc Date: 01/31/2002 08:28
Description of scan:
RUN 3 RC

Used wavelength: K-Alpha

K-Alpha1 wavelength (A): 1.78897
K-Alpha2 wavelength (A): 1.79285
K-Alpha2/K-Alpha1 intensity ratio: 0.50000
K-Alpha wavelength (A): 1.78897
K-Beta wavelength (A):

Peak search parameter set: As Measured Intensities
Set created: 04/28/1999 12:06
Peak positions defined by: Minimum of 2nd derivative
Minimum peak tip width (*2Theta): 0.00
Minimum peak tip width (*2Theta): 1.00
Peak base width (*2Theta): 2.00
Minimum significance: 0.60

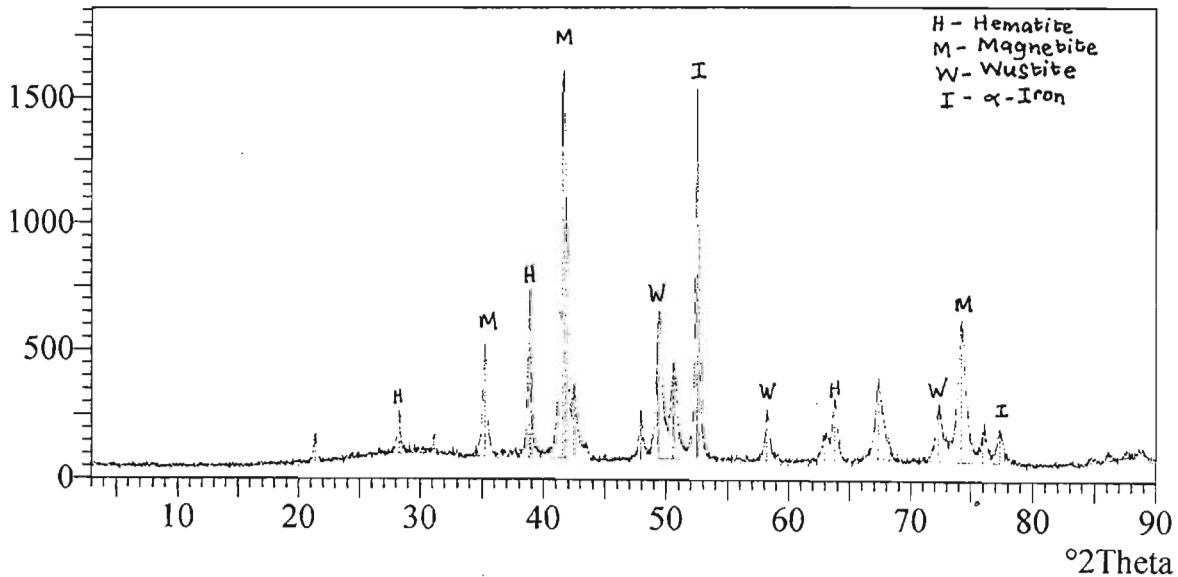
d-spacing (A)	Relative Intensity (%)	Angle (*2Theta)	Peak Height (counts/s)	Background (counts/s)	Tip Width (*2Theta)	Significance
1.48334	36.22	74.17297	543.81	75.53	0.56000	8.01
1.45447	7.67	73.90192	115.20	73.47	0.16000	0.66
1.45248	8.48	77.28086	127.37	71.85	0.16000	0.63
1.32884	1.39	84.61839	20.85	73.75	0.32000	0.63
1.31107	2.18	86.04004	52.70	84.22	0.48000	1.94
1.29377	1.09	87.47837	16.38	97.14	0.40000	1.05

d-spacing (A)	Relative Intensity (%)	Angle (*2Theta)	Peak Height (counts/s)	Background (counts/s)	Tip Width (*2Theta)	Significance
4.83287	7.29	21.33195	109.45	67.63	0.10000	0.88
4.24663	0.88	24.31898	13.21	82.53	0.24000	0.63
3.67040	11.37	28.21020	170.72	99.49	0.20000	3.29
3.33914	4.75	31.07611	70.95	99.03	0.10000	0.99
2.96041	30.79	35.17333	462.19	88.30	0.10000	1.05
2.84852	1.53	36.60297	23.02	86.82	0.32000	0.69
2.69269	43.36	38.80346	650.90	84.54	0.10000	1.71
2.68725	33.15	38.83512	497.71	84.45	0.06000	0.72
2.52625	100.00	41.47355	1501.29	81.77	0.20000	7.68
2.51376	77.31	41.68911	1160.69	81.55	0.12000	0.87
2.47398	19.19	42.39152	288.07	80.82	0.20000	2.40
2.41599	3.75	43.46019	56.30	79.71	0.24000	1.90
2.33901	1.10	44.96716	16.56	78.15	0.24000	0.70
2.20285	11.98	47.91468	179.90	79.79	0.20000	3.08
2.14680	34.71	49.24771	521.06	81.02	0.10000	0.69
2.09602	24.56	50.52337	368.66	82.19	0.32000	6.84
2.02500	96.81	52.42737	1453.47	83.93	0.20000	14.84
1.83988	12.21	58.17730	183.38	77.58	0.24000	3.87
1.71355	5.91	62.93439	88.68	80.02	0.40000	1.73
1.69321	15.74	63.77827	236.35	79.80	0.28000	4.98
1.61439	19.74	67.29306	296.35	86.17	0.32000	5.20
1.59465	4.29	68.23974	64.39	82.91	0.28000	1.13
1.51732	13.38	72.24529	200.85	77.82	0.48000	8.09

X'Pert Graphics & Identify
Graph: run3rc

User-1
01/31/2002 10:20

counts/s



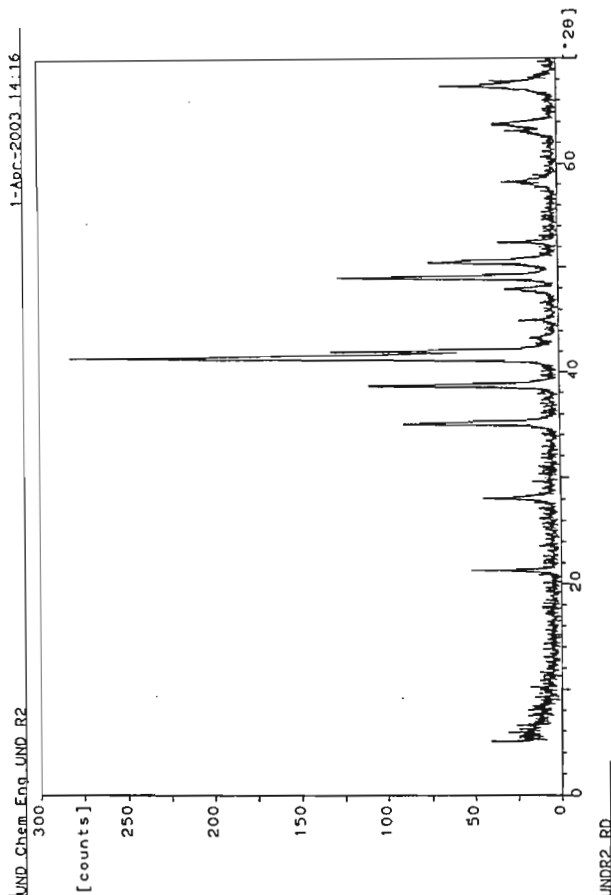
Sample identification: undr2
 Data measured at: 1-Apr-2003 11:53:00

Diffractometer type: PW3710 BASED
 Tube anode: Co
 Generator tension [kV]: 40
 Generator current [mA]: 40
 Wavelength Alpha1 [Å]: 1.78896
 Wavelength Alpha2 [Å]: 1.79285
 Intensity ratio (alpha2/alpha1): 0.500
 Divergence slit: 1/4°
 Receiving slit: 0.1
 Monochromator used: YES

Start angle [°2θ]: 5.000
 End angle [°2θ]: 70.000
 Step size [°2θ]: 0.020
 Maximum intensity: 265.6900
 Time per step [s]: 1.000
 Type of scan: STEP

Peak positions defined by: Top of smoothed peak
 Minimum peak tip width: 0.00
 Maximum peak tip width: 1.00
 Peak base width: 2.00
 Minimum significance: 0.75
 Number of peaks: 16

Angle [°2θ]	d-value α1 [Å]	d-value α2 [Å]	Peak width [°2θ]	Peak int [counts]	Back. int [counts]	Rel. int [%]	Signif.
2.285	4.8434	4.8539	0.160	38	4	14.5	1.63
2.115	3.6826	3.6906	0.200	36	6	13.5	2.32
2.110	2.9656	2.9720	0.280	81	4	30.5	5.80
2.715	2.6986	2.7045	0.280	98	4	36.9	6.95
2.455	2.5273	2.5328	0.360	266	4	100.0	13.12
2.060	2.4926	2.4980	0.200	110	4	41.5	3.36
2.290	2.4250	2.4303	0.320	9	4	3.4	0.92
2.005	2.3371	2.3422	0.160	16	3	6.0	1.18
2.885	2.2041	2.2089	0.320	26	3	9.8	1.88
2.045	2.1551	2.1598	0.120	119	3	44.7	1.45
2.480	2.0977	2.1023	0.200	61	3	22.9	1.66
2.460	2.0238	2.0282	0.240	25	3	9.4	3.11
2.245	1.8379	1.8419	0.560	22	3	8.3	4.22
2.880	1.7149	1.7186	0.320	12	3	4.4	1.19
2.755	1.6938	1.6974	0.560	27	3	10.2	5.29
2.340	1.6134	1.6169	0.280	53	4	20.1	2.30



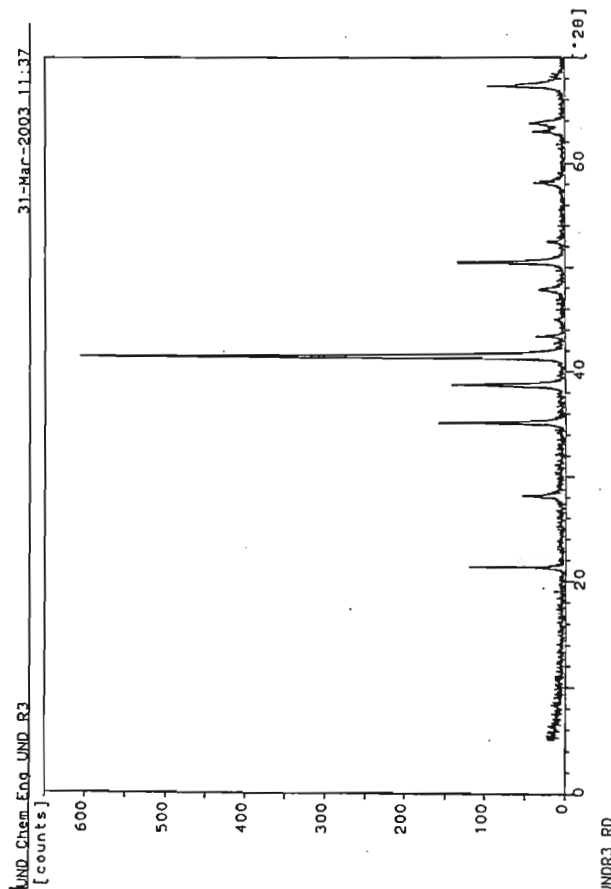
Sample identification: undr3
 Data measured at: 31-Mar-2003 10:37:00

Diffractometer type: PW3710 BASED
 Tube anode: Co
 Generator tension [kV]: 40
 Generator current [mA]: 40
 Wavelength Alpha1 [Å]: 1.78896
 Wavelength Alpha2 [Å]: 1.79285
 Intensity ratio (alpha2/alpha1): 0.500
 Divergence slit: 1/4°
 Receiving slit: 0.1
 Monochromator used: YES

Start angle [°2θ]: 5.000
 End angle [°2θ]: 70.000
 Step size [°2θ]: 0.020
 Maximum intensity: 595.3600
 Time per step [s]: 1.000
 Type of scan: STEP

Peak positions defined by: Top of smoothed peak
 Minimum peak tip width: 0.00
 Maximum peak tip width: 1.00
 Peak base width: 2.00
 Minimum significance: 0.75
 Number of peaks: 17

Angle [°2θ]	d-value α1 [Å]	d-value α2 [Å]	Peak width [°2θ]	Peak int [counts]	Back. int [counts]	Rel. int [%]	Signif.
3.335	4.8322	4.8427	0.080	114	4	19.2	1.79
3.550	4.3832	4.3928	0.800	2	4	0.3	0.89
3.150	3.6781	3.6861	0.240	42	5	7.1	3.21
3.125	2.9644	2.9708	0.080	154	4	25.8	0.86
3.720	2.9165	2.9229	0.040	7	4	1.1	0.81
3.760	2.6956	2.7014	0.080	137	4	23.0	0.83
3.450	2.5276	2.5331	0.160	595	4	100.0	9.75
3.365	2.4210	2.4263	0.060	34	3	5.7	0.97
3.985	2.3381	2.3432	0.240	7	3	1.2	1.92
3.960	2.2009	2.2057	0.100	24	3	4.0	0.81
3.505	2.0967	2.1013	0.140	130	3	21.8	3.19
3.415	2.0254	2.0298	0.200	14	3	2.4	1.16
3.335	1.9200	1.9241	0.480	2	3	0.3	0.99
3.150	1.8407	1.8447	0.400	24	3	4.0	3.01
3.985	1.7123	1.7160	0.240	30	3	5.1	2.24
3.780	1.6932	1.6968	0.200	40	3	6.7	1.09
3.885	1.6146	1.6181	0.240	81	3	13.6	3.22



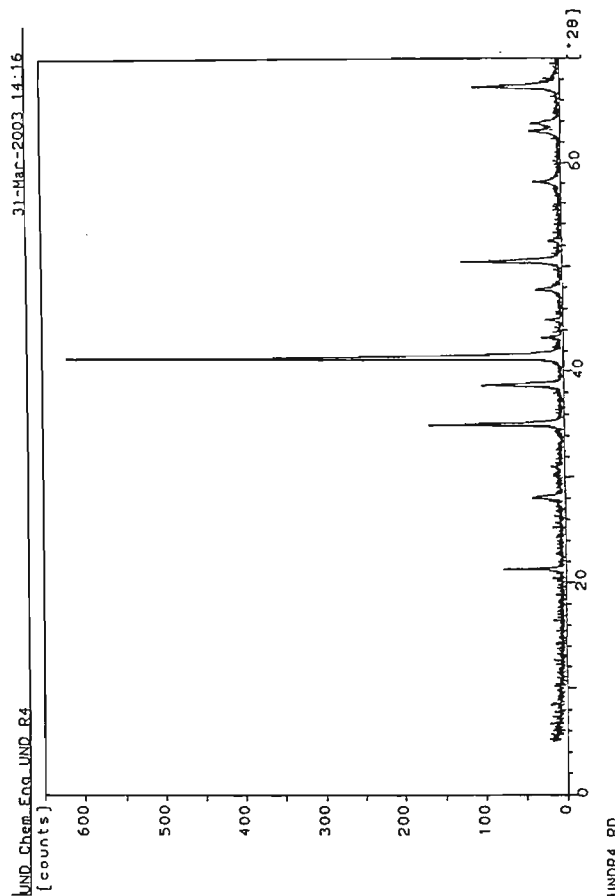
Sample identification: undr4
 Data measured at: 31-Mar-2003 11:37:00

Diffractometer type: PW3710 BASED
 Tube anode: Co
 Generator tension [kV]: 40
 Generator current [mA]: 40
 Wavelength Alpha1 [Å]: 1.78896
 Wavelength Alpha2 [Å]: 1.79285
 Intensity ratio (alpha2/alpha1): 0.500
 Divergence slit: 1/4°
 Receiving slit: 0.1
 Monochromator used: YES

Start angle [°2θ]: 5.000
 End angle [°2θ]: 70.000
 Step size [°2θ]: 0.020
 Maximum intensity: 615.0400
 Time per step [s]: 1.000
 Type of scan: STEP

Peak positions defined by: Top of smoothed peak
 Minimum peak tip width: 0.00
 Maximum peak tip width: 1.00
 Peak base width: 2.00
 Minimum significance: 0.75
 Number of peaks: 17

angle [°2θ]	d-value α1 [Å]	d-value α2 [Å]	Peak width [°2θ]	Peak int [counts]	Back. int [counts]	Rel. int [%]	Signif.
.620	8.1385	8.1562	0.200	6	5	0.9	0.88
.270	4.8468	4.8573	0.100	72	5	11.7	2.32
.070	3.6884	3.6964	0.160	30	6	4.9	0.84
.600	3.3898	3.3972	0.960	3	5	0.4	0.94
.115	2.9652	2.9716	0.140	159	4	25.8	4.24
.700	2.6996	2.7055	0.180	98	4	15.9	3.45
.410	2.5300	2.5355	0.100	615	4	100.0	3.36
.335	2.4226	2.4279	0.200	18	3	2.9	1.83
.960	2.3394	2.3444	0.160	14	3	2.3	1.12
.830	2.2065	2.2113	0.280	26	3	4.2	2.59
.500	2.0969	2.1015	0.120	108	3	17.6	1.74
.435	2.0247	2.0291	0.200	11	3	1.8	1.02
.235	1.8980	1.9021	0.040	2	3	0.3	0.79
.105	1.8420	1.8460	0.400	21	3	3.4	2.68
.980	1.7124	1.7161	0.200	30	3	4.9	1.72
.765	1.6935	1.6972	0.280	24	3	3.9	1.77
.260	1.6151	1.6186	0.200	92	4	15.0	2.84



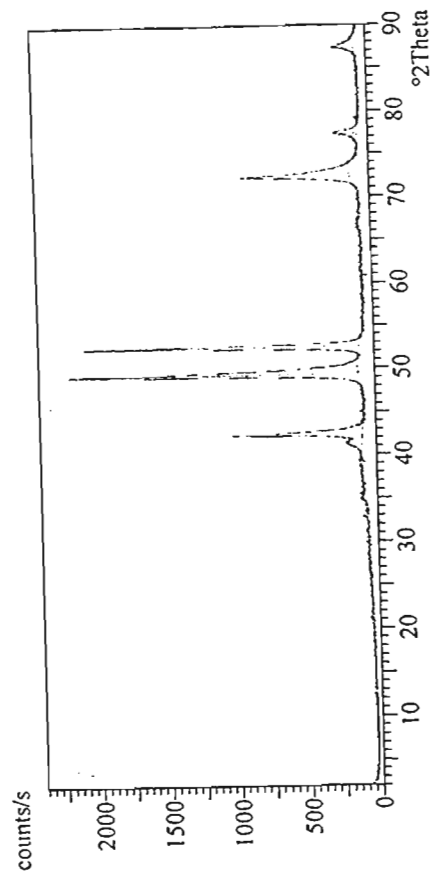
Description:
 ID1-T
 Original scan: id1t Date: 11/15/2002 09:58
 Description of scan:
 ID1-T

Used wavelength: K-Alpha
 K-Alpha1 wavelength (Å): 1.78897
 K-Alpha2 wavelength (Å): 1.79285
 K-Alpha2/K-Alpha1 intensity ratio: 0.50000
 K-Alpha wavelength (Å): 1.78897
 K-Beta wavelength (Å):

Peak search parameter set: As Measured Intensities
 Set created: 04/28/1999 12:06
 Peak positions defined by: Minimum of 2nd derivative
 Minimum peak tip width (*2Theta): 0.00
 Minimum peak tip width (*2Theta): 1.00
 Peak base width (*2Theta): 2.00
 Minimum significance: 0.60

d-spacing (Å)	Relative Intensity (%)	Angle (*2Theta)	Peak Height (counts/s)	Background (counts/s)	Tip Width (*2Theta)	Significance
4.95237	1.01	20.81143	20.66	43.66	0.12000	0.81
4.87564	0.53	21.14264	10.77	49.34	0.48000	0.71
3.33888	0.61	31.07856	12.52	69.25	0.48000	0.83
3.16727	1.50	32.80872	30.73	72.62	0.16000	0.78
2.99284	1.17	34.77995	24.01	83.47	0.48000	1.49
2.88205	0.69	36.16230	14.11	93.80	0.16000	0.65
2.54910	4.77	41.08493	97.72	101.10	0.48000	2.42
2.48078	44.08	42.26979	902.99	95.19	0.12000	3.31
2.33768	0.85	44.99418	17.34	83.28	0.12000	0.62
2.14521	100.00	49.28658	2048.52	115.21	0.20000	13.11
2.02436	95.66	52.44519	1959.58	105.12	0.12000	4.20
1.77383	0.45	60.56526	9.28	70.41	0.16000	1.10
1.76896	0.78	60.74973	16.07	70.37	0.04000	0.68
1.76580	0.00	60.86967	0.00	70.34	0.04000	1.32
1.75337	0.55	61.34774	11.33	70.30	0.48000	1.40
1.71014	1.89	63.07351	38.79	71.08	0.06000	0.82
1.62725	0.86	66.69161	17.61	75.62	0.96000	1.05
1.57077	0.34	69.42436	6.95	79.64	0.80000	0.95
1.51893	39.03	72.15630	799.63	133.81	0.08000	1.15
1.43222	8.02	77.29733	164.23	77.56	0.20000	0.67
1.36682	0.57	81.75201	11.71	65.90	0.16000	1.03
1.29680	7.02	87.22235	143.75	86.77	0.16000	1.03

User-1
 11/15/2002 11:14
 X'Pert Graphics & Identify
 Graph: id1t



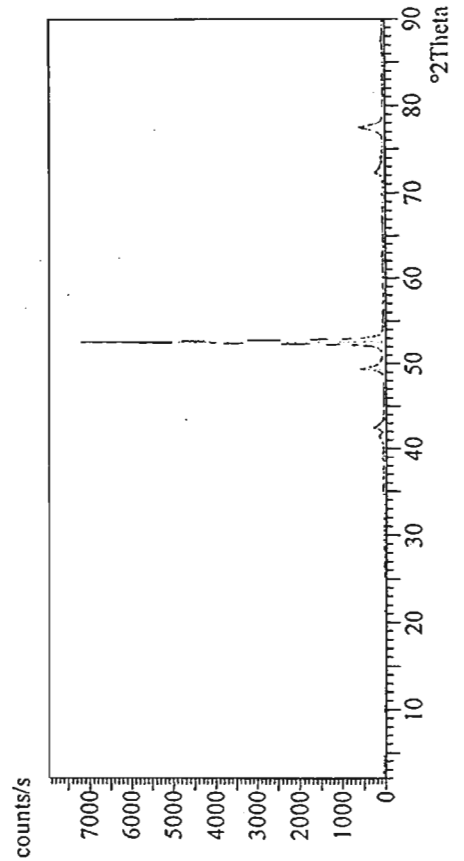
Description:
 ID1-M
 Original scan: id1m Date: 11/15/2002 08:26
 Description of scan:
 ID1-M

Used wavelength: K-Alpha
 K-Alpha1 wavelength (Å): 1.78897
 K-Alpha2 wavelength (Å): 1.79285
 K-Alpha2/K-Alpha1 intensity ratio: 0.50000
 K-Alpha wavelength (Å): 1.78897
 K-Beta wavelength (Å):

Peak search parameter set: As Measured Intensities
 Set created: 04/28/1999 12:06
 Peak positions defined by: Minimum of 2nd derivative
 Minimum peak tip width (*2Theta): 0.00
 Minimum peak tip width (*2Theta): 1.00
 Peak base width (*2Theta): 2.00
 Minimum significance: 0.60

d-spacing (Å)	Relative Intensity (%)	Angle (*2Theta)	Peak Height (counts/s)	Background (counts/s)	Tip Width (*2Theta)	Significance
7.02650	0.07	14.62733	5.18	35.45	0.14000	0.74
4.84238	0.10	21.28956	6.86	38.97	0.48000	1.04
3.88186	0.09	26.64431	6.56	43.81	0.64000	1.07
3.81821	0.22	27.09692	15.01	44.05	0.12000	0.77
3.64076	0.30	28.14474	20.66	45.47	0.06000	0.63
2.96399	0.47	35.12946	32.76	52.11	0.32000	0.76
2.86343	0.37	36.40564	25.55	52.93	0.40000	1.26
2.78283	0.41	37.49870	28.39	53.64	0.32000	0.78
2.69204	0.62	38.81311	42.93	54.49	0.24000	1.50
2.65359	0.41	39.39856	28.32	54.87	0.24000	0.63
2.53498	1.71	41.32422	118.69	56.11	0.40000	4.21
2.47459	3.37	42.38068	234.49	56.79	0.20000	2.73
2.33818	0.19	44.98409	12.97	58.48	0.48000	0.96
2.26759	0.12	46.46518	8.02	59.43	0.64000	0.63
2.14473	7.14	49.29832	496.90	80.93	0.16000	3.69
2.02276	100.00	52.48968	6960.47	91.58	0.28000	75.69
1.90773	0.23	55.92214	15.82	62.06	0.24000	1.30
1.81709	0.21	58.97850	14.90	58.53	0.24000	0.61
1.75755	0.19	61.18600	13.17	59.62	0.64000	1.16
1.72364	0.37	62.52383	25.72	60.37	0.08000	0.84
1.62699	0.20	66.70373	13.59	64.06	0.48000	0.89
1.56003	0.13	69.97183	9.35	66.17	0.64000	0.80
1.51947	2.39	72.12663	166.22	64.96	0.16000	0.69

User-1
 11/15/2002 11:16
 X'Pert Graphics & Identify
 Graph: id1m



Description: ID1-B

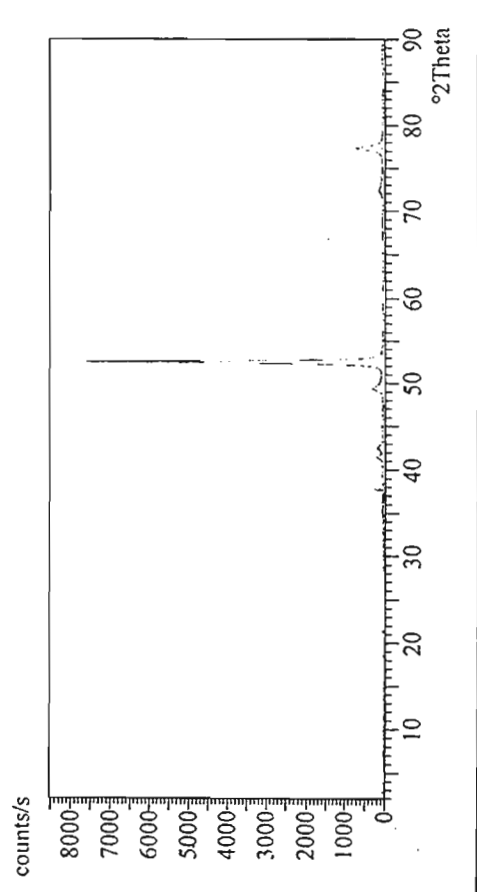
Original scan: id1b Date: 11/14/2002 10:53
 Description of scan: ID1-B

Used wavelength: K-Alpha
 K-Alpha wavelength (Å): 1.78897
 K-Alpha2 wavelength (Å): 1.79285
 K-Alpha2/K-Alpha intensity ratio: 0.50000
 K-Alpha wavelength (Å): 1.78897
 K-Beta wavelength (Å):

Peak search parameter set: As Measured Intensities
 Set created: 04/28/1999 12:06
 Peak positions defined by: Minimum of 2nd derivative
 Minimum peak tip width (*2Theta): 0.00
 Minimum peak tip width (*2Theta): 1.00
 Peak base width (*2Theta): 2.00
 Minimum significance: 0.60

d-spacing (Å)	Relative Intensity (%)	Angle (*2Theta)	Peak Height (counts/s)	Background (counts/s)	Tip Width (*2Theta)	Significance
10.50725	0.21	9.76701	15.78	31.36	0.06000	0.65
4.82280	0.21	21.37701	16.04	37.87	0.36000	1.65
3.88932	0.10	26.59227	7.51	41.02	0.64000	0.76
3.61301	0.14	28.66788	10.93	42.46	0.32000	0.89
2.95936	0.56	35.18624	43.31	50.73	0.32000	1.04
2.87889	0.72	36.20330	55.50	51.73	0.06000	1.30
2.76766	3.48	37.71195	266.65	53.21	0.06000	0.83
2.65556	0.41	39.36820	31.47	54.84	0.16000	1.55
2.53626	1.60	41.30230	123.08	56.73	0.16000	0.65
2.52003	1.60	41.58059	122.99	57.01	0.16000	0.70
2.47517	1.84	42.37022	140.95	57.78	0.12000	0.77
2.34290	0.46	44.88844	34.89	60.25	0.16000	1.09
2.14471	3.11	49.29883	238.51	79.75	0.28000	3.80
2.02420	100.00	52.44968	7668.96	89.51	0.28000	88.40
1.82017	0.21	58.86888	16.17	56.66	0.48000	0.63
1.74793	0.23	61.55953	17.66	56.36	0.24000	0.62
1.71776	0.12	62.76178	9.14	56.57	0.96000	1.37
1.64271	0.32	67.37257	24.69	63.13	0.24000	0.66
1.51847	1.18	72.18168	90.68	60.40	0.40000	1.93
1.49177	0.72	73.56947	55.24	61.40	0.04000	0.63
1.48034	0.48	74.34861	37.08	61.96	0.56000	1.58
1.43176	8.70	77.32669	667.40	64.10	0.32000	10.11
1.33194	0.11	84.37574	8.05	53.30	0.48000	0.88

User-1 11/14/2002 13:50 X'Pert Graphics & Identify Graph: id1b



Philips Analytical

Description: ID2-T

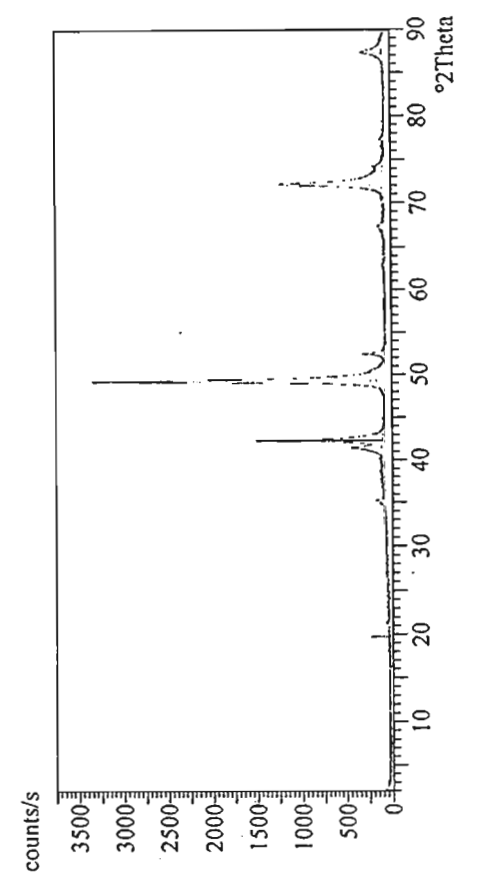
Original scan: id2t Date: 11/19/2002 11:40
 Description of scan: ID2-T

Used wavelength: K-Alpha
 K-Alpha wavelength (Å): 1.78897
 K-Alpha2 wavelength (Å): 1.79285
 K-Alpha2/K-Alpha intensity ratio: 0.50000
 K-Alpha wavelength (Å): 1.78897
 K-Beta wavelength (Å):

Peak search parameter set: As Measured Intensities
 Set created: 04/28/1999 12:06
 Peak positions defined by: Minimum of 2nd derivative
 Minimum peak tip width (*2Theta): 0.00
 Minimum peak tip width (*2Theta): 1.00
 Peak base width (*2Theta): 2.00
 Minimum significance: 0.60

d-spacing (Å)	Relative Intensity (%)	Angle (*2Theta)	Peak Height (counts/s)	Background (counts/s)	Tip Width (*2Theta)	Significance
5.23755	11.32	19.66663	364.67	44.65	0.04000	13.92
4.84092	0.74	21.29609	23.77	48.24	0.40000	1.57
2.95766	2.52	35.20713	81.16	91.00	0.28000	3.48
2.52812	10.58	41.44145	340.77	115.81	0.20000	3.52
2.48181	43.52	42.25146	1401.85	108.80	0.10000	2.78
2.47667	39.36	42.34329	1267.76	108.01	0.06000	0.93
2.30459	0.39	45.67639	12.49	86.27	0.10000	0.66
2.14791	100.00	49.22056	3221.25	161.79	0.24000	28.96
2.02652	6.19	52.38513	199.48	88.24	0.14000	2.33
1.91360	0.34	55.73571	10.80	73.59	0.96000	0.98
1.71098	0.50	63.03932	16.02	76.70	0.48000	1.34
1.61311	1.70	67.33533	54.74	84.35	0.40000	1.77
1.52126	31.30	72.02896	1008.30	91.01	0.08000	0.73
1.51820	34.20	72.19673	1101.62	91.01	0.16000	2.78
1.48215	2.79	74.24244	89.76	84.30	0.32000	1.11
1.44414	0.39	76.54297	12.64	77.27	0.32000	0.61
1.43166	1.17	77.33319	37.61	75.45	0.24000	0.75
1.29725	6.89	87.18419	222.05	84.88	0.20000	1.61
1.29337	5.67	87.51203	182.76	86.45	0.24000	1.08

User-1 11/19/2002 13:46 X'Pert Graphics & Identify Graph: id2t



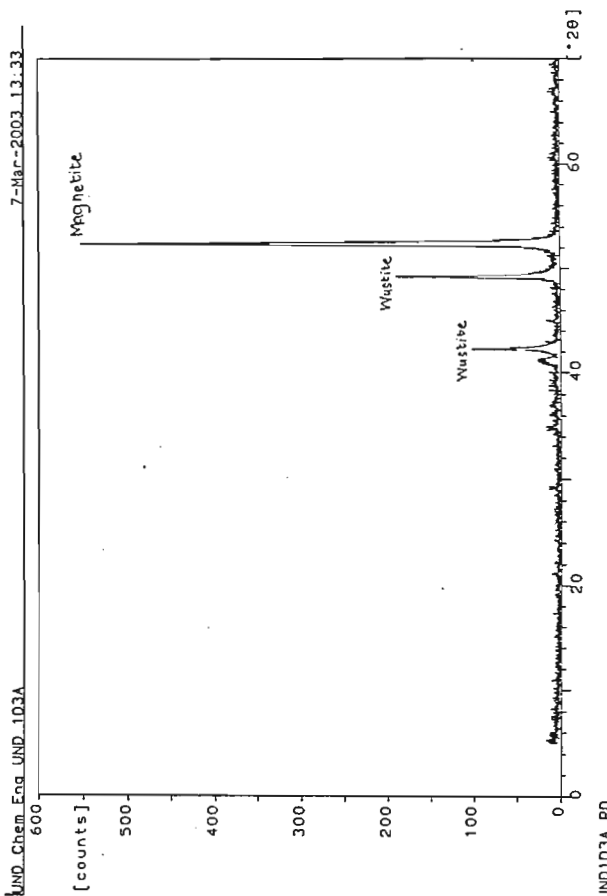
Philips Analytical

Sample identification: und1d3a
 Data measured at: 7-Mar-2003 11:42:00

Diffractionmeter type: PH3710 BASED
 Tube anode: Co
 Generator tension [kV]: 40
 Generator current [mA]: 40
 Wavelength Alpha1 [Å]: 1.78896
 Wavelength Alpha2 [Å]: 1.79285
 Intensity ratio (alpha2/alpha1): 0.500
 Divergence slit: 1/4°
 Receiving slit: 0.1
 Monochromator used: YES
 Start angle [°2θ]: 5.000
 End angle [°2θ]: 70.000
 Step size [°2θ]: 0.020
 Maximum intensity: 542.8900
 Time per step [s]: 1.000
 Type of scan: STEP

Peak positions defined by: Top of smoothed peak
 Minimum peak tip width: 0.00
 Maximum peak tip width: 1.00
 Peak base width: 2.00
 Minimum significance: 0.75
 Number of peaks: 12

Angle [°2θ]	d-value α1 [Å]	d-value α2 [Å]	Peak width [°2θ]	Peak int [counts]	Back. int [counts]	Rel. int [%]	Signif.
.170	4.8694	4.8800	0.240	4	2	0.7	1.40
.305	3.5361	3.5438	0.320	3	3	0.6	1.04
.960	2.9779	2.9844	0.240	8	3	1.4	1.39
.140	2.8838	2.8900	0.400	5	4	0.9	1.21
.090	2.8124	2.8185	0.480	4	4	0.7	1.29
.290	2.5370	2.5425	0.200	19	5	3.6	1.13
.280	2.4802	2.4856	0.120	85	5	15.6	2.07
.000	2.3374	2.3425	0.120	6	4	1.2	1.08
.245	2.1469	2.1516	0.200	182	5	33.6	7.79
.450	2.0242	2.0286	0.160	543	5	100.0	6.12
.705	1.7701	1.7740	0.480	4	3	0.7	1.34
.890	1.6230	1.6265	0.480	3	3	0.6	1.68

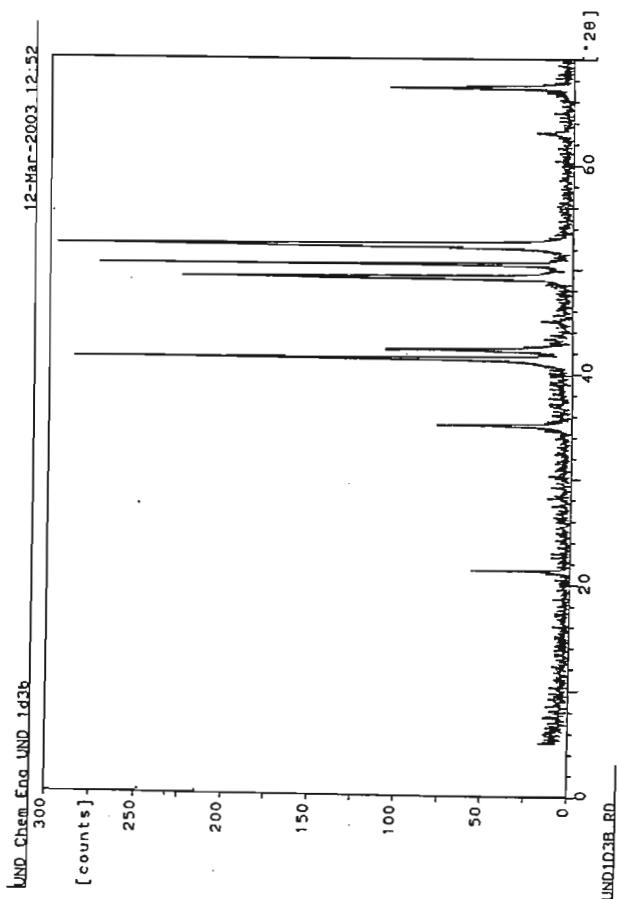


Sample identification: und1d3b
 Data measured at: 12-Mar-2003 9:11:00

Diffractionmeter type: PH3710 BASED
 Tube anode: Co
 Generator tension [kV]: 40
 Generator current [mA]: 40
 Wavelength Alpha1 [Å]: 1.78896
 Wavelength Alpha2 [Å]: 1.79285
 Intensity ratio (alpha2/alpha1): 0.500
 Divergence slit: 1/4°
 Receiving slit: 0.1
 Monochromator used: YES
 Start angle [°2θ]: 5.000
 End angle [°2θ]: 70.000
 Step size [°2θ]: 0.020
 Maximum intensity: 285.6100
 Time per step [s]: 1.000
 Type of scan: STEP

Peak positions defined by: Top of smoothed peak
 Minimum peak tip width: 0.00
 Maximum peak tip width: 1.00
 Peak base width: 2.00
 Minimum significance: 0.75
 Number of peaks: 13

Angle [°2θ]	d-value α1 [Å]	d-value α2 [Å]	Peak width [°2θ]	Peak int [counts]	Back. int [counts]	Rel. int [%]	Signif.
315	4.8367	4.8472	0.080	55	3	19.2	1.41
115	2.9652	2.9716	0.060	64	4	22.4	1.11
425	2.5291	2.5346	0.080	282	6	98.8	1.87
345	2.4766	2.4820	0.080	90	5	31.6	0.75
025	2.3362	2.3412	0.160	11	4	3.8	1.10
220	2.1479	2.1526	0.080	222	4	77.7	0.83
465	2.0983	2.1028	0.060	272	4	95.3	1.64
370	2.0247	2.0296	0.040	121	4	42.4	1.49
435	2.0271	2.0315	0.100	266	4	93.0	0.78
000	2.0247	2.0291	0.080	286	4	100.0	1.23
265	1.7119	1.7157	0.320	11	3	3.8	1.50
265	1.6150	1.6185	0.080	102	3	35.7	1.26
420	1.6117	1.6152	0.080	59	3	20.8	0.83



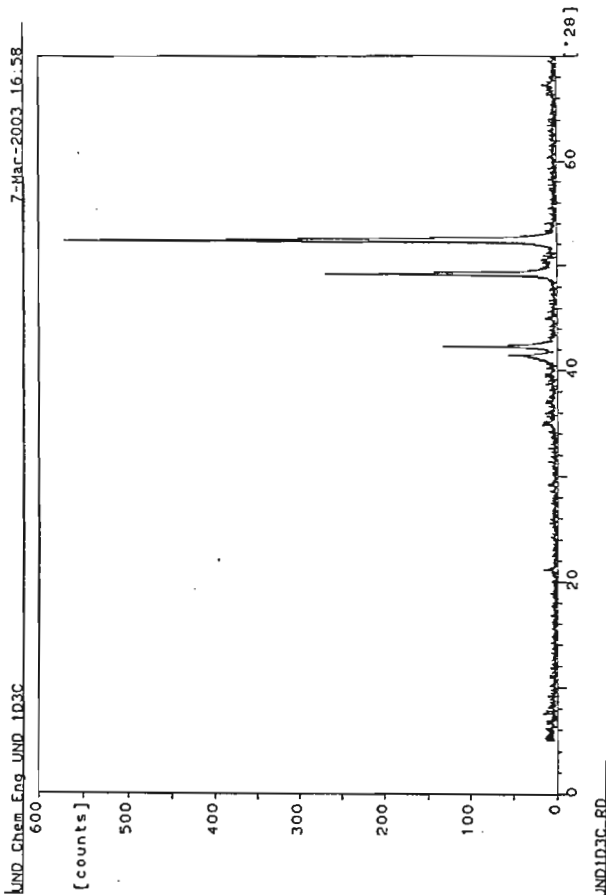
Sample identification: und1d3c
 Data measured at: 7-Mar-2003 13:37:00

Diffractometer type: PW3710 BASED
 Tube anode: Co
 Generator tension [kV]: 40
 Generator current [mA]: 40
 Wavelength Alpha [Å]: 1.78896
 Wavelength Alpha2 [Å]: 1.79285
 Intensity ratio (alpha2/alpha): 0.500
 Divergence slit: 1/4°
 Receiving slit: 0.1
 Monochromator used: YES

Start angle [°2θ]: 5.000
 End angle [°2θ]: 70.000
 Step size [°2θ]: 0.020
 Maximum intensity: 556.9600
 Time per step [s]: 1.000
 Type of scan: STEP

Peak positions defined by: Top of smoothed peak
 Minimum peak tip width: 0.00
 Maximum peak tip width: 1.00
 Peak base width: 2.00
 Minimum significance: 0.75
 Number of peaks: 15

gle	d-value	d-value	Peak width	Peak int	Back. int	Rel. int	Signif.
2θ	α1 [Å]	α2 [Å]	[°2θ]	[counts]	[counts]	[%]	
200	10.0623	10.0842	0.480	2	3	0.4	1.00
230	4.8558	4.8664	0.240	5	2	0.9	2.27
155	3.5539	3.5616	0.960	2	3	0.3	0.88
040	2.9713	2.9778	0.240	8	4	1.4	0.92
995	2.8194	2.8255	0.480	4	4	0.7	0.77
430	2.5288	2.5343	0.160	45	5	8.1	1.36
280	2.4802	2.4856	0.080	128	5	22.9	1.26
005	2.3371	2.3422	0.240	7	4	1.2	1.79
705	2.2120	2.2168	0.120	4	3	0.7	0.99
215	2.1481	2.1528	0.120	253	4	45.4	3.95
455	2.0987	2.1032	0.240	11	4	2.0	0.83
430	2.0249	2.0293	0.120	557	4	100.0	5.06
455	1.7768	1.7806	0.240	3	3	0.5	0.83
865	1.7152	1.7190	0.960	2	3	0.4	0.78
190	1.6166	1.6201	0.480	7	3	1.2	1.42



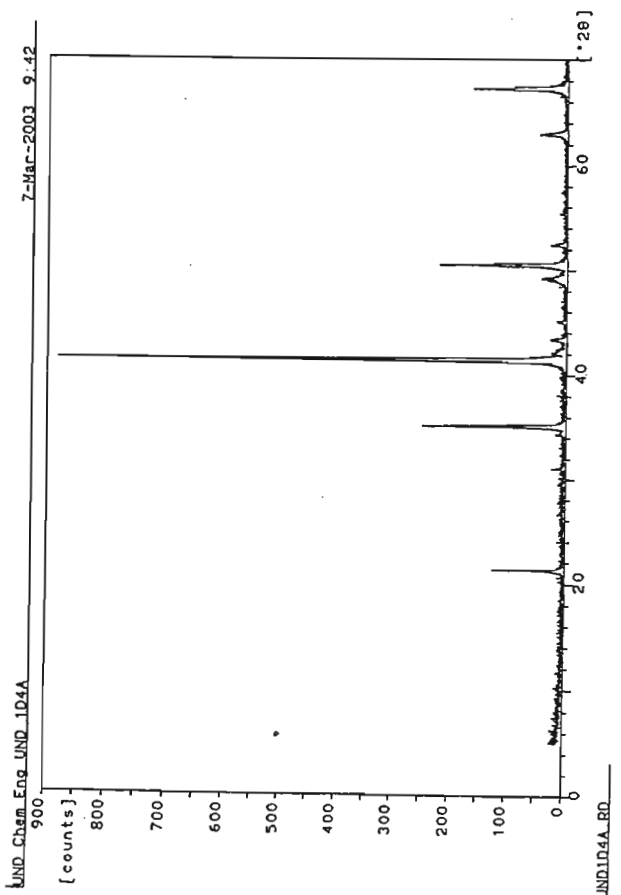
Sample identification: und1d4a
 Data measured at: 5-Mar-2003 13:28:00

Diffractometer type: PW3710 BASED
 Tube anode: Co
 Generator tension [kV]: 40
 Generator current [mA]: 40
 Wavelength Alpha [Å]: 1.78896
 Wavelength Alpha2 [Å]: 1.79285
 Intensity ratio (alpha2/alpha): 0.500
 Divergence slit: 1/4°
 Receiving slit: 0.1
 Monochromator used: YES

Start angle [°2θ]: 5.000
 End angle [°2θ]: 70.000
 Step size [°2θ]: 0.020
 Maximum intensity: 882.0900
 Time per step [s]: 1.000
 Type of scan: STEP

Peak positions defined by: Top of smoothed peak
 Minimum peak tip width: 0.00
 Maximum peak tip width: 1.00
 Peak base width: 2.00
 Minimum significance: 0.75
 Number of peaks: 14

le	d-value	d-value	Peak width	Peak int	Back. int	Rel. int	Signif.
θ	α1 [Å]	α2 [Å]	[°2θ]	[counts]	[counts]	[%]	
50	16.9221	16.9589	0.640	5	7	0.6	0.77
00	4.8400	4.8505	0.100	121	4	13.7	3.36
65	3.5057	3.5133	0.400	3	4	0.4	0.94
60	3.3408	3.3481	0.080	14	4	1.6	0.92
10	2.9656	2.9720	0.140	237	4	26.9	6.35
20	2.5294	2.5349	0.120	882	4	100.0	7.22
35	2.4216	2.4268	0.200	22	3	2.5	2.22
70	2.3340	2.3390	0.240	9	3	1.0	1.87
15	2.1564	2.1610	0.240	21	3	2.4	0.76
30	2.0977	2.1023	0.120	219	3	24.8	3.40
50	2.0242	2.0286	0.160	23	3	2.6	2.64
15	1.8610	1.8650	0.320	3	2	0.3	0.90
10	1.7127	1.7164	0.240	40	3	4.5	2.92
5	1.6154	1.6189	0.160	159	3	18.0	4.30

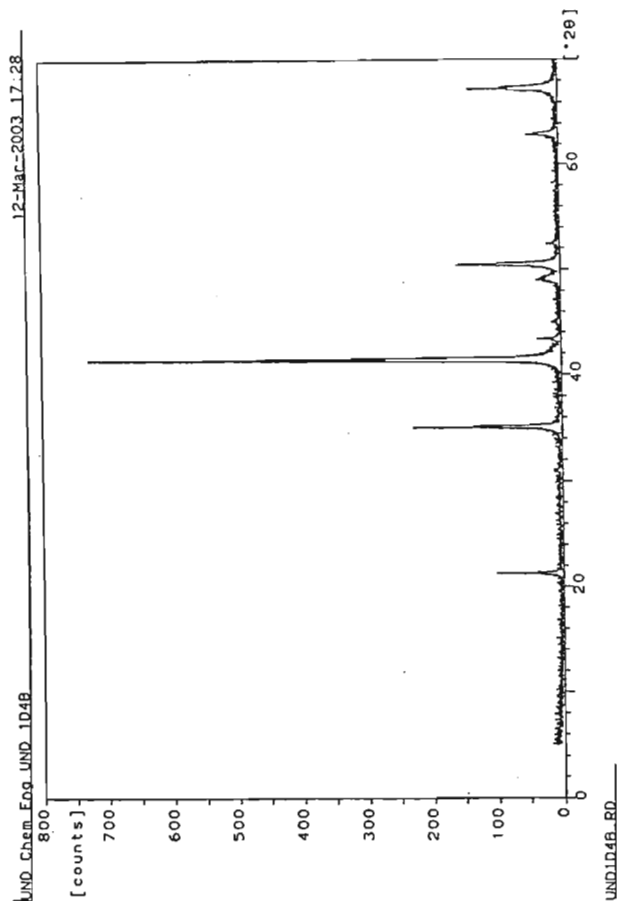


Sample identification: und1B4D
 Data measured at: 12-Mar-2003 13:55:00

Diffractionmeter type: PW3710 BASED
 Tube anode: Co
 Generator tension [kV]: 40
 Generator current [mA]: 40
 Wavelength Alpha1 [Å]: 1.78896
 Wavelength Alpha2 [Å]: 1.79285
 Intensity ratio (alpha2/alpha1): 0.500
 Divergence slit: 1/4°
 Receiving slit: 0.1
 Monochromator used: YES
 Start angle [°2θ]: 5.000
 End angle [°2θ]: 70.000
 Step size [°2θ]: 0.020
 Maximum intensity: 723.6100
 Time per step [s]: 1.000
 Type of scan: STEP

Peak positions defined by: Top of smoothed peak
 Minimum peak tip width: 0.00
 Maximum peak tip width: 1.00
 Peak base width: 2.00
 Minimum significance: 0.75
 Number of peaks: 12

Angle [°2θ]	d-value α1 [Å]	d-value α2 [Å]	Peak width [°2θ]	Peak int [counts]	Back. int [counts]	Rel. int [%]	Signif.
2.270	4.8468	4.8573	0.120	98	4	13.5	3.87
2.995	3.3477	3.3549	0.160	5	4	0.7	1.11
3.085	2.9676	2.9741	0.140	207	4	28.7	5.21
3.405	2.5302	2.5357	0.140	724	4	100.0	9.14
3.345	2.4221	2.4274	0.060	32	3	4.5	0.78
3.050	2.3349	2.3400	0.320	7	3	0.9	1.06
3.140	2.1512	2.1559	0.560	23	3	3.2	4.92
3.460	2.0985	2.1030	0.140	130	3	18.0	2.87
3.460	2.0238	2.0282	0.240	11	3	1.5	1.65
3.900	1.8479	1.8519	0.280	1	3	0.1	0.94
3.955	1.7130	1.7168	0.160	38	4	5.3	0.98
3.245	1.6154	1.6189	0.080	132	4	18.3	1.00

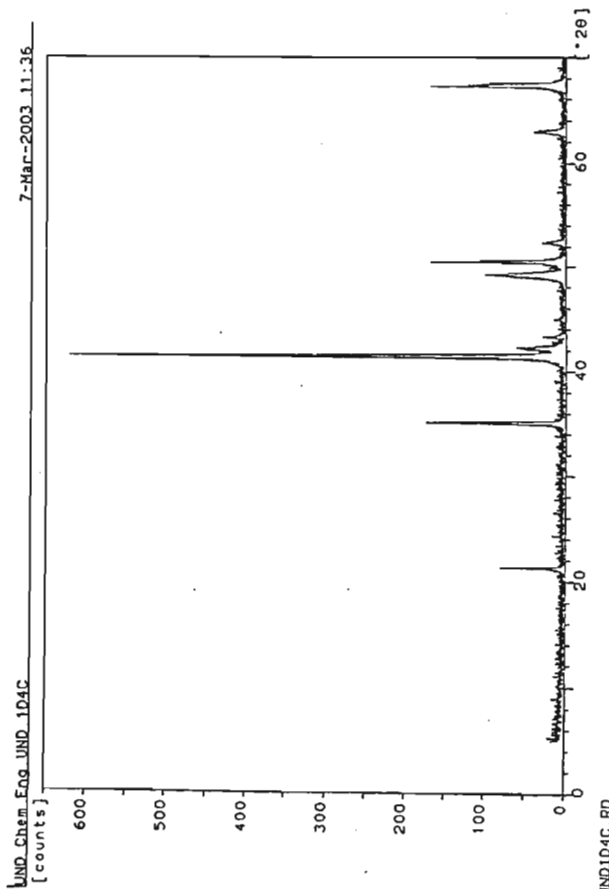


Sample identification: und1d4c
 Data measured at: 7-Mar-2003 9:45:00

Diffractionmeter type: PW3710 BASED
 Tube anode: Co
 Generator tension [kV]: 40
 Generator current [mA]: 40
 Wavelength Alpha1 [Å]: 1.78896
 Wavelength Alpha2 [Å]: 1.79285
 Intensity ratio (alpha2/alpha1): 0.500
 Divergence slit: 1/4°
 Receiving slit: 0.1
 Monochromator used: YES
 Start angle [°2θ]: 5.000
 End angle [°2θ]: 70.000
 Step size [°2θ]: 0.020
 Maximum intensity: 615.0400
 Time per step [s]: 1.000
 Type of scan: STEP

Peak positions defined by: Top of smoothed peak
 Minimum peak tip width: 0.00
 Maximum peak tip width: 1.00
 Peak base width: 2.00
 Minimum significance: 0.75
 Number of peaks: 14

Angle [°2θ]	d-value α1 [Å]	d-value α2 [Å]	Peak width [°2θ]	Peak int [counts]	Back. int [counts]	Rel. int [%]	Signif.
15	4.8367	4.8472	0.140	74	4	12.0	5.38
25	4.2456	4.2548	0.100	9	4	1.5	0.75
05	3.0677	3.0744	0.060	4	4	0.7	0.78
25	2.9644	2.9708	0.160	169	4	27.5	7.25
15	2.5297	2.5352	0.120	615	4	100.0	6.51
70	2.4808	2.4862	0.160	46	4	7.5	1.19
30	2.4229	2.4282	0.120	21	4	3.4	0.92
55	2.3391	2.3442	0.120	10	3	1.7	1.01
35	2.1473	2.1520	0.120	98	3	15.9	1.23
70	2.0973	2.1019	0.080	161	3	26.2	1.61
10	2.0245	2.0289	0.320	18	3	3.0	2.34
70	1.8343	1.8383	0.240	3	2	0.4	0.80
15	1.7135	1.7172	0.160	35	3	5.7	1.20
15	1.6152	1.6187	0.080	166	4	27.1	1.14



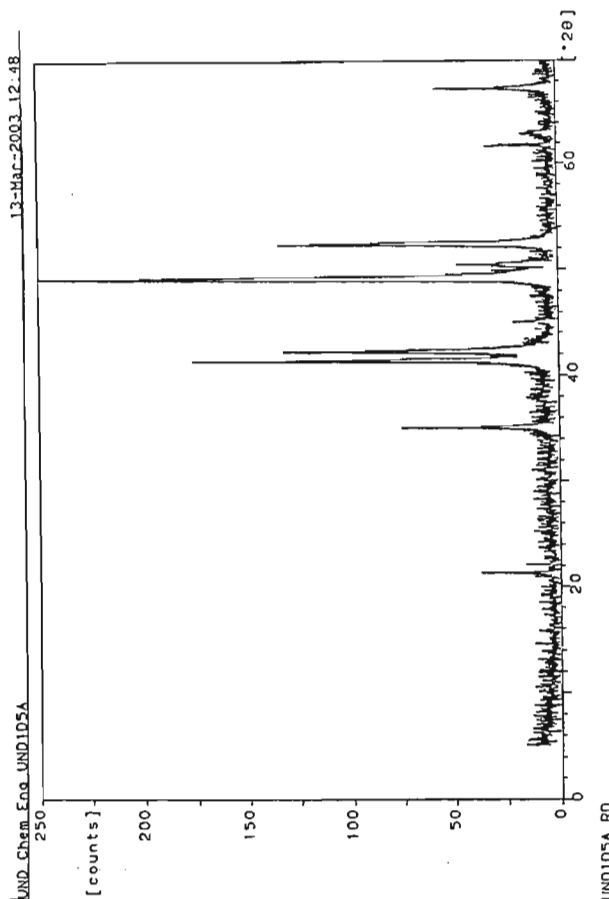
Sample identification: und1d5a
 Data measured at: 13-Mar-2003 11:14:00

Diffraction type: PW3710 BASED
 Tube anode: Co
 Generator tension [kV]: 40
 Generator current [mA]: 40
 Wavelength Alpha1 [Å]: 1.78896
 Wavelength Alpha2 [Å]: 1.79285
 Intensity ratio (alpha2/alpha1): 0.500
 Divergence slit: 1/4°
 Receiving slit: 0.1
 Monochromator used: YES

Start angle [°2θ]: 5.000
 End angle [°2θ]: 70.000
 Step size [°2θ]: 0.020
 Maximum intensity: 228.0100
 Time per step [s]: 1.000
 Type of scan: STEP

Peak positions defined by: Top of smoothed peak
 Minimum peak tip width: 0.00
 Maximum peak tip width: 1.00
 Peak base width: 2.00
 Minimum significance: 0.75
 Number of peaks: 14

Angle [°2θ]	d-value α1 [Å]	d-value α2 [Å]	Peak width [°2θ]	Peak int [counts]	Back. int [counts]	Rel. int [%]	Signif.
1.310	4.8378	4.8483	0.100	31	3	13.8	0.93
2.105	4.6658	4.6760	0.080	11	3	4.8	1.19
6.620	3.8853	3.8938	0.040	5	4	2.1	0.75
5.105	2.9660	2.9724	0.080	44	5	19.1	0.85
1.395	2.5308	2.5363	0.080	164	7	71.9	1.19
2.255	2.4816	2.4870	0.160	114	6	50.2	3.54
5.040	2.3354	2.3405	0.160	13	4	5.7	1.31
9.120	2.1520	2.1567	0.080	228	5	100.0	0.88
0.455	2.0987	2.1032	0.240	30	4	13.3	2.00
2.405	2.0258	2.0302	0.160	125	4	55.0	1.81
1.740	1.7433	1.7471	0.040	30	4	13.3	2.40
1.885	1.7396	1.7434	0.060	24	4	10.5	1.49
2.970	1.7127	1.7164	0.240	10	3	4.2	1.53
7.250	1.6153	1.6188	0.120	37	3	16.3	1.41



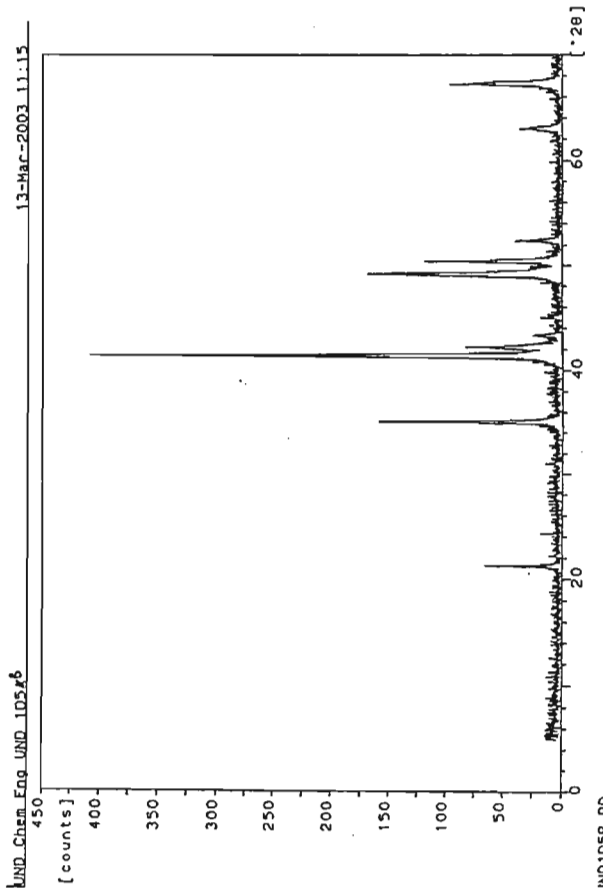
Sample identification: und1d5b
 Data measured at: 13-Mar-2003 8:40:00

Diffraction type: PW3710 BASED
 Tube anode: Co
 Generator tension [kV]: 40
 Generator current [mA]: 40
 Wavelength Alpha1 [Å]: 1.78896
 Wavelength Alpha2 [Å]: 1.79285
 Intensity ratio (alpha2/alpha1): 0.500
 Divergence slit: 1/4°
 Receiving slit: 0.1
 Monochromator used: YES

Start angle [°2θ]: 5.000
 End angle [°2θ]: 70.000
 Step size [°2θ]: 0.020
 Maximum intensity: 404.0100
 Time per step [s]: 1.000
 Type of scan: STEP

Peak positions defined by: Top of smoothed peak
 Minimum peak tip width: 0.00
 Maximum peak tip width: 1.00
 Peak base width: 2.00
 Minimum significance: 0.75
 Number of peaks: 14

Angle [°2θ]	d-value α1 [Å]	d-value α2 [Å]	Peak width [°2θ]	Peak int [counts]	Back. int [counts]	Rel. int [%]	Signif.
190	19.7563	19.7992	0.240	4	7	1.1	0.93
300	4.8400	4.8505	0.100	61	3	15.1	1.29
275	4.6307	4.6407	0.240	3	4	0.8	0.92
050	3.3419	3.3491	0.120	8	4	1.9	0.81
110	2.9656	2.9720	0.100	151	5	37.4	1.91
405	2.5302	2.5357	0.180	404	5	100.0	10.07
275	2.4805	2.4859	0.120	79	5	19.6	0.94
360	2.4213	2.4266	0.200	14	4	3.4	1.10
015	2.3367	2.3417	0.160	12	3	2.9	1.28
200	2.1487	2.1534	0.240	154	4	38.1	4.75
460	2.0985	2.1030	0.080	114	4	28.3	1.12
480	2.0231	2.0275	0.120	34	4	8.3	0.89
970	1.7127	1.7164	0.240	30	3	7.5	2.41
250	1.6153	1.6188	0.200	76	4	18.7	1.82



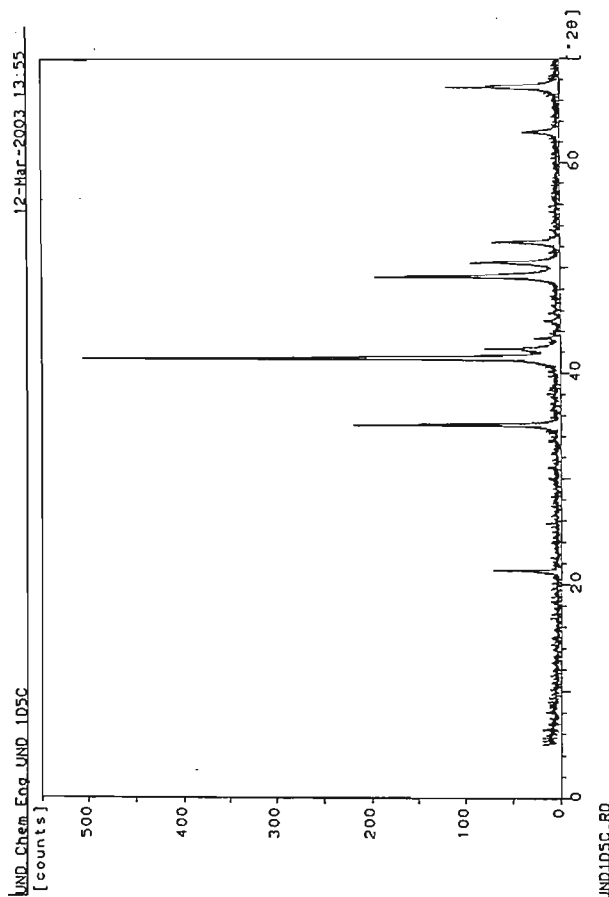
Sample identification: und1d5c
 Data measured at: 12-Mar-2003.12:51:00

Diffractionmeter type: PW3710 BASED
 Tube anode: Co
 Generator tension [kV]: 40
 Generator current [mA]: 40
 Wavelength Alpha [Å]: 1.78896
 Wavelength Alpha2 [Å]: 1.79285
 Intensity ratio (alpha2/alpha): 0.500
 Divergence slit: 1/4°
 Receiving slit: 0.1
 Monochromator used: YES

Start angle [°2θ]: 5.000
 End angle [°2θ]: 70.000
 Step size [°2θ]: 0.020
 Maximum intensity: 484.0000
 Time per step [s]: 1.000
 Type of scan: STEP

Peak positions defined by: Top of smoothed peak
 Minimum peak tip width: 0.00
 Maximum peak tip width: 1.00
 Peak base width: 2.00
 Minimum significance: 0.75
 Number of peaks: 12

Angle [°2θ]	d-value α1 [Å]	d-value α2 [Å]	Peak width [°2θ]	Peak int [counts]	Back. int [counts]	Rel. int [t]	Signif.
8.100	12.6649	12.6924	0.400	2	6	0.4	0.81
1.300	4.8400	4.8505	0.120	55	4	11.3	2.38
5.115	2.9652	2.9716	0.160	213	5	44.0	8.66
1.415	2.5297	2.5352	0.120	484	6	100.0	5.27
2.290	2.4796	2.4850	0.080	64	5	13.2	1.05
3.330	2.4229	2.4282	0.200	14	4	3.0	1.36
5.010	2.3369	2.3420	0.160	10	3	2.0	0.78
9.165	2.1502	2.1549	0.060	177	4	36.5	0.75
0.470	2.0981	2.1026	0.080	90	4	18.6	1.02
2.430	2.0249	2.0293	0.200	66	3	13.6	2.88
2.940	1.7134	1.7171	0.160	29	3	6.0	0.75
7.250	1.6153	1.6188	0.120	104	4	21.5	1.91



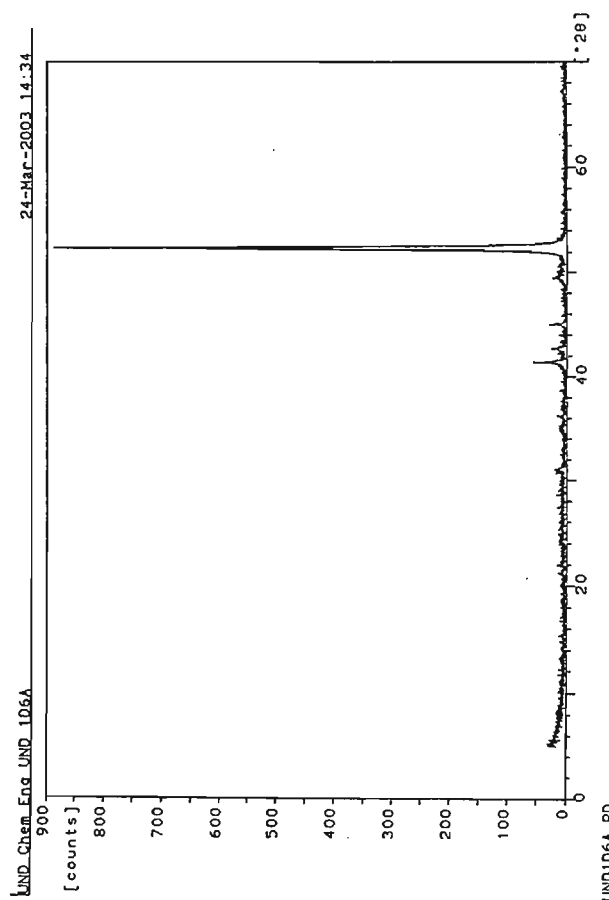
Sample identification: und1d6a
 Data measured at: 24-Mar-2003 11:58:00

Diffractionmeter type: PW3710 BASED
 Tube anode: Co
 Generator tension [kV]: 40
 Generator current [mA]: 40
 Wavelength Alpha [Å]: 1.78896
 Wavelength Alpha2 [Å]: 1.79285
 Intensity ratio (alpha2/alpha): 0.500
 Divergence slit: 1/4°
 Receiving slit: 0.1
 Monochromator used: YES

Start angle [°2θ]: 5.000
 End angle [°2θ]: 70.000
 Step size [°2θ]: 0.020
 Maximum intensity: 784.0000
 Time per step [s]: 1.000
 Type of scan: STEP

Peak positions defined by: Top of smoothed peak
 Minimum peak tip width: 0.00
 Maximum peak tip width: 1.00
 Peak base width: 2.00
 Minimum significance: 0.75
 Number of peaks: 15

Angle [°2θ]	d-value α1 [Å]	d-value α2 [Å]	Peak width [°2θ]	Peak int [counts]	Back. int [counts]	Rel. int [t]	Signif.
2.275	19.4382	19.4804	0.480	10	13	1.2	1.11
2.295	5.3375	5.3490	0.240	2	4	0.2	0.97
2.230	4.8558	4.8664	0.320	6	4	0.7	1.03
0.060	4.6752	4.6854	0.320	4	5	0.6	0.82
0.050	3.3419	3.3491	0.120	14	6	1.7	1.08
0.955	2.9783	2.9848	0.480	4	4	0.5	1.30
0.155	2.8826	2.8889	0.240	5	5	0.6	1.45
0.410	2.5300	2.5355	0.060	53	4	6.8	1.13
0.670	2.4586	2.4639	0.160	18	3	2.2	0.81
0.040	2.3354	2.3405	0.160	18	3	2.4	1.27
0.495	2.1367	2.1414	0.240	12	4	1.6	1.08
0.400	2.0260	2.0304	0.100	784	4	100.0	3.12
0.490	2.0228	2.0271	0.060	640	4	81.6	0.91
0.175	1.6608	1.6644	0.480	1	3	0.1	0.80
0.060	1.6193	1.6229	0.960	3	3	0.4	1.75



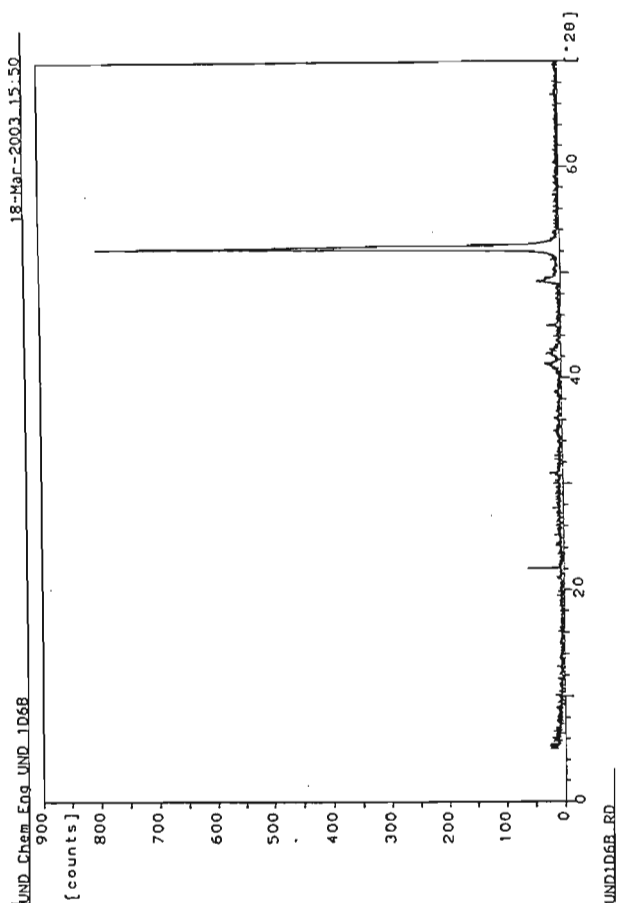
Sample identification: und1d6b
 Data measured at: 18-Mar-2003 13:09:00

Diffractometer type: PW3710 BASED
 Tube anode: Co
 Generator tension [kV]: 40
 Generator current [mA]: 40
 Wavelength Alpha1 [Å]: 1.78896
 Wavelength Alpha2 [Å]: 1.79285
 Intensity ratio (alpha2/alpha1): 0.500
 Divergence slit: 1/4°
 Receiving slit: 0.1
 Monochromator used: YES

Start angle [°2θ]: 5.000
 End angle [°2θ]: 70.000
 Step size [°2θ]: 0.020
 Maximum intensity: 784.0000
 Time per step [s]: 1.000
 Type of scan: STEP

Peak positions defined by: Top of smoothed peak
 Minimum peak tip width: 0.00
 Maximum peak tip width: 1.00
 Peak base width: 2.00
 Minimum significance: 0.75
 Number of peaks: 11

Angle [°2θ]	d-value α1 [Å]	d-value α2 [Å]	Peak width [°2θ]	Peak int [counts]	Back. int [counts]	Rel. int [%]	Signif.
0.080	4.6711	4.6812	0.080	55	4	7.0	2.00
0.000	3.3471	3.3544	0.160	12	6	1.6	1.14
0.895	2.9833	2.9898	0.400	6	4	0.7	1.11
1.185	2.8803	2.8866	0.240	7	4	0.9	1.29
1.660	2.7023	2.7082	0.240	5	3	0.6	1.07
1.165	2.5444	2.5499	0.240	17	3	2.1	0.87
1.300	2.4791	2.4845	0.240	16	3	2.0	1.13
1.010	2.3369	2.3420	0.160	17	3	2.1	1.26
1.190	2.1492	2.1538	0.160	30	5	3.9	1.05
1.385	2.0265	2.0309	0.180	784	6	100.0	13.07
1.045	1.6197	1.6232	0.800	3	3	0.3	0.90



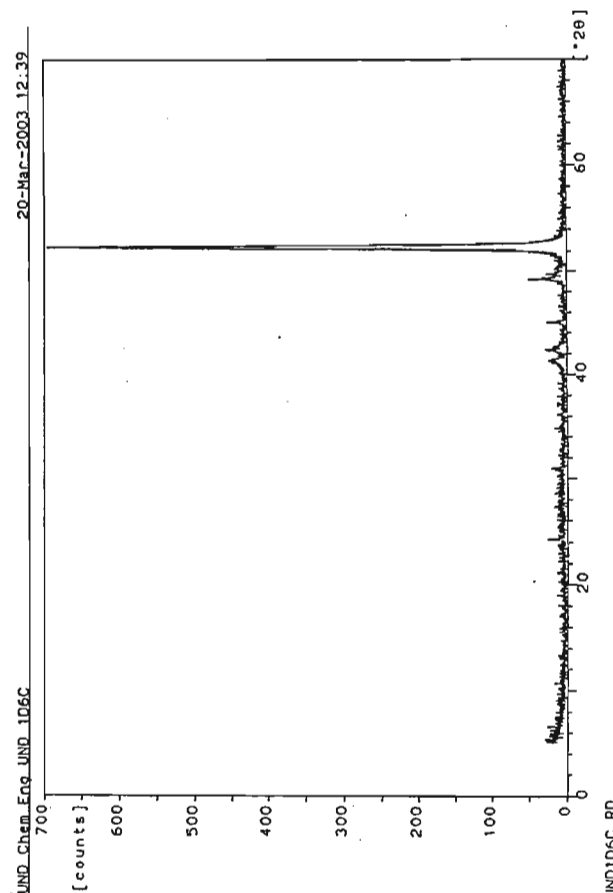
Sample identification: und1d6c
 Data measured at: 20-Mar-2003 11:04:00

Diffractometer type: PW3710 BASED
 Tube anode: Co
 Generator tension [kV]: 40
 Generator current [mA]: 40
 Wavelength Alpha1 [Å]: 1.78896
 Wavelength Alpha2 [Å]: 1.79285
 Intensity ratio (alpha2/alpha1): 0.500
 Divergence slit: 1/4°
 Receiving slit: 0.1
 Monochromator used: YES

Start angle [°2θ]: 5.000
 End angle [°2θ]: 70.000
 Step size [°2θ]: 0.020
 Maximum intensity: 691.6900
 Time per step [s]: 1.000
 Type of scan: STEP

Peak positions defined by: Top of smoothed peak
 Minimum peak tip width: 0.00
 Maximum peak tip width: 1.00
 Peak base width: 2.00
 Minimum significance: 0.75
 Number of peaks: 13

Angle [°2θ]	d-value α1 [Å]	d-value α2 [Å]	Peak width [°2θ]	Peak int [counts]	Back. int [counts]	Rel. int [%]	Signif.
1.280	4.2533	4.2626	0.100	16	6	2.3	0.90
1.980	3.3492	3.3565	0.120	13	6	1.9	0.86
1.910	2.9820	2.9885	0.480	3	4	0.4	0.83
1.165	2.8818	2.8881	0.240	5	5	0.8	1.38
1.315	2.5355	2.5410	0.400	13	4	1.9	1.80
1.280	2.4802	2.4856	0.200	13	4	1.9	1.18
1.995	2.3376	2.3427	0.160	18	4	2.7	0.95
1.165	2.1502	2.1549	0.060	45	4	6.5	0.90
1.650	2.1305	2.1351	0.120	18	4	2.7	0.99
1.385	2.0265	2.0309	0.220	692	4	100.0	15.93
1.230	1.8677	1.8718	0.400	3	3	0.4	0.85
1.360	1.7793	1.7832	0.200	4	2	0.5	0.80
1.785	1.6252	1.6288	0.960	1	3	0.2	0.87



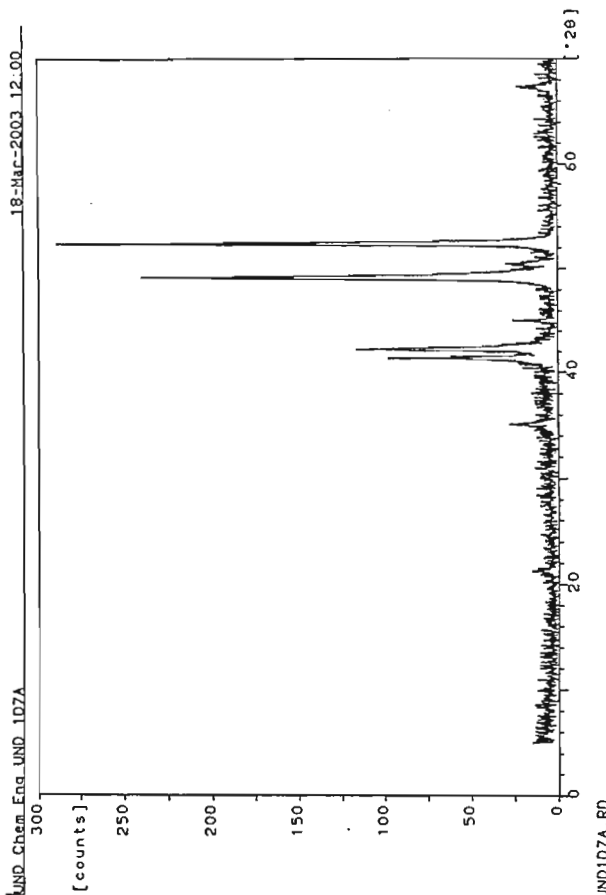
Sample identification: und1d7a
Data measured at: 18-Mar-2003 11:01:00

Diffractometer type: PW3710 BASED
Tube anode: Co
Generator tension [kV]: 40
Generator current [mA]: 40
Wavelength Alpha1 [Å]: 1.78896
Wavelength Alpha2 [Å]: 1.79285
Intensity ratio (alpha2/alpha1): 0.500
Divergence slit: 1/4°
Receiving slit: 0.1
Monochromator used: YES

Start angle [°2θ]: 5.000
End angle [°2θ]: 70.000
Step size [°2θ]: 0.020
Maximum intensity: 285.6100
Time per step [s]: 1.000
Type of scan: STEP

Peak positions defined by: Top of smoothed peak
Minimum peak tip width: 0.00
Maximum peak tip width: 1.00
Peak base width: 2.00
Minimum significance: 0.75
Number of peaks: 13

Angle [°2θ]	d-value α1 [Å]	d-value α2 [Å]	Peak width [°2θ]	Peak int [counts]	Back. int [counts]	Rel. int [t]	Signif.
405	18.9710	19.0122	0.640	1	8	0.4	0.78
665	6.5637	6.5779	0.120	4	4	1.3	1.21
310	4.8378	4.8483	0.480	8	4	2.9	2.30
970	3.3503	3.3576	0.240	4	5	1.5	0.85
100	2.9664	2.9728	0.160	19	6	6.8	1.00
410	2.5300	2.5355	0.200	83	6	29.0	3.19
260	2.4813	2.4867	0.240	104	5	36.4	4.25
030	2.3359	2.3410	0.240	18	4	6.2	2.96
215	2.1481	2.1528	0.180	213	5	74.6	3.83
425	2.0998	2.1044	0.240	18	5	6.5	1.01
410	2.0256	2.0300	0.160	286	4	100.0	6.00
965	1.7128	1.7165	0.480	4	3	1.4	0.76
250	1.6153	1.6188	0.320	12	4	4.3	1.30



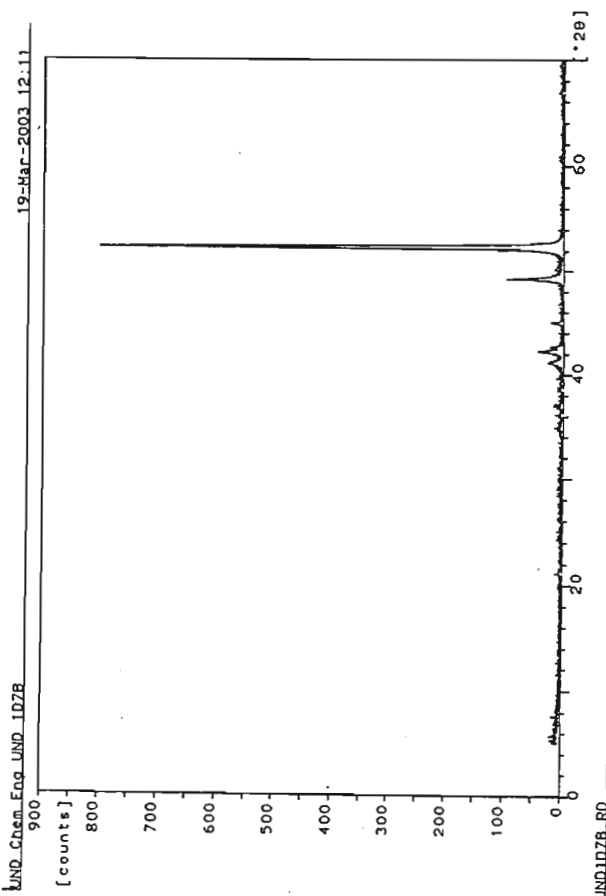
Sample identification: und1d7b
Data measured at: 19-Mar-2003 10:14:00

Diffractometer type: PW3710 BASED
Tube anode: Co
Generator tension [kV]: 40
Generator current [mA]: 40
Wavelength Alpha1 [Å]: 1.78896
Wavelength Alpha2 [Å]: 1.79285
Intensity ratio (alpha2/alpha1): 0.500
Divergence slit: 1/4°
Receiving slit: 0.1
Monochromator used: YES

Start angle [°2θ]: 5.000
End angle [°2θ]: 70.000
Step size [°2θ]: 0.020
Maximum intensity: 795.2400
Time per step [s]: 1.000
Type of scan: STEP

Peak positions defined by: Top of smoothed peak
Minimum peak tip width: 0.00
Maximum peak tip width: 1.00
Peak base width: 2.00
Minimum significance: 0.75
Number of peaks: 13

Angle [°2θ]	d-value α1 [Å]	d-value α2 [Å]	Peak width [°2θ]	Peak int [counts]	Back. int [counts]	Rel. int [t]	Signif.
80	19.0591	19.1005	0.960	4	7	0.5	0.80
50	4.8740	4.8846	0.240	5	3	0.6	1.14
40	2.9796	2.9860	0.800	5	3	0.7	1.34
60	2.8822	2.8885	0.240	6	3	0.8	1.77
15	2.8179	2.8240	0.400	4	4	0.6	1.06
30	2.5429	2.5484	0.320	19	4	2.4	1.42
50	2.4813	2.4867	0.200	37	4	4.7	1.97
15	2.3367	2.3417	0.240	14	3	1.7	2.76
15	2.1494	2.1540	0.060	90	5	11.3	1.28
15	2.0254	2.0298	0.200	795	5	100.0	16.89
15	1.8268	1.8308	0.960	1	2	0.2	1.09
30	1.7705	1.7744	0.640	3	2	0.3	0.98
30	1.6226	1.6261	0.480	4	3	0.5	1.16



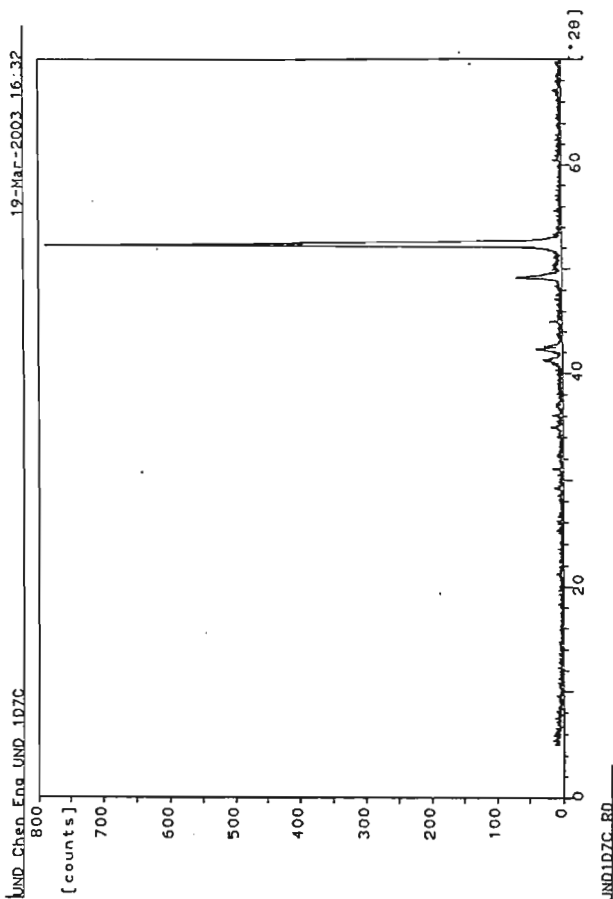
Sample identification: und1d7c
 Data measured at: 19-Mar-2003 14:11:00

Diffractionmeter type: PW3710 BASED
 Tube anode: Co
 Generator tension [kV]: 40
 Generator current [mA]: 40
 Wavelength Alpha1 [Å]: 1.78896
 Wavelength Alpha2 [Å]: 1.79285
 Intensity ratio (alpha2/alpha1): 0.500
 Divergence slit: 1/4°
 Receiving slit: 0.1
 Monochromator used: YES

Start angle [°2θ]: 5.000
 End angle [°2θ]: 70.000
 Step size [°2θ]: 0.020
 Maximum intensity: 772.8400
 Time per step [s]: 1.000
 Type of scan: STEP

Peak positions defined by: Top of smoothed peak
 Minimum peak tip width: 0.00
 Maximum peak tip width: 1.00
 Peak base width: 2.00
 Minimum significance: 0.75
 Number of peaks: 18

Angle [°2θ]	d-value α1 [Å]	d-value α2 [Å]	Peak width [°2θ]	Peak int [counts]	Back. int [counts]	Rel. int [t]	Signif.
3.395	19.0061	19.0474	0.480	3	6	0.3	0.91
3.330	5.6159	5.6280	0.800	1	2	0.1	0.78
3.260	4.8490	4.8596	0.960	3	2	0.4	1.13
3.240	3.5438	3.5515	0.240	6	3	0.8	1.39
3.045	3.3424	3.3497	0.160	8	3	1.1	1.24
2.930	2.9804	2.9869	0.240	10	3	1.3	2.13
2.100	2.8869	2.8931	0.240	5	3	0.7	1.22
1.925	2.8245	2.8307	0.320	6	3	0.7	0.80
1.245	2.5396	2.5451	0.320	19	4	2.5	1.70
1.270	2.4808	2.4862	0.200	32	4	4.2	2.04
1.635	2.4605	2.4659	0.120	15	3	2.0	0.97
1.000	2.3374	2.3425	0.120	12	3	1.6	2.07
1.150	2.1508	2.1555	0.100	55	6	7.1	0.97
1.385	2.0265	2.0309	0.140	773	5	100.0	6.71
1.525	2.0215	2.0259	0.060	467	5	60.4	0.87
1.660	1.7713	1.7752	0.480	3	2	0.4	1.13
1.690	1.7195	1.7233	0.480	2	2	0.3	0.80
1.955	1.6216	1.6251	0.480	3	3	0.4	0.94



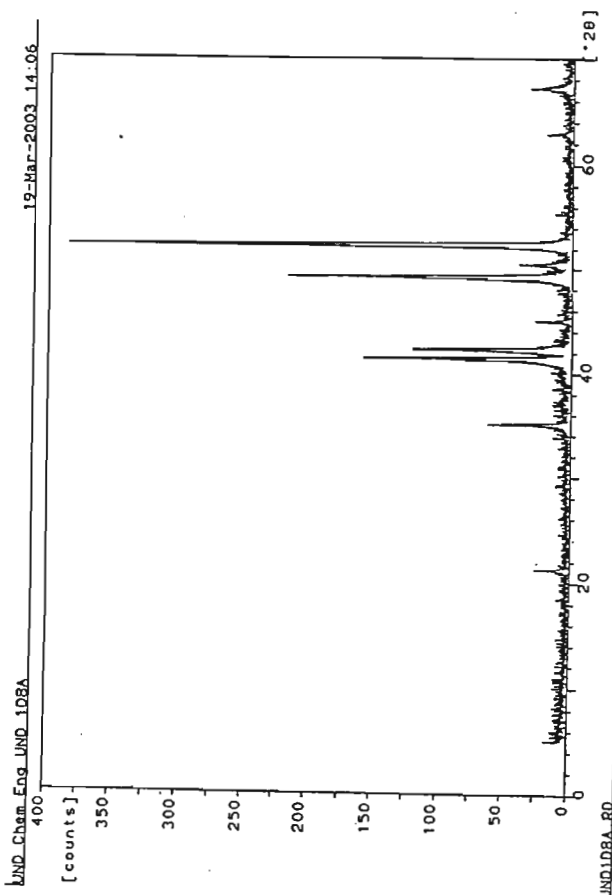
Sample identification: und1d8a
 Data measured at: 19-Mar-2003 12:18:00

Diffractionmeter type: PW3710 BASED
 Tube anode: Co
 Generator tension [kV]: 40
 Generator current [mA]: 40
 Wavelength Alpha1 [Å]: 1.78896
 Wavelength Alpha2 [Å]: 1.79285
 Intensity ratio (alpha2/alpha1): 0.500
 Divergence slit: 1/4°
 Receiving slit: 0.1
 Monochromator used: YES

Start angle [°2θ]: 5.000
 End angle [°2θ]: 70.000
 Step size [°2θ]: 0.020
 Maximum intensity: 349.6900
 Time per step [s]: 1.000
 Type of scan: STEP

Peak positions defined by: Top of smoothed peak
 Minimum peak tip width: 0.00
 Maximum peak tip width: 1.00
 Peak base width: 2.00
 Minimum significance: 0.75
 Number of peaks: 15

Angle [°2θ]	d-value α1 [Å]	d-value α2 [Å]	Peak width [°2θ]	Peak int [counts]	Back. int [counts]	Rel. int [t]	Signif.
2.270	4.8468	4.8573	0.160	17	3	4.8	1.24
2.080	2.9680	2.9745	0.100	49	4	14.0	1.38
1.140	2.8087	2.8148	0.480	5	3	1.5	1.68
1.565	2.7087	2.7146	0.200	7	3	2.1	0.84
1.395	2.5308	2.5363	0.100	156	3	44.7	2.14
1.285	2.4799	2.4853	0.100	112	3	32.1	0.96
1.985	2.3381	2.3432	0.060	21	3	6.1	1.24
1.230	2.1475	2.1522	0.060	216	4	61.8	2.67
1.450	2.0989	2.1034	0.160	35	4	10.0	1.37
1.395	2.0262	2.0306	0.120	350	4	100.0	3.01
1.455	1.9225	1.9267	0.240	3	3	0.7	0.81
1.080	1.8143	1.8182	0.480	1	2	0.3	0.86
1.615	1.7725	1.7764	0.800	3	2	0.8	1.14
1.925	1.7138	1.7175	0.320	9	3	2.6	1.20
1.220	1.6159	1.6194	0.160	27	3	7.7	0.77

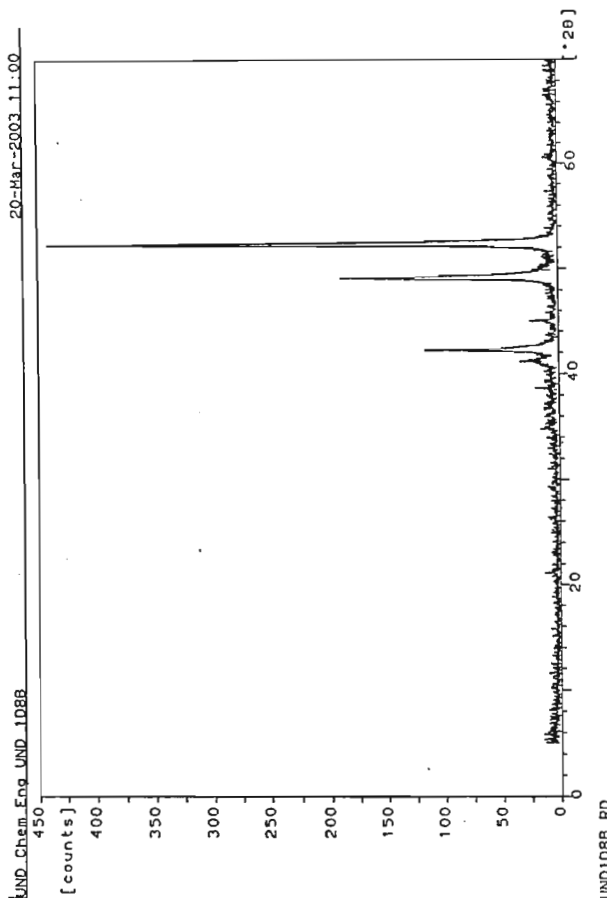


Sample identification: und1d8b
 Data measured at: 20-Mar-2003 9:24:00

Diffractionmeter type: PW3710 BASED
 Tube anode: Co
 Generator tension [kV]: 40
 Generator current [mA]: 40
 Wavelength Alpha1 [Å]: 1.78896
 Wavelength Alpha2 [Å]: 1.79285
 Intensity ratio (alpha2/alpha1): 0.500
 Divergence slit: 1/4°
 Receiving slit: 0.1
 Monochromator used: YES
 Start angle [°2θ]: 5.000
 End angle [°2θ]: 70.000
 Step size [°2θ]: 0.020
 Maximum intensity: 408.0400
 Time per step [s]: 1.000
 Type of scan: STEP

Peak positions defined by: Top of smoothed peak
 Minimum peak tip width: 0.00
 Maximum peak tip width: 1.00
 Peak base width: 2.00
 Minimum significance: 0.75
 Number of peaks: 13

Angle [°2θ]	d-value α1 [Å]	d-value α2 [Å]	Peak width [°2θ]	Peak int [counts]	Back. int [counts]	Rel. int [t]	Signif.
1.205	4.8615	4.8720	0.320	5	3	1.2	0.76
1.400	4.8177	4.8281	0.120	0	3	0.0	0.94
1.9160	3.5533	3.5610	0.480	2	3	0.5	1.44
4.865	2.9858	2.9923	0.240	5	4	1.3	0.78
6.915	2.8253	2.8314	0.480	4	5	0.9	0.77
1.155	2.5449	2.5505	0.320	14	6	3.5	0.99
2.240	2.4825	2.4878	0.200	94	5	23.1	3.33
5.000	2.3374	2.3425	0.160	16	4	3.9	0.98
9.170	2.1500	2.1546	0.240	166	7	40.8	5.64
2.380	2.0267	2.0311	0.160	408	6	100.0	5.68
4.705	1.9468	1.9510	0.240	2	3	0.5	0.77
0.590	1.7732	1.7770	0.480	3	3	0.6	1.67
6.765	1.6257	1.6292	0.960	3	3	0.7	0.80

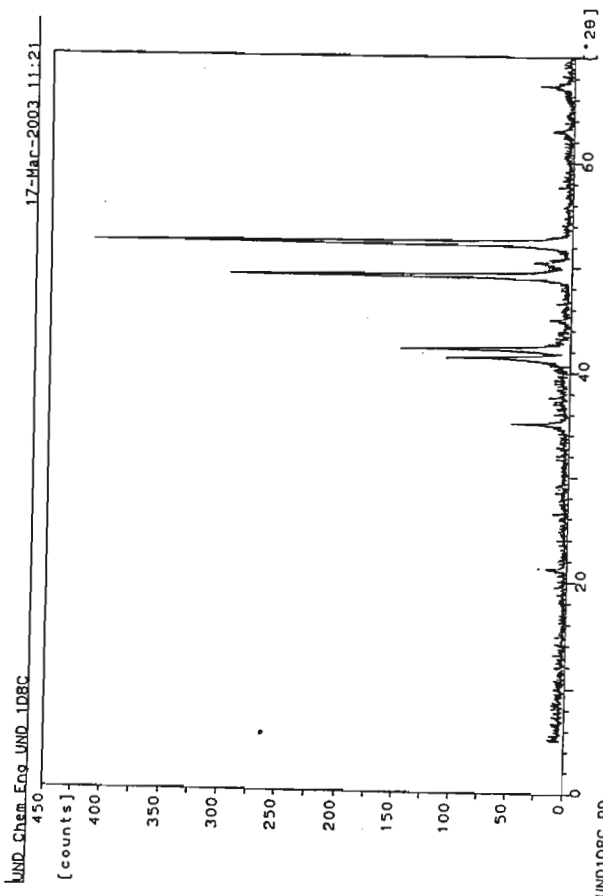


Sample identification: und1d8c
 Data measured at: 17-Mar-2003 9:49:00

Diffractionmeter type: PW3710 BASED
 Tube anode: Co
 Generator tension [kV]: 40
 Generator current [mA]: 40
 Wavelength Alpha1 [Å]: 1.78896
 Wavelength Alpha2 [Å]: 1.79285
 Intensity ratio (alpha2/alpha1): 0.500
 Divergence slit: 1/4°
 Receiving slit: 0.1
 Monochromator used: YES
 Start angle [°2θ]: 5.000
 End angle [°2θ]: 70.000
 Step size [°2θ]: 0.020
 Maximum intensity: 376.3600
 Time per step [s]: 1.000
 Type of scan: STEP

Peak positions defined by: Top of smoothed peak
 Minimum peak tip width: 0.00
 Maximum peak tip width: 1.00
 Peak base width: 2.00
 Minimum significance: 0.75
 Number of peaks: 13

Angle [°2θ]	d-value α1 [Å]	d-value α2 [Å]	Peak width [°2θ]	Peak int [counts]	Back. int [counts]	Rel. int [t]	Signif.
2.220	4.8581	4.8686	0.160	14	3	3.8	1.01
0.075	2.9684	2.9749	0.080	45	4	11.9	0.88
3.65	2.5326	2.5381	0.080	104	5	27.6	0.96
2.220	2.4836	2.4890	0.080	144	5	38.3	0.80
9.95	2.3376	2.3427	0.120	12	4	3.1	0.97
1.20	2.1520	2.1567	0.100	276	4	73.2	1.77
2.40	2.1471	2.1518	0.080	282	4	75.0	1.38
4.65	2.0983	2.1028	0.120	26	4	6.9	1.17
3.65	2.0272	2.0316	0.100	376	4	100.0	1.91
1.35	1.8127	1.8167	0.120	3	2	0.9	0.84
7.05	1.7701	1.7740	0.960	3	2	0.7	0.82
0.35	1.7135	1.7172	0.240	12	2	3.1	0.88
1.25	1.6158	1.6193	0.400	15	3	4.0	2.00

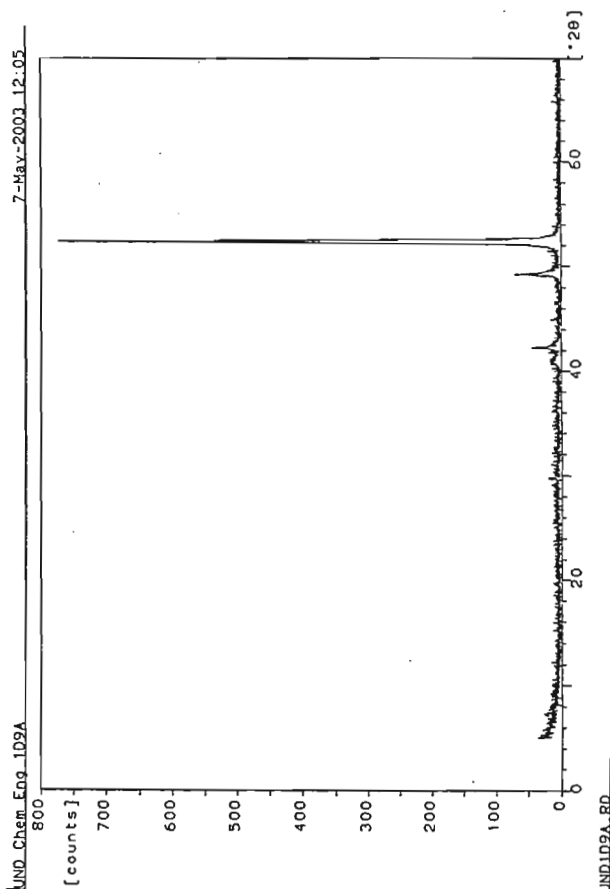


Sample identification: UND1D9A
 Data measured at: 5-May-2003 12:10:00

Diffractionmeter type: PW3710 BASED
 Tube anode: Co
 Generator tension [kV]: 40
 Generator current [mA]: 40
 Wavelength Alpha1 [Å]: 1.78896
 Wavelength Alpha2 [Å]: 1.79285
 Intensity ratio (alpha2/alpha1): 0.500
 Divergence slit: 1/4°
 Receiving slit: 0.1
 Monochromator used: YES
 Start angle [°2θ]: 5.000
 End angle [°2θ]: 70.000
 Step size [°2θ]: 0.020
 Maximum intensity: 750.7600
 Time per step [s]: 1.000
 Type of scan: STEP

Peak positions defined by: Top of smoothed peak
 Minimum peak tip width: 0.00
 Maximum peak tip width: 1.00
 Peak base width: 2.00
 Minimum significance: 0.75
 Number of peaks: 8

Angle [°2θ]	d-value α1 [Å]	d-value α2 [Å]	Peak width [°2θ]	Peak int [counts]	Back. int [counts]	Rel. int [%]	Signif.
.340	8.3224	8.3405	0.560	0	5	0.1	0.76
.000	7.3397	7.3556	0.800	1	4	0.1	0.82
.775	3.4815	3.4891	0.120	7	7	1.0	1.02
.555	2.8521	2.8583	0.960	3	5	0.3	1.14
.010	2.5536	2.5591	0.480	10	4	1.3	2.52
.290	2.4796	2.4850	0.160	32	4	4.3	1.44
.245	2.1469	2.1516	0.200	55	5	7.3	2.59
.365	2.0272	2.0316	0.140	751	6	100.0	7.65

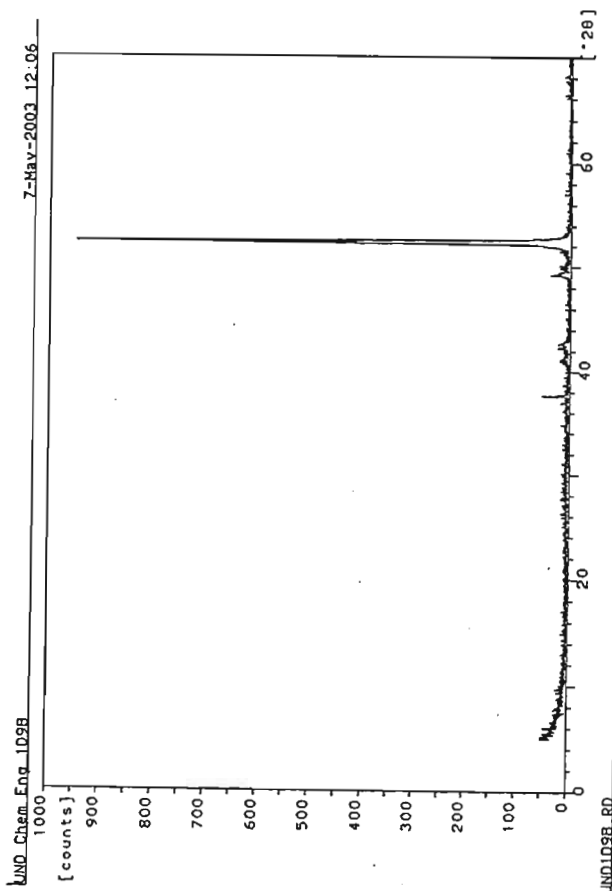


Sample identification: und1d9b
 Data measured at: 2-May-2003 9:19:00

Diffractionmeter type: PW3710 BASED
 Tube anode: Co
 Generator tension [kV]: 40
 Generator current [mA]: 40
 Wavelength Alpha1 [Å]: 1.78896
 Wavelength Alpha2 [Å]: 1.79285
 Intensity ratio (alpha2/alpha1): 0.500
 Divergence slit: 1/4°
 Receiving slit: 0.1
 Monochromator used: YES
 Start angle [°2θ]: 5.000
 End angle [°2θ]: 70.000
 Step size [°2θ]: 0.020
 Maximum intensity: 864.3600
 Time per step [s]: 1.000
 Type of scan: STEP

Peak positions defined by: Top of smoothed peak
 Minimum peak tip width: 0.00
 Maximum peak tip width: 1.00
 Peak base width: 2.00
 Minimum significance: 0.75
 Number of peaks: 10

Angle [°2θ]	d-value α1 [Å]	d-value α2 [Å]	Peak width [°2θ]	Peak int [counts]	Back. int [counts]	Rel. int [%]	Signif.
.35	5.7865	5.7991	0.480	1	4	0.1	0.81
.75	4.2542	4.2634	0.120	4	4	0.5	0.78
.15	3.5420	3.5497	0.240	6	6	0.7	1.06
.15	2.7745	2.7806	0.060	50	5	5.8	2.45
.75	2.5426	2.5481	0.480	9	4	1.0	2.15
.0	2.4564	2.4617	0.240	14	4	1.6	1.77
.5	2.1469	2.1516	0.200	26	5	3.0	1.75
.5	2.0262	2.0306	0.180	864	6	100.0	14.81
.5	1.8158	1.8197	0.320	4	2	0.4	1.05
.5	1.5954	1.5988	0.240	6	3	0.7	1.74



Sample identification: und1d9c
 Data measured at: 2-May-2003 12:09:00

Diffractometer type: PW1710 BASED
 Tube anode: Co
 Generator tension [kV]: 40
 Generator current [mA]: 40
 Wavelength Alpha1 [Å]: 1.78896
 Wavelength Alpha2 [Å]: 1.79285
 Intensity ratio (alpha2/alpha1): 0.500
 Divergence slit: 1/4°
 Receiving slit: 0.1
 Monochromator used: YES

Start angle [°2θ]: 5.000
 End angle [°2θ]: 70.000
 Step size [°2θ]: 0.020
 Maximum intensity: 846.8100
 Time per step [s]: 1.000
 Type of scan: STEP

Peak positions defined by: Top of smoothed peak
 Minimum peak tip width: 0.00
 Maximum peak tip width: 1.00
 Peak base width: 2.00
 Minimum significance: 0.75
 Number of peaks: 8

Angle [°2θ]	d-value α1 [Å]	d-value α2 [Å]	Peak width [°2θ]	Peak int [counts]	Back. int [counts]	Rel. int [%]	Signif.
7.735	3.7320	3.7401	0.240	5	6	0.6	0.94
0.990	2.5547	2.5603	0.240	8	3	1.0	0.90
2.570	2.4641	2.4694	0.640	10	3	1.2	1.78
1.995	2.3376	2.3427	0.240	5	3	0.6	0.93
1.265	2.1461	2.1507	0.200	24	4	2.8	1.67
1.595	2.0932	2.0978	0.060	8	4	1.0	0.77
1.415	2.0254	2.0298	0.120	847	4	100.0	5.80
1.545	2.0208	2.0252	0.100	488	4	57.7	1.14

